Dissertation zur Erlangung des Doktorgrades

der Fakultät für Chemie und Pharmazie

der Ludwig-Maximilians Universität München

Synthesis and Characterization of a Metal-Salen Base Pair for the Assembly of

Programmed Metal Arrays inside the DNA Double Helix

Synthese und Charakterisierung eines Metall-Salen Basenpaars für den Aufbau von

programmierten Metallanordnungen im Inneren von DNA-Doppelhelices

Guido Clever

aus

Bad Neuenahr

2006

Ltd. Doolittle: „Wenn Zusammenhänge logisch sind, dann sind sie das unabhängig von ihrem Ursprung."

Bombe # 20:   „Hmmm…"

Dark Star (John Carpenter, 1974)

Meiner Familie und Michi gewidmet.

<u>Parts of this work were published or presented on conferences</u>

G. H. Clever, K. Polborn, T. Carell, *Angew. Chem. Int. Ed.* **2005**, *44,* 7204 - 7208.
"A Highly DNA-Duplex-Stabilizing Metal-Salen Base Pair"

G. H. Clever, Y. Söltl, H. Burks, W. Spahl, T. Carell, *Chem. Eu. J.* **2006**, *12,* 8708 - 8718.
"Metal-Salen-Base-Pair Complexes Inside DNA: Complexation Overrides Sequence Information"

G. H. Clever, T. Carell, *Angew. Chem.* **2006**, in press (DOI: anie.200603099).
"Controlled Stacking of 10 Transition Metal Ions inside a DNA Duplex"

K. Tanaka*, G. H. Clever*, Y. Takezawa, Y. Yamada, C. Kaul, M. Shionoya, T. Carell, *Nature Nanotech.* **2006**, in press (DOI: 10.1038/nnano.2006.141).
"Programmable Self-Assembly of Metal Ions inside Artificial DNA Duplexes"

G. H. Clever, T. Carell, *Coll. Symp. Ser.* (M. Hocek, Ed), *Vol 7,* p. 389 - 391. Institute of Org. Chem and Biochem., Academy Of Sciences of the Czech Rep., Prague **2005**.
"Assembly of a Highly DNA-Duplex-Stabilizing Metal-Salen Base Pair"

Poster presentations on JCF meeting, Heidelberg **2004** (poster prize); ORCHEM, Bad Nauheim **2004**; Nanobionics III, Marburg **2005**; NAC XIII, Prague **2005**; Summer School FrontChem, Tokyo **2006**; Int. COE Symposium, Tokyo **2006**.

Oral presentations on Volkswagen Foundation meeting, Aachen **2005**; "Roche Symposium for Leading Scientists of the next decade"; Basel **2005**, FCI stipend meeting, Munich **2006**.

Table of contents

1   Summary

The controlled assembly of functional nanoscale materials from molecular entities is regarded as a key subject of future nanotechnology. Currently, the use of DNA, which features superior self organization properties, is heavily investigated. The aim of this work was the development of new systems for the controlled binding of multiple metal ions to the inside or outside of modified DNA double strands.

In the "metal-base pair concept", the natural DNA base pairs are replaced by flat metal complexes. The placement of metals inside the chiral DNA environment may result in enantioselective catalytic activity of these hybrid compounds. Furthermore, the incorporation of numerous metal-base pairs into oligonucleotides may lead to compounds with interesting electronic and magnetic properties.

In this thesis a new kind of metal-base pair based on the well known salen ligand was developed. A new feature that differentiates the metal-salen base pair from other known metal-base pairs is the crosslinking character of the metal salen complex, which resulted in a greatly enhanced structural stability of the DNA.

The synthesis of the ligand-nucleoside precursor comprised the preparation of a suitable protected salicylic aldehyde and an organo-cuprate mediated *C*-glycosylation as the key step (Sum.-Fig. 1, Chapter 4.2.1).
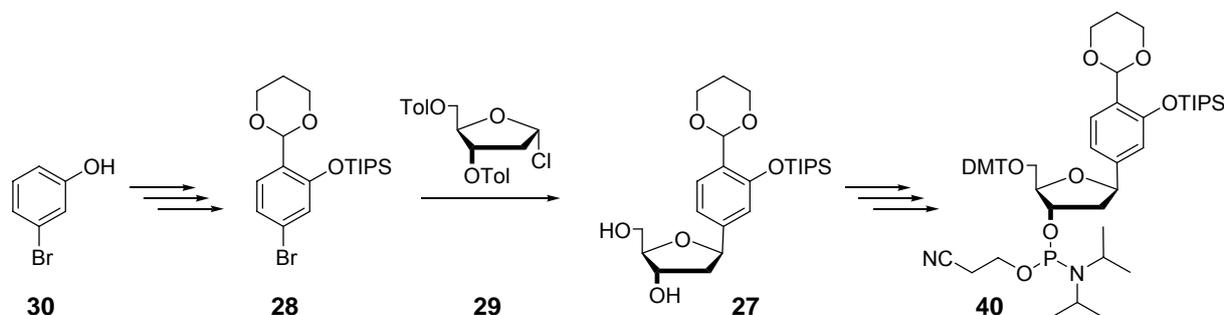
Sum.-Fig. 1: Synthesis of the protected salicylic aldehyde nucleoside **27** and the phosphoramidite **40**.

The correct β-configuration of the nucleoside was confirmed by X-ray crystallography. An X-ray structure of the corresponding monomeric copper-salen base pair showed a very good geometrical match with natural *Watson-Crick* base pairs (Chapter 4.2.2).

The ligand-nucleoside precursor was incorporated into numerous oligonucleotides by automated DNA synthesis to obtain duplexes with the ability to coordinate up to ten metal ions inside the helix. The assembly of the salen complexes was performed after hybridization of the complementary sequences and thereby preorganization of the salicylic aldehydes opposite to each other (Sum.-Fig. 2, Chapter 4.4).
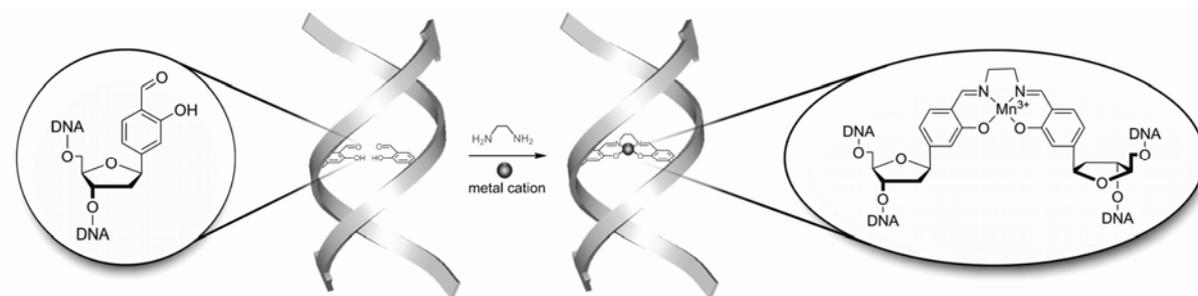
Sum.-Fig. 2: Schematic representation of the assembly of the metal-salen base pair inside the DNA.

The addition of excess ethylenediamine and 1 eq of Mn^{2+} or Cu^{2+} increased the melting temp. by 28 °C and 42 °C, respectively (Sum.-Fig. 3a, Chapter 4.4.2). This is the highest increase in melting point which was ever achieved with a metal-base pair.
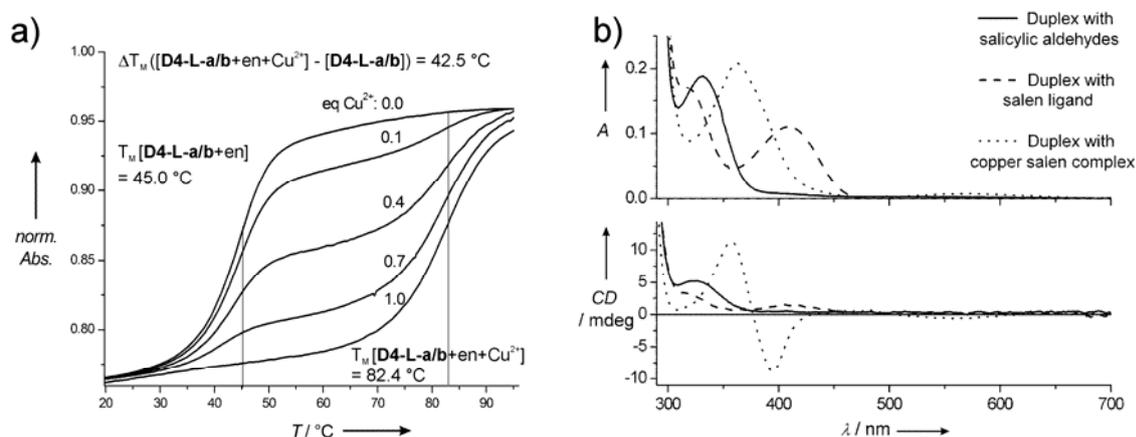
Sum.-Fig. 3: a) UV-melting curve of strand **D4-L-a/b** showing the high duplex stabilization of 42.5 °C; b) Comparison of (top) UV spectra and (bottom) CD spectra of DNA **D4-L-a/b** containing one pair of salicylic aldehydes prior and after assembly of a copper salen complex.

The complexation of these and other metal ions such as Fe^{3+}, VO^{2+} and Zn^{2+} was examined by UV and CD spectroscopy. The CD spectra showed the typical features of B-DNA at lower wavelengths and a chirality transfer from the DNA onto the salen chromophore at wavelengths above 300 nm (Sum.-Fig. 3b, Chapter 4.4.3). High res. ESI mass spectrometry proofed the correct assembly of the salen complexes inside the DNA double strands (Chapter 4.4.4).

The interplay of the sequence context and the number and position of one and more pairs of salicylic aldehydes in the double helix was studied with a variety of different specially designed oligonucleotides. It was found, that the salen complex formation is – depending on the used metal ion – so strong, that it can override sequence information and presumably force the DNA duplex to adopt unnatural secondary structures (Chapter 4.5.1).

Side reactions resulting from the kinetically driven intrastrand salen assembly, thereby leading to unspecific hairpin formation, were investigated. A reaction of salicylic aldehyde-containing single strands with ethylenediamine and metal ions was also observed (Chapters 4.5.3 and 4.5.4).

The high stability of the metal-salen base pair allowed the stacking of up to ten metal ions inside a DNA double strand (Sum.-Fig. 4, Chapter 4.6).
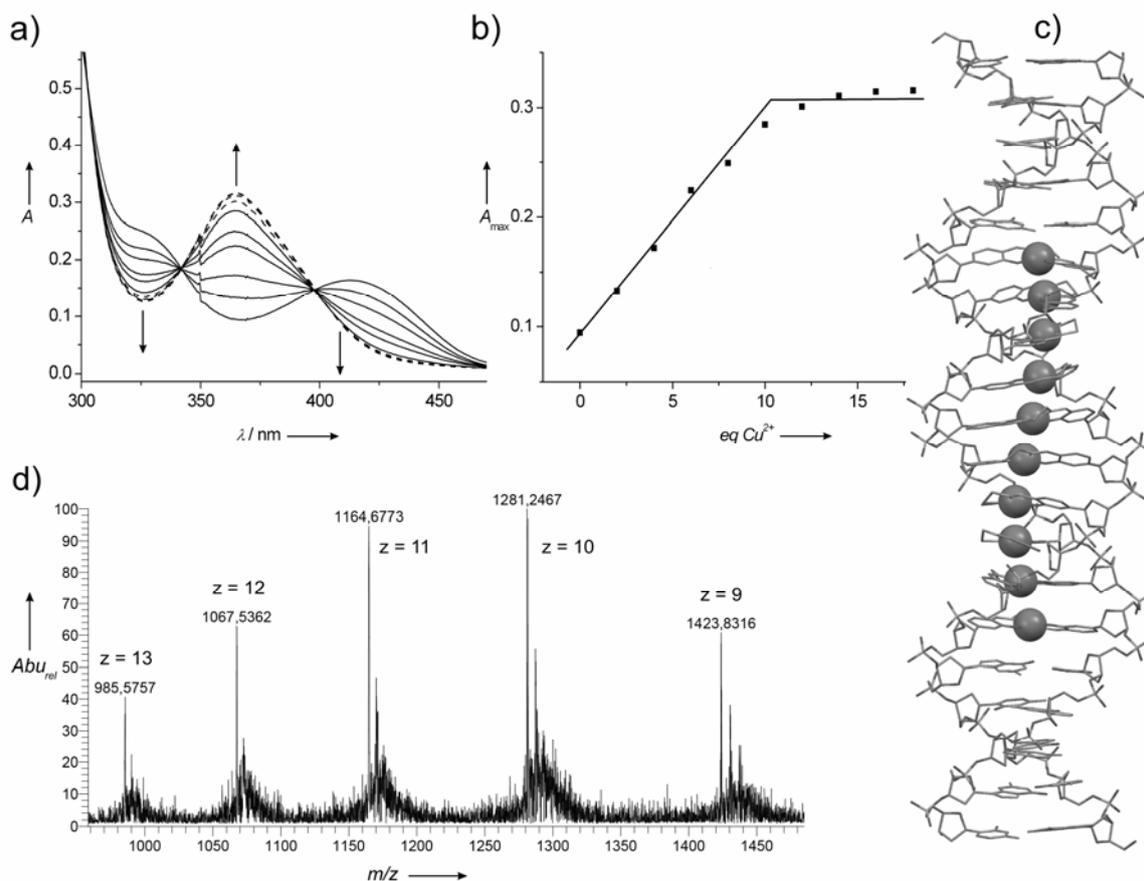
Sum.-Fig. 4: Stacking of 10 metal ions inside DNA. a) UV titration; b) plot of UV abs. max. against the ratio [Cu^{2+}]/[duplex]; c) model structure of 10 metal-salen complexes inside a perfect B-DNA; d) high resolution ESI-MS spectrum of [**D19-L-a/b**+10en+10Mn].

Utilizing the ability of **TT**-mismatches to coordinate Hg^{2+}-ions to give the **T**-Hg^{2+}-**T** base pair, DNA oligonucleotides were prepared, which allowed the selective mixing of up to ten Cu^{2+} and Hg^{2+}-ions inside the duplexes in sequences like Cu^{2+}-Hg^{2+}- Cu^{2+}-Hg^{2+}- Cu^{2+}-Hg^{2+}- Cu^{2+}-Hg^{2+}- Cu^{2+}-Hg^{2+} (Chapter 4.6).

EPR spectroscopic measurements in collaboration with *Dr. O. Schiemann*, Frankfurt University, delivered data, which is in full accordance with the formation of the copper(II)salen complexes inside the modified DNA strands (Sum.-Fig. 5). Two directly neighbored copper(II)salen complexes were found to interact in an antiferromagnetic manner (Chapter 4.4.6).
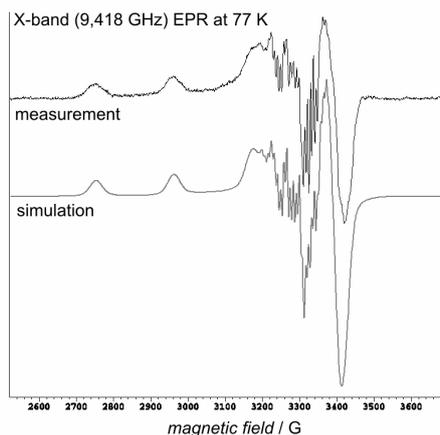
Sum.-Fig. 5: X-band EPR spectrum of strand **D4-L-a/b** containing one copper(II)salen base pair.

In the course of this work, several other ligand-modified nucleosides were synthesized and two of them were incorporated into DNA strands. Metal coordination to the DNA was, however, not yet achieved with these compounds (Sum.-Fig. 6).
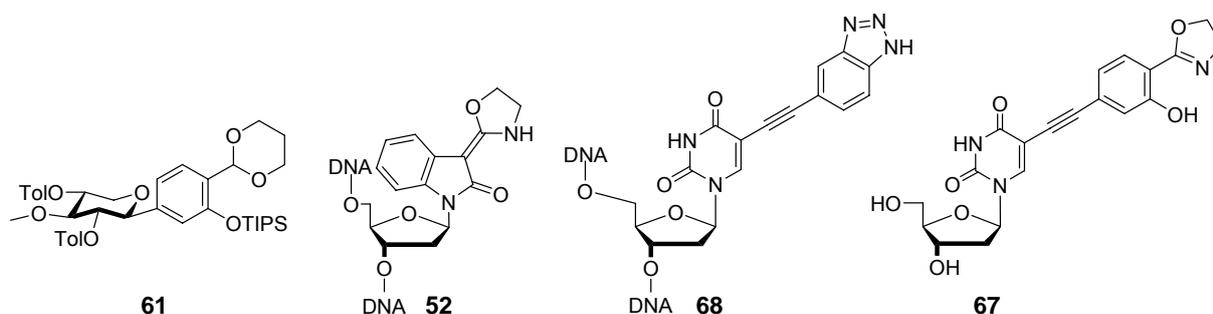
Sum.-Fig. 6: Other ligand-modified nucleosides prepared in this work. **52** and **68** were incorporated into oligonucleotides.

Azide-modified glutathione was synthesized and used as a ligand for nanoscopic gold clusters in collaboration with the group of *Prof. U. Simon*, RWTH Aachen. The clusters were successfully coupled to alkyne-modified DNA strands by means of the "click chemistry" approach. The assembly of the clusters along the DNA stretches was visualized by atomic force microscopy (Sum.-Fig. 7, Chapter 5.3).
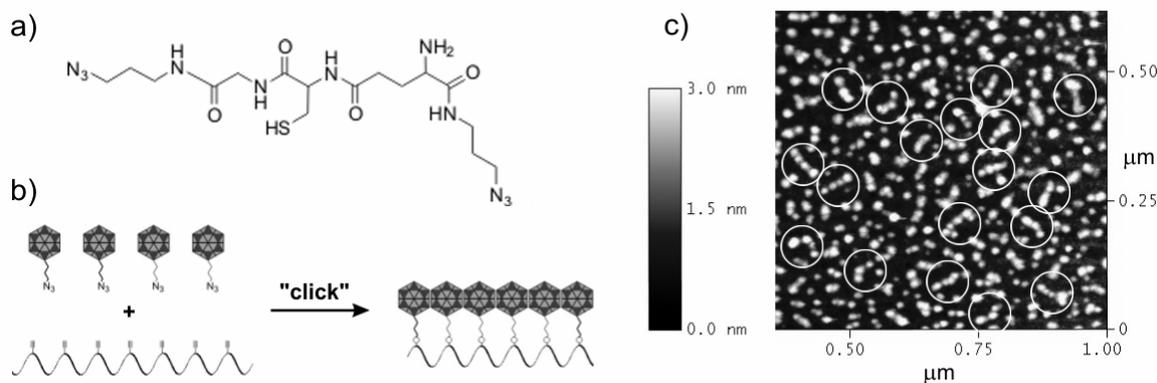
Sum.-Fig. 7: "Clicking clusters to DNA". a) the synthesized azide-modified glutathione ligand; b) reaction of azide-labeled clusters with alkyne-hypermodified DNA; c) AFM picture of clusters on DNA.

2 Zusammenfassung

Der kontrollierte Aufbau von funktionellen Materialien im Nanometerbereich aus molekularen Einheiten wird als zentrales Thema zukünftiger nanotechnologischer Entwicklungen betrachtet. Gegenwärtig wird dafür der Einsatz von DNA aufgrund ihrer herausragenden Selbstorganisationseigenschaften intensiv untersucht. Das Ziel dieser Arbeit war die Entwicklung von neuen Systemen, um gezielt eine Reihe von Metallen innerhalb oder außerhalb eines modifizierten DNA Doppelstrangs zu koordinieren.

Im Zuge des "Metall-Basenpaar-Konzepts" werden die natürlichen DNA-Basenpaare durch planare Metallkomplexe ersetzt. Die Platzierung von Metallen in der chiralen Umgebung der DNA eröffnet dabei im Prinzip Möglichkeiten zur Anwendung dieser Hybridsysteme in der enantioselektiven Katalyse. Des Weiteren verspricht der Einbau von mehreren dieser Metall-Basenpaare in Oligonukleotide die Möglichkeit, Systeme mit interessanten elektronischen und magnetischen Eigenschaften hervorzubringen.

Im Zuge dieser Arbeit wurde ein neuartiges Metall-Basenpaar entwickelt, welches auf dem bekannten Salenliganden basiert. Eine herausstechende Eigenschaft, die das Metall-Salen-Basenpaar von allen anderen bekannten Basenpaaren unterscheidet, ist der Vernetzungscharakter des Metall-Salenkomplexes welcher zu einer stark erhöhten strukturellen Stabilität der entsprechenden DNA-Doppelstränge führte.

Die Synthese des Ligand-modifizierten Nukleosidvorläufers erforderte die Darstellung eines geeignet geschützten Salicylaldehydes und eine Organo-Kuprat-vermittelte *C*-Glycosylierung als Schlüsselschritte (Sum.-Fig. 1, Kapitel 4.2.1).

Die gewünschte β-Konfiguration des Nukleosids wurde durch eine Kristallstrukturanalyse belegt. Die Kristallstruktur des entsprechenden monomeren Kupfer-Salen-Basenpaares zeigte eine sehr gute strukturelle Übereinstimmung mit den natürlichen *Watson-Crick*-Basenpaaren (Kapitel 4.2.2).

Das Ligand-modifizierte Nukleosid wurde mittels automatisierter DNA-Synthese in zahlreiche Oligonukleotide eingebaut. So wurden Doppelstränge erhalten, die bis zu zehn Metallionen im Inneren der Helix koordinieren konnten. Die Bildung der Salenkomplexe erfolgte im Anschluss an die Hybridisierung der jeweils komplementären Doppelstränge, da eine Präorganisation des Systems von Nöten

war um ein Gegenüberliegen der Salicylaldehyde zu erzwingen (Sum.-Fig. 2, Kapitel 4.4).

Die Zugabe von Ethylendiamin im Überschuss und einem Äquivalent Mn^{2+} bzw. Cu^{2+} erhöhte den Schmelzpunkt der DNA um 28 °C bzw. 42 °C (Sum.-Fig. 3a, Kapitel 4.4.2). Dies ist der höchste Schmelzpunktanstieg, der jemals mit einem Metall-Basenpaar erreicht wurde.

Die Komplexierung von diesen und anderen Metallen wie Fe^{3+}, VO^{2+} und Zn^{2+} wurde mittels UV- und CD-Spektroskopie ermittelt. Die CD-Spektren zeigen im unteren Wellenlängenbereich einen für B-DNA typischen Verlauf. Oberhalb von 300 nm war ein Chiralitätstransfer von der DNA auf den Salen-Chromophor erkennbar (Sum.-Fig. 3b, Kapitel 4.4.3). Hochauflösende ESI-Massenspektren bestätigten des Weiteren die Bildung der Salenkomplexe im Inneren der Doppelstränge (Kapitel 4.4.4).

Das Zusammenspiel der umgebenden DNA-Sequenz mit der Zahl und Position der Salicylaldehydpaare in der Doppelhelix wurde mit speziell gestalteten Oligonukleotiden untersucht. Dabei stellte sich heraus, dass Bildung der Salenkomplexe je nach verwendetem Metall teilweise so dominierend ist, dass sie die Sequenzinformation überschreibt und wahrscheinlich zur Ausbildung von ungewöhnlichen DNA-Sekundärstrukturen führt (Kapitel 4.5).

Des Weiteren wurden Nebenreaktionen untersucht, die aufgrund der kinetisch begünstigten Intrastrang-Salenkomplexbildung zum Entstehen unspezifischer Haarnadelstrukturen führten. Ebenfalls wurde eine Reaktion von Salicylaldehyd-enthaltenden Einzelsträngen mit Ethylendiamin und Metallionen beobachtet (Kapitel 4.5).

Die hohe Stabilität, die der DNA durch die Metall-Salen-Basenpaare verliehen wurde ermöglichte das Stapeln von bis zu zehn aufeinander folgenden Metallionen im Inneren eines DNA-Doppelstranges (Sum.-Fig. 4, Kapitel 4.6).

Die Fähigkeiten von **TT**-Fehlpaarungen Quecksilber(II)ionen zu koordinieren und somit **T**-Hg^{2+}-**T**-Basenpaare zu bilden wurde genutzt, um Oligonukleotide zu synthetisieren, die ein kontrolliertes Mischen von Cu^{2+} und Hg^{2+}-Ionen im Inneren der Duplexe erlaubten. So wurde zum Beispiel die sequentielle Abfolge Cu^{2+}-Hg^{2+}- Cu^{2+}-Hg^{2+}- Cu^{2+}-Hg^{2+}- Cu^{2+}-Hg^{2+}- Cu^{2+}-Hg^{2+} realisiert (Kapitel 4.6).

ESR-spektroskopische Messungen in Zusammenarbeit mit *Dr. O. Schiemann*, Universität Frankfurt, lieferten Daten, die in vollem Einklang mit der Bildung von

Kupfer(II)Salenkomplexen innerhalb der modifizierten DNA-Stränge sind. Zwei direkt benachbarte Kupfer(II)Salenkomplexe gingen dabei eine antiferromagnetische Wechselwirkung miteinander ein (Sum.-Fig. 5, Kapitel 4.4.6).

Im Laufe dieser Arbeit wurden außerdem mehrere andere Ligand-modifizierte Nukleoside hergestellt von denen zwei in DNA Stränge eingebaut wurden. Die Koordination von Metallen an DNA konnte mit diesen Verbindungen (bisher) jedoch nicht beobachtet werden (Sum.-Fig. 6).

In Kollaboration mit der Gruppe von *Prof. U. Simon*, RWTH Aachen, wurde ein mit zwei Azid-Funktionalitäten modifiziertes Glutathion synthetisiert und als Ligand für nanoskopische Goldcluster eingesetzt. Die Cluster wurden anschließend mittel "Click-Chemie" erfolgreich an Alkin-modifizierte DNA-Stränge gekuppelt. Die Anordnung mehrerer dieser Cluster entlang der DNA-Stränge wurde durch *Atomic Force Mikroskopie* (AFM) untersucht (Sum.-Fig. 7, Kapitel 5.3).

3　Introduction

3.1　Bionanotechnology

3.1.1 Structure and function of biopolymers

Most natural materials that convey structure, complex functions and information processing to living organisms consist of biological oligomers and polymers. Whereas proteins are the main materials for functional units (enzymes, channels, carriers) and structural components (cytoskeleton, bone matrix, hair), and polysaccharides play a role in signaling processes (e.g. glycosylation patterns) and energy storage (nourishing carbohydrates), oligonucleotides are mainly responsible for genetic information storage, processing and inheritance.

A biological example for the use of oligonucleotides for functions beyond its role as information carrier is the structural and catalytic function of RNA in the ribosome. There, nature makes use of the specific base pairing features to build up a defined 3-dimensional structure of a combination of nucleic acids and protein components. It has been shown that the RNA-components of the ribosomal subunits even maintain their 3-dimensional structure when the protein components are absent.[1]

Currently, tremendous efforts are undertaken to understand and predict protein structures by experimental approaches and computational methods. Although rather small structural motifs such as sheet and helical structures are well understood, we are still far away from an *ab initio* tertiary structure prediction of complex polypeptides.

On the other hand, the structural features of oligonucleotides are much better understood. After *Erwin Chargaff* and *G. R. Wyatt* estimated the ratios of the DNA components to be **A** : **T** = **G** : **C** = 1 : 1 and the fibrous linear arrangement of the nucleotides was shown by *Maurice Wilkins* and *Rosalind Franklin* through X-ray measurements, *James D. Watson* and *Francis Crick* proposed 1953 in their seminal work in *Nature* a structural model for the double helical DNA.[1, 2]

Detailed discussions of the structural features of oligonucleotide double strands of different base composition and under different conditions can be found elsewhere.[3] Figure 1 displays the most important structures for double helical DNA.

A-DNA   B-DNA   Z-DNA
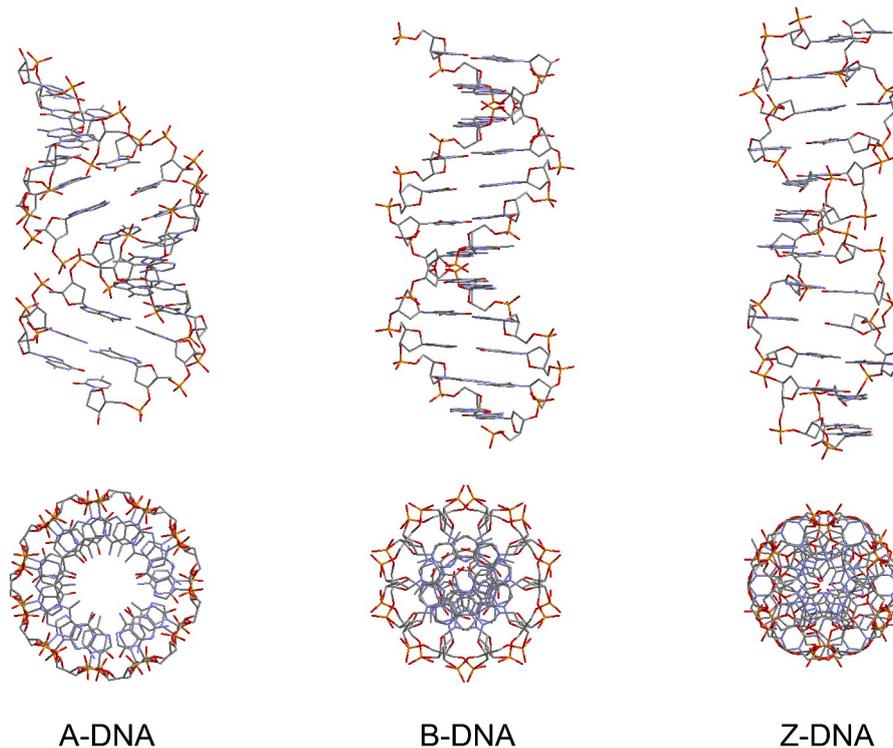
Figure 1: The three most important DNA secondary structure families in side view (top) and along the helix axis (bottom). A-DNA features a right handed double helix with the strongly tilted base pairs aligned around a central hollow cavity. It is found for DNA at high humidity and the most common RNA duplex structure. The structure of B-DNA is discussed in the text. Z-DNA features a left handed helix with pair wise clustered base pairs and is mainly found in CpG alternating sequences. The less common C-, D- and E-DNA families, triple helical structures and quadruplexes are not presented here.

Here, only a brief overview is given of those structural features of B-DNA which are of interest for the understanding of the results obtained in this thesis (Figure 1 middle). B-DNA is believed to be the most common DNA secondary structure in natural genetic material and it was the DNA structure that was first elucidated.[2] It features a right handed double helix with a base distance of 0.34 nm and a helical twist per base of 36 °. The helix makes a complete turn every 3.4 nm, thus there are about 10 base pairs per turn. The base-pair centers are located on the helix axis. Base stacking in B-DNA is limited to intrastrand interactions without interstrand overlap interactions. The duplex stability of DNA in water was found to be a result of the π stacking interactions, the hydrogen bonding between the complementary nucleobases and the differences of hydration energies of double strands and the corresponding single strands.[4] On the outside of B-DNA, the spaces between the intertwined strands form two helical grooves of different width (minor groove and major groove).

The structural features of the canonical *Watson-Crick* **AT**-base pair found in B-DNA are summarized in Figure 2.
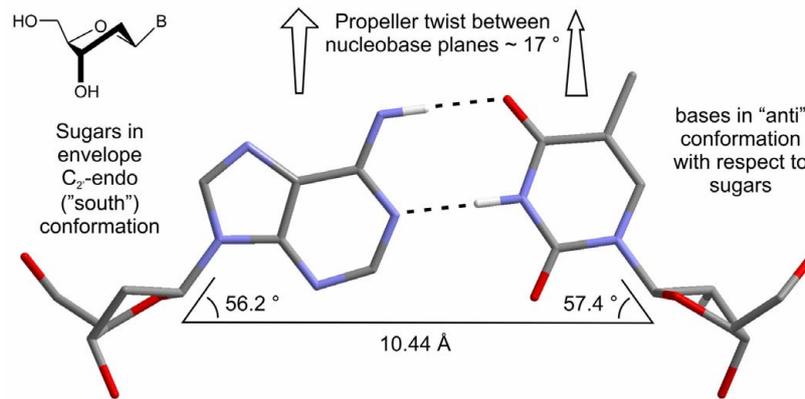
Figure 2: Parameters describing the canonical *Watson-Crick* AT base pair.

The 2'-deoxyribose sugars adopt an envelope $C_{2'}$-endo ("south") conformation in B-DNA. The bases are oriented in the anti-conformation with the hydrogen bond donor and acceptor atoms pointing away from the sugar moieties. The distance between the C1' atoms in the **AT** base pair is 10.44 Å (**GC**: 10.72 Å) and the angle between the glycosidic bonds and the line connecting the C1' atoms is 56.2 ° for adenosine and 57.4 ° for thymidine (54.4 ° for guanosine, 55.7 ° for cytidine). The angle between the planes defined by the flat nucleobases is known as "propeller twist" θ_P and is 17 ° for the **AT** base pair (11 ° for **GC**).

3.1.2 Nature as paragon for nanotechnology

Two approaches to construct defined (functional) nanoscale objects were foreseen and accelerated by the physicist Richard P. Feynman in his famous talk at the annual meeting of the American Physical Society at Caltech (1959) when he called on scientists to make use of the "plenty of room at the bottom".[5] The classical "top-down" approach, which relies on a progressive miniaturization of man-made objects by the development of smaller and smaller tools, has been rivalled by the successful developments of the "bottom-up" approach, which relies on the chemist's skill to design and arrange functional building blocks in nanoscale environments. Since the advent of bottom-up nanotechnology, numerous examples of simple functional elements, molecular machines and self organized aggregates have been presented in the literature[6,7] and some developments have already made it to the commercial market.[8] Nanotechnology is widely regarded as the next major step after information technology in the technological development of the modern world. The vast amount

of money that has been invested into this field is an indicator of the hope and expectation that surrounds nanotechnology.[9] From a critical point of view, however, it should be mentioned that many products that today are decorated with the buzzword "nano" were known long before as "pigments" and "powders".

In bottom-up nanotechnological research, biological structures often play the role as paragon or even are used as building material for artificial model systems. Examples of biological "nano machines" that inspired many scientists are the unidirectional, cyclic operating ATPase, the controlled movement of the bacterial flagella, multienzyme complexes which sequentially modify a bound substrate in a multistep transformation, channels for ions or small molecules, ribosomes and oligonucleotide polymerases and many more.[1]

Learning from nature, man-made nanoscale devices can be described by the following criteria:

1. Composition:
    a. Purely artificial (rotaxanes, catenanes, …)
    b. Bio-Artificial hybrids (conjugates of proteins or amino acids or DNA or nucleosides with artificial components…)
    c. Derivatives and unnatural arrangement of natural components (cyclodextrins, peptides from β-amino acids…)
    d. Mainly unmodified natural components (3D-structures built from unmodified DNA strands, functional fusion proteins…)

2. Function:
    a. Static structural features (self assembly, scaffold function…)
    b. Molecular motion (rotation, translation, mechanical switching…)
    c. Substrate processing (catalysis, carrier function…)
    d. Quantum mechanical behavior (electronic features, magnetism, spectroscopic features…)
    e. Information storage and processing
    f. Interaction with other functional units
    g. Self-replication

The motivation to generate nanoscale devices derived from biological systems is based on the sophistication of natural materials that have been optimized over millions of years as a result of evolution. Furthermore, the great deal of knowledge that has been accumulated over the last 50 years about the structure and function of the biopolymers enables us to exploit this knowledge for new technological developments and applications.

Examples of artificial oligonucleotide-based nanoscale objects are presented in the following Chapters, with a focus on metal incorporation into DNA in Chapter 3.3.

3.1.3 Examples of oligonucleotide-based nanoscale objects

With regard to the functional classifications of nanoscale objects or devices introduced in the previous section, several examples of DNA-based systems that illuminate different aspects of bionanotechnology will be presented in this section.

Fascinating examples of structurally static architectures have been built up by DNA and RNA strands. Different approaches make use of either unmodified oligonucleotides or strands carrying junction nodes or other functionalities at their ends. Some examples are presented in Figure 3.

This figure is only available in the printed version of this thesis due to copyright reasons

Figure 3: Examples of static nanoscale constructs that were generated from oligonucleotides. a) Seeman's DNA cube, b) von Kiedrowski's "nano cyclobutadiene" (the balls present the covalent junctions of the strands) and c) the repetitive unit of Jaegers "Jigsaw Puzzles" composed of RNA strands. Each unit is fitted with four overhanging "arms" which allow interaction with the neighboring puzzle pieces. [a: reprinted by permission from reference 10, Wiley-VCH, © 1998; b: reprinted by permission from reference 11, Wiley-VCH, © 1999; c: reprinted by permission from reference 12, Science AAAS, © 2004]

Seeman et al. were the pioneers in this field when they generated defined 3-dimensional structures from a set of complementary deoxyoligonucleotides such as

the cube in Figure 3a.[10] The sequences were chosen in such a way that every strand unambiguously had its unique position resulting in predictable topological properties of the molecular architecture. The group of *von Kiedrowski* synthesized tripodal DNA building blocks by connecting three oligonucleotides at one of their ends by covalent bonds and used several of these tripods with matching sequences to generate nanoscale structures such as "nano cyclobutadiene", so called by the author because of its resemblance with the corresponding hydrocarbon (Figure 3b).[11] An example of an RNA-based construct was presented by *Jaeger et al.*[12] They prepared puzzle units called "tectosquares" which were programmed with respect to their geometry, topology, directionality, and addressability to self-assemble into a variety of complex nanoscopic designs with predefined periodic and aperiodic patterns (Figure 3c). Especially interesting is that this construct uses intermolecular RNA loop-loop interactions, called "kissing loops", which were discovered in ribosomal and viral RNA.[13]

The sequence-specific programming of large tertiary structures from a mix of hundreds of well chosen oligonucleotides recently culminated in the generation of the amazing surface patterns shown in Figure 4.[14]
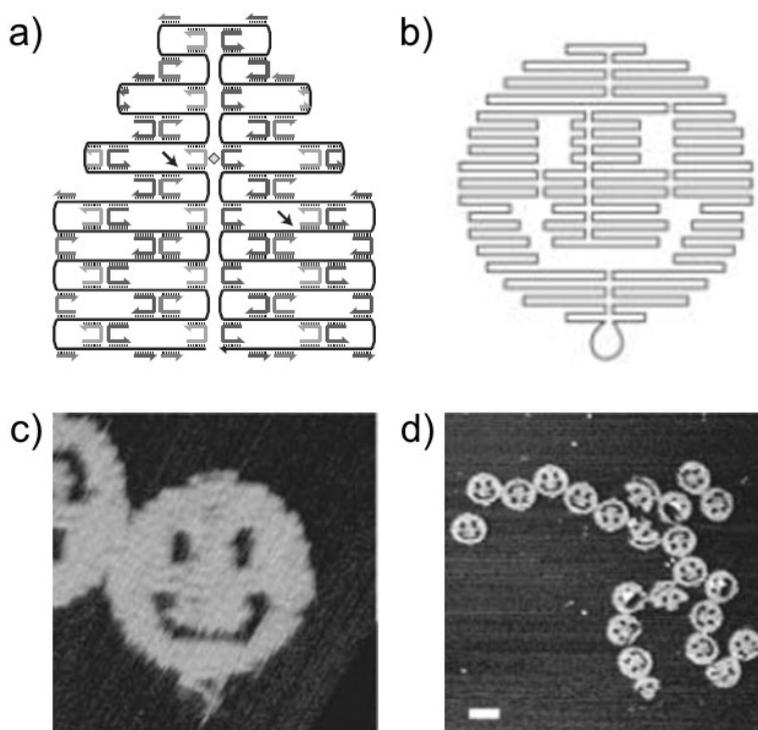
Figure 4: "DNA origami" by *Paul Rothemund*. a) Interaction of the long scaffold strand (e.g. genomic DNA from the virus *M13mp18*) with numerous specifically designed short "staple" strands, b) schematic design of a "nano smiley", c) and d) AFM pictures of the resulting constructs on a mica surface (white scale bar in d = 100 nm). [Reprinted by permission from reference 14, Macmillan Publishers Ltd, © 2006]

Rothemund used naturally occurring long single stranded DNA strands (e.g. the 7,249 nucleotide long genomic DNA from the virus *M13mp18* as a scaffold, which self-organized into predefined shapes by the addition of numerous specifically designed short single stranded "staple" sequences. The concept and the resulting AFM images are shown in Figure 4.

Several other groups have reported the use of DNA sequences for the generation of e.g. surface-bound lattices or soluble constructs with the ability to coordinate to proteins, organic or inorganic nanoparticles.[15]

As an example, efficient conjugation of carbon nanotubes to DNA and PNA has been achieved, and the ability of these covalently bonded adducts to hybridize to nucleic acid complements has been verified.[16, 17]

Several molecular machines that exhibit controlled motion in nanoscale dimensions were constructed from oligonucleotides.[18]. One early example of the manifestation of a mechanical movement was published by *Seeman* and coworkers.[19]   They connected two double crossover constructs via a short double stranded sequence, which could be switched from B- to Z-form DNA and back by addition or removal of $[Co(NH_3)_6]^{3+}$ (Figure 5a). Two different fluorescent dyes attached near the molecular hinge enabled a FRET-based read-out of the switching event. The same group presented another example whose mechanical function relies on an entirely different effect.[20] Here, an even more complicated construct contained several crossover junctions, which can adopt two different topological states (PX and JX_2) dependent on the presence of specific "set" strands which act as fuels (Figure 5b). Removal of the temporarily incorporated set strands by biotinylated antisense oligonucleotides and addition of new set strands caused switching between the two states. This event was monitored by AFM spectroscopy, which revealed a reorganization of the bulky DNA attachments (Figure 5c). Even a "walking robot" which sequentially sets one "foot" in front of the other has been realized by this approach.[21, 22]
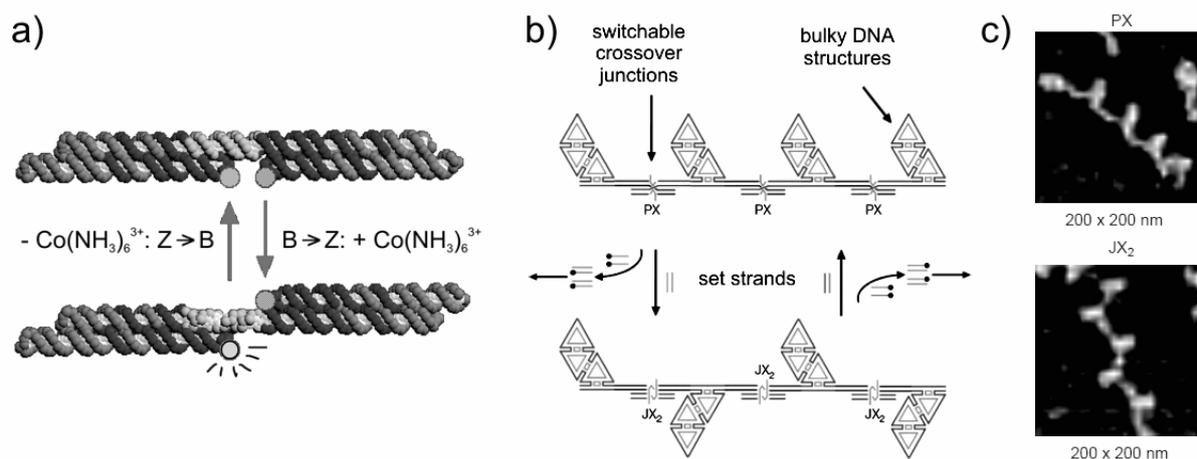
Figure 5: Examples for DNA-based molecular machines. a) The B → Z transition of a DNA double crossover construct is induced by addition of a chemical agent and leads to a mechanical response, which is measurable by a FRET experiment, b) a complex DNA structure containing switchable crossover junctions (PX and JX$_2$)with different topologies which interconvert upon addition or removal of specific set sequences, c) the switching results in a topological reorganization of the constructs which can be monitored by AFM. [a: reprinted by permission from reference 19, Macmillan Publishers Ltd, © 1999; b and c: reprinted by permission from reference 20, Macmillan Publishers Ltd, © 2002]

Regarding DNA-based catalytically active systems, progress has been made in recent years. Although the topic of natural and artificial ribozymes[23, 24, 25] and deoxyribozymes[26,27,28] will not be discussed here, some examples will be given for artificial DNA-hybrid compounds that have shown catalytic activity.

Several examples of oligonucleotide-bound metal complexes such as copper-phenanthroline,[29] copper-terpyridine,[30] iron-EDTA[31] and dysprosium(III)-texaphyrin[32] that can cleave their counterstrand have been reported.

Krämer et al. used catalytic metal complexes which were bound to the ends of oligonucleotides or PNA strands and accelerated reactions such as ester hydrolysis of substrates bound to a template strand.[33,34,35]

An elegant supramolecular approach of DNA-based catalysis in water was presented by *Feringa et al.*[36, 37] The concept is depicted in Figure 6.
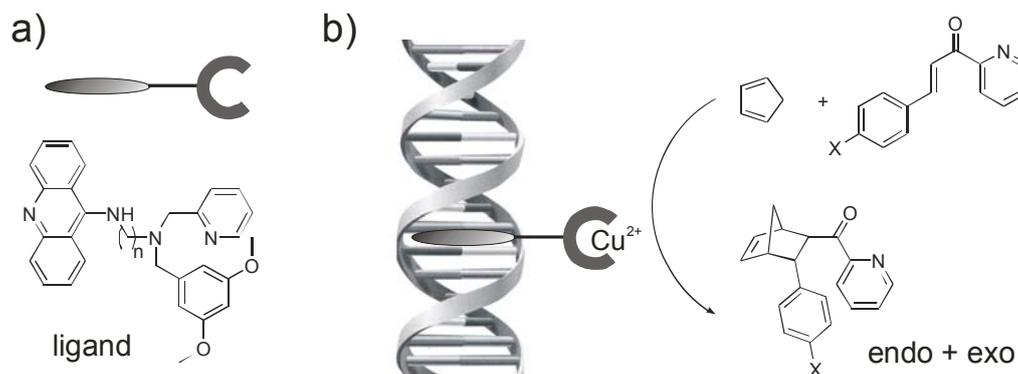
Figure 6: Enantioselective catalysis of Diels Alder reactions with a supramolecular hybrid system composed of DNA as the carrier of asymmetry and an intercalating Cu^{2+} complex.

This system was used successfully in enantioselective Diels-Alder reactions of cyclopentadiene with acceptor-substituted dienophiles. Here, the catalytic center (the Cu^{2+} complex) and the carrier of the chiral information (unmodified DNA) are two separate molecules, which interact by means of a stacking interaction between the DNA base pairs and the acridine unit, which is covalently bound to the achiral metal complex. The transfer of chirality from the DNA onto the metal catalyst proofed to be efficient enough to allow certain reactions to proceed with enantiomeric excesses (ee) of up to 99 %.

Non-catalytic reactions of DNA-bound substrates that only react together when they are brought in close proximity by hybridization of the DNA strands with each other (or a substrate) have been termed "DNA programmed reactions" and have been investigated mainly by *Liu et al.*[38, 39, 40, 41] They have explored a variety of organic reactions in this context and applied the concepts of combinatorial chemistry and cascade reactions to the field of oligonucleotide templated synthesis.

Another function that has been studied intensively in recent years is electric conductance through DNA.[42] The two principal mechanisms of charge transport trough DNA are (a) transfer of positive charges ("holes") and (b) excess electron transfer. Both processes have biological importance. Hole transfer is directly involved in DNA-damage formation.[43, 44, 45]

Excess electron transfer through DNA was found to be a natural occurring process in the repair of photo damages such as the **TT**-dimers by the corresponding repair enzymes ("photolyases").[46, 47, 48, 49, 50]

These findings were of great interest for testing DNA as a molecular wire for nanotechnological applications. It turned out, however, that the charge conducting properties of unmodified DNA strands are of too low fidelity and reliability to use native DNA in molecular electronic circuits. *Porath et al.* connected DNA strands by nano electrodes and observed large-bandgap semiconducting behavior.[51]

Two new strategies were thus envisioned to make use of DNA for the generation of molecular wires: (1) doping or even complete substitution of the *interior* of the double helix with materials such as metals or redoxactive organic moieties and (2) using DNA as a programmable scaffold for the deposition of conductive materials such as reduced metal layers or metal clusters with their own unique electronic properties on the *outside* of the DNA strands.

The first approach was one of the motivations behind the metal-base pair concept, which is the main topic of this work.

The second approach was elaborated by *Braun* and *Eichen*[52, 53] with their method of *in situ* metal reduction on DNA strands that were uniformly labeled with reducing molecules and later refined by *Burley et al.* by using a modular "click chemistry"[54] approach to attach the reducing functionalities to the DNA strands.[55] This topic is addressed in Chapters 5 of this thesis.

Of current interest are constructs in which **every base** (or base pair) carries a modification. The basis for these approaches came from chemically modified antisense oligonucleotides. The difficulty of this topic is to maintain duplex stability and specific hybridization whilst introducing major non-natural modifications into the whole system. Examples for the arrangement of functional elements along the outside of an entire DNA strand are *Seeman's* covalently "stitched nylon thread" along a DNA strand[56], multiple stacked pyrene molecules on the outside of the double helix by *Wengel*[57] and the works on the modular polyfunctionalization of long DNA strands via "click chemistry" by *Carell et al.*[58]

DNA-based nano constructs which make use of metal complexation as a tool for connectivity of different subunits can be divided into two subgroups. Examples of the first group utilize ligands which are bound to the (end-standing) phosphate groups of DNA single strands to connect the DNA strands in an intermolecular fashion with other oligonucleotides or other functional components.[59] Examples for this approach were given e.g. by *Han et al.* who assembled complex structures from DNA single strands with attached terpyridine units by formation of stable bis(terpyridine)iron(II) complexes between the oligonucleotides.[60] Star-shaped constructs with several oligonucleotide "rays" protruding from a central Ni(II)-cyclam or Ru(II)-tris(bipyridyl) complex which might give 3-dimensional DNA networks after hybridization of complementary strands were reported by *Steward* and *McLaughlin*.[61, 62]

A slightly different strategy uses the sequence-specific formation of DNA double strands as a template effect for the formation of metal complexes from ligands that are bound to the phosphates at the 3' or 5' ends of single stranded oligo-nucleotides.[59] The works of *Sheppard* and *Gothelf* will be discussed here in detail as they made use of the salen complex, which is central to this thesis (Figure 7).

a)

b)
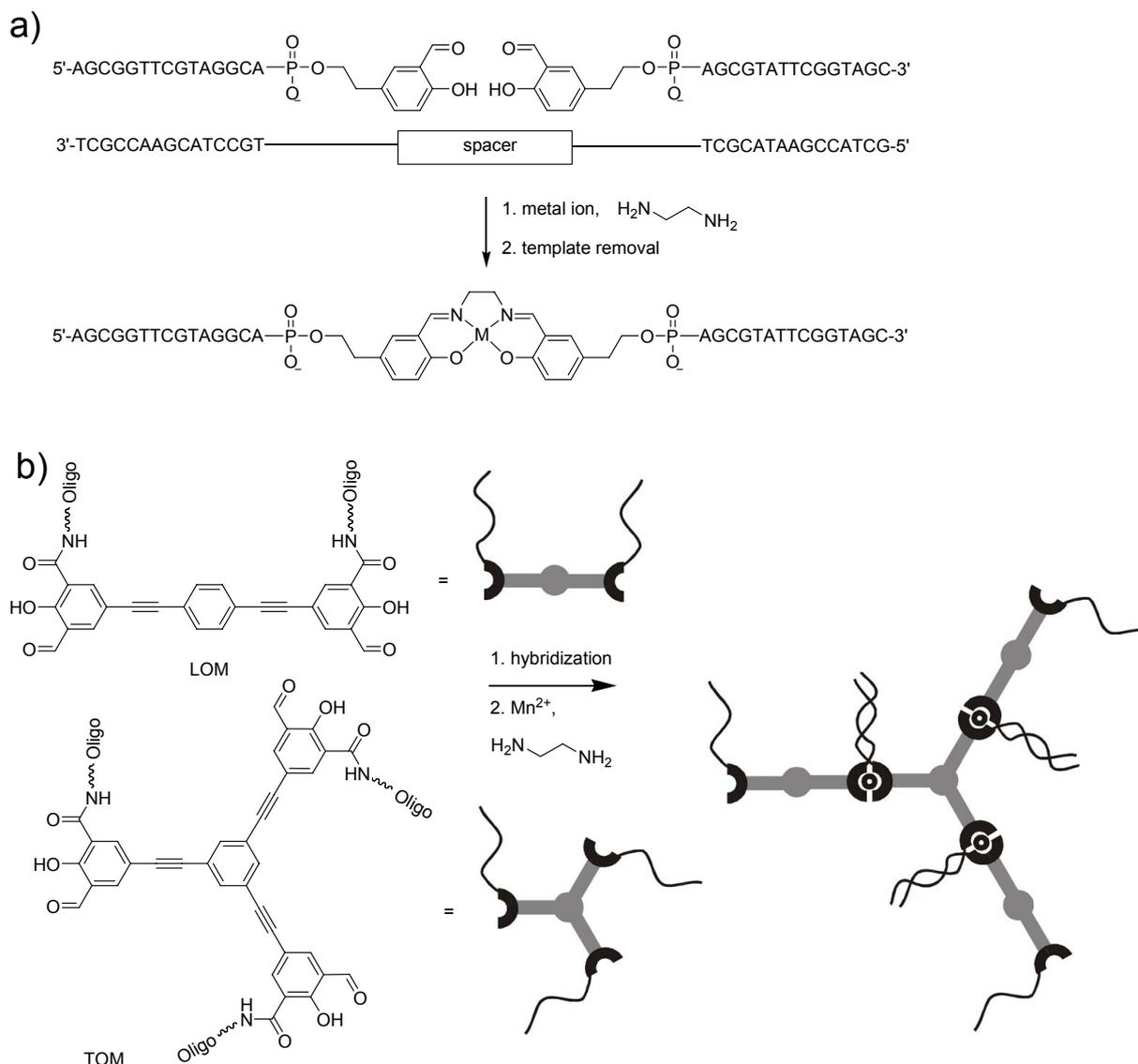
Figure 7: Two approaches for DNA-template-directed metal-salen complex formation. a) The formation of *side-on* salen complexes on an oligonucleotide template, b) the synthesis of DNA programmed architectures that are ultimately linked together by covalent metal-salen complexes.

In the early report from *Czlapinski* and *Sheppard*, the DNA-programmed synthesis of a metal salen complex *side-on* a DNA template in the presence of ethylenediamine and Mn(II) or Ni(II) was shown (Figure 7a).[63, 64] In a later publication they showed that a *side-on* nickel salen complex can be used for the site-specific cleavage of the template strand.[65]

In the strategy by *Gothelf et al.*, two or three salicylic aldehyde groups are contained within the same compound enabling the assembly and covalent coupling of multiple modules.[66, 67, 68, 69, 70] The linear oligonucleotide-functionalized module (LOM) and the tripodal oligonucleotide-functionalized module (TOM), both containing salicylic aldehydes, were synthesized (Figure 7b). Oligonucleotides attached at each

terminus, were encoded to link up other building blocks containing complementary sequences.

The salicylic aldehyde groups of two modules were brought in close proximity when their complementary DNA sequences were annealed together and resulted in manganese–salen complex formation between two salicylic aldehyde groups in the presence of ethylenediamine and Mn(II). Depending on the encoding of LOMs and TOMs with different DNA sequences, assembly and covalent coupling of the modules into a variety of predetermined nanostructures was shown (Figure 7b).

The second type of constructs that uses metal complexation for producing connectivity between different parts is known as metal-base pairing where coordinative forces between metal ions and ligand-like nucleosides substitute hydrogen bonding between strand and counterstrand of a DNA double helix. As this concept is the topic of this thesis it will be discussed in more detail in Chapter 3.3 of the introduction and in Chapter 4 of the discussion part.

3.2   *Hypermodification of the DNA backbone and bases*

A vast number of chemically modified nucleotides[71, 72, 73] and single- or double-stranded oligonucleotides functionalized with lipophilic groups or peptides[74, 75] have been intensively studied in an attempt to optimize the biological activity of antisense oligonucleotides[76] and for the diagnosis of single nucleotide polymorphisms (SNPs) in genes.[77] Out of this contemporary research, many chemical developments and nucleotide modifications have emerged that will be of great importance for the progress in nucleic acid nanotechnology.

A variety of modified backbones such as pyranosyl nucleic acids (Chapter 4.2.5), oligonucleotide phosphorthioates,[78] locked nucleic acids (LNA),[79, 80] propylene glycol nucleic acids (GNA)[81] and peptidic nucleic acids (PNA)[82] were described in recent years (Figure 8).
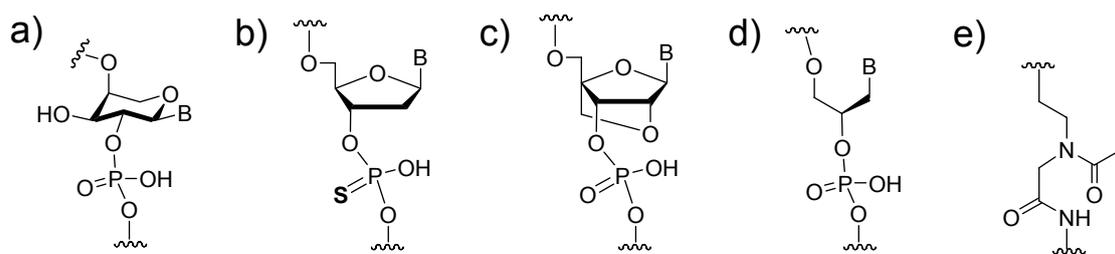
Figure 8: Examples for backbone modifications in oligonucleotides. a) an example of pyranosyl nucleic acids, b) phosphorthioate backbone, c) locked nucleic acids (LNA), d) propylene glycol nucleic acids (GNA) and e) peptidic nucleic acids (PNA). B = base.

Also many artificial nucleobases have been synthesized to investigate the factors that are responsible for DNA duplex stability and base pairing specificity in the hybridization process,[83, 84] in transcription by polymerases[85, 86] and interaction with DNA binding enzymes.[87, 88]

Kool et al. incorporated steric base surrogates in which fluorine atoms substitute the carbonyl and amino groups of the natural nucleobases into oligonucleotides to study the role of the hydrogen bond donors and acceptors on the hybridization and polymerization of the oligonucleotides.[89, 90]

Extended, benzannelated purine and pyrimidine nucleobases were used successfully to prepare hypermodified DNA duplexes of much higher diameter than the natural structure.[91]

3.3 Metal coordination inside/to nucleic acids

3.3.1 Metal coordination to unmodified DNA

Interaction of metal salts with unmodified DNA was examined even long before its secondary structure was elucidated.[92] Complexes of metal ions with DNA were later named M-DNA. The research field of M-DNA can be split into (1) reports on the formation of non-canonical base pairs from the natural nucleobases under participation of metal ions; (2) the substitution of hydrogen atoms that are part of the *Watson-Crick* base pairing by metal ions;[93] (3) the reversible binding of metals to parts of the DNA which are not involved in base pairing[94] and (4) the persistent distortion or crosslinking of DNA duplexes by metals which form kinetically and/or thermodynamically inert complexes (mainly by platinum).[95] Only examples of the first two classes will be discussed here. Also not mentioned here are any reports on the

intercalation of metal complexes into the base stack but references to intercalating salen complexes can be found in Chapter 3.4.2.

Katz found in 1952 a substantial decrease of the viscosity of natural DNA upon addition of $HgCl_2$, which he attributed to a decrease in the overall size of the molecule.[96] First he believed that mercury ions bind the phosphate groups in an intrastrand fashion. But after *Thomas* proved binding of Hg^{2+} to the nucleobases by UV spectroscopy,[97] *Katz* proposed as early as 1963 the formation of Hg^{2+}-thymine (1:2) complexes in DNA double strands by a slippage process that brings thymine bases in both strands together.[98] His structural suggestion for the **T**-Hg^{2+}-**T** base pair **1** can be found as an illustration in his original paper and was later shown to be a correct assumption (Figure 9).

1
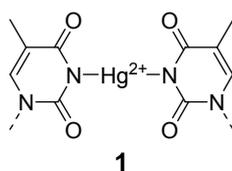
Figure 9: The structure of the T-Hg^{2+}-T base pair suggested by *Katz* in 1963.

A crystal structure of 1-methylthymine with Hg^{2+} (2:1) further supported this idea[99] and binding studies further showed that the strength of the Hg^{2+} interaction increased with increasing AT content.[100] *Gruenwedel* comprehensively studied the interaction of mercury(II) ions with DNA strands by UV and CD spectroscopy and found major secondary structure transitions upon Hg^{2+} binding.[101]

This concept was picked up later by *Buncel et al.* and *Marzilli et al.* who verified the formation of **T**-Hg^{2+}-**T** inter- and intrastrand crosslinks in double strands containing one or more **TT** mismatches by UV and CD spectroscopic titrations and NMR spectroscopy.[102, 103] Ten years later, *Ono et al.* essentially repeated this approach and additionally provided melting curve experiments and ESI mass spectra of mercury containing duplexes.[104, 105]

Studies about the substitution of the imino protons that are bound to the N3 position of thymine and the N1 position of guanine in native base pairs by Zn^{2+}, Co^{2+} and Ni^{2+} ions at high pH were conducted by Lee *et al.* (Figure 10).[106, 107]

Zn-AT   Zn-GC
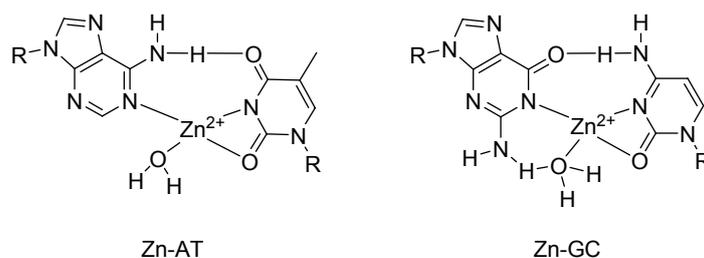
Figure 10: Suggested structure of the Zn^{2+}-coordinated **AT** and **GC** base pairs in M-DNA.

The electronic properties of M-DNA allowed an energy transfer between different dyes bound to remote ends of the metallized duplex and the authors suggested the use of M-DNA as a molecular wire.[108] The electron conductance of a 15 μm long M-DNA strand was measured between two gold electrodes and a metal-like conductance was found (in contrast to native B-DNA which has been suggested to display semiconducting properties).[109]

3.3.2 The metal-base pair concept and examples

The intercalation of metal complexes into DNA duplexes[110] and the attachment of metal complexes to the oligonucleotide ends[59] or outer sphere of the DNA by nucleoside attached linkers[111, 112] is connected to a major alteration of DNA's double helical structure and spatial dimensions.

In contrast, there have been several efforts to incorporate metal ligands with geometries similar to the natural base-pairs into DNA double strands, recently.

The metal-base pair concept is defined by the arrangement of a metal coordinating ligand on facing positions of a DNA duplex and the formation of a metal complex between these two ligands in the middle of the double helix, thereby substituting the natural hydrogen bonding interaction in canonical *Watson-Crick* base pairs by coordinative forces.

The first example of an artificial ligand potentially suitable for the coordination of metal ions inside the DNA double helix was reported by *Tanaka* and *Shionoya* in 1999.[113] They synthesized the *o*-phenylenediamine-palladium complex **2** and later its derivatives **3**[114], **4**[115] and **5**[116] (Figure 11) in solution but did not report the incorporation of these nucleosides into oligonucleotides.

2: X = Y = NH$_2$, M = Pd^{2+}
3: X = O$^-$, Y = NH$_2$, M = Pd^{2+}
4: X = Y = O$^-$, M = Cu^{2+}
5: X = Y = O$^-$, M = B^{3+}
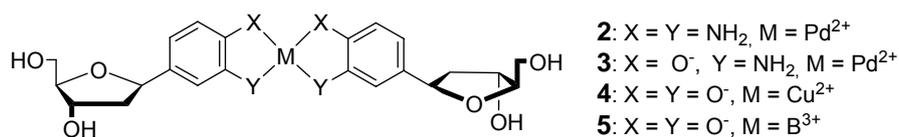
Figure 11: The monomeric metal-base pairs **2**, **3**, **4** and **5** prepared by Tanaka and Shionoya.

In fact the first successful formation of a metal-base pair inside a DNA duplex was reported in 2000 by *Meggers, Romesberg* and *Schultz*.[117] A combination of a pyridine-2,6-dicarboxylate ("Dipic") as a planar tridentate ligand and a pyridine nucleoside ("Py") were incorporated opposite each other in two complementary oligonucleotide strands. The addition of Cu^{2+} resulted in formation of the copper-base pair Dipic-Py (**6**, Figure 12) and thereby significant stabilization of the DNA duplex. Other metal salts such as CeCl$_3$, Mn(NO$_3$)$_2$, Fe(SO$_4$)$_2$, Co(NO$_3$)$_2$, Ni(NO$_3$)$_2$, Zn(NO$_3$)$_2$, Pd(NO$_3$)$_2$, and K$_2$PtCl$_4$ did not result in any duplex stabilization.

6: X = O
7: X = NH
8: X = NCH$_3$
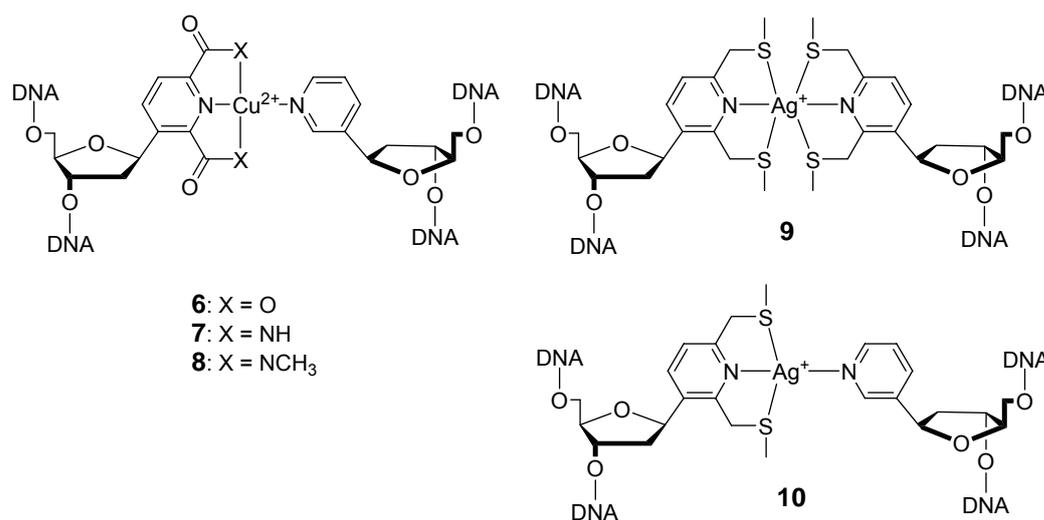
Figure 12: The metal-base pairs Dipic-Py **6**, Dipam-Py **7**, MeDipam-Py **8**, SPy-SPy **9**, and Spy-Py **10** from the Schultz group.

The tridentate character of the pyridine-2,6-dicarboxylate moiety is primarily responsible for the tight binding to Cu^{2+} (whereas Zn^{2+}, Ni^{2+}, Pd^{2+} and Pt^{2+} where only loosely bound) and subsequently allows the coordination of the oppositely arranged pyridine nucleobase to the copper atom's fourth coordination site. They suggested that the [3+1] arrangement of the donor atoms in the ligands might be superior over a [2+2] arrangement but subsequent studies on various ligands with a [2+2] distribution of donor atoms did not support this hypothesis. Another reason for their choice of an unsymmetrical metal-base pair was the vision to create a new, artificial base pairing system that can be replicated by DNA polymerases and is orthogonal to the *Watson-*

Crick base pairs. This plan, however, could not be fulfilled to the present day by any group.

The derivative "Dipam-Py" **7** leads to an even higher duplex stabilization than its predecessor (in contrast the combination "MeDipam-Py" **8** does not form a stable metal-base pair at all).[118]

The combinations "SPy-SPy" **9** (Figure 12) and "SPy-Py" **10** which can selectively bind Ag$^+$ ions were subsequently incorporated into oligonucleotides and characterized by the same group.[119] They also managed to incorporate two metal-base pairs **6** into the palindromic *Dickerson-Drew*[120] dodecamer sequence and obtained a crystal structure, which was found to exist in a Z-DNA conformation.[121] The latter fact was attributed to be a special feature of the prepared sequence. Solution studies on other sequences containing two metal-base pairs **6** revealed a preference for a B-DNA conformation.[121]

Several other metal base pairs followed these initial reports (Figure 13).
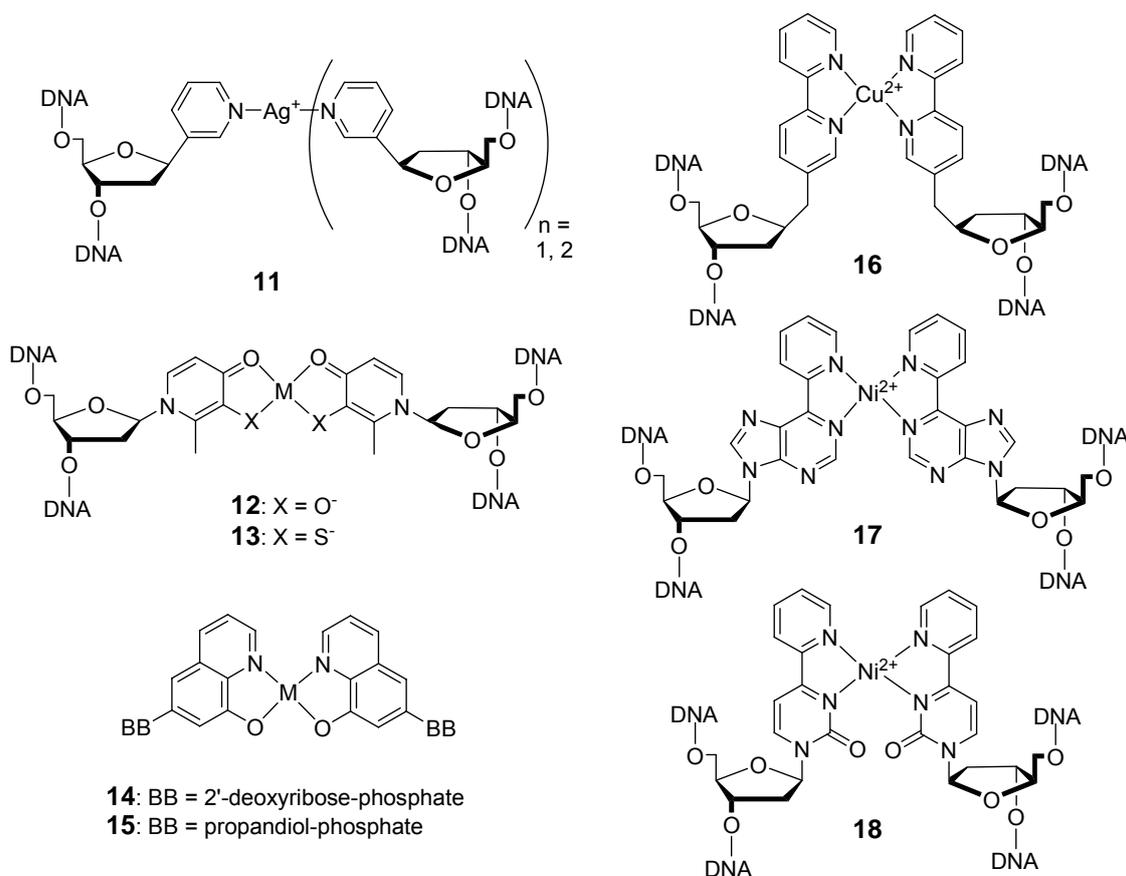
Figure 13: Further examples of currently known metal-base pairs.

Shionoya et al. used the very simple pyridine nucleoside "Py" (**11**) for the formation of double and triple helices by coordinating central Ag$^+$ ions[122] (*Schultz et al.*, however,

were not able to reproduce this Py-Ag$^+$-Py base pairing in an alternative sequence context[119]). *Shionoya* and *Tanaka* also prepared the hydroxypyridone ("HP") base pair **12** that was successfully utilized for the complexation of Cu^{2+} ions inside DNA double strands.[123] The synthesis of its 3-sulfur substituted analogue **13** is currently being pursued by this group to allow the coordination of soft metals such as gold or palladium.[124]   Five consecutive copper-hydroxypyridone base pairs **12** were successfully incorporated in a double strand and characterized by UV and CD titration experiments, EPR spectroscopy and ESI mass spectrometry.[125]   The electron spins on adjacent Cu^{2+} centers were found to be aligned parallel and coupled in a ferromagnetic manner with a spin state of 5/2 for the total system. The distance between the copper centers was roughly estimated to be 3.7 ± 0.1 Å (in contrast to 3.3 – 3.4 Å in the canonical B-type DNA).

The theoretical investigations of this system by *Di Felice et al.* showed that the total magnetization of the ferromagnetic wire depends linearly on the number of planes in the stack.[126] The combination of interplane spin coupling and intraplane metal-hydroxypyridone coupling was regarded as a very important feature for electronic and magnetic applications because the preparation of a high spin state was – in accordance with the EPR measurements by *Shionoya* – supported by the calculations. Although the nature of the σ- and π-frontier orbitals, with nodes between the stacked planes, does not support bandlike electron conduction, it was anticipated that the efficient metal-ligand orbital hybridization may suggest alternative mechanisms, for example, driven by a redox activity of the inner cations. Furthermore, they speculated that the same features might be shown by any kind of stack consisting of similar copper(II)-base pairs with a comparable square planar coordination environment.

Using a 8-hydroxyquinoline ("HQ") ligand, *Meggers et al.* not only prepared the 2'-deoxyribosyl-based metal-base pair "dHQ-dHQ" **14** but also its linear-backbone analogue "pHQ-pHQ" **15** basing on the propylene glycol backbone introduced in Chapter 3.2.[81, 127] *Tor et al.* coupled a 2,2'-bipyridine ("Bipy") ligand via a methylene spacer to 2'-deoxyribose and obtained metal base pair **16**, which displayed a slight duplex stabilization after addition of Cu^{2+}.[128] The geometry of this metal base pair, however, does not suggest a smooth incorporation into the double helical structure without major disturbances.

It is worth mentioning that a similar nucleoside carrying a bipyridyl unit directly connected to the sugar C1' atom (i.e. **16** without the methylene group) was investigated by *Leumann et al.* for its effect on duplex stabilization in the absence and presence of transition metal ions. Whereas the duplex stabilization by two opposing bipyridine bases of this kind (in absence of any metal ions) could be undoubtedly shown,[129] the influence of transition metal ions on this system remained unclear.[130] The two metal base pairs "PyA-PyA" **17** and "PyC-PyC" **18**, derivatives of the natural nucleobases adenine and cytidine, were prepared by *Switzer et al.*[131, 132] Both metal-base pairs **17** and **18** showed a strong preference for the binding of Ni^{2+} over other transition metal ions such as Co^{2+}, Cu^{2+}, Zn^{2+}, Fe^{2+} and Mn^{2+}. Finally, the metal base pair concept has recently also been shown to work for PNA duplexes (not shown).[133]

Three coordination geometries are in principle possible for the arrangement of two bidentate ligand nucleosides around a central metal ion: square planar, D_2^d and tetrahedral. For maintaining the B-DNA like structure with aromatic stacking of the nucleobases in the double helix, it was envisioned that the optimal coordination geometry of a metal-base pair should be square planar or at most D_2^d.[132]
When metal ions are incorporated that favor additional axial ligands in their coordination sphere, their needs should be satisfied with loosely bound solvent molecules or bridging donor atoms from the neighboring bases. Metals that require a tight binding of apical ligands perpendicular to the base pair plane are anticipated to cause major distortions of the double helical structure (if they are coordinated at all).

For the characterization of the successful formation of metal-base pairs inside the DNA double helix, several techniques have been applied which are summarized in Table 1. These techniques can be divided into methods which yield a rather indirect answer on the impact of metal coordination on the DNA duplex structure (e.g. melting point studies and CD spectroscopy) and methods which yield more quantitative information (metal titrations, high resolution mass spectrometry).

Method and information outcome	Restrictions and implications	Reference or Chapter
DNA Melting point experiments: Thermal stability of the DNA duplex in presence or absence of metal ions, kinetics of assembly	- Thermal stress for the system (heating to 90 °C) - dependent on sequence and additives - no structural information (metal position) - difficult for coordination >1 metals/duplex	4.4.2
UV spectroscopy: Visualization of electronic transitions assignable to the metal-complex	- relatively low information content	4.4.3.1
CD spectroscopy: DNA secondary structure and chirality of metal complex	- difficult interpretation for extensively modified DNA such as stacked metal arrays	4.4.3.2
EPR spectroscopy: Coordination environment of bound metal, distance and spin coupling of multiple metal centers	- paramagnetic metals required - relatively large amounts of DNA required - prone to disturbances by minor impurities - time consuming	4.4.6
Spectroscopic titrations: Stoichiometry of metals : duplex	- high complexation constant required - exact determination of DNA concentration crucial	4.6.2, 4.6.3
Mass spectrometry: High resolution stoichiometry of metals : duplex, oxidation state of metal	- difficult for non-covalently crosslinked duplexes - absence of alkali metal cations required - time consuming screening of conditions and suitable mass spectrometric method	4.4.4
NMR spectroscopy: Coordination environment of metal, molecular structure of oligonucleotide duplex	- no paramagnetic metals tolerated - large amounts of DNA required - time consuming measurement and interpretation	[103]
X-ray crystallography: molecular structure of oligonucleotide duplex or subunits	- large amounts of DNA required - time consuming screening process - structure in crystal might deviate from that in solution	4.2.2, [121]

Table 1: Overview of the characterization techniques that have been used for the examination of the known metal-base pairs.

Table 2 gives an overview about which of the oligonucleotide incorporated metal-base pairs discussed above was characterized by which methods.

Metal-base pair	Highest ΔT_M (K)[a]	Methods[b]	Reported metals	Max. M per duplex	Reference or chapter
1 (T-T)	+10 (AT: +3)	T_M, Tit$_{UV}$, Tit$_{CD}$, NMR, ESI-MS	Hg^{2+}	5	[105], 4.6.3
6 (Dipic-Py)	n.d.[c] (AT: -2.6)	T_M, EPR, CD, X-ray	Cu^{2+}	4[d]	[117, 118, 121]
7 (Dipam-Py)	+15 (AT: +3.9)	T_M	Cu^{2+}	4[d]	[118]
9 (SPy-SPy)	+19.1 (AT: +3.4)	T_M	Ag^+	3 (isolated)	[119]
10 (Spy-Py)	+11.5 (AT: -4.1)	T_M	Ag^+	3 (isolated)	[119]
11 (Py-Py)	+6.8 (AT: -5.5)	T_M, NMR	Ag^+	1	[122]
12 (HP-HP)	+13.1 (AT: +5.9)	T_M, Tit$_{UV}$, Tit$_{CD}$, EPR, ESI-MS	Cu^{2+}	5	[123, 125]
14 (dHQ-dHQ)	+28.9 (AT: +23.7)	T_M	Cu^{2+}	1	[127]
15 (pHQ-pHQ)	n.d.[c] (AT: +29.2)	T_M, CD	Cu^{2+}	1	[127]
16 (Bipy-Bipy)	+7.5 (AT: n.d.)	T_M, UV	Cu^{2+}	1	[128]
17 (PyA-PyA)	+18.1 (AT: +9.8)[e]	T_M	Ni^{2+}, Co^{2+}	3[d]	[131]
18 (PyC-PyC)	+16.5 (AT: +4.4)[e]	T_M	Ni^{2+}, Co^{2+}	1	[132]

Table 2: a) Highest reported values for strands containing one metal base pair. The first value corresponds to the stabilization of the ligand-containing strands upon addition of metal, the value in parenthesis denotes the stabilization relative to a native **AT** base pair. Care must be taken when comparing the measured duplex stabilizations for different metal-base pairs because partly different sequences, buffers and concentrations were used; b) T_M = melting point experiment (thermal de- and renaturing), Tit$_{UV}$ = UV spectroscopic titration, Tit$_{CD}$ = CD spectroscopic titration; c) no sigmoid melting curve without metal seen; d) presumed stacking of metals only supported by a single T_M value, no other characterization reported; e) for Ni^{2+}.

A comparison of the metal-base pairs known so far yields the following picture: most reported duplex stabilizations are in the range of +5 to +20 K for one incorporated metal-base pair. The highest reached duplex stabilization prior to the practical work for this thesis (2003) was +19.1 K with the SPy-Ag^+-SPy base pair[119] (subsequently exceeded in 2005 by the dHQ-Cu^{2+}-dHQ base pair[127] and our own results). Reliable

data on metal stacking inside the DNA double helix was so far only reported by *Shionoya*[125] and *Ono*.[105] Geometrical comparisons of the artificial metal-base pairs with natural base pairs were either not discussed at all or only calculated. Only *Schultz et al.* were able to obtain a crystal structure of their metal-base pair.[121] None of the DNA duplexes containing the metal-base pairs were reported to have been used in catalysis experiments and most of the metal-ligand combinations have not been tested as catalysts at all. All the reported metal-base pairs consist of two separate mono- bi- or tridentate ligands around the central metal ion. No covalent crosslinking of the ligands to form a single multidentate ligand has been reported. The diversity of coordinated metals by the known metal base pairs is rather low.

3.4 Coordination chemistry: salen complexes and metal stacking

3.4.1 Monomeric and oligomeric salen complexes

Salen (N,N-bis-salicylidene-ethylenediamine) is a tetradentate chelate ligand providing two nitrogen and two oxygen donor atoms to coordinate a metal in a square planar or slightly distorted (D_2^d) square-planar fashion.[134] Thereby it shares similarities with porphyrine-type ligands but is much easier to synthesize and handle. The basic salen ligand **19** is synthesized by the condensation of two salicylic aldehyde molecules **20** with one molecule ethylenediamine **21** resulting in the formation of two Schiff-base moieties (Figure 14).
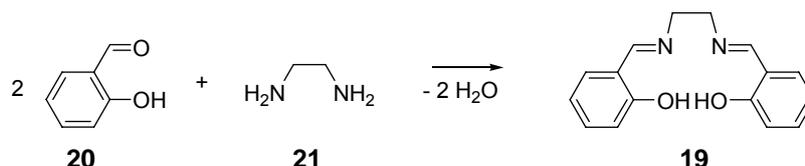
Figure 14: Synthesis of the salen ligand **19**.

The assembly of the ligand usually occurs spontaneously[135] and may also be promoted by a metal template.[63] The use of numerous differently substituted salicylic aldehyde derivatives as well as different chiral ethylenediamines and longer-chain diamines has been reported to create a plethora of chiral and non-chiral ligands with preferences for different metals and solvents.[135] The variety of coordinated metal ions is expressed by the vast number of references that can be found for metal-salen complexes in chemical databases: for each of about 20 different metals more than

100 publications are available, with Co, Mn, Cu, Ni, Fe, Cr and V as the most prominent metals that were studied.[136] Metal salen complexes of these elements are widely used in catalysis. Because of the high versatility and fidelity of salen complexes they have been ranked among the "privileged ligands for catalysis" by *Jacobsen*.[137]

The most prominent application of salen complexes is the asymmetric epoxidation of unfunctionalized alkenes, which was independently developed by *Eric Jacobsen* and *Tsutomu Katsuki* in 1990.[138, 139] Chromium and manganese are the metals mainly used as catalytically active metals in the epoxidation catalysts and the topic has been extensively reviewed.[140] Examples for other reactions catalyzed by salen complexes are cyclopropanations,[141] oxidations[142] and kinetic resolutions.[143]

Salen complexes of metals such as manganese(III) have been used for the construction of single molecule magnets because the strong ligand field in the basal plane of the salen ligand is known to result in pronounced magnetic anisotropies of the coordinated metal ions.[144] Spin coupling has been shown for *in-plane* arranged salen complexes as well as for stacked dimers of two manganese salen complexes (Figure 15). This is of particular interest, as the work described in this thesis details another way of arranging multiple manganese salen complexes (Chapter 4.6).
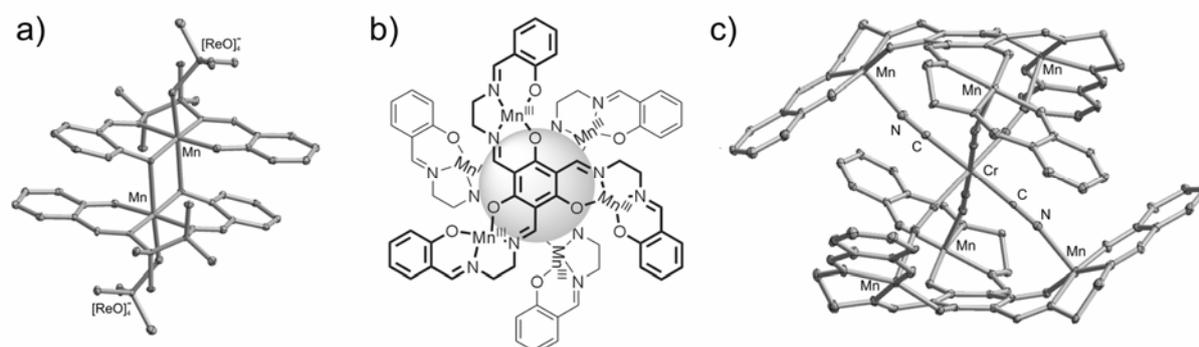
Figure 15: Single molecule magnets composed of Mn(III) salen complexes. a) Two stacked Mn-salen complexes with the salen-oxygen atoms bridging the metal centers, b) schematic representation of two triplesalencomplexes forming a sandwich structure with an internal $[Cr(CN)_6]^{3-}$ fragment (represented by the grey sphere) and c) side view of the crystal structure of this aggregate (the substituents on the salen ligands have been omitted for clarity).

The crystal structure of a single molecule magnet composed of two stacked Mn(III) salen complexes with two terminal $[ReO_4]^-$ ligands is shown in Figure 15a. The

system has a spin ground state S_t = 8/2 and also exhibits a slow relaxation of its magnetization.[145]

Figure 15b depicts a schematic drawing and Figure 15c the crystal structure of a Mn$_6$Cr-complex, which is a sandwich structure composed of two bowl-shaped C_3-symmetriy triple-salen complexes **22** that coordinate a central [Cr(CN)$_6$]$^{3-}$ fragment. The compound has an anisotropic, high ferrimagnetic spin ground state S_t = 21/2 with a slow relaxation of its magnetization, which is typical for single molecule magnets.[146]

3.4.2 Interaction of metal-salen complexes with DNA

Metal-salen complexes have been shown to bind to DNA in an intercalating fashion and have been used for the manipulation and structural characterization of DNA.[147, 148] The cleavage of the DNA backbone by salen complexes has been extensively studied.[149] *Griffin et al.* found that the manganese(III) salen complex in combination with an oxidizing reagent acts as a minor groove binder and cleaves DNA with a considerable **AT**-specifity.[150] Non oxidative (hydrolytic) cleavage was achieved with oxo-bridged di-iron salen complexes.[151] On the other hand, it was shown by *Bailly et al.* that copper(II) salen complexes can cleave DNA under reducing conditions.[152] *Burrows* and *Rokita* investigated the covalent binding of nickel(II) salen complexes to accessible guanine bases in DNA via the formation of a new carbon-carbon bond.[153]

3.4.3 Metal stacks and arrays in solid state structures and in solution

In solid state structures, several examples of principally infinite metal chains surrounded by organic ligands have been realized because of the interest in their unusual and highly anisotropic optical, electrical and magnetic properties.[154] A theoretical work by *Little* in 1964 even predicts that 1D conducting materials may exhibit high-temperature superconductivity.[155]

Discrimination has to be made between compounds with direct metal-metal contacts and compounds with ligand separated metal centers that nevertheless are close enough to result in intermetallic interaction. Additionally, chains with equidistantly

arranged metal centers must be differentiated from dimer chains with a pair wise arrangement of the metal centers resulting from a *Peierls* distortion (Figure 16).
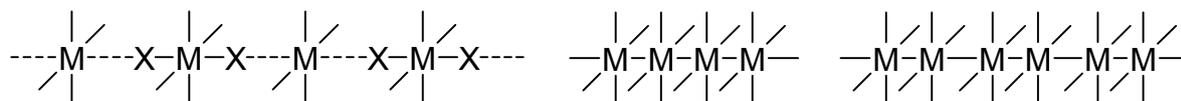
Figure 16: Examples for metal arrangements in linear chain compounds. The ligands are omitted for clarity.

There are examples for chains in which either all metal centers are equal, all centers are composed of the same element but in different oxidation states or two different metals are alternately arranged.[154]

For example, the platinum group metals (Ru, Rh, Pd, Os, Ir, Pt) form two groups of linear chain compounds: (1) the halide-bridged mixed valence chain compounds with alternating arrangement of planar d^8 and six-coordinate d^6 centers and (2) the metal-metal bonded chains composed of identical components. The latter compounds often exist in fractionally oxidized forms (Figure 17).
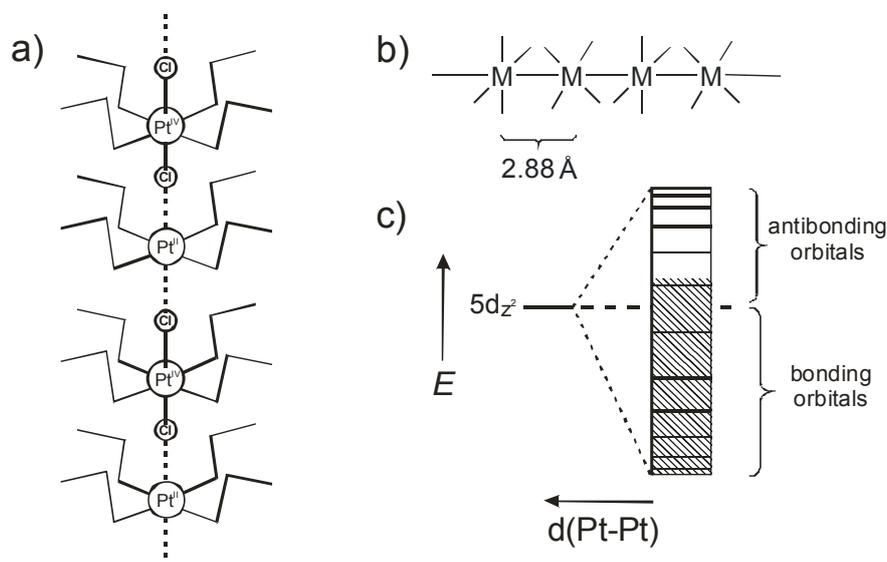
Figure 17: Examples of metal chain compounds from platinum group metals in solid state materials. a) 1-D structure of "*Wolfframs* Red"; b) Metal stacking in the "Platinum Blue" salts (ligands omitted); c) band model of the *Krogmann* salt $K_2[Pt(CN)_4]Cl_{0,32} \cdot 2,6\ H_2O$. Reduction increases the M-M-bonding because electrons are removed from anti-bonding orbitals.

An example of the halide-bridged $\cdots Pt^{II}\cdots X\text{-}Pt^{IV}\text{-}X\cdots$ compounds is "Wolfframs Red" salt tetrakis(ethylamine)-platinum(II)dichlorotetrakis(ethylamine)platinum(IV)tetra-chloride-tetrahydrate.[156] The mixed valence character was revealed by the special spectroscopic properties and the atom distances in the crystal structure of this

compound.[157] Examples for the compounds with direct Pt-Pt interactions can be found in the group of the exceptionally dark blue "Platinum Blue" compounds, the first of which was prepared by *K. A. Hofmann* by the reaction of $PtCl_2(CH_3CN)_2$ with $AgNO_3$.[158] When these oligomeric to polymeric compounds were partially reduced, the charge was found to be delocalized over several platinum atoms and the Pt-Pt distance even decreased. The shortest Pt-Pt distances in these chain compounds was determined to be 2.88 Å in the non-stoichiometric but well-defined compound $K_2[Pt(CN)_4]Cl_{0,32}$ · 2,6 H_2O. *Krogmann* was able to explain the structural and spectroscopic features of this metal chain compound with a delocalized band model.[159]

Little information is available about soluble systems which are not based on a covalently bound polydentate ligand as a scaffold but result from polymerization of monomeric metal complexes, as such systems are usually difficult to characterize. They are intermediate states of the formation of the solid state metal chain compounds discussed above. *Malatesta* and *Canziani* reported that, upon recrystallization of the compound $K_2[Ir_2(CO)_4Br_5]$ the color of the solution gradually turns from yellow, red and green to violet before the solid state chain compound $K_x\{[Ir(CO)_2Br_2]^{-0.6}\}_n$ finally separates as bronze-shining long needles.[160]

Of the well characterized metal-chain compounds in solution, most known systems of defined stoichiometry and chain length are based on linear, covalently bonded polydentate ligands, which provide the scaffold for the formation of the metal chain.[161] Usually, the synthesis of these extended ligands of finite length is time consuming and low yielding. Two different examples of polynuclear complexes in solution are depicted in Figure 18.

a)

b)
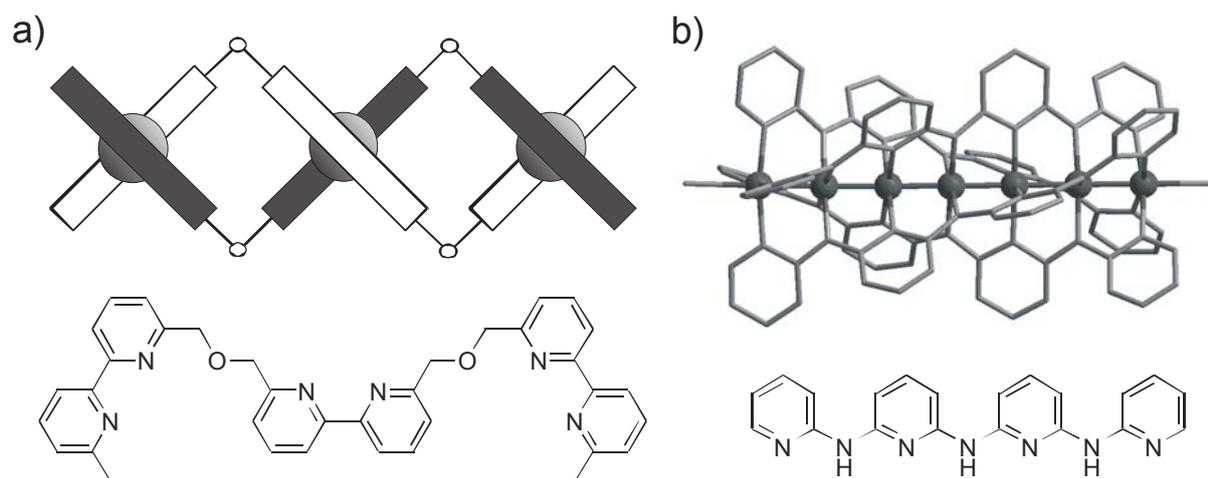
Figure 18: Examples for the controlled linear arrangement of several metal ions in soluble ligand systems. a) Lehn's helicate containing three Zn^{2+} ions tetrahedrally coordinated by bipy chain ligands; b) A chain of 7 Cr^{2+} ions displaying close metal-metal contacts was prepared by *Peng et al.*

Lehn et al. published several reports about the synthesis and characterization of polynuclear, helical complexes that spontaneously form upon mixing the specially designed ligands and metal ions such as Zn^{2+} (Figure 18a)[162]

Peng et al. synthesized several polymetallic chain compounds with direct metal-metal contacts like $[Cr_7(\mu_7\text{-teptra})_4Cl_2]$ where four tetrapyridyltriamine ("teptra") ligands are helically wrapped around a central Cr_7-chain, which is perfectly linear. The crystal structure and one of the ligands is shown in Figure 18b.[163] Recently, the same group reported the quantitative measurements of the single-molecule conductance of these 1D multinuclear metal strings.[164] By STM measurements they found that the conductance values correlate well with the d-orbital electronic coupling between adjoining metal atoms with interesting effects for the odd-numbered chains.

Hierarchical linear arrangements of several different metals coordinated by synthetic ligands were developed by *Albrecht et al.*[165]

The use of oligonucleotides as a polydentate ligand scaffold for the linear arrangement of metals in solution has just recently been developed by the pioneering works in the field of the metal-base pairs (Chapter 3.3.2). Although, conductance measurements with these systems have not been realized up to now, interesting magnetic effects were already indicated.

4 Part I: Coordination of metals inside the DNA duplex

4.1 Aims of project (part I)

The currently known metal-base pairs highlight the development from simple ligands to carefully designed systems with sophisticated properties (Chapter 3.3.2).

The new metal-base pair described in this work is based on the well known salen complex, which is one of the most widely used systems in catalysis. Its main features are the acceptance of a great variety of metal ions, accessibility of derivatives carrying additional functions and the successful application in aqueous media and hence biocompatibility (Chapter 3.4.1).

A modular assembly of the metal complex inside DNA starting from preorganized oligonucleotide precursors, an auxiliary building block (a vicinal diamine) and a metal ion should be established as a new feature among the metal-base pairs.

This modular strategy was thought to be a great advantage over all other known metal-base pairs as it permits the introduction of a source of diversity with the ability to attach additional functionality in the assembly process. From one nucleotide-based ligand precursor (a salicylic aldehyde nucleotide), a wide variety of metal-complexes inside the DNA duplex could be generated by variation of the metal core and the diamine component. The formation of an interstrand metal-salen complex obviously results in a crosslink between the two single strands composing the DNA duplex, which was hoped to have a tremendous influence on the duplex stability. This feature should allow the stacking of several metal-complexes inside the DNA double helix.

The main goal of the project was to synthesize and incorporate a salicylic aldehyde-modified nucleobase into deoxyoligonucleotides. Once a suitable assembly protocol was in place, the assembly of one and multiple interstrand salen complexes inside the DNA double helix should be investigated (Chapters 4.2.1, 4.2.2, 4.3 - 4.7).

Additionally, it was planned to synthesize a 2-[2-hydroxyphenyl-]oxazoline base pair consisting of a similar set of donor atoms but lacking any crosslinking abilities compared to the metal-salen base pair (Chapters 4.2.3 and 4.2.4).

As an alternative to the nucleosides with the natural 2'-deoxyribose backbone, it was further planned to prepare a hypermodified nucleoside building block carrying a ligand attached to a xylopyranose backbone sugar. Artificial pyranosyl-based oligonucleotides were reported to yield extremely stable duplexes. (Chapter 4.2.5).

4.2　Synthesis of ligand nucleosides

4.2.1 Synthesis of the salicylic aldehyde nucleobase

As a promising new candidate for a metal-base pair the salen ligand **19** was chosen for incorporation into oligonucleotide double strands. The reasons for this choice were (a) the high geometrical match of the flat metal-salen complex with the natural *Watson-Crick* base pairs; (b) the intriguing new feature of covalent interstrand-crosslinking upon assembly of the complex in DNA and (c) the variety of applications and tolerated metals of salen complexes as demonstrated in thousands of publications.

Figure 19 conceptionally depicts the design of the metal-salen base pair by merging the structure of a native *Watson-Crick* base pair with the salen ligand.
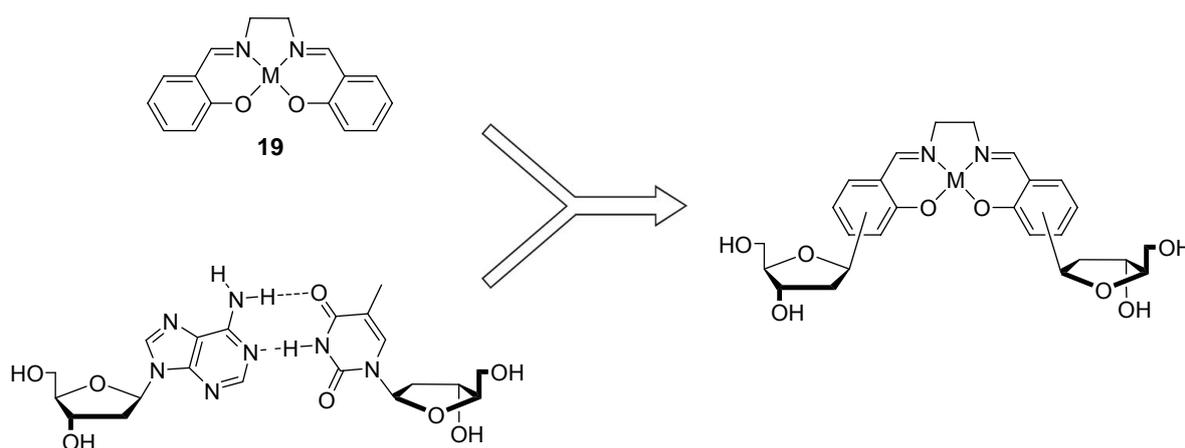
Figure 19: Formal combination of a salen complex with a canonical base pair to obtain a metal-salen base pair.

In order to create a salen-based metal-base pair which fits optimally into the double helix structure, the position of the salicylic aldehyde by which it is connected to the C1' position of 2'-deoxyribose had to be chosen carefully. If either the C4-atom or the C5-atom was chosen, the metal-base pair structures **23** or **24**, which are shown in Figure 20, would result.
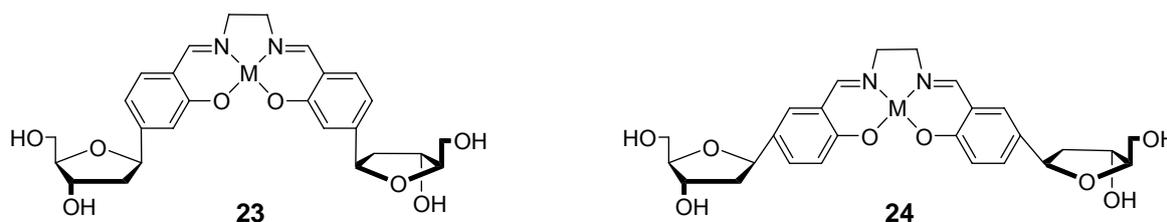
Figure 20: Depiction of the two examined metal-salen base pairs **23** and **24** with connection of the ligand to the sugar either *meta* or *para* to the oxo-substituent (for detailed geometric considerations see Chapter 4.2.2).

Initial studies focused on connecting the salicylic aldehyde via its C4-atom to the sugar to obtain structure **23** in the DNA duplex. Based on a structural analysis, this constitution was expected to fit better into the DNA than its isomer **24**. For completeness, a comparison of complex **23** is made to system **24** whose synthesis and characterization is described in the diploma thesis of *Y. Söltl*.[166, 167]

Because the crosslinking metal-salen complex was supposed to be assembled in the DNA double strand as the last step of the synthetic route, the salicylic aldehyde nucleobase **25** had to be synthesized as a precursor for generation of the salen-complex. The free nucleoside **25** and its isomer **26** are depicted in Figure 21.
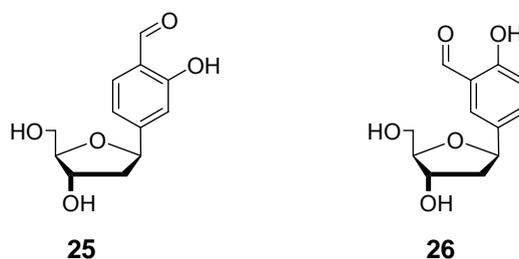
Figure 21: Salicylic aldehyde nucleobases **25** and **26**[166] described in this work.

Two of such ligand precursors situated in the appropriate complementary positions of a duplex structure may assemble in the presence of a proper metal and ethylenediamine to give a metal-salen complex (Figure 22). This complex was thought to stack inside the duplex structure presenting the metal in the minor groove. In contrast to the metal-base pairs investigated so far (Chapter 3.3.2), the salen-base pair requires the metal and also ethylenediamine for assembly. Although the imine formation is known to be generally highly reversible, the coordination of the metal to the salen complex was anticipated to yield a stable, covalently bound crosslink.[168]
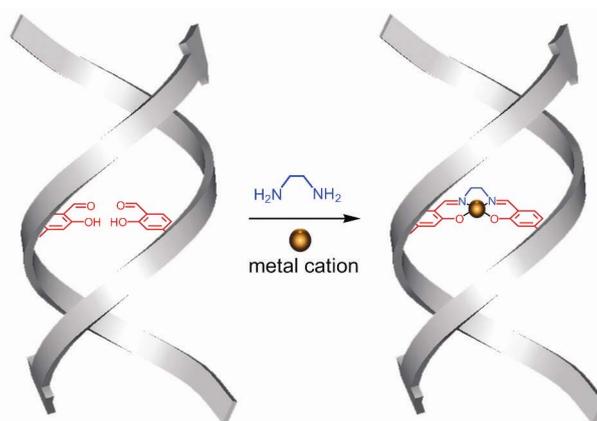
Figure 22: Assembly concept of the interstrand metal-salen base pair in a preorganized duplex.

A retrosynthetic analysis of the free salicylic aldehyde **25** in DNA goes back to the protected salicylic aldehyde nucleobase **27**, which in turn is formed via a metal-mediated *C-C*-coupling reaction between the protected ligand **28** and the glycosyl donor **29**.
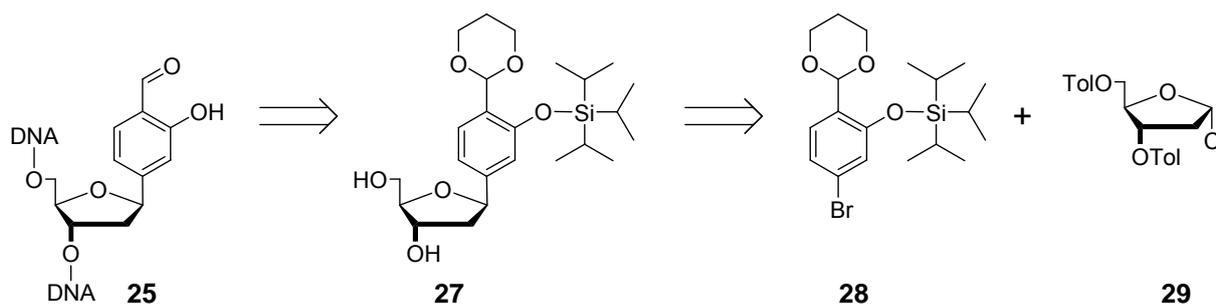
Figure 23: Retrosynthetic analysis of the salicylic aldehyde nucleobase **25** in a DNA oligonucleotide.

The protecting groups on the ligand **28** were chosen to comply with the ligand synthesis and the subsequent DNA chemistry: the protecting groups had to be insensitive towards the reagents used for the planned cuprate coupling (namely *t*-butyllithium) and the subsequent removal of the sugar's protecting groups.

It was also necessary that the modified bases cause no problems during automated DNA synthesis using the standard reagents for the *coupling* (lutidine as base, nucleophilic activation), *capping* (acylating reagents) and *oxidation* (aqueous iodine) steps. Any reactivity of the modified base towards one of these reagents may have led to faulty couplings, truncation or branching of the oligonucleotides.

It was anticipated that the acetal protecting group would show some reactivity towards the acidic detritylation step (2 % CHCl$_2$COOH in CH$_2$Cl$_2$) but this was not

expected to pose a problem as free aldehydes have previously been shown to comply with DNA synthesis.[169, 170]

Finally, the ligand's protecting groups had to be removed after the DNA synthesis. This has been accomplished both for acetals and silyl protecting groups in several examples before: *Nielsen et al.* and *Czlapinski et al.* successfully used acetals in their DNA-salicylic aldehyde constructs as protecting groups for the aldehyde functionality (Chapter 3.1.3).

For the protection of the phenolic oxygen atom, both groups used a benzoyl group which could not be used in this work due to the reasons explained above. On the other hand, silyl protecting groups are used extensively for the protection of the aliphatic 2'-hydroxyl group of ribose in automated RNA synthesis. Silyl protection of phenolic hydroxyl groups in a DNA synthesis context was only reported rarely before.[171] Nevertheless it was decided to use a silyl protecting group for the preparation of the ligand precursor **25**. The success of the chosen protecting group strategy is illustrated by the results described in Chapter 4.3.2.

The first task in the preparation of the salicylic aldehyde nucleobase **25** was the synthesis of the protected bromide **28** (Scheme 1).
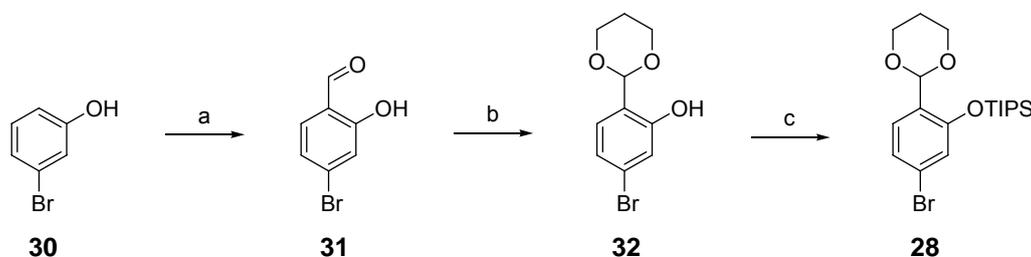
Scheme 1: Synthesis of the protected ligand building block **28**. a) $(CH_2O)_n$, NEt_3, $MgCl_2$, MeCN, 80 °C, 10 h, 49 %; b) 1,3-propanediol, $HC(OEt)_3$, $N(nBu)_4Br_3$, r.t., 24 h, 86 %; c) TIPS-OTf, $NEt(iPr)_2$, CH_2Cl_2, r.t., 12 h, 87 %.

First, *ortho*-formylation of 3-bromophenol **30** with paraformaldehyde in the presence of $MgCl_2$ and triethylamine yielded 4-bromosalicylic aldehyde **31**.[172]

The formylation was followed by an acetalization. The standard method for the preparation of cyclic acetals from benzaldehydes (diol, cat. acid, removal of water) did not result in any product formation. However, a special procedure for the acetal protection of salicylic aldehydes that uses $N(nBu)_4Br_3$ as a catalyst and triethylorthoformate as water-removing agent successfully yielded 1,3-dioxane **32**.[173]

Finally, tri-*iso*-propylsilyl (TIPS) protection of the phenolic hydroxyl group under standard conditions (TIPS-OTf, NEt(iPr)$_2$) yielded the protected ligand **28**.

The ^{1}H-NMR spectrum of **28** shows some characteristic signals which helped trace the existence and integrity of the protected salicylic aldehyde in the following synthetic steps: the 1,3-dioxane ring is locked in a single chair conformation by the bulky aromatic substituent which leads to the appearance of 4 characteristic signals for the 6 hydrogen atoms of the propylene unit (C5-H$_{ax}$: δ 1.4 ppm; C5-H$_{eq}$: δ 2.1 ppm; C4-H$_{ax}$/C6-H$_{ax}$: δ 3.9 ppm; C4-H$_{eq}$/C6-H$_{eq}$: δ 4.2 ppm). The sharp singlet resonance at δ 5.8 ppm was assigned to the single hydrogen atom at the carbon between the two oxygen atoms. The aromatic hydrogen atoms give rise to two doublets and one doublet of doublets between δ 6.8 – 7.6 ppm. The signals of the TIPS group (one doublet and one septet) can be found between δ 1.0 and 1.5 ppm (Figure 24).
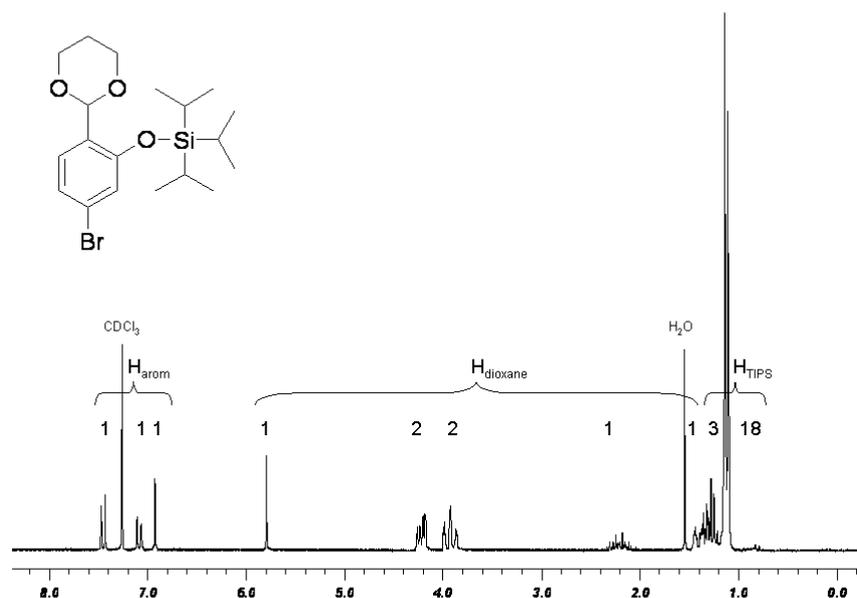
Figure 24: ^{1}H-NMR spectrum of compound **28** showing all expected signals (300 MHz, CDCl$_3$).

The first step of the synthesis of compound **28** is worth a more detailed discussion: in contrast to 5-bromosalicylic aldehyde (used to prepare the metal-salen base pair **24**), which is easily prepared by bromination of salicylic aldehyde, its isomer 4-bromosalicylic aldehyde **31** carries the bromine substituent *meta* to the hydroxyl group and *para* to the formyl group and therefore is less readily accessible. The

synthesis of compound **31** from commercially available 3-bromophenol **30** was described in the literature in 6 consecutive steps![174]

Here, only one step with yields between 20 and 50 % was needed according to a method for the direct *ortho*-formylation of phenols published by *Casiraghi et al.* and *Hofsløkken et al.* to accomplish the same transformation.[172, 175] The reaction is based on a Lewis-acid mediated activation of formaldehyde and reaction with the phenol in a site-selective manner. *Casiraghi* reported in 1980 that the use of tin tetrachloride as *Lewis*-acid and tri-*n*-butylamine as base in dry toluene was superior to the use of magnesium salts and triethylamine. The reproducibility of this method in the course of this work was, however, troublesome.

In contrast, the method reported in 1999 by *Hofsløkken* explicitly relies on the use of a magnesium salt (dry MgCl$_2$) and triethylamine in acetonitrile as the solvent. This method was found to give much better and more reliable results, although never more than 50 % yield of the desired isomer **31** were obtained.

The mechanism of this ortho-formylation is thought to proceed via two consecutive *Lewis*-acid catalyzed steps in "one pot" (Scheme 2).
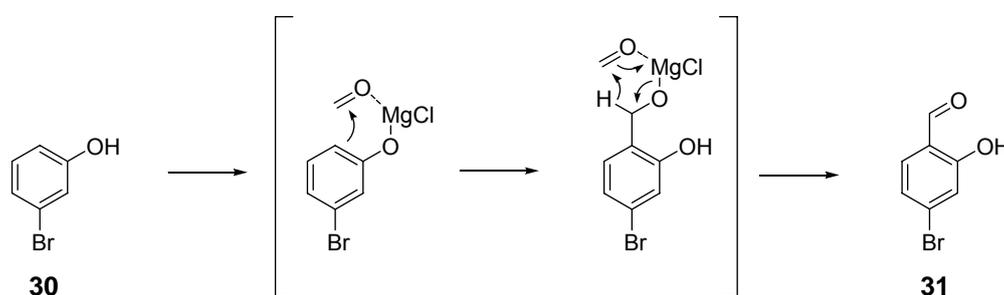
Scheme 2: Assumed mechanism for the orthoformylation of 3-bromophenol **30**.

First, the *Lewis*-acid MgCl$_2$ coordinates to the deprotonated phenolic oxygen and to one molecule of formaldehyde and thereby directs the electrophilic aromatic substitution into the *ortho* position to the phenolic oxygen. From the two possible *ortho* positions the position *para* to the bromine substituent is highly preferred due to steric reasons and only a trace of the unwanted isomer 6-bromosalicylic aldehyde was isolated. The intermediate product of this first step is a benzylic alcohol. A subsequent oxidation of this intermediate benzylic alcohol to the final product 4-bromosalicylic aldehyde **31** has to occur in the reaction mixture. This is expected to be an *Oppenauer*-oxidation-type reaction involving again MgCl$_2$ as Lewis acid and formaldehyde as oxidizing reagent.

The second key intermediate for the planned metal-mediated *C-C*-coupling reaction was the toluoyl protected 2'-deoxyribosyl chloride **29**, which was prepared according to Scheme 3.
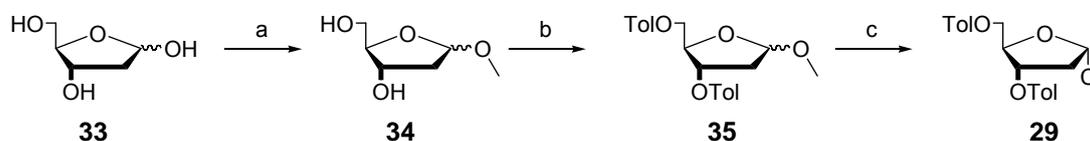
Scheme 3: Synthesis of the toluoyl protected 2'-deoxyribosyl chloride **29**. a) 0.1 % HCl in MeOH; b) TolCl, py, 78 % over 2 steps; c) HCl, HOAc, 83 %.[176]

2'-Deoxyribose **33** was first treated with a catalytic amount of HCl in methanol to afford the methylacetal **34**.[176] Protection of the free hydroxyl groups was achieved with toluoylic acid chloride to yield compound **35**. This was finally reacted in neat glacial acetic acid with HCl gas until the glycosyl chloride **29** precipitated as a white powder consisting exclusively of the α-anomer (anomeric effect). The compound had to be washed thoroughly with dry ether to remove all traces of acid and was stored at -20 °C.

The metal-mediated *C*-glycosylation between the brominated ligand precursor **28** and the glycosyl donor **29** was the key step of the nucleoside synthesis. Scheme 4 summarizes the elaborated methods for the preparation of *C*-nucleosides.
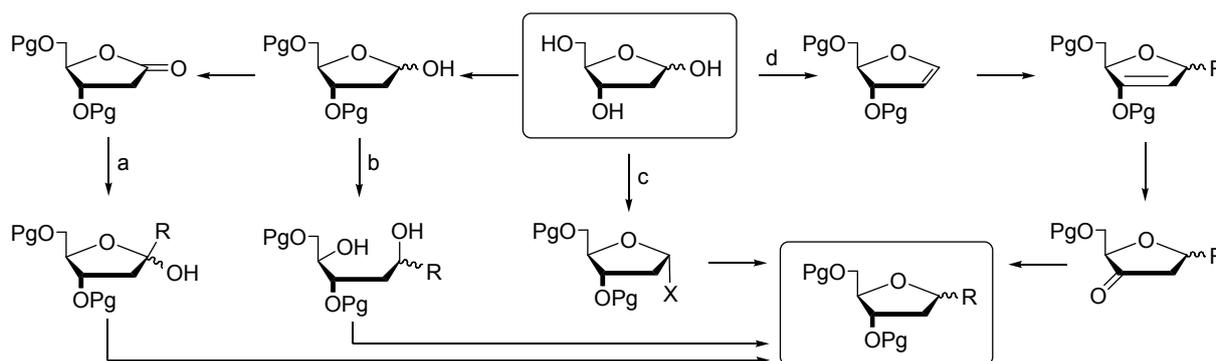
Scheme 4: Methods for the preparation of *C*-nucleosides. a) Addition of a metal-organic compound to ribonolactone and subsequent reductive cleavage of the 1'-hydroxyl group;[177] b) addition of a metal-organic compound to the 1'-unprotected sugar and subsequent Mitsunobu ring closure;[178] c) direct nucleophilic substitution of a leaving group at C1' with a metal-organic species such as organocuprates[179] or organocadmium compounds[180]; d) *Heck*-coupling to a glycal with double bond migration, then cleavage of 3'-protecting group and stereoselective reduction of the resulting carbonyl group at C3'.[181]

In this work, approach c) was found to give the best results. A sequence of lithium-bromine exchange at the protected ligand **28** and subsequent transmetallation to copper(I) to perform a cuprate coupling on glycosyl chloride **29** was developed after screening of different reagents, solvents, reaction temperatures and times. In conclusion, the following aspects of the reaction were optimized:

- A lithiation of the aromatic ligand was chosen because generation of a *Grignard*-reagent failed (presumably due to the high electron density). The use of *t*-BuLi was found to be more effective than other lithiation reagents.

- A glycosyl chloride was chosen from a variety of electrophilic glycosyl donors (bromide, lactone, trichloracetimidate). The use of 2'-deoxyribonolactone was not successful.

- CuBr • SMe$_2$ was used as the copper reagent as its insolubility in ether was found to be an indispensable indicator for the difficult transmetallation step.

- Freshly dried (Na) and chemically deoxygenated (benzophenone) diethylether was found to be the best solvent for the lithiation and transmetallation. Due to the poor solubility of glycosyl chloride **29** in ether, this compound was dissolved in dry dichloromethane prior to addition of the cuprate.

- The temperature control during the transmetallation step was found to be very important. Best results were obtained when the mixture was warmed to about − 30 °C until almost all of the CuBr • SMe$_2$ had dissolved.

- Workup consisted of an aqueous quenching of the reaction mixture with ammonium chloride buffer which was set to pH ≈ 8 to ensure the stability of the acetal protecting group.

The synthetic sequence to nucleoside **38**, which was developed in this work, is shown in Scheme 5.
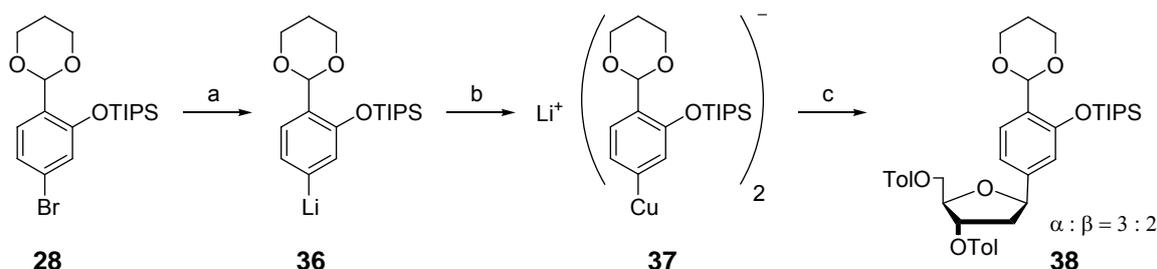
Scheme 5: *C*-glycosylation sequence to the protected ligand nucleoside **38**. a) 2 eq *t*-BuLi, Et$_2$O, − 78 °C, 2 h; b) CuBr · SMe$_2$, − 78 °C to − 30 °C, 20 min; c) **29**, CH$_2$Cl$_2$, 12h, − 78 °C to r.t., 78 % (α : β = 3 : 2).

The protected ligand **28** was reacted with 2 eq. *t*-butyllithium at − 78 °C in diethylether to give the lithiated compound **36** as a yellow solution. The metallation was complete within 2 hours as proven by quenching an aliquot of the reaction mixture with D_2O and subsequent NMR spectroscopic visualization of the newly introduced deuterium atom in the 4-position. The lithiated ligand **36** was subsequently transmetallated by transferring it to a precooled (− 78 °C) suspension of CuBr • SMe_2 (1 eq) in diethylether. The mixture of lithiated ligand and copper(I) salt had to be warmed carefully to about − 30 °C under heavy stirring until almost all CuBr • SMe_2 had dissolved to give an orange-beige solution (a color change to green or brown and the formation of a dark precipitate indicated decomposition of the cuprate).

After complete transmetallation, the ligand cuprate **37** was immediately cooled down again to − 78 °C and transferred to a precooled (− 78 °C) solution of 2'-deoxyribosyl chloride **29** in dry dichloromethane. Subsequently, the reaction mixture was slowly allowed to warm up to room temperature. The final color of the mixture varied between yellow and dark green-brown. For the workup, aqueous ammonium chloride buffer (pH ≈ 8) was added to complex the copper by forming the blue copper tetraamine complex.

The reaction usually produced a variety of side products (Figure 25) besides the desired β-nucleoside β-**38** and its anomer α-**38**.
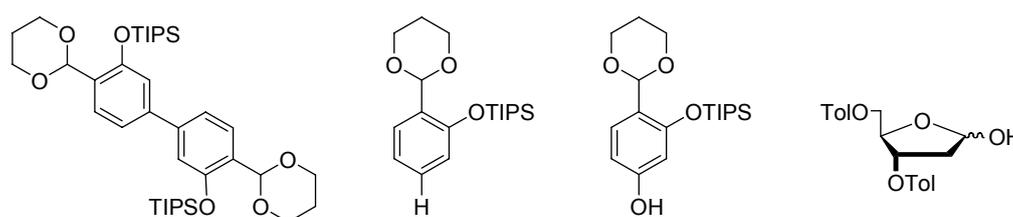
Figure 25: Side products of the organo-cuprate coupling reaction. The ligand dimer (left) was isolated in yields of up to 55 % with respect to the amount of ligand precursor **28** used in the coupling reaction. The latter three compounds were only isolated in traces.

The anomers β-**38** and α-**38** could be separated by silica gel column chromatography. The ^{1}H-NMR spectrum of the nucleoside β-**38** is depicted in Figure 26.
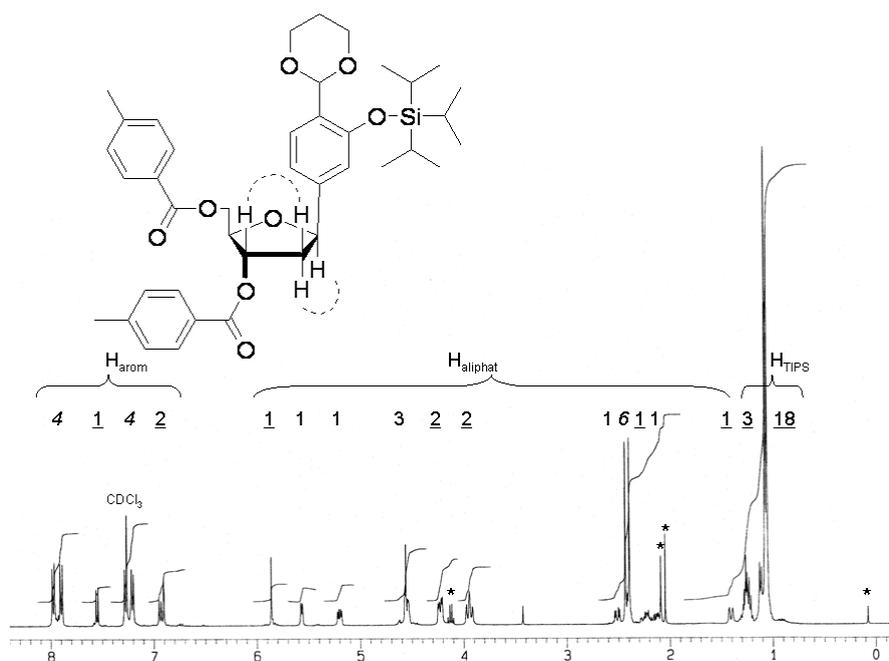
Figure 26: ^{1}H-NMR spectrum of the glycosylation product β-**38** (400 MHz, CDCl$_3$). Comparison with the ^{1}H-NMR spectra of the ligand precursor **28** (Figure 24) and the glycosyl donor **29** shows that all expected signals are present. The observed significant NOESY contacts are marked in the structure diagram by dashed lines. The numbers indicate the relative integral size (underlined = ligand, italic = toluoyl, normal font = sugar, * = impurities; scale in ppm).

Both the NMR signals corresponding to the protected ligand and to the sugar moiety can be clearly differentiated in the spectrum of nucleoside β-**38** (compare to the ^{1}H-NMR spectrum of the ligand building block **28**, Figure 24). The configuration at C1' of both anomers was assigned by evaluation of the NOESY contacts between the hydrogen atoms C1'-H, C2'-H, and C3'-H. Additionally, compound β-**38** was fully deprotected and crystallized to unambiguously prove its configuration (Chapter 4.2.2).

The further steps leading to the phosphoramidite that was needed for the incorporation into oligonucleotides by automated DNA synthesis are depicted in Scheme 6.
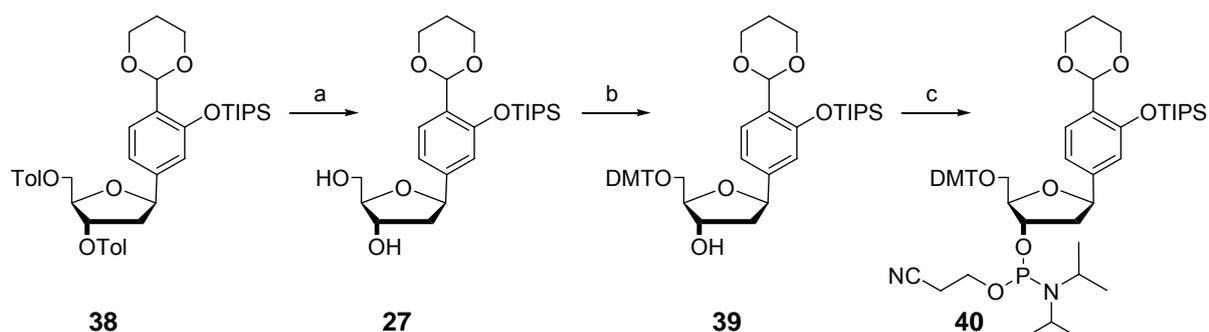
Scheme 6: Synthesis of phosphoramidite **40** for the automated DNA synthesis. a) K$_2$CO$_3$, MeOH, r.t., 2 h, 72 %; b) DMT-Cl, pyridine, 3 h, 67 %; c) (*i*Pr$_2$N)(NCCH$_2$CH$_2$O)PCl, NEt(*i*Pr)$_2$, THF, r.t., 2 h, 78 %.

First, the toluoyl protecting groups of nucleoside β-**38** were cleaved by transesterification with methanol under *Zémplen* conditions.[182] The free nucleoside **27** was reacted with 4,4'-dimethoxytritylchloride (DMT-Cl) to the 5'-DMT compound **39**. The use of 1.3 equivalents of DMT-Cl was found to be sufficient to obtain the product **39** in good yields without significant amounts of double protected material. The product was subsequently reacted with the phosphorylating agent (*i*Pr$_2$N)(NCCH$_2$CH$_2$O)PCl under strictly anhydrous and anaerobic conditions to obtain phosphoramidite **40**. This compound also had to be purified under anaerobic conditions to avoid oxidation of the phosphorus atom by a quick silica gel filtration in a closed apparatus. Precipitation from hexane, commonly used as final purification step of modified phosphoramidites, was not feasible due to the very low polarity of the product **40** and was also not found to be necessary. The ligand-phosphoramidite **40** was characterized by ^{1}H-, ^{13}C- and ^{31}P- NMR spectroscopy and high resolution mass spectrometry and used in the automated oligonucleotide synthesis described in Chapter 4.3.1.

4.2.2 Synthesis and X-ray structure of a monomeric Cu^{2+}-salen-base pair

In order to unambiguously establish the configuration at C1' of the nucleoside **27**, an attempt was undertaken to obtain a crystal structure of the nucleoside or of one of its directly accessible derivatives. Removal of all protecting groups from the β-nucleoside **27** yielded the free nucleoside **25** which showed tendencies to crystallize from different solvents. Crystals suitable for X-ray analysis were finally obtained by slow evaporation of a solution of **25** in EtOAc.[183] The synthesis of **25** is depicted in Scheme 7, the crystal structure which clearly shows the desired β-configuration is illustrated in Figure 27.
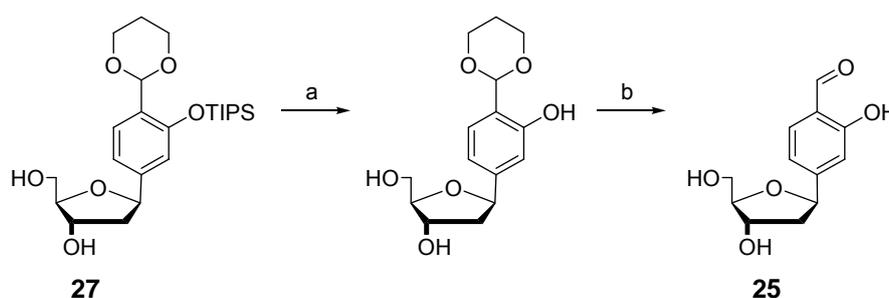
Scheme 7: Complete deprotection to obtain the free salicylic aldehyde nucleoside **25**. a) TBAF, THF, 3 h; b) HCl, H$_2$O, THF, 2 h, 32 % over two steps.
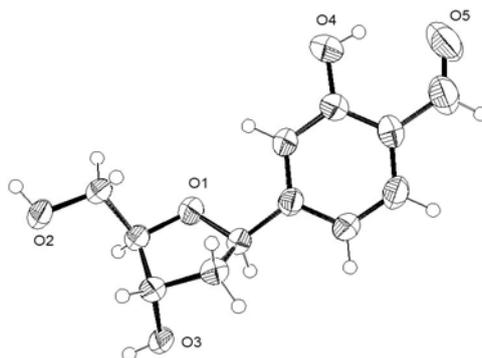
Figure 27: X-ray structure of salicylic aldehyde nucleoside **25**.[183]

Additionally, the copper-salen complex of this monomeric ligand-nucleoside was prepared and crystallized. Therefore, compound **25** was reacted with 0.5 eq ethylenediamine in methanol to give the corresponding salen ligand **41** (Scheme 8).
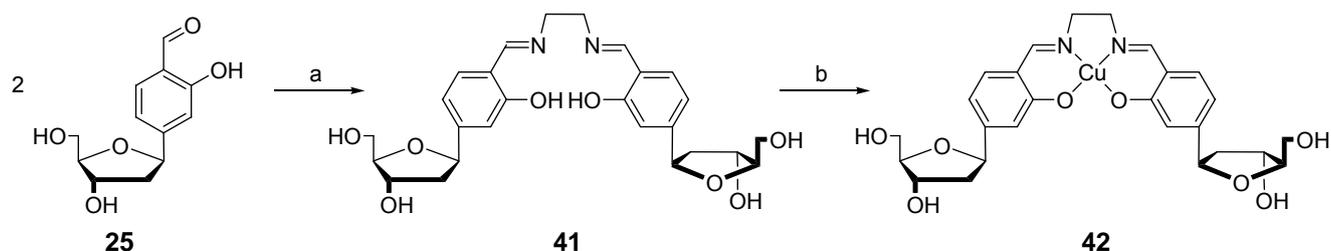
Scheme 8: Synthesis of the monomeric copper-salen base pair **42**. a) 1 eq ethylenediamine, MeOH; b) 1 eq Cu(acac)$_2$, MeOH, quant.

Treatment of the chelate ligand with 1 eq. Cu(acac)$_2$ in methanol yielded the copper salen complex **42** as a purple solution from which dichroic green-purple crystals were grown by slowly cooling this solution from 65 °C down to room temperature. Figure 28 shows the structure following X-ray diffraction of the resulting crystals.[184]
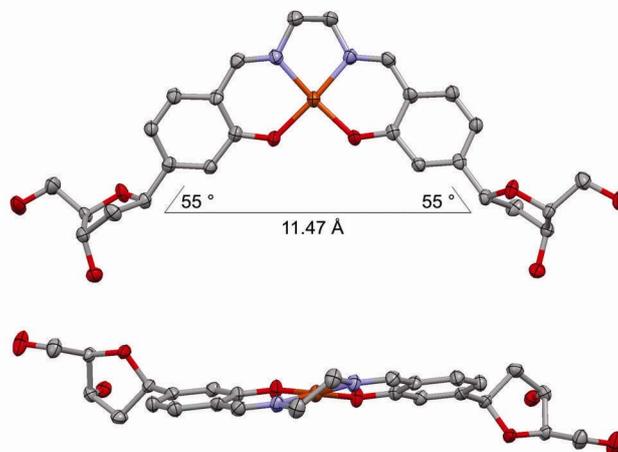
Figure 28: X-ray structure of monomeric copper-salen base pair **42** (top and side view).[184]

The metal-base pair **42** displays a tetrahedrally distorted square-planar coordination geometry of the copper centre as reported for similar copper salen complexes.[185] The molecule has a C2-axis which goes through the copper atom and the middle of the ethylene bridge. The salicylic aldimine moieties are oriented in an anti-conformation with respect to the sugars, the distance between the C1' atoms of the two sugars is 11.47 Å, which is similar to **AT** (10.44 Å) and **GC** (10.72 Å) *Watson-Crick* base-pairs. The angle between the *C*-glycosidic bond and the line connecting the C1' atoms is, with 55°, in excellent agreement with a normal base pair.

The chelate rings exhibit the Δ configuration which resembles surprisingly closely the propeller twist of a native *Watson-Crick* base pair. The dihedral angle between the planes defined by the aromatic rings was found to be θ_P = + 22°. This is slightly larger than in natural base pairs (ca. + 10°) but of the same sign (Figure 29a). Nevertheless, no circular dichroism was observed for a solution of **42** in water, which might be the result of a 1 : 1 mixture of molecules with the chromophore (the copper chelate) in either Δ or Λ configuration. This means that the homochiral sugar moieties might have no influence on the configuration of the chelate in solution. This feature stands in contrast to the fixed configuration of the chelate ring in the crystal lattice and in the DNA duplex (Chapter 4.4.3.2).

The 2'-deoxyribose sugar rings exhibit a $C_{2'}$-endo ("south") conformation, which is common for B-type DNA (Figure 29b).[186]
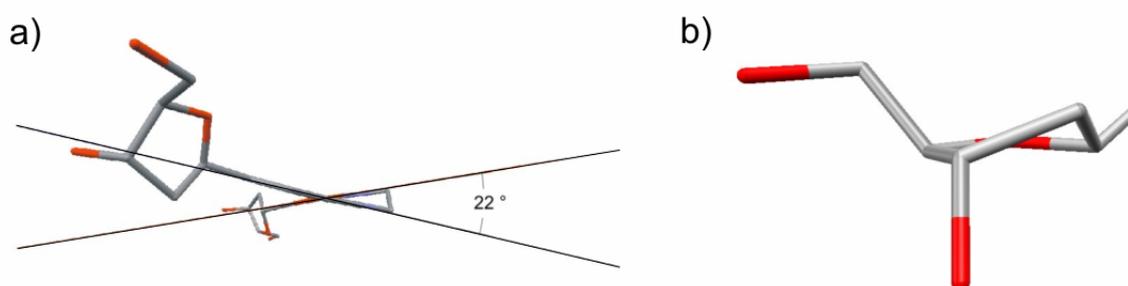
Figure 29: a) View of the X-ray structure of monomeric copper-salen base pair **42** along the intersection of the two planes that are defined by the aromatic rings of the salicylic aldehydes; b) detail from X-ray structure of monomeric copper-salen base pair **42** showing the sugar pucker in the C_{2}-endo ("south") conformation.

The superposition depicted in Figure 30 shows the high geometrical match of the deoxyribosyl substituted Cu-salen complex and a normal **AT**-*Watson-Crick* base pair.
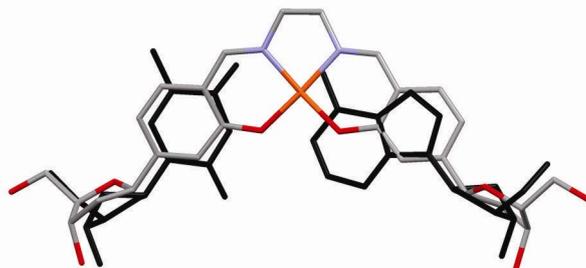
Figure 30: Superposition of the -ray structure of monomeric copper-salen base pair **42** with a canonical *Watson-Crick* A-T base pair (black).

Attempts to crystallize the corresponding vanadyl complex in a similar manner starting from VO(acac)$_2$ resulted in the formation of purple microcrystals, which were, however, not suitable for X-ray crystallography.

An NMR study was performed with salicylic aldehyde **25** in deuterated methanol. After addition of 0.5 eq ethylenediamine, the ^{1}H- and ^{13}C-NMR spectra changed significantly and indicated quantitative formation of the salen ligand in solution by the shift of the aldehyde associated ^{1}H-NMR signal at 10 ppm upfield to 8.4 ppm, which is typical for salicylic aldimines. Addition of Pd(OAc)$_2$ resulted again in a significant shift, especially of the NMR signals of the atoms near the coordinated metal ion.[187]

Attempts towards obtaining a crystal structure of an entire DNA duplex containing one or more metal-salen base pairs showed that it was possible to crystallize a 12mer double strand containing one manganese-salen base pair (**[D16-L-a/b**+en+Mn], for sequence see Table 3) under appropriate conditions. A preliminary examination in a synchrotron beam line yielded, however, only structural features of very low resolution, which showed that the crystals consist of DNA and also contain manganese ions. No clear structural information was obtained, yet. The reason for this might be a random disorganized orientation of the DNA and/or a contamination of the crystal with excess manganese ions. Experiments with other metal-salen containing DNA strands are currently under way.

4.2.3 Attempts to prepare a hydroxyphenyl-oxazoline nucleoside

Besides the development of the salicylic aldehyde **25** for preparation of the metal-salen base pair, another bidentate ligand of similar geometry was planned to be incorporated into DNA oligonucleotides.
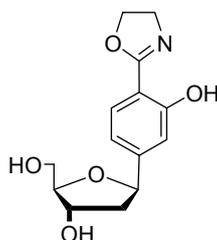
Figure 31: Depiction of the planned hydroxyphenyl-oxazoline ligand base **43**.

Similar to the salen ligand, a pair of these hydroxyphenyl-oxazoline ligands **43** was expected to coordinate a range of transition metal ions via the two nitrogen and two oxygen donor atoms in a square planar or tetrahedral coordination sphere. Similar mononuclear complexes of various substituted hydroxyphenyl-oxazolines have been reported before and were used for catalytic dehydrogenations,[188] Diels-Alder reactions,[189] epoxidations of allylic alcohols[190] and in photoluminescent materials[191]. These ligands are structurally related to the very versatile phosphanyl-oxazoline (PHOX) ligands developed by *Helmchen* and *Pfaltz*.[192] In the known complexes of the hydroxyphenyl-oxazoline complexes with the stoichiometry ML$_2$, the two separate ligands were generally arranged *anti* around the central metal. When these ligands are incorporated into DNA double strands as base surrogates facing each other, one would expect a *syn* arrangement in the metal complex **44** due to the preorganization in the DNA duplex (Scheme 9; compare to Chapter 4.4.1).
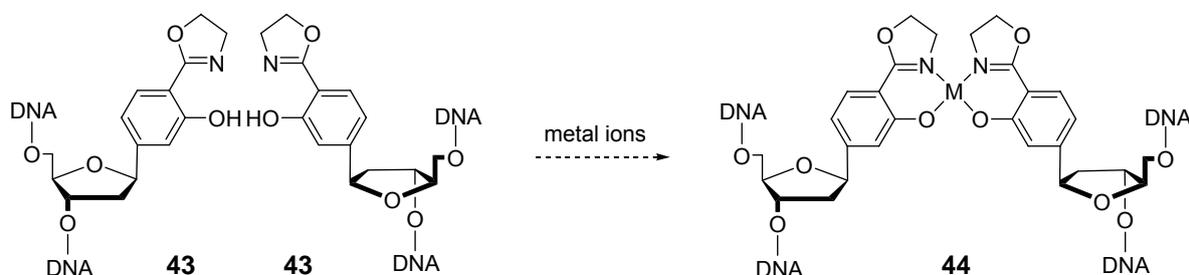
Scheme 9: Planned assembly of the bis(hydroxyphenyl-oxazoline) base pair **44** inside DNA.

In contrast to the salen ligand, a pair of the ligands **43** in the complex **44** is not connected by a covalent bridge and therefore is expected to show significant differences in coordination behavior and stabilizing influence on the DNA duplex.

A key intermediate for the preparation of **43** is a 2-[4-bromo-2-hydroxyphenyl-]oxazoline carrying a protecting group on the phenolic hydroxyl group (**45** in Scheme 10).
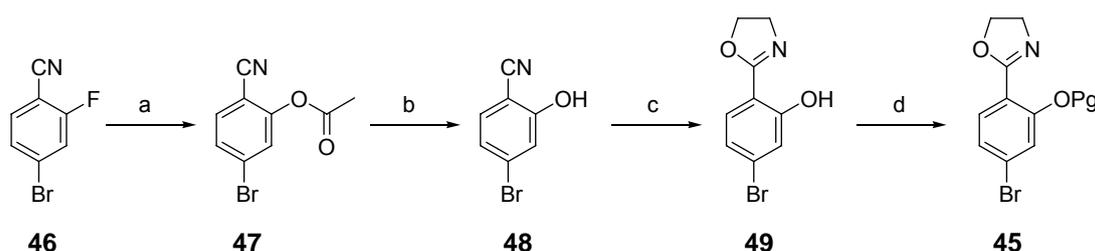
Scheme 10: Synthesis of the protected hydroxyphenyl-oxazoline building block **45**. a) KOAc, 18-crown-6, MeCN, 100 °C, 36 h; b) NaOH$_{(aq)}$, 24 h, 70 %;[193] c) dry ethanolamine, cat. ZnCl$_2$, PhCl, 4 h, reflux, 62 %; d) see main text.

For the generation of the oxazoline ring, the approach starting from a nitrile was chosen as the most efficient way among several methods of synthesizing oxazolines. 4-Bromo-2-fluorobenzonitrile **46** was first reacted in a nucleophilic aromatic substitution with a mixture of potassium acetate and the crown ether 18-crown-6 to 2-acetoxy-4-bromobenzonitrile **47**, which was instantly saponified to yield 4-bromo-2-hydroxybenzonitrile **48**.[193] This compound was subsequently transformed to 2-[4-bromo-2-hydroxyphenyl-]oxazoline **49** by treatment with ethanolamine and a catalytic amount of zinc(II)chloride in dry chlorobenzene.[194] This one-step method was found to be both superior in yield and time to the three-step sequence starting from the corresponding salicylic acid, which is widely used for the preparation of 2-aryloxazolines.

Subsequently, the hydroxyl group required protection for the planned organometallic *C*-glycosylation. Unexpectedly, this protection turned out to be very difficult with a range of standard hydroxyl protecting groups being unsuccessful if tried on this position.[195] The TIPS protecting group, which proved to be the most amenable choice for the synthesis of the salicylic aldehyde nucleoside **27**, could not be used to protect molecule **49** due to its instability during silica gel chromatography.

It was found that **49** could be protected with the benzyl, the pivaloyl and the methoxymethyl (MOM) protecting groups. Unfortunately, none of the differently

protected hydroxyphenyl-oxazolines could be successfully used in a *C*-glycosylation reaction to obtain a ligand-nucleoside (Figure 32).
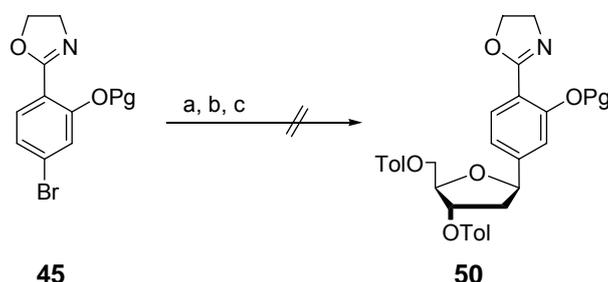
Figure 32: Attempt to prepare a protected hydroxyphenyl-oxazoline nucleoside **50** by a metal-organic coupling reaction. a) 2 eq *t*-BuLi, Et$_2$O, − 78 °C, 2 h; b) CuBr · SMe$_2$, − 78 °C to − 30 °C, 20 min; c) **29**, CH$_2$Cl$_2$, 12h, − 78 °C to r.t.

Because the attempts to perform the *C*-glycosylation failed, the synthesis of hydroxyphenyl-oxazoline nucleoside **43** was not pursued any further.

On the other hand, the hydroxyphenyl-oxazoline functionality was successfully attached to the 5-position of 2'-deoxyuridine via an alkyne linker. The perspective to use this compound for the coordination of metal ions to the exterior of the DNA duplex is discussed in Chapter 5.2.

The synthesis of another nucleoside based on the structure of hydroxyphenyl-oxazoline **49** is discussed in Chapter 4.2.4.

4.2.4 Incorporation of an oxazolinylidene-indolone nucleoside into DNA

Attempts to synthesize a nucleoside containing a hydroxyphenyl-oxazoline ligand were unsuccessful mainly due to difficulties in performing the copper-mediated *C*-glycosylation (Chapter 4.2.3). Therefore, a simpler synthetic procedure was developed for an altered ligand, which contains a similar arrangement of donor atoms.[196]

The troublesome *C*-glycosylation of a sugar moiety with an (aromatic) ring can be circumvented if the ring contains a nitrogen atom with a free valence as in the case of the natural DNA bases. Another example is *Shionoya's* hydroxypyridone ligand (**12**). Likewise, a new ligand based on the hydroxyphenyl-oxazoline system was developed by formally transforming the phenyl ring of structure **43** into the pyrrole ring of structure **51** (Figure 33).
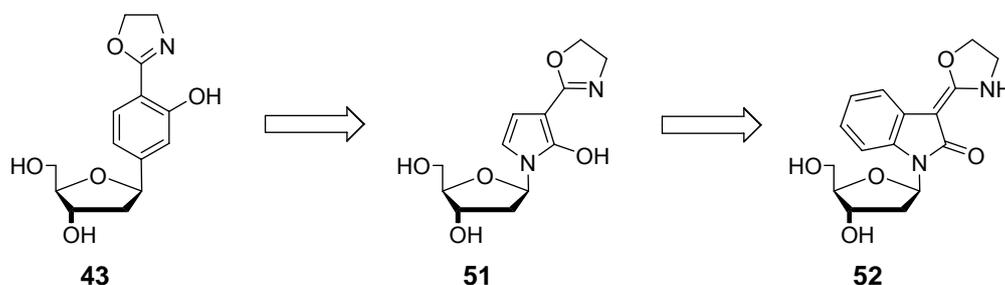
Figure 33: Formal transformation of the hydroxyphenyl-oxazoline nucleoside **43** via the hypothetic hydroxypyrrole-oxazoline **51** into the 3-(2-oxazolidinylidene-)indol-2-one nucleoside **52**.

Although compound **51** is difficult to synthesize, the derivative **52** is easily accessible according to published methods for the preparation of compound **53** (Figure 34).[197]
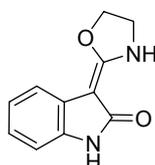
Figure 34: Free 3-(2-oxazolidinylidene-)indol-2-one ligand **53**. Note that compound **53** appears in the literature as the tautomer shown here (C=O double bond) whereas the hydroxyphenyl-oxazoline in **43** is believed to exist as depicted in Figure 33 (C=N double bond).[197]

The resulting ligand **52** (Figure 33) is accessible from the commercially available compound isatin (**54**), which is an industrial intermediate in the fabrication of indigo. This strategy of a simple and quick synthetic access from isatin, however, implied that the final ligand **52** contains an additional benzene ring and therefore is sterically more bulky than the parental system.

Ligands similar to molecule **53** are known to form complexes with a couple of transition metal ions (Cu^{2+}, Ni^{2+}, Co^{2+}).[198] The synthesis of the DNA building block is summarized in Scheme 11.
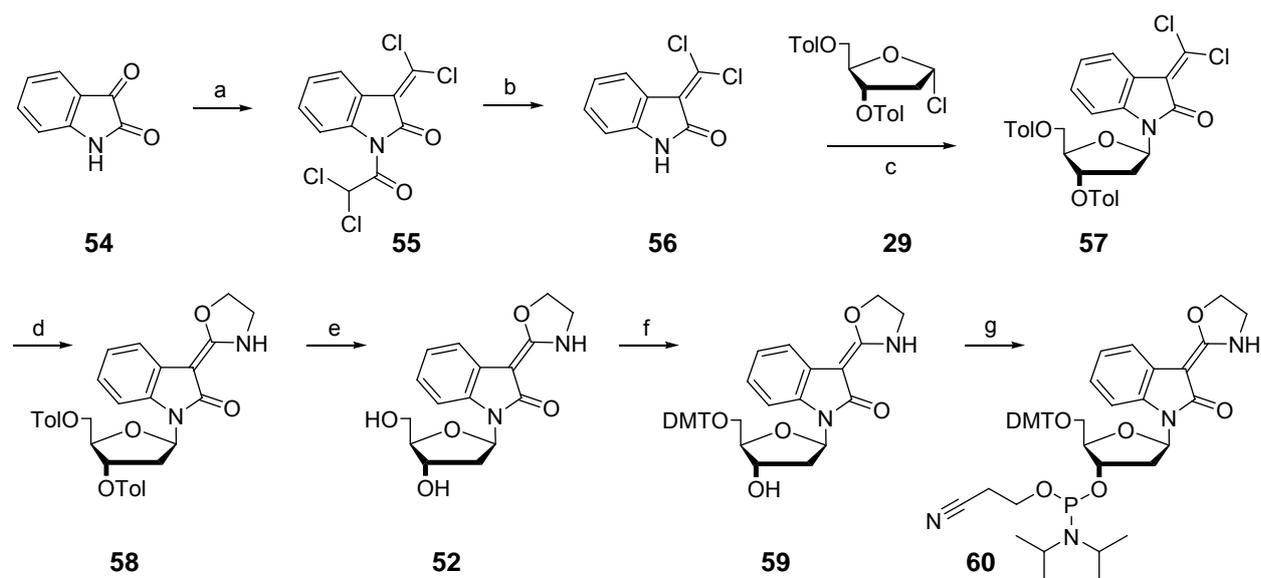
Scheme 11: Synthesis of the 3-(2-oxazolidinylidene-)indol-2-one nucleoside **52** and the corresponding phosphoramidite **60**. a) $CHCl_2COCl$, NEt_3, $CHCl_3$, 20 °C, 1 h, 80 %; b) $NaOH_{(aq)}$, 89 %; c) **29**, DBU, dry MeCN, 17 h, 37 % (18 % β, 19 % α); d) ethanolamine, THF, 35 %; e) K_2CO_3, MeOH, 54 %; f) DMT-Cl, pyridine, 65 %; g) CED-Cl, $NEt(iPr)_2$, THF, r.t., 32 h, yield not determined.

In contrast to the three consecutive steps in the synthesis of the free ligand **53**, the order of the steps for the synthesis of the glycosylated ligand **52** was changed. First, isatin **54** was reacted with a mixture of dichloroacetylchloride and triethylamine in chloroform (which leads to *in situ* formation of dichloroketene) to the acylated dichloromethyleneindolone **55**. Besides the unavoidable acylation of the nitrogen atom, the dichloroketene reacts in a [2+2] cycloaddition with the carbonyl group in 3-position to a spiro-annelated β-lactone, which fragments under cycloreversion and loss of CO_2 to compound **55**. Afterwards, the unwanted dichloroacetyl group is removed from N1 by saponification with aqueous NaOH to yield molecule **56**. The *N*-glycosylation using glycosyl donor **29** and DBU was performed with a total yield of 37 % to give nucleoside **57** (19 % α, 18 % β). Side reactions were not examined but a hydrolysis or polymerization of a fraction of compound **56** is probable. The anomers could be differentiated by the *through space* coupling of the hydrogen atoms at C1', C2' and C3' using ¹H-NOESY-NMR spectroscopy. The closure of the oxazoline ring of molecule **58** by treatment of **57** with ethanolamine in THF yielded the protected ligandoside **58** in 35 % yield. The ring closure was performed after the glycosylation to avoid the regioselectivity problems that were expected when the ligand **53** would have been taken for the reaction (due to its two nucleophilic nitrogen atoms). Deprotection of the sugar hydroxyl group yielded nucleoside **52** and subsequent DMT protection afforded compound **59**.

Interestingly, a protection of the free NH group of molecule **59** (or OH-group of its tautomer) was not possible with a variety of protecting groups (SEM, TES, TIPS). The DMT group could selectively be introduced onto the sugar's 5'-position in moderate yields. However, generation of the phosphoramidite **60** was certainly complicated by the free NH functionality: a mixture of two phosphorylated compounds (each as a mixture of diastereomers) was isolated. Although silica column chromatography of **60** resulted in partial decomposition, it was decided to use the impure phosphoramidite for DNA synthesis. The coupling of the ligand nucleoside was of medium performance and the raw DNA material consisted of a mixture of the expected product and failure sequences.[199]

One hairpin and two complementary single strands containing nucleoside **52** were synthesized, purified by RP-HPLC and characterized by high resolution ESI mass spectrometry (Figure 35).

D28-In-a	5'-CACATTAITGTTGTA-3'
D28-In-b	3'-GTGTAATIACAACAT-5'
D29-In	5'-GTAGAITTTTITCTAC-3'

Figure 35: Duplex **D28-In-a/b** and hairpin **D29-In** containing the 3-(2-oxazolidinylidene-)indol-2-one nucleoside **52** prepared in this work.

According to the standard protocol, the melting temperature was measured in the absence and presence of metal ions (not shown). Even without any metal ions, the melting temperature of the duplex was, with 45.2 °C, 4 K higher than the melting temperature of a similar duplex containing the salicylic aldehyde bases **25** (Chapter 4.4.2). This small effect can be explained with the additional π-surface introduced with the two nucleosides **52**. Unfortunately, addition of metal ions did not alter the melting point of the duplex or the hairpin containing nucleoside **52**. ESI mass spectrometric analysis likewise did not furnish any data supporting a coordination of metal ions by the nucleosides **52**. Figure 36 shows the ESI spectra of the oligonucleotides **D28-In-a/b** and **D29-In**.
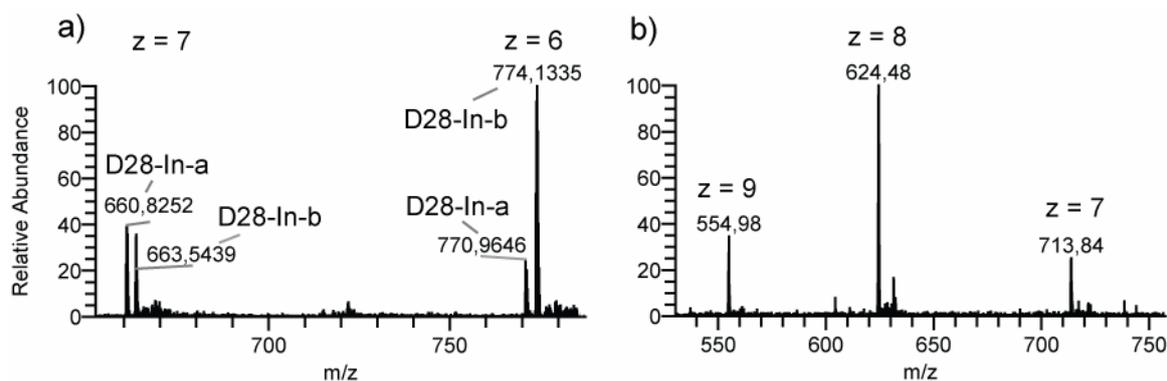
Figure 36: a) ESI mass spectrum of a mixture of **D28-In-a** and **D28-In-b**. The duplex breaks up into its single strand components under ESI conditions. Found for [**D28-In-a**-7H$^+$]$^{7-}$:660.5391; calculated for [$C_{154}H_{185}N_{50}O_{91}P_{14}$]$^{7-}$: 660.5382; found for [**D28-In-b**-7H$^+$]$^{7-}$:663.1140; calculated for [$C_{154}H_{183}N_{56}O_{87}P_{14}$]$^{7-}$: 663.1129; b) ESI mass spectrum of hairpin **D29-In**. Found for [**D29-In**-8H$^+$]$^{8-}$: 624.2293; calculated for [$C_{170}H_{202}N_{49}O_{100}P_{15}$]$^{8-}$: 624.2281. In both cases, no metal complexation could be observed in the ESI experiments.

The reason for the incapability of the strands **D28-In-a/b** and **D29-In** to coordinate metal ions might be that the nucleobases **52** exist in a conformation with the benzene rings pointing away from the sugar moieties into the middle of the DNA duplex. This means that the potentially coordinating parts of the molecules are not facing each other in the DNA duplex and a metal ion cannot be coordinated between the complementary strands.

4.2.5 Synthesis of 3'-O-methylxylose-based *C*-nucleosides

Scientists have over the years introduced modifications into the backbone of oligonucleotides for several reasons (Chapter 3.2).[200,201,202] In the course of investigating the early chemical evolution of life, *Eschenmoser et al.* posed the question as to why ribofuranose was chosen by nature as the building block of nucleic acids. Thereafter, various oligonucleotides with backbones consisting of threofuranose (TNA),[203,204] different pentofuranoses, pentopyranoses[202,205,206,207,208] and hexopyranoses[202] were systematically synthesized and examined. From an evolutionary point of view, TNA is very exciting as it could have been formed by abiotic processes with a high probability and is able to hybridize to RNA. In contrast to the hexopyranosyl nucleic acids, which show bad performance in specific base pairing, the pentopyranosyl nucleic acids are able to form double strands with interesting properties. The repetitive monomers of four different pentopyranosyl nucleic acids are depicted in Figure 37.

β-D-Ribopyranosyl   β-D-Xylopyranosyl   α-L-Lyxopyranosyl   α-L-Arabinopyranosyl
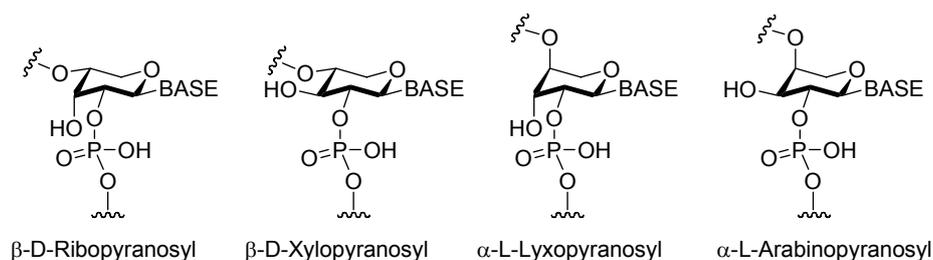
Figure 37: The four different pentopyranosyl (4'→2') backbone sugars examined by *Eschenmoser*.

Remarkably, double strands consisting of one of the above mentioned pentopyranosyl nucleic acids have higher stabilities and pair with higher selectivity than pentofuranosyl nucleic acids (RNA, DNA).[206,207] The duplex structure of these systems differs significantly from RNA or DNA structures which was shown by *Schlönvogt et al.* in NMR experiments.[209] The crystal structure of an octameric hexopyranosyl duplex was recently determined by *Egli et al.*[210]

Homoduplexes between complementary pentopyranosyl oligonucleotides are almost linear with only a slight left handed helicity. Single stranded pentopyranosyl oligonucleotides are not able to form hetero duplexes with DNA or RNA so they make up a base pairing system which is orthogonal to the natural oligonucleotides. These interesting features of the pentopyranosyl nucleic acids made *Eschenmoser* and others believe that they may be well suited candidates for the development of new nucleic acid-based nano materials.[208]

In the research group of *Carell* several attempts were performed to synthesize pentopyranosyl oligonucleotides for the linear arrangement of multiple redox-active flavin functionalities for the generation of molecular wires.[211, 212, 213]

Of interest up to now was the functionalization of methylxylose-based oligonucleotides with the ligands introduced in Chapters 4.2.1 - 4.2.4 to generate hypermodified oligonucleotide structures that combine the concepts of metal base pairs with the properties of the pentopyranosyl nucleic acids. Compound **61** was chosen as the target of synthesis (Figure 38).
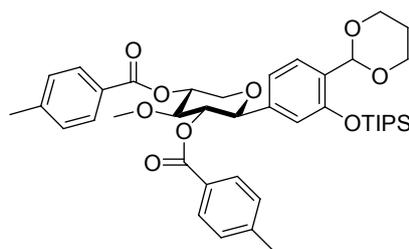
Figure 38: The protected salicylic aldehyde substituted methylxylose sugar **61** as a synthetic goal.

The synthesis of the fully protected methylxylose sugar **62** which was the starting material for the glycosylation experiments was carried out according to the procedure described by *Behrens* (Scheme 12).[211]
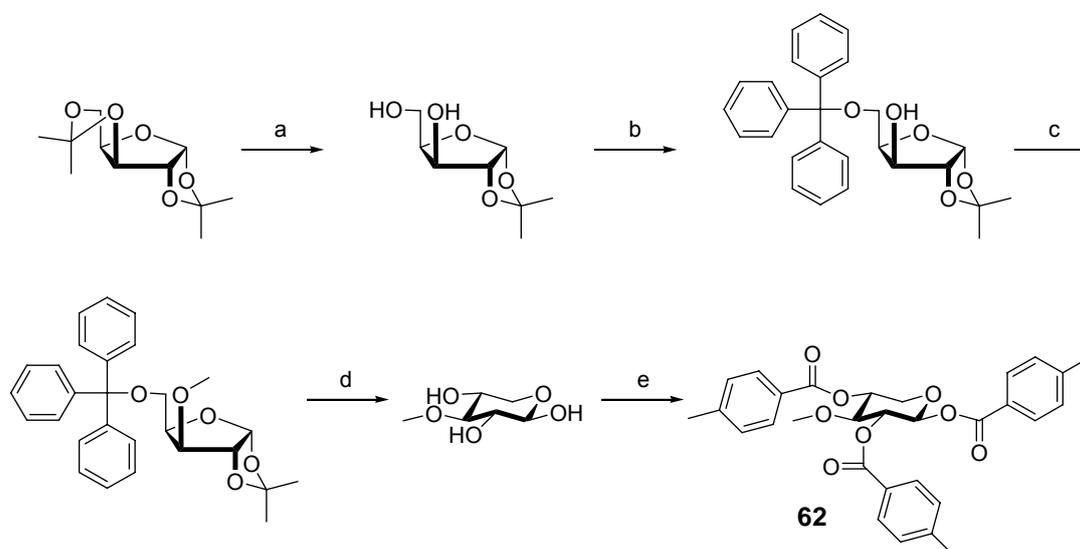
Scheme 12: Synthesis of 3'-*O*-methyl-1',2',4'-tri-*O*-toluoylxylose **62**. a) AcOH : HCO$_2$H : H$_2$O = 10 : 4 : 3, 93 %; b) tritylchloride, NEt$_3$, pyridine, 90 %; c) MeI, NaOH, DMSO, 92 %; d) 90 % TFA, 95 %; e) TolCl, DMAP, pyridine, 61 %.

A glycosyl donor moiety suitable for the cuprate-based *C*-glycosylation with the ligands according to the protocols described in Chapter 4.2.1 had to be synthesized. The first choice was a glycosyl chloride similar to the 2'-deoxyribosyl chloride **29**. For its synthesis, a special protocol for the C1'-chlorination of the fully toluoyl protected compound **62** was chosen, which did not require the use of gaseous HCl. This method uses an excess of dichloromethyl-methylether and a catalytic amount of zinc chloride and yielded methylxylosyl chloride **63** in good yields and purity.[214]

The preparation of the corresponding glycosyl bromide **64** was undertaken when the rather low reactivity of chloride **63** in the *C*-glycosylation reactions became evident (see below).[215] Both glycosyl halides exist according to their ¹H-NMR spectra as single anomers (presumably with α-configuration). The syntheses are depicted in Scheme 13.
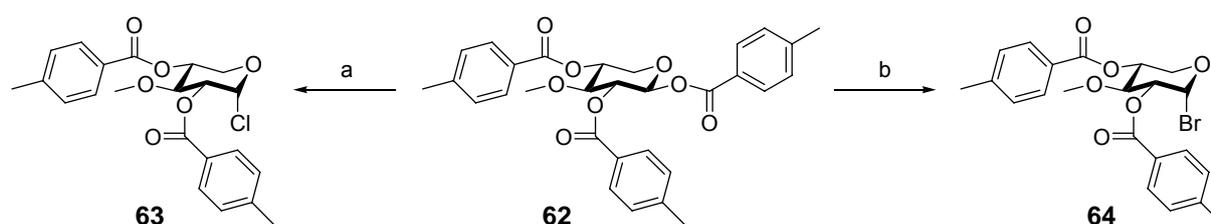
Scheme 13: Synthesis of methylxylosyl chloride **63** (left) and methylxylosyl bromide **64** (right). a) dichloromethyl-methylether, cat. ZnCl$_2$, CHCl$_3$, 62 %; b) Ac$_2$O, CH$_2$Cl$_2$, 33 % HBr in HOAc, 59 %.

Both glycosyl halides were examined for their application in the desired *C*-glycosylation. It was found that xylosyl chloride **63** is much less reactive towards aromatic cuprate reagents at the usually very low reaction temperatures (− 78 °C) compared to the ribosyl chloride **29**.

This was recognized to be a serious problem for carrying out the *C*-glycosylation with the *Gilman*-cuprate **37** derived from the brominated ligand **28**: at the low reaction temperatures which were sufficient for the cuprate couplings with **29**, methylxylosyl chloride **63** did not react at all with the ligand cuprate. When the temperature was carefully raised to 0 °C, only decomposition products of the cuprate (dimerized ligand, hydrolysis products; see Figure 25) were observed but the glycosyl chloride **63** remained unreacted. A model reaction for the cuprate coupling to **63** was subsequently carried out (Scheme 14).
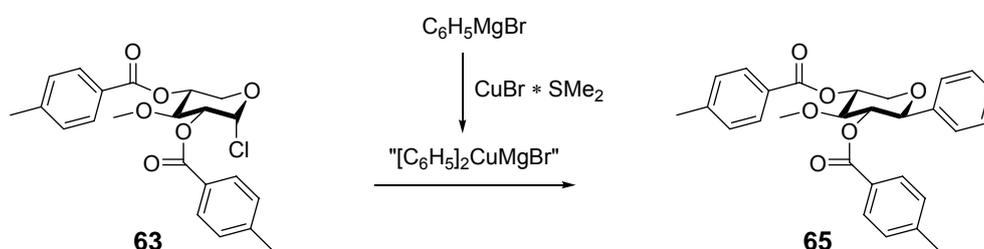
Scheme 14: C1'-phenylation of **63** as model reaction for the introduction of a ligand by a metal-organic *C*-glycosylation (Solvent: THF, yield 80 %).

In this case, a *Normant*-cuprate (= Grignard reagent-derived cuprate) was used instead of a *Gilman*-cuprate (= organolithium reagent-derived cuprate) because *Normant*-cuprates are known for their higher thermal stability. In this model reaction, an unsubstituted phenyl ring was chosen as the residue which was to be coupled to the sugar C1'-atom. The cuprate coupling was then carried out at higher temperatures (0 °C) with the *Normant*-reagent, which was obtained after transmetallation of the freshly prepared phenyl-*Grignard* reagent C_6H_5MgBr onto CuBr • SMe$_2$ in THF.

In this instance, the cuprate coupling proceeded smoothly and the product 3'-*O*-methyl-1'-phenyl-2',4'-di-*O*-toluoyl-D-xylopyranose **65** could be obtained. The β-nucleoside β-**65** crystallized from the solvent (EtOAc : hexane) immediately after column chromatography to give long, colorless needles. An X-ray structure of β-**65** confirmed the β-configuration at C1' and the exact constitution with the phenyl ring attached to the sugar C1'-atom (Figure 39).
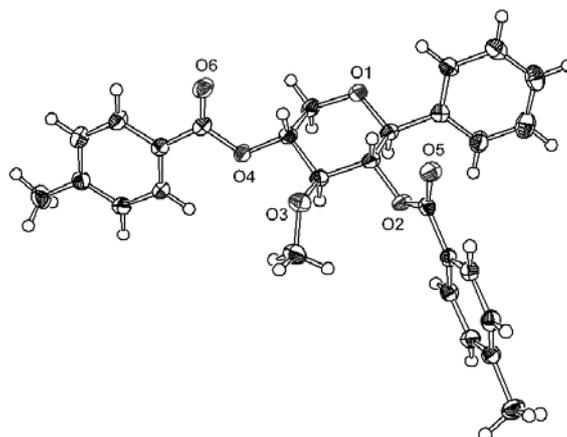
Figure 39: X-ray structure of the toluoyl protected C-glycoside **65**.

Subsequently, glycosyl bromide **64** (Scheme 13) was synthesized, which is much more reactive towards nucleophilic substitution than chloride **63**. This was also expressed by its instability against hydrolysis. Compound **64** had to be freshly prepared and could only be used as a crude material (purity by NMR ≈ 90 %) because it did not survive column chromatography.

Now, the cuprate coupling of **37** with **64** led to the formation of the desired ligand-substituted methylxylose nucleoside β-**61** and its α-anomer but in low yields (29 % anomeric mixture) and partial cleavage of the acetal protecting group (Scheme 15).
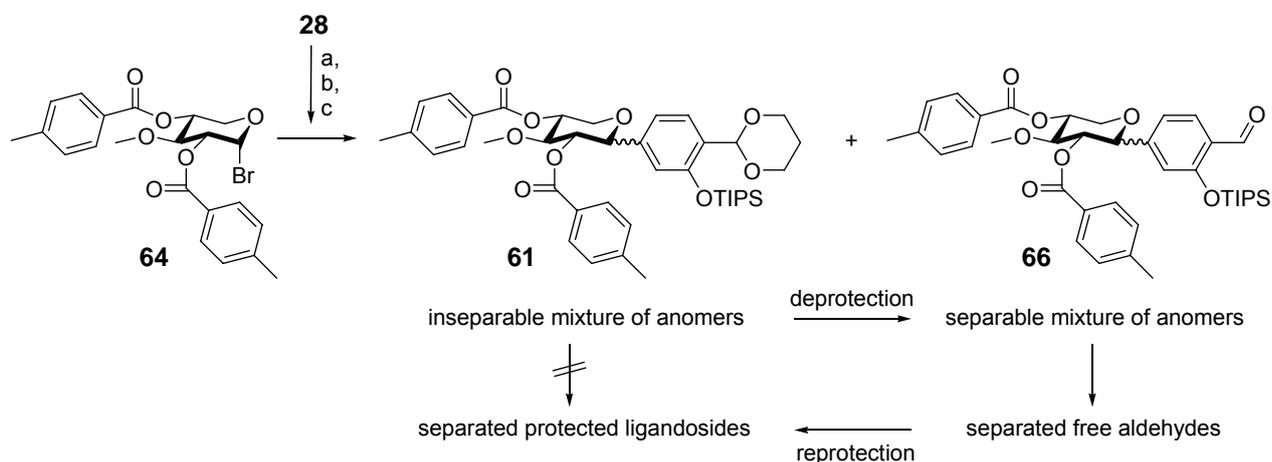
Scheme 15: Synthesis of the ligand-substituted methylxylose nucleoside **61** and partial cleavage of the acetal to the aldehyde **66** (both as α/β mixtures). A successful strategy for the separation of the anomers is schematically shown under the structures. a) **28**, 2 eq *t*-BuLi, Et$_2$O, − 78 °C, 2 h; b) CuBr · SMe$_2$, − 78 °C to − 30 °C, 20 min; c) **64**, CH$_2$Cl$_2$, 12h, − 78 °C to r.t.

It proved to be difficult to separate the fully protected anomers by column chromatography, but the isolated anomeric mixture of the corresponding deprotected aldehydes α-**66** and β-**66** could be easily separated by silica gel flash

chromatography. By first deprotecting the aldehydes, separation of anomers and finally reprotecting the aldehydes as cyclic acetals, the desired nucleoside anomers α-**61** and β-**61** were obtained in pure form (but in very low quantities). The configuration at the sugar C1'-atom was assigned by a comparison of the ^{1}H-NMR spectra of the free aldehydes α-**66** and β-**66** with the ^{1}H-NMR spectrum of the model compound β-**65** whose stereochemistry was assigned by X-ray crystallography (Figure 40).
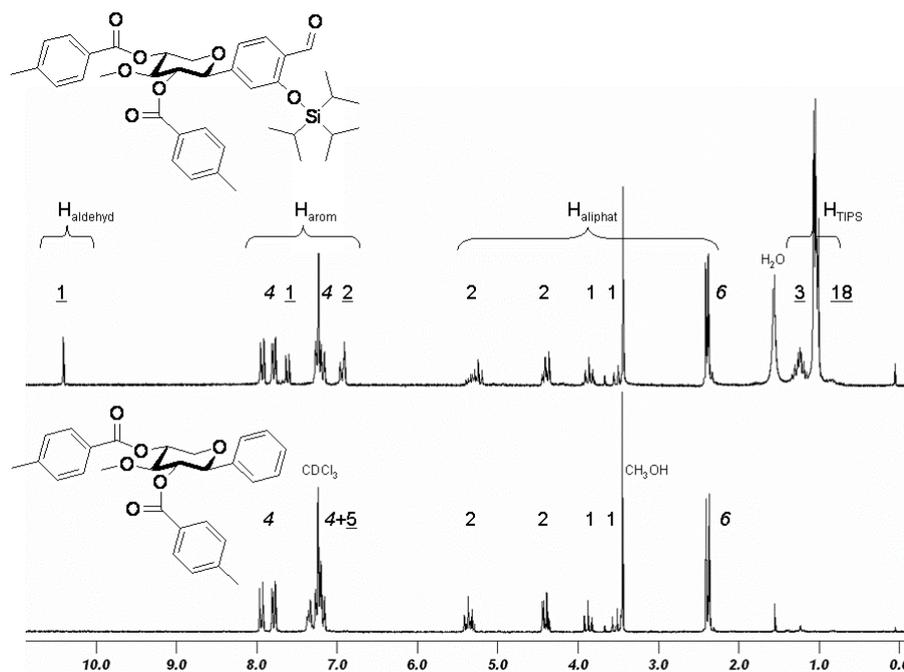
Figure 40: Indirect assignment of the configuration of salicylic aldehyde **66** (and consequently of the fully protected synthetic target **61**) by comparison of the ^{1}H-NMR spectra of the free aldehyde β-**66** (top) with the model compound β-**65** (bottom). The configuration of β-**65** was assigned by X-ray crystallography. The numbers indicate the relative integral size (underlined = ligand, italic = toluoyl, normal font = sugar; 200 MHz, $CDCl_3$; scale in ppm).

In conclusion, it could be shown that the desired ligand-modified methylxylose nucleoside β-**61** can be synthesized, although optimization of the purification process and of the yields is still required. A preparation of methylxylose-based oligonucleotides carrying multiple metal-salen complexes promises to be possible with this approach. Parallel efforts by co-workers in the *Carell* group on the difficult methylxylose chemistry have, however, shown that the production of intact oligonucleotides in fair yields is very time consuming and often even unsuccessful. Furthermore, the success of the metal-salen base pair concept in double stranded 2'-deoxyribosyl nucleic acids shifted the focus away from methylxylose-based oligonucleotides (see following Chapters).

4.3   Incorporation of the salicylic aldehyde nucleoside into oligonucleotides

4.3.1 Automated DNA synthesis

The DNA oligonucleotides were synthesized on a PerSeptive Biosystems Expedite 8900 Synthesizer and an *Äkta Oligopilot 10* (Amersham Biosciences) using *Ultramild Bases* (Glen Research) and following standard phosphoramidite protocols for the solid support oligonucleotide synthesis. The coupling times for the ligand nucleosides were similar to the coupling of the normal bases. The use of controlled pore size glass beads (CPG) as solid support material was found to give the desired oligonucleotides in better yields and with higher purities compared to polystyrene resin. This effect may be assigned to the very unpolar character of the tri-*iso*-propylsilyl protected salicylic aldehyde monomer, which may lead to an unfavorable interaction of the free phosphoramidite or of the growing DNA strand with the unpolar polystyrene matrix during the coupling reaction. A similar effect is known for solid phase synthesis of polypeptides carrying many unpolar residues. Details about the DNA synthesis procedure are given in the experimental section of this work, the process of automated oligonucleotide synthesis in general is reviewed elsewhere.[216] The oligonucleotide synthesis was monitored online by measurement of the UV-Vis absorption of the reagents leaving the solid support cartridge: Every consecutive coupling step finishes with the cleavage of the 5'-DMT protecting group ("detritylation"). At $\lambda = 500$ nm, this process can be monitored due to the strong absorption of the deeply red 4,4'-dimethoxytrityl cation, which is released upon acidic cleavage of the DMT group.

For this work, modified oligonucleotides carrying up to ten artificial nucleobases were synthesized, so an excellent coupling fidelity of the modified nucleoside in the automated synthesis was important to be able to produce full length oligonucleotides in high yields and purities. A representative chart of the trityl-values (absorption at $\lambda = 500$ nm) along with an online conductivity measurement during the synthesis of the oligonucleotide 5'-GCGCG**LLLLLLLLLL**GGCCG-3' (**D19-L-a**) on the DNA synthesizer Äkta Oligopilot 10 is depicted in Figure 41. Similar heights of the trityl- and conductivity-peaks throughout the synthesis of this 20mer oligonucleotide

containing 10 consecutive ligand nucleobases **25** indicated a successful synthesis (prior to the following characterization by HPLC and mass spectrometry).

Figure 41: Online monitoring of the synthesis of **D19-L-a**. Large black peaks: Detritylation signals (λ = 500 nm).

A listing of all DNA strands containing the salicylic aldehyde nucleobase **25** (**L**) synthesized for this work is given in Table 3. Figure 42 shows the two modifications that were incorporated into the oligonucleotides.

Figure 42: The salicylic aldehyde nucleobase **L** (left) and the 1',2'-dideoxyribose spacer **D** (right).

No.	Sequence[a]	Chap.	No.	Sequence	Chap.
D1-L[b]	5'-TGTACG**L**CGTACA-3'	4.4.2.2, 4.5.1.1	D9-L-a D9-L-b	5'-CACATT**LL**TGTTGTA-3' 3'-GTGTAA**LL**ACAACAT-5'	4.4.2.4 4.4.6
D2-L[b]	5'-GTA**L**AGTTTTCT**L**TAC-3'	4.4.2.2	D10-L-a D10-L-b	5'-CACATT**L**A**L**GTTGTA-3' 3'-GTGTAA**L**T**L**CAACAT-5'	4.5.3
D3-L[b]	5'-GTAGA**L**TTTT**L**TCTAC-3'	4.4.2.2	D11-L-a D11-L-b	5'-CACATT**L**G**L**GTTGTA-3' 3'-GTGTAA**L**C**L**CAACAT-5'	4.5.3
D4-L-a[c] D4-L-b	5'-CACATTA**L**TGTTGTA-3' 3'-GTGTAAT**L**ACAACAT-5'	4.4.2.3 4.4.6	D12-L-a D12-L-b	5'-CACATT**LDL**GTTGTA-3' 3'-GTGTAA**LDL**CAACAT-5'	4.5.3
D5-L-a D5-L-b	5'-CACATT**LD**TGTTGTA-3' 3'-GTGTAA**DL**ACAACAT-5'	4.5.1.2	D13-L-a D13-L-b	5'-CACAT**L**AAT**L**TTGTA-3' 3'-GTGTA**L**TTA**L**AACAT-5'	4.5.3
D6-L-a D6-L-b	5'-CACATT**LDD**GTTGTA-3' 3'-GTGTAA**DDL**CAACAT-5'	4.5.1.2	D14-L-a D14-L-b	5'-CGGA**L**GAC**L**AGCG-3' 3'-GCCT**L**CTG**L**TCGC-5'	4.4.2.4 4.6.1
D7-L-a D7-L-b	5'-CACATT**DLD**GTTGTA-3' 3'-GTGTAA**DLD**CAACAT-5'	4.5.1.2	D15-L-a D15-L-b	5'-GCGGA**L**GC**L**AGCGG-3' 3'-CGCCT**L**CG**L**TCGCC-5'	4.4.6
D4-L-a D8-L-b	5'-CACATTA**L**TGTTGTA-3' 3'-GTGTA**L**TTACAACAT-5'	4.5.1.2	D16-L-a D16-L-b	5'-CGCGAATTC**L**CG-3' 3'-GCGCTTAAG**L**GC-5'	4.2.2 4.5.4

No.	Sequence	Chap.

D17-L-a[e]
D17-L-a
D17-L-b
D17-L-b[e]
	5'-CTC**L**TGG
	            CGT**L**GTCCTC**L**TGG-3'
	3'-GAG**L**ACCGCA**L**CAG
	                        GAG**L**ACC-5'
		4.5.2

D18-L-a D18-L-b	5'-GCGCG**LLLLL**GGCCG-3' 3'-CGCGC**LLLLL**CCGGC-5'	4.6.2
D19-L-a D19-L-b	5'-GCGCG**LLLLLLLLLL**GGCCG-3' 3'-CGCGC**LLLLLLLLLL**CCGGC-5'	4.4.3.2 4.6.2
D20-L	5'-**LLLLLLLLL**-3'	4.6.2
D21-L-a D21-L-b	5'-GCGCG**TLT**GGCCG-3' 3'-CGCGC**TLT**CCGGC-5'	4.6.3
D22-L-a D22-L-b	5'-GCGCG**TLTLT**GGCCG-3' 3'-CGCGC**TLTLT**CCGGC-5'	4.6.3
D23-L-a D23-L-b	5'-GCGCG**LTTTL**GGCCG-3' 3'-CGCGC**LTTTL**CCGGC-5'	4.6.3
D24-L-a D24-L-b	5'-GCGCG**LTLTLTLTLT**GGCCG-3' 3'-CGCGC**LTLTLTLTLT**CCGGC-5'	4.6.3
D25-L-a D25-L-b	5'-GCGCG**LTTTTLLLLT**GGCCG-3' 3'-CGCGC**LTTTTLLLLT**CCGGC-5'	4.6.3

Table 3: All modified oligonucleotides containing the salicylic aldehyde nucleobase discussed in this work. a) The structures represented by **L** and **D** are depicted in Figure 42; b) Self-complementary single strands capable of forming hairpin structures; c) Strand **D4-L*-a/b** discussed in Chapter 4.4.2.3 contains the isomeric salicylic aldehyde **26** instead of the parental structure **25**.

4.3.2 Deprotection of the incorporated nucleosides

After the automated oligonucleotide synthesis, the DNA strands had to be cleaved from the solid support and all protecting groups had to be removed from the bases and the backbone. In modern DNA synthesis technology based on cyanoethylphosphoramidites, the standard method for both processes is the treatment of the solid-phase bound oligonucleotides with aqueous bases (usually ammonia) for several hours.[216] The incorporated modified nucleoside **27** carries two protecting groups (cyclic acetal and TIPS) which do not occur in unmodified DNA synthesis products. The developed method for the deprotection of the salicylic aldehyde nucleoside **27** is depicted in Scheme 16.
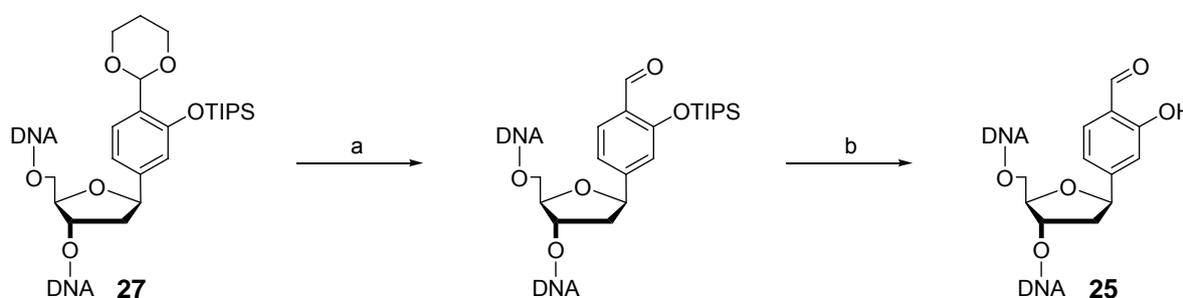
Scheme 16: Deprotection of the ligand precursor **27** in the synthesized oligonucleotides to the salicylic aldehyde **25**. a) 2 % CHCl$_2$COOH + 1 % H$_2$O in CH$_2$Cl$_2$, 1 – 2 h, quant.; b) NH$_{3\ (aq)}$: EtOH = 3 : 1, 8 - 16 h, quant.

The acetal protected aldehyde functionality of **27** was found to be cleaved by treatment with 2% dichloroacetic acid in water-containing dichloromethane, the same reagent which is used for the cleavage of the 5'-DMT protecting groups during DNA synthesis. Therefore, following the synthesis, the resin-bound oligonucleotide was subjected to a slow steady flow of the acid reagent (10 mL / h) for 1 h (one or two ligand nucleosides) or 2 h (more than two ligand nucleosides), respectively. The flow-through method was found to be more effective than treating the resin-bound oligonucleotide with the acid reagent batch-wise in a closed vessel, presumably because steady removal of the released 1,3-propanediol drives the deprotection to completion. The acid treatment was followed by washing the resin with dichloromethane. The acetal cleavage at the solid phase was found to be superior to a deprotection in solution after cleavage of the strands from the resin because the acid treatment of the beads could be more easily controlled. Although acidic cleavage of the acetals in an aqueous solution of the oligonucleotide with acetic acid

is possible, the risk of partly depurinating the strands by this procedure is higher (compare Chapter 4.3.3).

Common fluoride reagents (TBAF in THF, HF in pyridine) in various concentrations were tested for their ability to cleave the silyl protecting group from the modified nucleoside. Although removal of the silyl protecting groups was achieved with these reagents, partly degradation of the oligonucleotides was encountered in some cases. Eventually it was found that even when no extra efforts were undertaken to remove the silyl protecting group from the phenolic oxygen and the resin-bound oligonucleotides were directly subjected to aqueous ammonia, the TIPS group was cleaved. This further simplified the deprotection strategy.

In conclusion, no additional reagent had to be used for the deprotection of the two protecting groups on the modified nucleoside in the DNA strands. The acetal can be cleaved by a prolonged treatment with the acidic detritylation reagent and the tri-*iso*-propylsilyl protecting group on the phenol is cleavable under the standard conditions used to remove the synthesized DNA from the solid support. Because no extra reagents besides the common ones had to be used for the complete deprotection of the oligonucleotides the protocol remained short and simple. Additionally, the risk of harming the DNA strands by treatment with non-standard reagents was prevented in this way.

4.3.3 Chromatographic purification of aldehyde carrying oligonucleotides

Upon treatment of the salicylic aldehyde containing oligonucleotides with aqueous ammonia the solution turned yellow (in contrast to unmodified DNA strands whose solutions are colorless). This phenomenon can be clearly attributed to the salicylic aldehydes and is in fact also observed when an aqueous solution of unsubstituted salicylic aldehyde is treated in the same way. The cause for this color change is either the formation of the salicylic aldimine (salen ligands are likewise deeply yellow) or the deprotonation of the phenolic hydroxyl group or both in combination (Scheme 17).
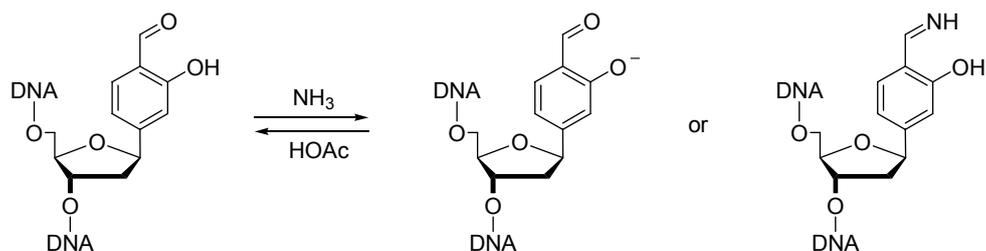
Scheme 17: Possible reactions of the salicylic aldehyde in DNA with aqueous ammonia and reversal of the reaction by addition of excess acetic acid.

The yellow color even remained when the aqueous ammonia was removed *in vacuo* and the oligonucleotides were redissolved in pure water. Although the color change itself did not impose any problems, the interaction of the ammonia with the incorporated salicylic aldehydes lead to the existence of an equilibrium of different species that showed different behavior on the HPLC column. This emerged as a severe complication, especially when more than one ligand was incorporated into one oligonucleotide because the HPL chromatogram then showed broad and multiple peaks in the region where elution of the product was expected (Figure 43a).
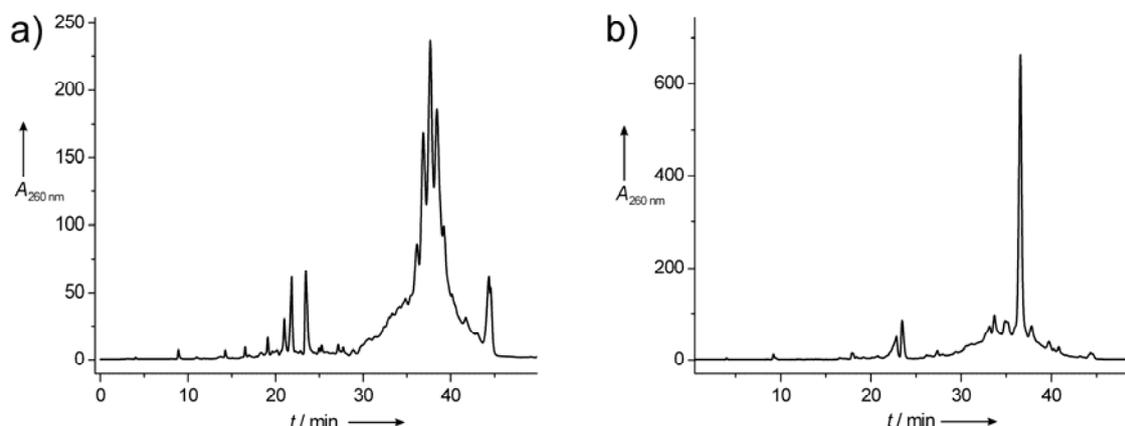
Figure 43: Preparative HPLC runs of the crude strands: a) **D18-L-a** in a solution containing ammonia and b) **D18-L-b** after addition of 20 % HOAc. Eluent: 100 mM NHEt₃OAc in (H$_2$O) : (MeCN : H$_2$O = 8 : 2), gradient: 0 - 40 % MeCN in 40 min, 3μ-RP-C$_{18}$ column.

When the fractions of **D18-L-a** (Figure 43a) that eluated between 35 and 45 min were analyzed by ESI mass spectrometry, all samples contained the desired oligonucleotide **D18-L-a** with the correct mass (presumably formed aldimines were hydrolyzed under ESI conditions). The strong peak broadening complicated the separation of the pure full length product from the shorter failure sequences or the slightly later eluting, incompletely deprotected strands.

This problem could be overcome by the addition of 20 % acetic acid to the aqueous solution of the crude oligonucleotides and incubation for 10 min at 35 °C prior to injection onto the preparative HPLC column. The yellow color of the strands almost completely disappeared and the preparative HPL chromatogram was significantly simplified (shown for the strand **D18-L-b** in Figure 43b). Now, the separation of the desired oligonucleotide product from the side products was feasible but care had to be taken, that the acid treatment was not carried out too long to avoid depurination of the strands (compare Chapter 4.3.2).

Noteworthy is the fact, that the presence of ammonia was no problem when the pH of the solution was near neutrality: The ESI experiments on the salen complex formation were carried out in highly concentrated NH_4OAc buffer (pH 8) without any visible reaction of the strands with ammonia (Chapter 4.4.4). The solutions of the salicylic aldehyde oligonucleotides in the ammonium acetate buffer were almost colorless until ethylenediamine was added (which itself lead to the appearance of a yellow color; Chapter 4.4.3) and ammonia was no competitor of the more nucleophilic ethylenediamine in terms of aldimine formation.

That the salicylic aldehyde function did not react with NH_2-groups of the natural nucleobases by an aldimine formation was supported by mass spectrometry and NMR experiments on mixtures of the four natural nucleosides with salicylic aldehyde. Exemplarily, the HPL chromatogram of the purified fractions of the oligonucleotide **D19-L-b** containing 10 consecutive salicylic aldehyde nucleobases **25** is depicted in Figure 44.
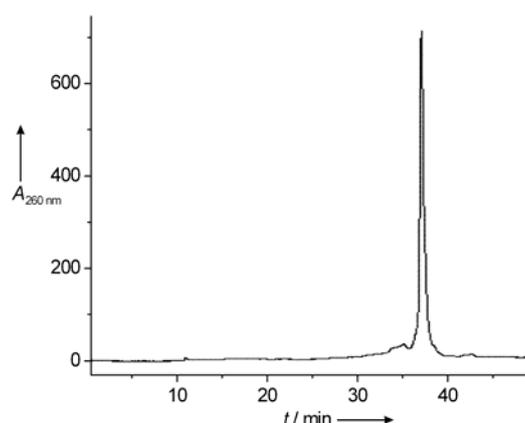
Figure 44: Analytical HPL chromatogram of the purified 20mer **D19-L-b** containing 10 consecutive modified bases **25**. Eluent: 100 mM $NHEt_3OAc$ in $(H_2O) : (MeCN : H_2O = 8 : 2)$, gradient: $0 - 40$ % MeCN in 40 min, 3μ-RP-C_{18} column.

Following chromatographic separation, the oligonucleotides were freed from remaining HPLC buffer (NEt$_3$OAc) and other ubiquitous ions by desalting with C-18 *Sepac*® reverse-phase cartridges. Besides the unavoidable contamination with Na$^+$, K$^+$ and NHEt$_3^+$ the ESI-MS experiments sometimes indicated contamination of the salicylic aldehyde containing oligonucleotide solutions with Fe^{3+} which was likewise effectively removed by the desalting step.

The concentration of the synthesized single strands was determined by UV spectrometry taking into account the extinction coefficient of the free salicylic aldehyde nucleobase, which was determined by UV spectroscopy.

4.4   Assembly of the metal-salen base pair

4.4.1 Hybridization and reaction with amines and metal ions

The formation of a double helical duplex from two complementary oligonucleotides by the action of π-stacking forces and hydrogen bonds is known as hybridization. It was anticipated that the salicylic aldehyde modified oligonucleotides should be subjected to hybridization prior to the planned salen complex formation to ensure perfect preorganization of the ligand precursors in the double helix. The melting temperatures of all synthesized duplexes were determined by temperature dependent UV spectroscopy (Chapter 4.4.2) and the complexation experiments were performed at temperatures at least 10 K under the estimated melting temperature after hybridization of the strands.

The sequences of the synthesized strands were initially chosen to arrange the salicylic aldehydes in strand and counterstrand directly facing each other like depicted in Figure 45. It was later found out that the arrangement of the ligand precursors in the double helix can in fact be handled more flexible and metal salen complexes are even formed when the helix structure is disturbed (Chapter 4.5.1.2). The interplay of salen complex formation and the DNA sequence is discussed in Chapter 4.5 for different cases.
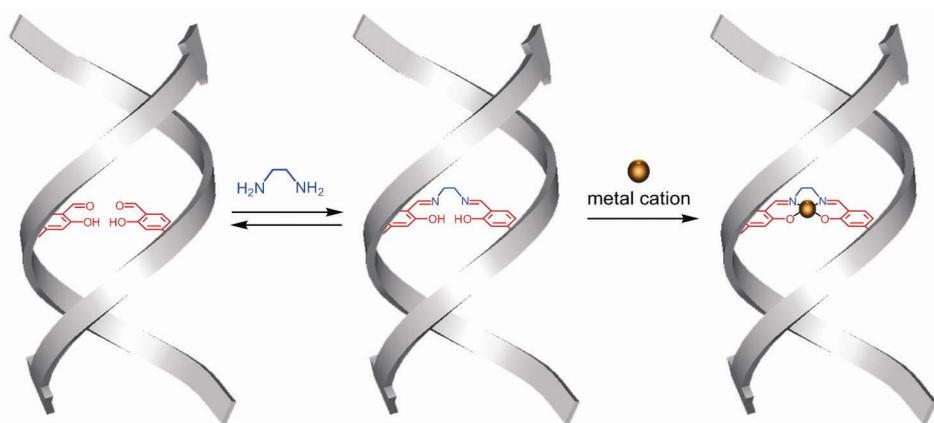
Figure 45: Depiction of the two-step assembly process of the metal-salen base pair inside the DNA duplex comprising first the reversible condensation of both facing salicylic aldehydes with one molecule of ethylenediamine and secondly the complexation of the metal ion to the stable salen complex.

In contrast to all other metal base pairs known in literature, the formation of the metal-salen base pair in DNA requires the addition of two further components to the hybridized double strand.

The first component is a diamine (here mostly ethylenediamine, abbreviated as en) which reacts with both oppositely arranged salicylic aldehydes in an equilibrium reaction to give the salen ligand inside the duplex (Figure 45 middle). In water, however, the salen ligand is unstable towards hydrolysis (see experiments in Chapter 4.4.2).

The second additive is a metal ion with an affinity to be complexed by the salen ligand (here examined: Cu^{2+}, Mn^{3+}, VO^{2+}, Fe^{3+}, Ni^{2+}, Zn^{2+}).

It was shown that the assembly of the salen complex inside DNA proceeds cooperatively. The diamine is first needed to form the ligand, while the coordinated metal prevents subsequently the hydrolysis of the formed imines (Chapter 4.4.2). This feature is a significant difference between all previously reported metal-base pairs and the salen concept. A covalent crosslink of both DNA single strands is combined with the metal complexation event.

The different experiments described in the following Chapters required different sample preparations in terms of DNA concentration, type and concentration of buffer and salt additive (which is needed for the backbone charge neutralization). A careful sample preparation was found to be very important to avoid reagent incompatibilities and to preserve reproducibility. Table 4 summarizes different sample preparations.

Experiment	DNA conc.	Buffer and conc.[a, b]	Salt and conc.[a]	Comment
Melting curves	2 μM – 6 μM	M.d., 10 mM	M.d., 10 mM-150 mM	OD at 260 nm should be < 1
CD/UV < 300 nm	2 μM – 6 μM	M.d., 10 mM	M.d., 10 mM-150 mM	OD at 260 nm should be < 1
CD/UV > 300 nm	10 μM – 30 μM	M.d., 10 mM	M.d., 10 mM-150 mM	OD at 350 nm should be < 1
HPLC	10 μM – 30 μM	M.d., 10 mM	M.d., 10 mM-150 mM	-
ESI	30 μM – 300 μM	NH_4OAc, 100 mM		Na^+, K^+… must be avoided
EPR	300 μM – 3 mM	NH_4OAc, 100 mM		Paramagnetic impurities must be avoided

Table 4: Different sample preparations for the different experiments carried out with the modified oligonucleotides containing one or more salicylic aldehydes. a) M.d. = Metal dependent. Buffers: CHES for Cu^{2+}, HEPES for Mn^{2+}, MOPS for Hg^{2+}. Salts: NaCl for all metals except for Hg^{2+}: $NaClO_4$ or $NaNO_2$; b) buffer pH must allow existence of the transition metal ions in solution without precipitation.

Special care had to be taken that certain additives do not react with the examined metal ions by complexation or precipitation. No buffers could be used that can act as chelate ligands themselves (like e.g. TRIS = tris(hydroxymethyl)aminomethane) because they reduce the effective concentration of free metal ions available for the complexation by the salen ligand. Furthermore, many premixed buffer formulations used in biochemistry contain EDTA, which is of course detrimental to the examined complexation experiments.

In the cases where the soft Hg^{2+}-ions were complexed by the DNA duplexes (Chapter 4.6), chloride was substituted by non-coordinating anions like nitrate or perchlorate. Manganese and iron ions were introduced as the doubly charged cations Mn^{2+} and Fe^{2+}, respectively, but they are known to be oxidized to Mn^{3+} and Fe^{3+} upon complexation under aerobic conditions. Some metals require a certain pH range to avoid precipitation of their hydroxides or oxides.

The studied metals were usually used in form of their sulfates. Stock solutions in bidest. water were stored in plastic vessels (Eppendorf) at room temperature and checked for precipitation prior to use.

Contamination with unwanted metals was avoided by using only analytical grade reagents ("puriss") and bidest. water for setting up all solutions. A need to treat the reagents with solid phase bound chelating reagents (Chelex 100) prior to use as

described by Schultz[117] and also by Tor[128] to remove contaminating metal ions was found to be not necessary (checked by high resolution mass spectrometry). In contrast, the use of Chelex 100 resin was rather found to be problematic because it releases its chelate ligands into the solution by a leaching process.

Diamine stock solutions were always freshly prepared in bidest. water because ethylenediamine is known to react with carbon dioxide to form (cyclic) urea derivatives.[217] Because the reaction of the diamine with the salicylic aldehydes is an equilibrium process, an excess of ethylenediamine (about 30 equivalents) was added to the hybridized DNA. The conversion into the salen ligand was finished within 30 minutes at room temperature accompanied by a color change to yellow (Chapter 4.4.3).

Subsequently, a solution of the examined metal ions was added and the sample was again incubated for at least 15 min (see titrations in Chapter 4.4.3) but usually for several hours. In most cases, the prepared samples were stable for several weeks.

For the duplexes containing only one pair of facing salicylic aldehydes, simultaneous addition of diamine and metal ions was no problem, but for duplexes containing more than one pair of salicylic aldehydes the order and time frame of the additions was found to be important (more information on this matter is discussed in Chapter 4.5.3). Examples of the reaction of different diamines (but also monoamines) and various metal ions with the oligonucleotides introduced in Table 3 (Chapter 4.3.1) and their characterization by thermal de- and renaturing studies, UV-Vis and CD-spectroscopy, mass spectrometry and some other techniques is discussed in the following Chapters.

4.4.2 Melting point studies

4.4.2.1 Introduction to melting point experiments

In order to determine the thermal stability of DNA duplexes containing the ligand precursor **25**, melting point measurements in the absence and presence of diamines and metal ions were performed.

The optical density of oligonucleotide solutions at λ = 260 nm is different for single strands and double strands, respectively.[1] Double strands have a lower extinction coefficient at λ = 260 nm than the corresponding mixture of single strands because the absorption of the bases' aromatic systems is quenched by the stacking

interactions in the double helix. When the temperature of the sample is raised above a temperature specific for the examined length and sequence (and conditions) the duplexes break up into the single strands ("melting") and the height of the UV absorption maximum increases ("hyperchromicity"). The "melting point" (T_M) of an oligonucleotide duplex is defined as the transition point of the absorption at λ = 260 nm plotted against the temperature (see examples below).

A highly simultaneous melting of the duplex is indicated by a sharp transition of the sigmoid melting curve, whereas the transition of the curve is flattened out when the examined process proceeds over a wider temperature (and time) frame. Details on the exact conditions of the experiments are given in the experimental section.

The discussed examples clearly show that the assembly of the metal base pair inside the DNA duplex was accompanied by a significant change in the melting temperature of the whole system. Selected melting profiles are discussed in more detail in the following paragraphs. A comprehensive list of melting points of the synthesized strands is given in Table 5 at the end of the Chapter.

4.4.2.2 Melting point experiments with hairpin structures

Initially, it was tried to use the palindromic DNA sequence **D1-L** (5'-TGTACG**L**CGTACA-3') carrying the salicylic aldehyde in the middle of its sequence to assemble a metal-salen base pair inside the homoduplex formed by the strands. However, it turned out that the oligonucleotide **D1-L** did not hybridize to form a double strand but instead gave a hairpin structure with the salicylic aldehyde uncomplexed in its loop. This was deduced from the observation of a concentration-independent melting point, which is typical for hairpins (because of the low entropic contribution to the free enthalpy of the melting process). Furthermore, addition of ethylenediamine and metal ions did not alter the melting temperature of the strand **D1-L** (see Chapter 4.5.1.1, Figure 69).

In contrast, the hairpins **D2-L** and **D3-L** which contain two salicylic aldehydes facing each other in their stem region are able to form an intramolecular metal-salen complex. Their melting profiles showed significant differences in absence or presence of ethylenediamine and the examined metal ions (Figure 46).
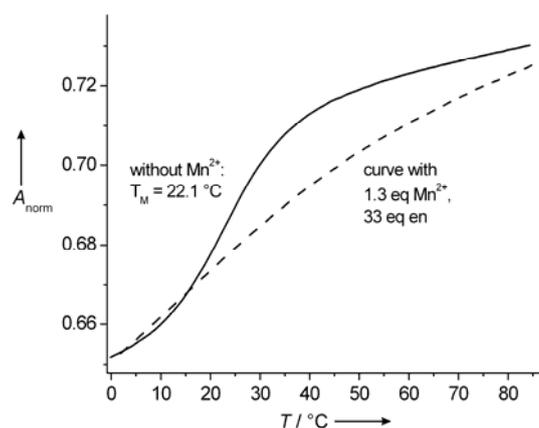
Figure 46: Melting profiles of the hairpin **D2-L** (3 μM) without and with 100 μM en and 4 μM Mn^{2+}.

The depicted melting curve is typical for hairpins. Without metal ions, a distinct melting point can be observed although the transition of the curve is broader as it is in the case of DNA double strands (see following Chapters). After assembly of the metal salen complex inside the DNA hairpin, the melting curve shows a more or less uniform rising instead of a clear transition point. Because this circumstance complicated a simple quantification of the melting curve experiments, more attention was given to oligonucleotide duplexes which are discussed in the next Chapter.

The lack of a clear melting point in the hairpins [**D2-L**+en+M] and [**D3-L**+en+M] containing a metal-salen complex is thought to result from the very high stability of the metal complex in the hairpin structure. Temperature dependent circular dichroism spectroscopy of the hairpin samples indicated, that even at high temperatures (> 80 °C) the metal salen complexes can stay intact inside the hairpin structures (Chapter 4.4.3). The correct assembly of salen complexes in **D2-L** and **D3-L** with different metals was proven by ESI mass spectrometry (Chapter 4.4.4).

4.4.2.3 Melting point experiments with DNA duplexes containing one pair of salicylic aldehydes

Most of the experiments on the metal-salen base pair were carried out with the duplex structure **D4-L-a/b** depicted in Figure 47 whose sequence was chosen according to the work of Shionoya et al. for the sake of comparability.

5'-CACATTA**L**TGTTGTA-3'
3'-GTGTAAT**L**ACAACAT-5'

Figure 47: Sequence of the DNA duplex **D4-L-a/b**.

Figure 48 displays a comparison of the melting curves of different duplexes of the type **D4-a/b** with different combinations of the ligand **25** (here "**L**") opposite the natural nucleobases (e.g. in **D4-A-a/-L-b** the strand **a** contains an adenine (A) instead of **L** and so on).
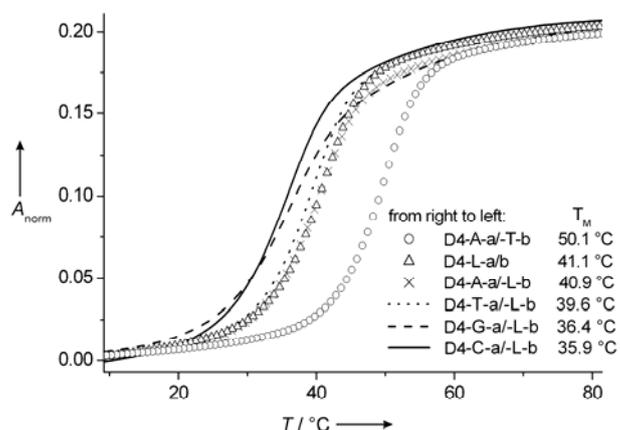
Figure 48: Graphical comparison of the melting curves of the sequence **D4** containing either an **AT** base pair, two facing ligands **LL** or a combination of ligand **L** opposite the four natural bases **A**, **T**, **G** and **C** (3 μM DNA, 150 mM NaCl, 10 mM TRIS buffer).

Under the chosen conditions (3 μM DNA, 150 mM NaCl, 10 mM buffer, details see Table 5) the unmodified double strand **D4-A-a/-T-b** containing an **AT**-base pair instead of the ligands **L** has a melting point of 50.1 °C. The salicylic aldehyde base pair (**LL**) in duplex **D4-L-a/b** was found to decrease the melting point by 9.0 K to 41.1 °C. The combinations of one ligand **L** opposite any of the natural bases **A**, **T**, **G** and **C** lead to an even higher destabilization as can be seen in Figure 48. The following diagram shows the effect upon addition of ethylenediamine (en) and/or copper(II) to duplex **D4-L-a/b**.
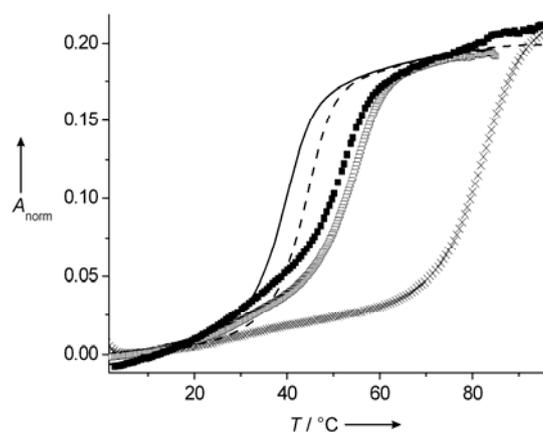
Figure 49: Graphical comparison of the melting curves of the sequence **D4-L-a/b** (1) without any additives (39.9 °C, solid line); (2) with only ethylenediamine (45.5 °C, dashed line); (3) with methylamine and Cu^{2+} (52.3 °C, black boxes); (4) with only Cu^{2+} (54.9 °C, open boxes) and (5) with ethylenediamine and Cu^{2+} (82.4 °C, crosses) (3 μM DNA, 150 mM NaCl, 10 mM CHES buffer).

Addition of an excess of ethylenediamine (en) to a solution containing the DNA duplex **D4-L-a/b** caused an increase of the melting temperature by 4.8 K. This stabilizing effect due to the crosslinking of both strands by the ethylenediamine is, however, surprisingly small. The reason is, that formation of the imine linkage in water is highly reversible, causing rapid hydrolysis of the crosslink during the melting point experiment.[218]

Experiments in which only Cu^{2+} (and no ethylenediamine) was added, are worth to be discussed in more detail for duplex **D4-L-a/b** and the similar sequence **D4-L*-a/b** containing the isomer **26** of the salicylic aldehyde **25** (see Figure 50 and Chapter 4.2.1).[166]

25   **26**

Figure 50: The two isomeric salicylic aldehyde nucleobases **25** and **26**.

As was mentioned before, the metal-salen complex **23** based on nucleoside **25** was expected to fit better into the DNA duplex than complex **24** based on nucleoside **26**. The better geometrical fit of the salen-complex that is generated from nucleobase **25** is particularly obvious after addition of only Cu^{2+} ions (no ethylenediamine). Only the perfectly preoriented system **D4-L-a/b** accepts the metal, resulting in a strong stabilization. Duplex **D4-L*-a/b**, in contrast, shows no stabilizing effect upon addition of Cu^{2+} ions, indicating that in a duplex where two salicylic aldehydes **26** (here **L***) face each other as a base pair, metal coordination in between is impossible. However, addition of ethylenediamine and copper results in dramatic melting point increases for both duplexes showing the strong cooperativity of the complex formation in DNA. The complexed metal prevents the hydrolysis of the imine bonds. The stability of the rigid salen complex is so dominating, that its formation occurs even when the preorganization of the salicylic aldehyde precursors in DNA is not optimal (as in duplex **D4-L*-a/b**). These observations are displayed in Figure 51.

Figure 51: Comparison of the thermal stability of the duplexes **D4-L-a/b** (open columns) and **D4-L*-a/b** (striped columns) with addition of ethylenediamine and/or Cu^{2+}

In the case of duplex **D4-L-a/b**, the addition of ethylenediamine plus one equivalent of Cu^{2+} induced a shift of the melting temperature to 82 °C by more than 30 K in respect to a normal **AT** base pair (+ 42.5 K in respect to the duplex containing the **LL** "base pair"). This is the most dramatic duplex stabilization ever observed with a metal-base pair.[219]

The hydroxypyridone ligand **12** used by Tanaka et al. in the same sequence context induced a stabilization of only 13 K when Cu^{2+} was added. In contrast, the assembly of the copper-salen base pair increased T_M by more than 40 K.[122, 220] The value measured by Tanaka et al. for their non-crosslinking metal-base pair is almost the same as the value measured with the salicylic aldehyde containing duplex **D4-L-a/b** when only Cu^{2+} is present. This comparison accentuates the role of the ethylenediamine crosslinking for the tremendous stability of [**D4-L-a/b**+en+Cu]. The cooperative character of the assembly process of the copper salen complex **23** in the DNA double helix is summarized graphically in Scheme 18.
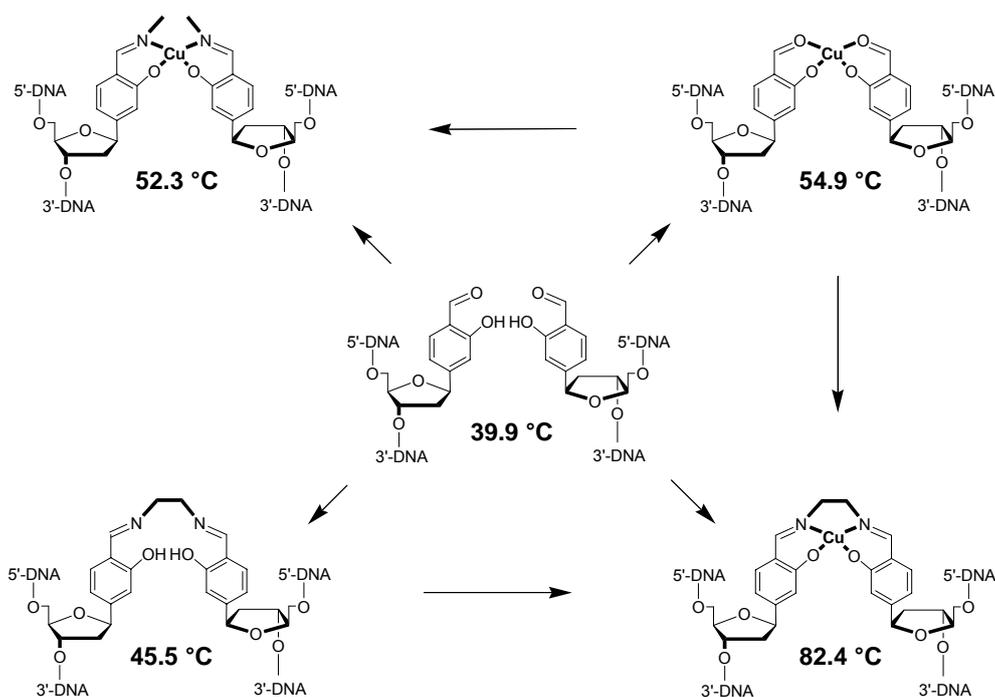
Scheme 18: The cooperativity of the assembly process leads to the observed tremendous stabilization of the DNA duplex.

In order to estimate the effect of the crosslinking, first Cu^{2+} and secondly methylamine was added to the **LL**-containing duplex **D4-L-a/b**. In this case, a much smaller stabilization of only 12 K was observed, which is in the range of the stabilization when copper alone was added. This fact reveals that indeed the combination of crosslinking by ethylenediamine and coordination of the metal is responsible for the superior stability of the copper-salen base pair in DNA.

No melting point alterations were observed in the absence of one or both salicylic aldehyde nucleobases showing that indeed formation of the salen complex inside the duplex is responsible for these dramatic shifts. Formation of the salen complex could be completely reversed by addition of an excess of EDTA to the DNA solution (not shown).

As mentioned in Chapter 4.4.1, the buffer and salt additives to the oligonucleotide samples can have a dramatic effect on the outcome of the experiments. Especially buffers that can act as ligands themselves demanded the addition of a great excess of metal ions to see an effect on the melting curve. A screening of various buffer substances enabled to reduce the amount of metal ions that were needed for a quantitative complex formation to one equivalent. Melting curve-based titration experiments for Cu^{2+} and Mn^{2+} are depicted in Figure 52.
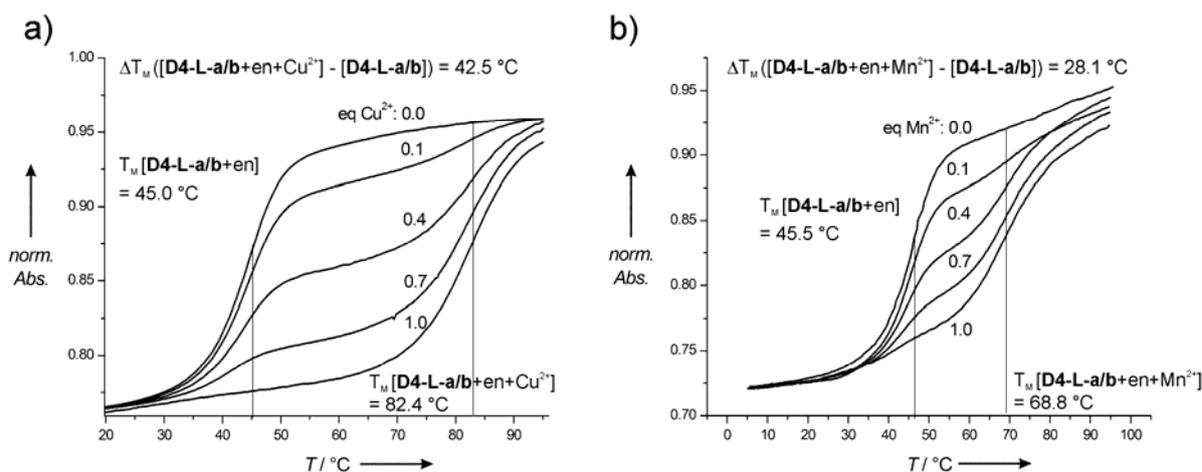
Figure 52: Melting profiles of 3 μM **D4-L-a/b** with 100 μM ethylenediamine (en) in the presence of various equivalents of (a) Cu^{2+} (0 - 1 eq.) and (b) Mn^{2+} (0 - 1 eq.). The samples contained 150 mM NaCl and 10 mM buffer (CHES pH 9 for Cu^{2+}, HEPES pH 9 for Mn^{2+}).

Addition of one equivalent of Mn^{2+} (which is known to be oxidized to Mn^{3+} upon complexation by salen ligands)[221] increased the T_M by 28.1 K to 68.8 °C.

In the cases of the free duplex **D4-L-a/b** and the duplexes containing ethylenediamine and copper, the thermal de- and renaturing profiles were superimposable. The measurements of the samples containing ethylenediamine, Mn^{2+} and the DNA duplex, however, reproducibly showed a strong hysteresis between the de- and renaturing profiles, which can be associated with a thermal instability of the Mn^{2+} salen complex when exposed to temperatures above T_M for elongated times. In these cases, the single transition in the heating curve can be assigned to the metal-increased high melting temperature whereas the cooling curve shows, that a fraction of the duplexes (ca. 50 %) re-hybridizes without re-incorporation of the metal (expressed by the lower melting point). However, after the time the measurement cycle spend at a temperature below T_M, the metal seems to be again fully incorporated and gives rise to a denaturing profile coinciding with the preceding denaturing curve. The melting curve and the assumed process are depicted in Figure 53.
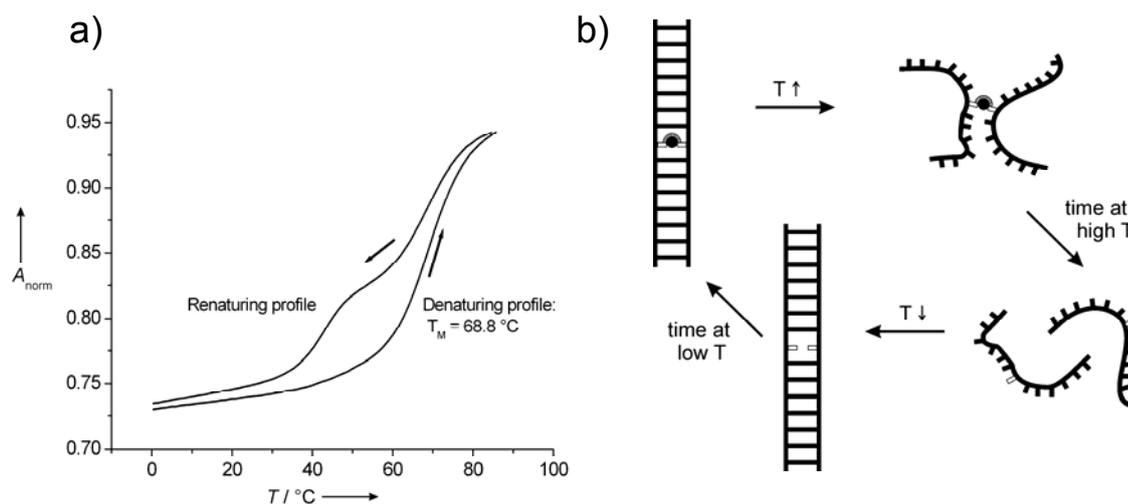
Figure 53: a) De- and renaturing profiles of 3 μM **D4-L-a/b** with 100 μM ethylenediamine (en) and 3 μM Mn^{2+}; b) assumed sequence of duplex denaturation and complex cleavage during the slow heating and renaturation and complex reassembly during the slow cooling of [**D4-L-a/b**+en+Mn] in the course of the melting curve measurement.

In contrast to the experiments with copper, Mn^{2+} did not cause any melting temperature shift when ethylenediamine was absent. This means that for the complexation of manganese, the preorganized tetradentate 2N+2O coordination environment and the crosslinking character of the salen ligand is essential for a successful complex formation inside the DNA duplex. This result was also supported by ESI mass spectrometry experiments.

It has to be mentioned, that melting point experiments are not necessarily the method of choice to test every kind of metal for its ability to form a salen complex in DNA, because finding proper conditions (kind and pH of buffer) was found to be very time and material consuming. When new metals were tested, the spectroscopic measurements were frequently hindered by the occurrence of turbidity, precipitation and the recording of irreproducible curves. Usually, ESI mass spectrometry was found to be a faster and more versatile and reliable technique for the screening of various metals under mild and uniform conditions (Chapter 4.4.4).

Addition of Zn^{2+} to **D4-L-a/b** resulted in an increase of T$_M$ by 7.7 K and a hysteresis between the de- and renaturing curve. Interestingly, addition of Ni^{2+} caused reproducibly a decrease of the melting temperature by 4.6 K. This might be an effect of unspecific DNA binding of Ni^{2+} after the salen complexes have been saturated with nickel ions.[94] For Zn and Ni, however, high metal salt concentrations were required to see the effects presented in Figure 54.
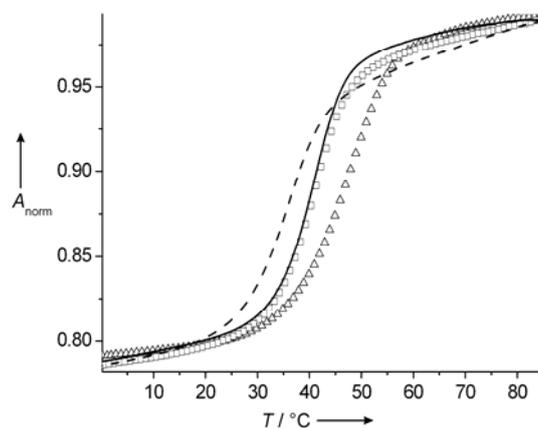
Figure 54: Melting profiles of 3 µM **D4-L-a/b** (solid line); with 100 µM ethylenediamine and 400 µM Zn^{2+} (open triangles: denaturing curve, open boxes: renaturing curve) and with 100 µM ethylenediamine and 400 µM Ni^{2+} (dashed line). 3 µM DNA, 10 mM TRIS buffer pH 7.4, 150 mM NaCl.

4.4.2.4 Melting point experiments with DNA duplexes containing two pairs of salicylic aldehydes

Several attempts were undertaken to perform similar melting point experiments with the synthesized strands containing more than one pair of salicylic aldehydes. In most cases, the obtained melting profiles showed significant differences when one, two or more equivalents of metal were added. However, most of these curves were too complex to interpret them accurately. The best interpretable set of melting profiles was obtained for the strand **D14-L-a/b** (Figure 55).

5'-CGGA**L**GAC**L**AGCG-3'
3'-GCCT**L**CTG**L**TCGC-5'

Figure 55: Sequence of duplex **D14-L-a/b** containing two remote pairs of salicylic aldehydes.

The double strand **D14-L-a/b** contains two remote pairs of salicylic aldehydes. The melting profiles for the pure duplex and the samples containing ethylenediamine and additionally one or two equivalents of Cu^{2+} are shown in Figure 56.
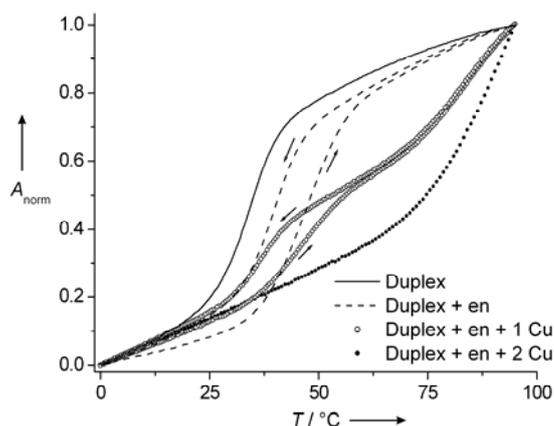
Figure 56: A comparison of melting curves of duplex **D14-L-a/b** in absence of any additive (solid line), with excess ethylenediamine ("en", dashed line), with en and one eq. Cu^{2+} (open circles) and with en and two eq. Cu^{2+} (closed circles). 3 μM DNA, 10 mM CHES buffer pH 9, 150 mM NaCl.

Without any ethylenediamine or metal, the double strand **D14-L-a/b** melts at T_M = 34.2 °C. Addition of ethylenediamine shifts the melting temperature to a much higher value accompanied by a characteristic hysteresis (averaged T_M = 41.6 °C). This hysteresis is explainable with the reversibility of the imine-linkage. When one equivalent of Cu^{2+} was added, the system showed two transitions, one at T_M = 41.2 °C (with hysteresis) and a second one at T_M = 82.9 °C (without hysteresis), indicating the presence of two species in solution. Under the conditions of the thermal de- and renaturing experiment, the assembly of the duplexes containing two Cu^{2+} ions proceeds cooperatively. When one equivalent of metal salt is added, half of the duplexes melt without any metal (T_M = 41.6 °C) and the second half is melting with two metal ions inside (T_M = 82.9 °C). This model was supported by the fact, that duplex [**D14-L-a/b**+2en+2Cu] containing two Cu^{2+} ions was also observed in the ESI mass spectrum of this sample.

Addition of a second equivalent of Cu^{2+} resulted in the occurrence of only one defined melting point at $T_M \approx$ 92.1 °C indicative for the formation of a single DNA duplex species [**D14-L-a/b** +2en+2Cu] complexing two Cu^{2+} ions.

The same melting point study with duplex **D9-L-a/b** yielded again melting profiles which showed significant changes upon addition of one or two equivalents of Cu^{2+}. However, the melting curves obtained in this case were slightly more complex. These results together with the ESI mass spectrometric data (Chapter 4.6.1) proof the formation of DNA duplexes with two metal ions inside. The high melting point of the sample near the limit of the measurement (95 °C) indicates that the two metal complexes in the duplex may not disassemble at all and only the four Watson Crick base pairs on either end of the duplexes dehybridize.

4.4.2.5 Tabular summary of the melting point experiments

Entry	Strand(s)[a]	Additive(s)		T_M / °C
1	**D2-L**		[b]	19.9
2	**D2-L**	100 µM en	6 µM Cu^{2+} [b]	65.2
3	**D2-L**		[c]	22.1
4	**D2-L**	100 µM en	4 µM Mn^{2+} [c]	[h]
5	**D2-T/A**		[g]	46.5
6	**D3-L**		[b]	35.4
7	**D3-L**	100 µM en	[b]	52.2
8	**D3-L**	100 µM en	4 µM Cu^{2+} [b]	76.5
9	**D3-L**		[c]	36.0
10	**D3-L**	100 µM en	[c]	51.6
11	**D3-L**	100 µM en	4 µM Mn^{2+} [c]	70.3[d]
12	**D4-L*-a/b**		[b]	35.7
13	**D4-L*-a/b**	100 µM en	[b]	40.5
14	**D4-L*-a/b**		4 µM Cu^{2+} [b]	36.8
15	**D4-L*-a/b**	100 µM en	4 µM Cu^{2+} [b]	71.6
16	**D4-L-a/b**		[b]	39.9
17	**D4-L-a/b**	100 µM en	[b]	45.0
18	**D4-L-a/b**		4 µM Cu^{2+} [b]	54.9
19	**D4-L-a/b**	100 µM en	4 µM Cu^{2+} [b]	82.4
20	**D4-L-a/b**	200 µM $MeNH_2$	4 µM Cu^{2+} [b]	52.3
21	**D4-L-a/b**	100 µM edh	[b]	73.4[f]
22	**D4-L-a/b**		[c]	40.7
23	**D4-L-a/b**	100 µM en	[c]	45.5
24	**D4-L-a/b**		6 µM Mn^{2+} [c]	40.7
25	**D4-L-a/b**	100 µM en	4 µM Mn^{2+} [c]	68,8[d]
26	**D4-L-a/b**		[g]	41.1
27	**D4-L-a/b**	100 µM en	400 µM Zn^{2+} [g]	48.8[d]
28	**D4-L-a/b**	100 µM en	400 µM Ni^{2+} [g]	36.5
29	**D4-A-a/-T-b**		[g]	50.1
30	**D5-L-a/b**		[b]	32.0
31	**D5-L-a/b**	100 µM en	4 µM Cu^{2+} [b]	66.8[e]
32	**D5-L-a/b**		[c]	33.4
33	**D5-L-a/b**	100 µM en	6 µM Mn^{2+} [c]	60.6[d]
34	**D6-L-a/b**		[b]	18.6
35	**D6-L-a/b**	100 µM en	4 µM Cu^{2+} [b]	59.1
36	**D6-L-a/b**		[c]	20.6
37	**D6-L-a/b**	100 µM en	4 µM Mn^{2+} [c]	53.2[d]
38	**D7-L-a/b**		[b]	20.9
39	**D7-L-a/b**	100 µM en	4 µM Cu^{2+} [b]	56.5[e]
40	**D7-L-a/b**		[c]	21.0
41	**D7-L-a/b**	100 µM en	6 µM Mn^{2+} [c]	57.8[d]

Table 5: Melting point experiments with the oligonucleotides **D2 – D7**. [a] For sequences see Table 3. All samples contained 3 µm DNA (duplex or hairpin) and 150 mM NaCl. Melting profiles were measured from 0 °C to 85 °C (for Cu^{2+}: 95 °C) with a slope of 0.5 °C/min. [b] All experiments using Cu^{2+} and corresponding controls were carried out in 10 mM CHES buffer at pH 9.0. [c] Mn^{2+} experiments: 10 mM HEPES buffer at pH 9.0. [d] Reproducible differences in de- and renaturing profiles due to thermal instability of the Mn-complex. The given T_M correspond to the denaturing profiles. [e] Additional transition of low intensity (Entry 31: 23.8 °C; Entry 39: 16.0 °C). [f] edh = O,O'-ethylenedihydroxylamine. [g] Measured in 10 mM TRIS buffer at pH 7.4; [h] No T_M determined.

4.4.3 UV-Vis and CD spectroscopy

4.4.3.1 UV-Vis spectroscopy

Further insight into the formation of the interstrand salen ligand and complexation of divalent metal ions was obtained by UV-Vis spectroscopic monitoring of the assembly process. The duplex **D4-L-a/b** has an absorption maximum at $\lambda = 260$ nm as expected for a double strand consisting primarily of natural nucleobases.[1] The salicylic aldehydes give rise to an additional absorption at $\lambda = 330$ nm due to the $\pi \rightarrow \pi^*$ transition of the aromatic chromophore.[222, 223]

Addition of an excess of ethylenediamine resulted in the appearance of a new band at $\lambda = 410$ nm. At the same time the absorption of the salicylic aldehyde at $\lambda = 330$ nm decreased over 20 minutes. The absorption at $\lambda = 410$ nm matches reported values for the deprotonated salen ligand. The existence of isosbestic points at $\lambda = 325$ nm and $\lambda = 358$ nm indicates an immediate formation of the salen ligand when an ethylenediamine molecule encounters the preorganized salicylic aldehydes (Figure 57a). In this model, the formation of the first imine bond is rate determining and the second imine bond formation is accelerated for entropic reasons.

Coordination of Cu^{2+} ions by the preformed salen ligand in DNA results in a shift of the absorption band to $\lambda = 360$ nm. In addition, a new band appears at $\lambda = 570$ nm, which is typical for the 2N+2O+Cu chromophore.[224]

The titration curve of [**D4-L-a/b**+en] with Cu^{2+} ions is depicted in Figure 57b. The overlaid curves show isosbestic points at $\lambda = 334$ nm and $\lambda = 395$ nm. The plot of the absorption at $\lambda = 360$ nm against the copper concentration shows a linear rise up to a ratio of duplex to Cu^{2+} of about 1:1 (inlay in Figure 57b).
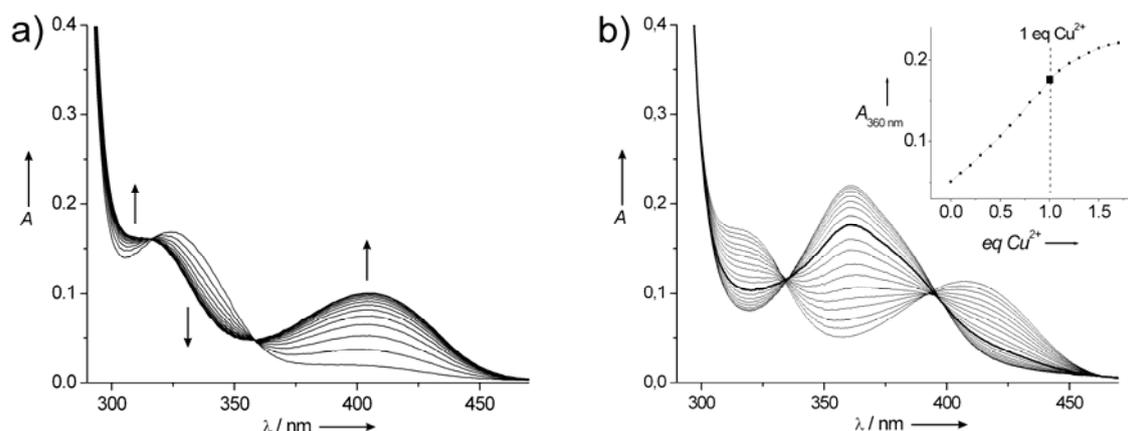
Figure 57. a) Time dependent evolution of the UV-Vis spectra of 30 μM **D4-L-a/b** after addition of 1 mM ethylenediamine in 10 mM CHES buffer and 150 mM NaCl. The measuring interval was 2 minutes; b) titration of [**D4-L-a/b**+en] (30 μM DNA, 1 mM en, 100 mM NH_4OAc_{aq} pH 8) with Cu^{2+} in steps of 0.1 eq; Thick line: 1.0 eq Cu^{2+}; Inlay: Plot of Abs_{360} against the ratio $[Cu^{2+}]/[$ **D4-L-a/b**+en].

Figure 58 compares the UV-Vis spectra of **D4-L-a/b**, [**D4-L-a/b**+en] and [**D4-L-a/b**+en+Cu].
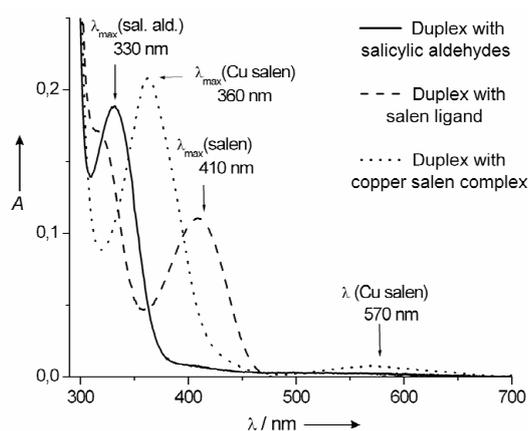
Figure 58: Electronic absorption bands of duplex **D4-L-a/b**, [**D4-L-a/b**+en] and [**D4-L-a/b**+en+Cu] (30 μM DNA, 1 mM en, 40 μM Cu^{2+}, 100 mM NH_4OAc_{aq} pH 8).

Similar measurements where carried out for the oligonucleotides containing several salen complexes (Chapter 4.6).

4.4.3.2 CD spectroscopy

Circular dichroism (CD) spectroscopy is based on the different absorption and refraction of left and right circularly polarized light. The source of the large CD effect of DNA double strand is the result of the fact that the chromophores (mainly the aromatic rings) are electronically coupled inside the asymmetric environment of the duplex. On the basis of the measured CD curve, an assignment to one of the structure groups (A, B, Z) can be made. Due to the considerable number of single

chromophores and the dependence of the CD spectrum on the nucleotide sequence, however, no detailed structural information can be extracted from the CD curve alone. Circular dichroism spectroscopy of the oligonucleotides containing the metal-salen base pair yielded plenty of information about the assembly process, the thermal stability of the salen complexes in different sequence contexts and the transfer of chirality from the surrounding DNA duplex onto the incorporated metal-salen complex. Additionally, it was the only appropriate method for carrying out the titrations of the mixed metal arrays described in Chapter 4.6.

First, the circular dichroism of the nucleobase-centered absorption band around $\lambda = 260$ nm is discussed. Figure 59 shows temperature dependent CD measurements of duplex **D4-L-a/b** and hairpin **D2-L** in absence and presence of ethylenediamine and manganese.

Hairpin **D2-L**   Duplex **D4-L-a/b**
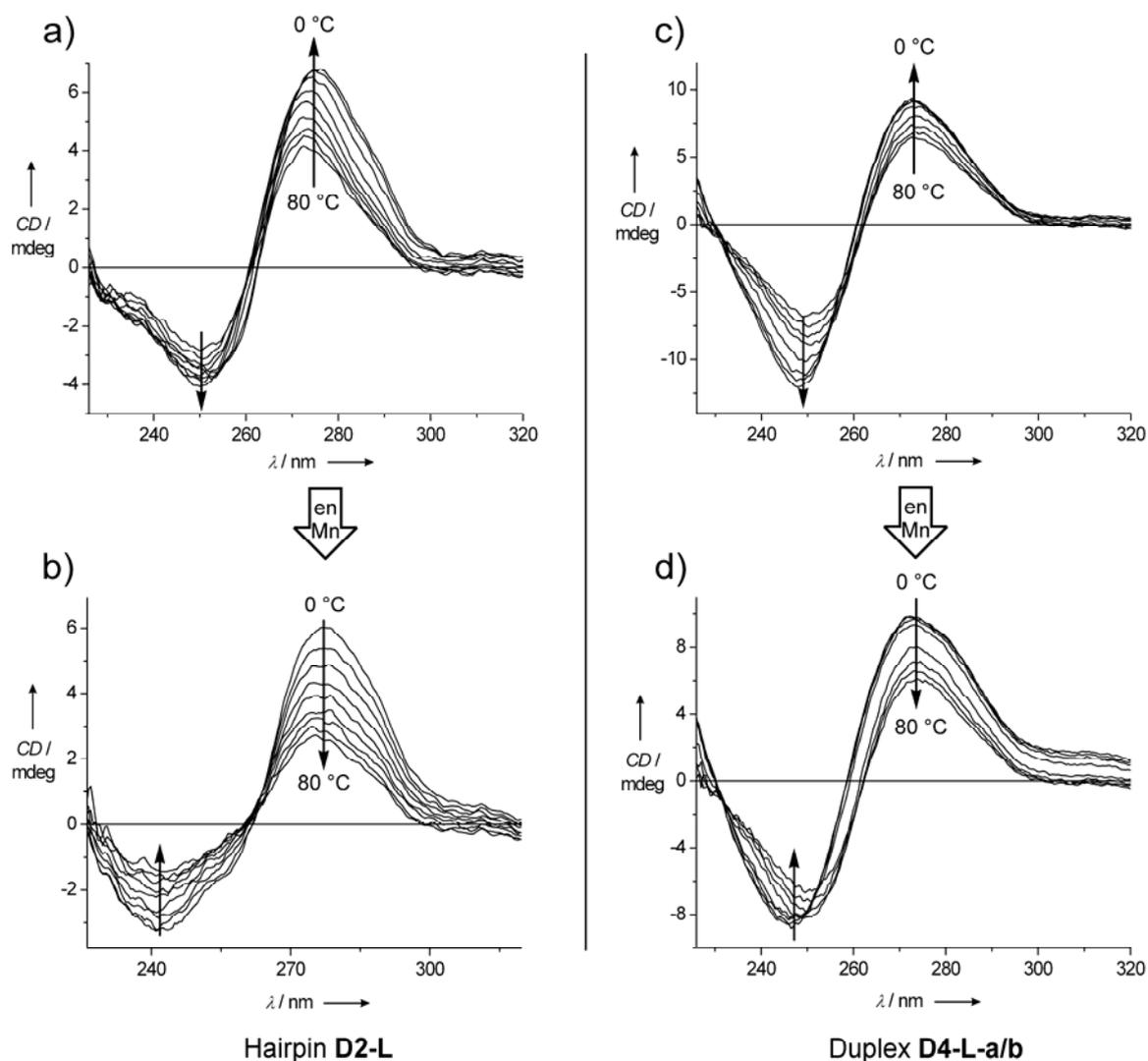
Figure 59: CD spectra at temperatures from 10 °C to 80 °C (in steps of 10 °C) of a) hairpin **D2-L**; b) hairpin **D2-L** with en and Mn; c) duplex **D4-L-a/b** and d) duplex **D4-L-a/b** with en and Mn. The DNA concentration was 3 µM in each case. 1.3 eq of Mn^{2+} and 33 eq of ethylenediamine were used. The samples contained 150 mM NaCl, 10 mM HEPES buffer pH 9.

Comparison of the curves of the **L**-containing DNA duplex **D4-L-a/b** and the DNA hairpin **D2-L** between 10 °C and 80 °C indicates the formation of the manganese salen complex inside the DNA duplex. The CD spectra measured between 80 °C and 10 °C show clearly formation of B-type DNA structures in all cases.[225] Addition of ethylenediamine and either Mn^{2+} or Cu^{2+} resulted in changes of the CD spectra below the individual melting temperatures indicating formation of the salen complex (only the Mn^{2+} spectra are shown). Above the melting temperatures, the obtained CD spectra of the duplex **D4-L-a/b** are undistinguishable from non-metal-containing DNA strands. The CD spectrum of the L-containing hairpin **D2-L** at 80 °C, however, features in the presence of Mn^{2+} even above the melting point clear differences compared to non-metal-containing hairpins, showing that the salen complex may stay to some extend intact in the hairpin even at rather high temperatures (Figure 60). Interesting is the comparison of these results to the UV spectroscopic melting point studies carried out with hairpin [**D2-L**+en+Mn] and duplex [**D4-L-a/b**+en+Mn] discussed in Chapter 4.4.2.2 and 4.4.2.3.
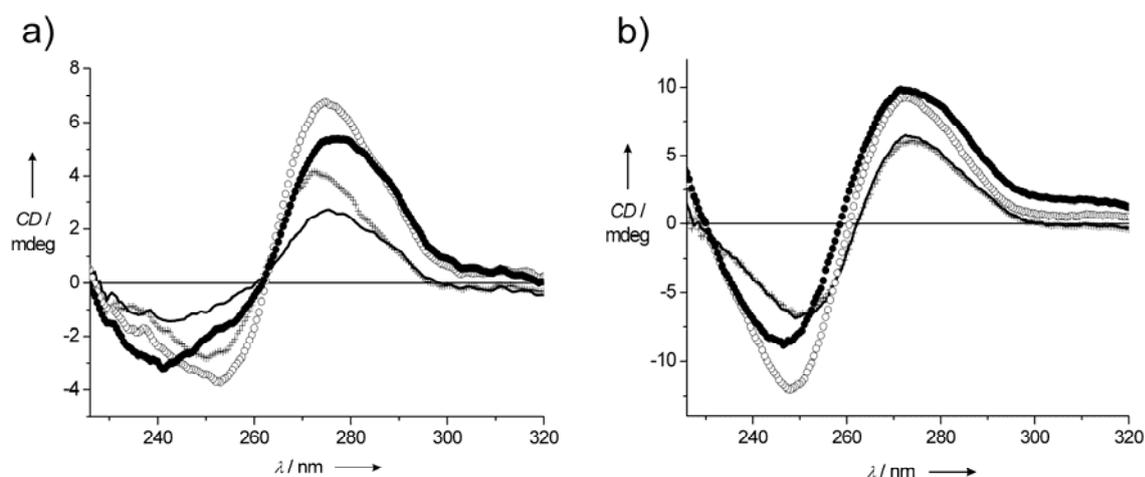
Figure 60: Comparison of CD spectra at 10 °C and 80 °C of (a) hairpin **D2-L** and (b) duplex **D4-L-a/b** in the absence and presence of ethylenediamine and Mn^{2+}. Open circles: 10 °C, no en, Mn; black circles: 10 °C, with en and Mn; crosses: 80 °C, no en, Mn; solid line: 80 °C, with en and Mn.

At higher DNA concentrations (15 μM) the circular dichroism of the salen-centered absorption bands between λ = 300 und 500 nm were studied in the absence or presence of ethylenediamine and copper. The free salicylic aldehydes as well as the uncomplexed salen ligand show only a minor CD signal inside the DNA double helix. When Cu^{2+} is added, the duplex [**D4-L-a/b**+en+Cu] features a strong CD-signal in the range of the absorption of the $\pi \rightarrow \pi^*$-transition (Figure 61).

This is in sharp contrast to the observation that an aqueous solution of the monomeric homochiral Cu-salen complex **42** shows no CD signal in the range between λ = 300 to λ = 700 nm. This can be explained by the assumption, that the chirality of the sugar moieties does not influence the chelate configuration and the monomeric copper-salen base pair in solution exists in a 1:1 mixture of diastereomers with Δ and Λ configured chelate rings, respectively. Because only the metal-ligand system gives rise to an electronic absorption between λ = 300 to λ = 700 nm, the result of this 1:1 mixture is zero net ellipticity in the CD spectrum of complex **42**. In the DNA duplex, however, the chiral information of the surrounding double helical structure is imprinted onto the salen complexes forcing it into a single fixed conformation, which gives rise to the observed strong CD band.
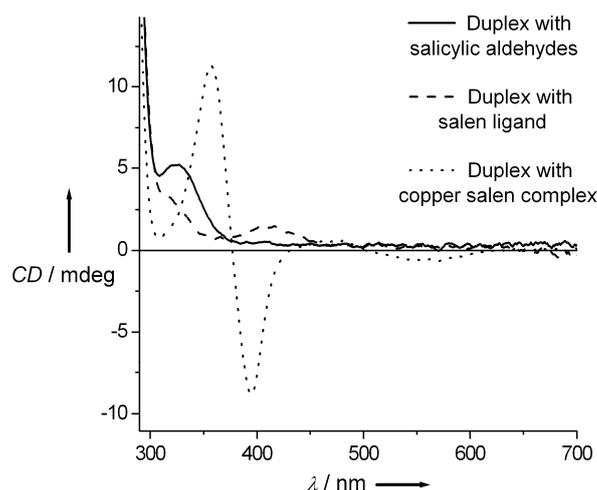
Figure 61: Circular dichroism spectra of **D4-L-a/b**, [**D4-L-a/b**+en] and [**D4-L-a/b**+en+Cu] (30 μM DNA, 1 mM en, 30 μM CuSO$_4$, 100 mM NH$_4$OAc pH 8).

The signal for the copper-salen containing duplex has a positive sign in the high energy region and a negative sign of the low energy part and corresponds according to studies by *Downing et al.* to a Δ configuration of the metal chelate inside the duplex.[224] In conclusion, the salen complex inside the DNA duplex adopts the same absolute configuration as in the crystal (see Chapter 4.2.2). Concerning the metal-based d-d transition around λ = 570 nm, only a small CD effect is observed.

CD spectroscopic measurements were also performed with the hypermodified duplex **D19-L-a/b**, which contains 10 consecutive pairs of salicylic aldehydes. A circular

dichroism study at temperatures between 0 °C and 80 °C of duplex **D19-L-a/b** prior and after assembly of the ten manganese-salen complexes is depicted in Figure 62.
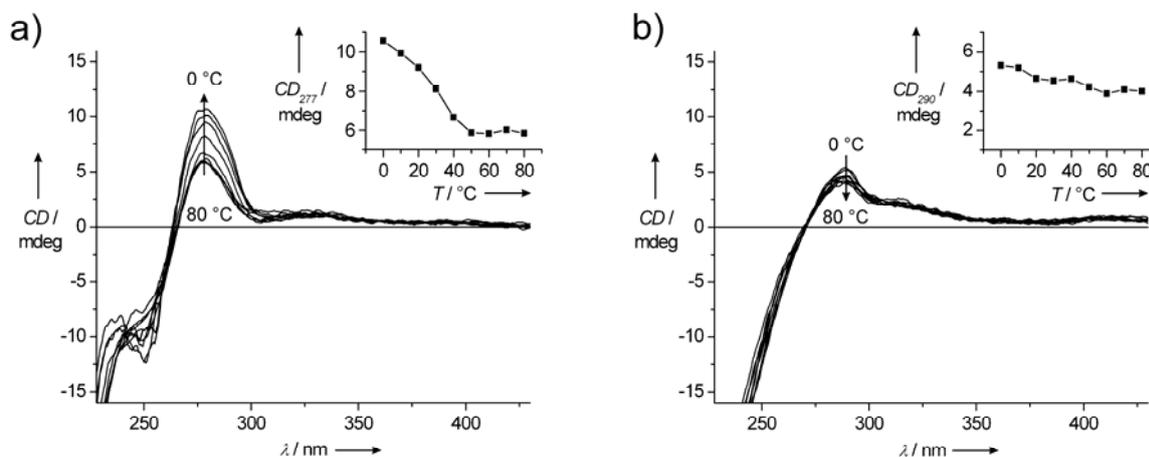
Figure 62. CD spectroscopic measurements of duplex **D19-L-a/b** containing ten consecutive pairs of salicylic aldehydes at temperatures between 0 °C and 80 °C in steps of 10 K. a) 3 μM duplex in 10 mM HEPES, 150 mM NaCl (80 °C → 0 °C). b) Same sample after 24 h incubation with 1 mM en and 40 μM Mn^{2+} (0 °C → 80 °C). The inlay graphs show a plot of the positive CD maximum against the temperature. HEPES = *N*-(2-hydroxyethyl)piperazine-*N'*-(2-ethanesulfonic acid). Blanks were subtracted for each temperature separately.

Without any ethylenediamine and Mn^{2+}, the spectra feature a positive band around λ = 277 nm, a negative band (shoulder) around λ = 249 nm and a crossover of the baseline at λ = 265 nm. These features can be attributed to a B-DNA-like secondary structure of the duplex.[226] When the temperature of the sample was slowly reduced from 80 °C to 0 °C, the CD curves changed as seen in Figure 62a. The inset in Figure 62a shows a plot of the positive CD maximum against the temperature. It suggests a melting of the duplex **D19-L-a/b** around 35 °C, in accordance with UV spectroscopic melting point studies (not shown). Addition of excess ethylenediamine and Mn^{2+} lead to a significant change of the CD spectrum with a diminishment of the positive band around λ = 290 nm and a vanishing of the band around λ = 249 nm (Figure 62b). A clear classification of the structure of the hyper-modified duplex [**D19-L-a/b**+10en+10Mn] basing on this data is difficult. Most important, however, was the observation that the spectra did not change when the temperature was raised (inset in Figure 62b). This is a clear sign for the expected high structural stability of the duplex caused by the multiple metal-salen crosslinks.

The CD titrations of the mixed-metal arrays are depicted in Chapter 4.6. Although a structural assignment for the duplexes containing five to ten consecutive homo- or

hetero-nuclear metal-salen complexes cannot be made based on the complex CD results, the observed large ellipticities suggest a helical conformation of the prepared duplexes containing the metal ions.

A complete structural characterization can only be made by means of a X-ray measurement or – with diamagnetic metals coordinated – by NMR spectroscopy.

4.4.4 ESI mass spectrometry

ESI mass spectrometry was described before for the analysis of covalent and noncovalent adducts and crosslinks of DNA single and double strands.[227, 228, 229] After many inconclusive experiments to analyze the metal-salen crosslinked oligonucleotides by MALDI-TOF-mass spectrometry the use of a Finnigan LTQ ESI-FTICR-mass spectrometer for the measurements was successful. The extremely high resolution and accuracy of the FTICR mass analyzer proofed to be a valuable advantage over older mass spectrometric equipment as it allows to correlate calculated with experimentally observed molecular weights with deviations in the 10 ppm range even for heavy biomolecules. Because mass spectrometry is faster and a far more direct proof of the "structure" than are melting point studies, a screening of several metals and diamine bridges was performed. The samples were prepared by hybridizing equimolar amounts of strand and counterstrand in 100 mM ammonium acetate buffer (pH 8) and subsequent incubation with the diamine and metal salt overnight at room temperature.

Usually, no chromatographic separation of the reaction mixture was performed prior to mass spectroscopic analysis (exception: see Chapter 4.4.5). Consequently, the species that are identified in the mass spectrum can be considered to reflect the real composition of the reaction mixture (apart from the unspecific adduct formation with ubiquitous cations seen in the mass spectrum). The complex formation inside the DNA duplex was therefore defined as "quantitative" when no remaining uncomplexed duplexes or excess single stranded material was left over in the reaction mixture.

Figure 63 displays an example, where the reaction of the double strand **D4-L-a/b** with ethylenediamine and Mn^{2+} was not complete, probably because of a lack of hybridization of strand and counterstrand.
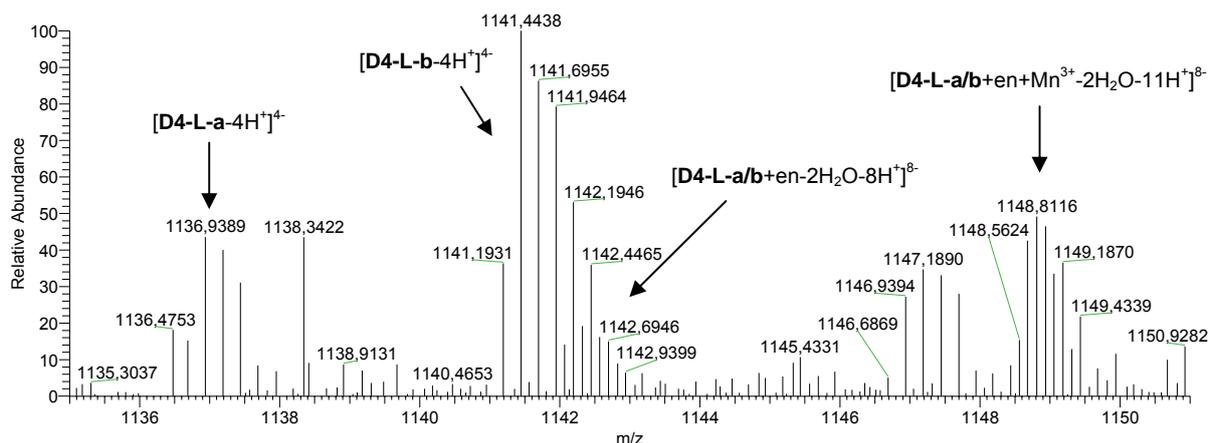
Figure 63: Example for an ESI mass spectrum of an incompletely reacted mixture of **D4-L-a/b** with ethylenediamine and Mn^{2+}. The single strand components can be differentiated from the double strand components by the peak distances in the isotope patterns.

Besides the expected double strand product containing the manganese-salen complex [**D4-L-a/b**+en+Mn^{3+}-$2H_2O$-$3H^+$] (peak at *m/z* = 1148), also the ethylenediamine-linked duplex [**D4-L-a/b**+en-$2H_2O$] (peak at *m/z* = 1142) and two signals for the single strands **D4-L-a** and **D4-L-b** (peaks at *m/z* = 1137 and 1141) were observed. Because the charge of the double strands is with *z* = 8 double the charge of the single strand (*z* = 4) in the examined region, the distance between double strands' isotope peaks is half that of the single strands. This feature can be easily seen by zooming into the high resolution ESI spectra (note that this cannot be seen in MALDI-TOF spectra!). In the regions of the mass spectrum, where the double strands containing odd-numbered charges appear, logically no peaks for the corresponding single strands can be found.

The problem of unspecific hairpin formation of strands containing two or more salicylic aldehydes is addressed in Chapter 4.5.3.

In all cases discussed below, the experimentally found molecular weights are in excellent agreement with the values calculated for the hairpins or duplexes containing the expected number of ethylenediamine units and metal ions. Table 6 shows the calculated molecular weights of the lowest-weight isotopomers along with the measured values (exemplarily for *m/z* with *z* = – 4 or – 9) for different strands containing one salen complex each. In each case, one molecule of diamine condenses with both salicylic aldehydes of the DNA strands along with the loss of two water molecules to form the crosslinking ligand which binds the metal ion.

All obtained molecular weights proof the presence of only one metal ion in the duplexes or hairpins (Table 6, entries 2 - 5). Interestingly, only in the case of Ni^{2+} molecular weights were determined, which indicate next to the formation of the expected mono-Ni^{2+} adduct [**D2-L**+en+Ni^{2+}–$2H_2O$–$2H^+$] also the presence of [**D2-L**+en+$2Ni^{2+}$–$2H_2O$–$4H^+$] and of [**D2-L**+en+$3Ni^{2+}$–$2H_2O$–$6H^+$], which is a sign for further unspecific and rather tight binding of additional Ni^{2+} to the oligonucleotide once the salen-ligand is saturated with metal.

Entry	Strand(s)[a]	Additive(s)		Species	Calc. mass	Exp. Mass	Δ [ppm]
1	**D2-L**	-	-	[M-4H$^+$]$^{4-}$	1209.4573	1209.4497	6.3
2	**D2-L**	en	Mn^{3+}	[M-5H$^+$]$^{4-}$	1228.4364	1228.4376	1.0
3	**D2-L**	en	Cu^{2+}	[M-4H$^+$]$^{4-}$	1230.6999	1230.6908	7.4
4	**D2-L**	en	Fe^{3+}	[M-5H$^+$]$^{4-}$	1228.6967	1228.6902	5.3
5	**D2-L**	en	VO^{2+}	[M-4H$^+$]$^{4-}$	1231.6997	1231.6973	1.9
6	**D2-L**	en	Ni^{2+}	[M-4H$^+$]$^{4-}$	1229.4488	1229.4299[b]	15.4
7	**D4-L-a/b**	-	-	[M$_a$-4H$^+$]$^{4-}$ [M$_b$-4H$^+$]$^{4-}$	1136.6993 1141.2048	1136.6887 1141.1948[c]	9.3 8.8
8	**D4-L-a/b**	en	Cu^{2+}	[M-9H$^+$]$^{9-}$	1021.7207	1021.7220	1.3
9	**D7-L-a/b**	edh[d]		[M-9H$^+$]$^{9-}$	961.3902	961.3792	11.4
10	**D2-L**	phen[d]	Cu^{2+}	[M-9H$^+$]$^{9-}$	1242.6998	1242.6840	12.7

Table 6: ESI mass spectrometry experiments with the oligonucleotides **9**, **13** and **15**. [a] For sequences see Table 3. All samples contained 30 μM DNA (duplex or hairpin) and 100 mM NH_4OAc (pH 8). DNA strands were first hybridized by slow cooling from 80 °C to 25 °C and then incubated for at least 12 h with the diamine and a solution of the metal sulfate at room temperature. [b] Additional peaks for [**D2-L**+en+2Ni-$2H_2O$-$4H^+$] and [**D2-L**+en+3Ni-$2H_2O$-$6H^+$] were observed. [c] Only single strand masses observed. [d] edh = O,O'-ethylenedihydroxylamine, phen = 1,2-phenylenediamine.

Addition of Mn^{2+} and Fe^{2+} to the ligand containing duplexes and hairpins resulted in oxidation to give Mn^{3+} and Fe^{3+} ions as clearly proven by the *m/z* values.[221] The charge of the coordinated metal can be deduced from the observed *m/z* value by comparison with the simulated isotope pattern. Saturation of the metal's coordination sites which are not occupied by the tetradentate salen ligand might be achieved by loosely bound water (or acetate) molecules or by interaction with the donor atoms of a neighboring salen ligand[145] or natural nucleobase. The former case is plausible basing on the observation that loosely bound apical ligands such as water easily decomplex from the salen complex in the gas phase.[230]

Only the peaks expected for the coordination of one iron(III) ion to the assembled salen ligand along with Na^+ and K^+ adducts appear in the spectrum of [**D2-L**+en+Fe^{3+}–$2H_2O$–$3H^+$] (Figure 64a).

The mass spectrum of the duplex [**D4-L-a/b**+en+Cu^{2+}–$2H_2O$–$2H^+$] is shown in Figure 64b as an example. Only the peaks calculated for the Cu-salen containing duplex are observed along with some Na^+, K^+ and $NHEt_3^+$ adducts of it. No uncomplexed single strands are visible and not more than one copper atom is complexed to the duplex. Although monomeric copper-salen complexes have been used for the cleavage of the DNA backbone (Chapter 3.4.2), no degradation of the DNA was observed with any of the constructs prepared in the course of this work.

The reaction of oligonucleotide duplex **D7-L-a/b** with *O,O'*-ethylenedihydroxylamine (edh) in absence of metal ions results in quantitative crosslinking to the bis-oxime compound [**D7-L-a/b**+edh–$2H_2O$] (Figure 64c).

1,2-Phenylenediamine can also be used as bridge, when oxygen is excluded (Table 6, entry 10).

Other examples for characteristic ESI mass spectra of metal-salen containing hairpins and duplexes are described in the following Chapters and are depicted either there or in the appendix (Chapter 7.1).

The mass spectra of the strands containing up to ten metals are discussed in Chapter 4.6.1 and 4.6.2, those of the mixed metal stacks are shown in Chapter 4.6.3.
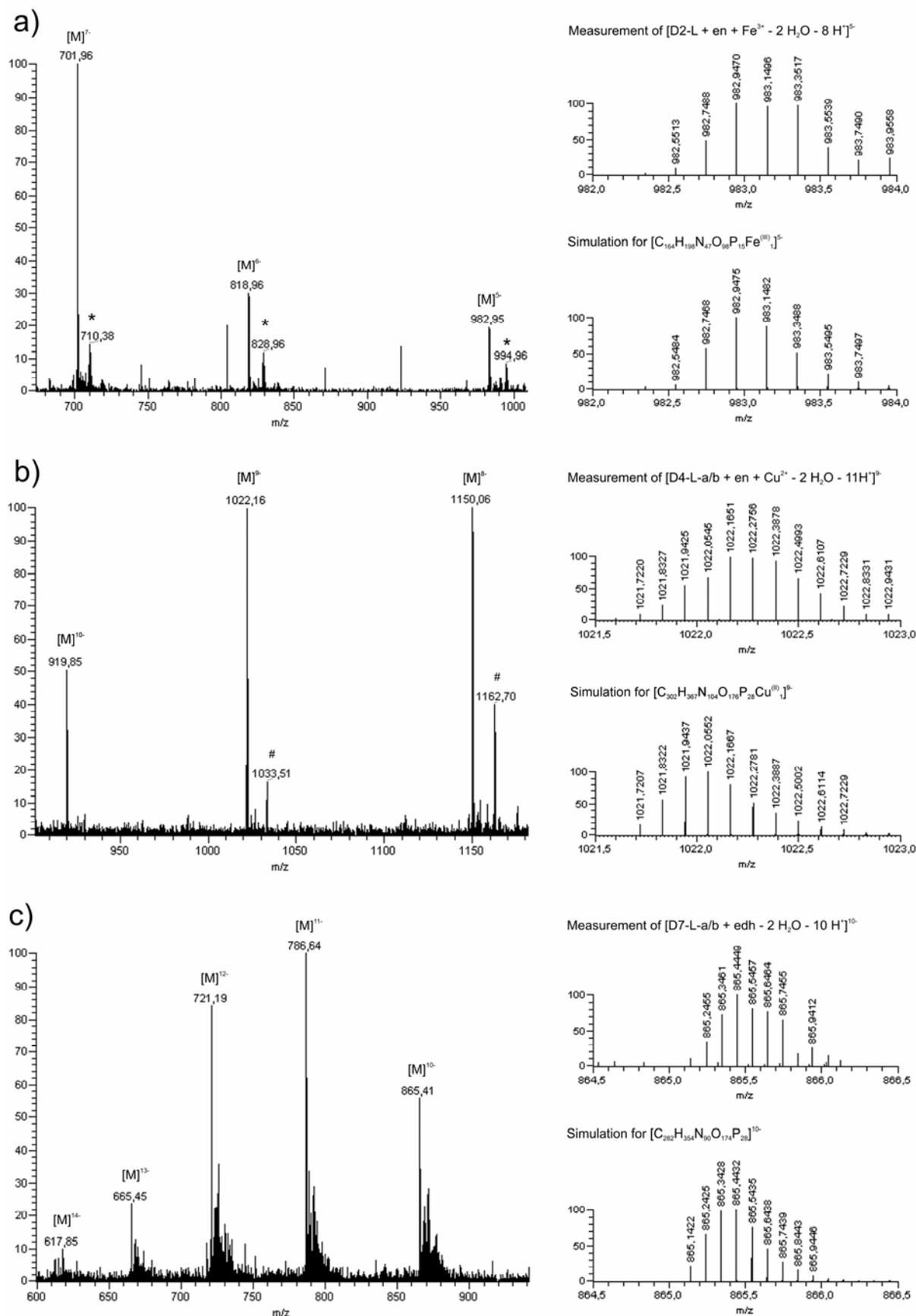
Figure 64: Selected ESI mass spectra and comparison of experimental data with calculated molecular weights. a) [**D2-L**+en+Fe^{3+}−$2H_2O$−$3H^+$]; b) [**D4-L-a/b**+en+Cu^{2+}−$2H_2O$−$2H^+$]; c) [**D7-L-a/b**+edh−$2H_2O$]; Adducts: * = [M + Na + K − 2H], # = [M + NEt_3].

4.4.5 Liquid chromatography-mass spectrometry (LC-MS)

The unusual high stability of the copper-salen complex in the DNA duplex has a great influence on the chromatographic behavior of the double strand **D4-L-a/b** (Figure 65). Injection of a hybridized probe of **D4-L-a/b** in 100 mM NH_4OAc buffer onto a C_{18}-RP HPLC column results in complete denaturation of the duplex. Consequently, two peaks, one for each single strand, are observed. When the duplex sample was incubated with an excess of ethylenediamine and Cu^{2+} prior to injection, only one peak was observed. Analysis of this peak by UV spectroscopy during the HPLC run revealed a bathochromic shift of the $\pi \rightarrow \pi^*$-band, which is indicative for the presence of the copper-salen complex.
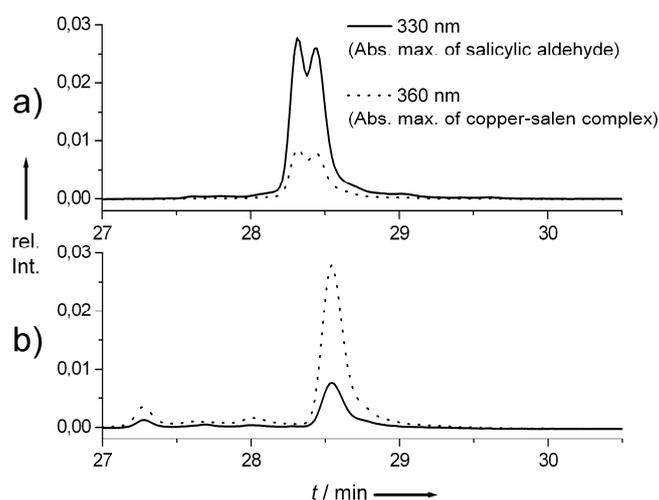
Figure 65: Comparison of HPL chromatograms of: a) 30 μM **D4-L-a/b** in 100 mM NH_4OAc (pH 8) and b) the same sample after incubation with 1 mM ethylenediamine and 100 μM Cu^{2+}. Eluent: 2 mM $NHEt_3OAc$ in (H_2O) : (MeCN : H_2O = 8 : 2), gradient: 0 – 40 % MeCN in 40 min, 3μ-RP-C_{18} column.

LC-MS analysis of this sample with the HPLC system coupled to an ESI-ICR spectrometer confirmed the exclusive presence of the Cu-salen duplex. Again, only one peak can be observed in the UV-Vis detector, which coincides with the occurrence of the expected UV-Vis and mass spectra for the duplex [**D4-L-a/b**+en+Cu] (Figure 66).

These results show that the Cu-salen containing DNA duplexes are so stable that they can in principle be isolated and purified by HPL chromatography. In the chromatography process, however, the excess ethylenediamine is removed from the sample containing the metal-salen base pair inside the DNA duplex. This was found to result in a slow disassembly of the metal complex at room temperature.
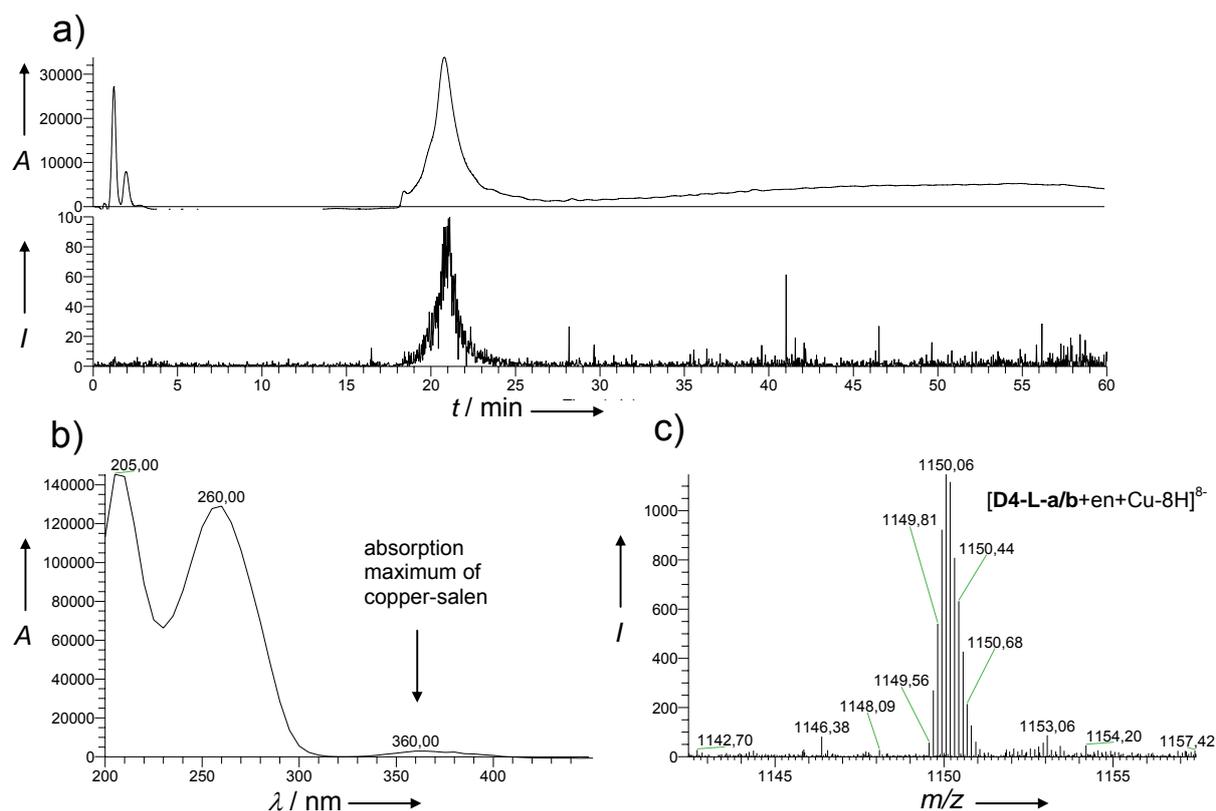
Figure 66: LC-MS measurement of duplex [**D4-L-a/b**+en+Cu]. a) Chromatogram (top: sum over UV-Vis traces from 200 – 600 nm, bottom: mass scan for m/z = 1149-1151); b) UV-Vis spectrum at t = 21 min; c) mass spectrum at t = 21 min. The absorption and intensity values are given in arbitrary units. Eluent: 2 mM NHEt$_3$OAc in (H$_2$O) : (MeCN), gradient: 0 – 40 % MeCN in 40 min, 3μ-RP-C$_{18}$ column.

4.4.6 EPR spectroscopy

To gain more information about the coordination environment of the copper(II) atoms inside the modified DNA oligonucleotide duplexes, electron paramagnetic resonance (EPR) experiments were conducted with the strands [**D4-L-a/b**+en+Cu], containing one copper(II)salen complex, and [**D9-L-a/b**+2en+2Cu], containing two neighbored copper(II)salen complexes. The measurements were performed by the group of *O. Schiemann* at the University of Frankfurt and the Technical University Munich.[231]

EPR spectroscopy examines the resonant absorption of electromagnetic radiation by paramagnetic ions or molecules in a magnetic field.

The samples are introduced into the magnetic field and irradiated with microwaves of several GHz (X-band EPR: ≈ 9 GHz). In the continuous wave method, the magnetic field is continuously changed and the EPR signal is usually visualized as the first derivative of the obtained spectrum.

A prerequisite to paramagnetism is the existence of at least one unpaired electron in the examined system which results in a total magnetic moment S ≠ 0. The applied magnetic field results in a quantitized splitting of the energy levels of the different spin states (*Zeeman* Effect). The energies of these levels follow the equation $E(m_s) = g \cdot \mu_B \cdot m_s \cdot B$ with g = molecule-specific *Landé*-factor, μ_B = *Bohr's* magneton $(9.27401 \times 10^{-24} \cdot J \cdot T^{-1})$, m_s = magnetic quantum number (m_s = -S, -S+1, ..., 0, ..., S+1, + S) and B = magnetic field strength. For one unpaired electron ($m_s = \pm \frac{1}{2}$) this results in the following condition for the resonance phenomenon to occur: $\Delta E = h \cdot \nu = g \cdot \mu_B \cdot B$ (ΔE = energy difference between the levels with $m_s = + \frac{1}{2}$ and $m_s = - \frac{1}{2}$, h = *Planck's* constant).

For the free electron, the *Landé*-factor g is only a function of the electron spin and has the value g_e = 2.002319. In molecules, deviations from g_e are caused by the chemical environment of the unpaired electron (spin-orbital magnetism, hyperfine coupling with nuclei, coupling with other unpaired electrons).

Interaction of the unpaired electrons with nuclei changes the resonance equation to $\Delta E = h \cdot \nu = g_e \cdot \mu_B \cdot (B_{ext} + A \cdot m_I)$ with B_{ext} = external magnetic field strength and $A \cdot m_I$ = force of magnetic field induced by the nucleus (A = hyperfine coupling constant and m_I = nuclear quantum number). A selection rule allows only an electronic spin flip without change of the nuclear spin.

The EPR signal splitting in the presence of several nuclei with different nuclear spin quantum numbers can be calculated using the equations for the spin multiplicity.

A more detailed consideration of the interactions of the unpaired electron with its environment shows, that the hyperfine coupling phenomenon has to be divided into an isotropic term (Fermi contact interaction of molecular orbitals with s-orbital-like symmetry and spin-polarization interaction of π-like orbitals) and an anisotropic term (dipolar interaction of unpaired electrons and nuclei through space). The latter dipolar interaction is a function of the distance of the interacting spins. Therefore its measurement yields structural information about the examined paramagnetic system.

Figure 67 depicts the EPR-spectrum of the DNA double strand **D4-L-a/b** containing one copper(II)salen base pair. The pattern of the hyperfine coupling clearly indicates the coordination of the copper(II) ions by the 2N+2O-coordination sphere of the salen ligand. The measurement is even in the *shf*-region (super hyper fine coupling) in perfect accordance with the corresponding simulation.[231]
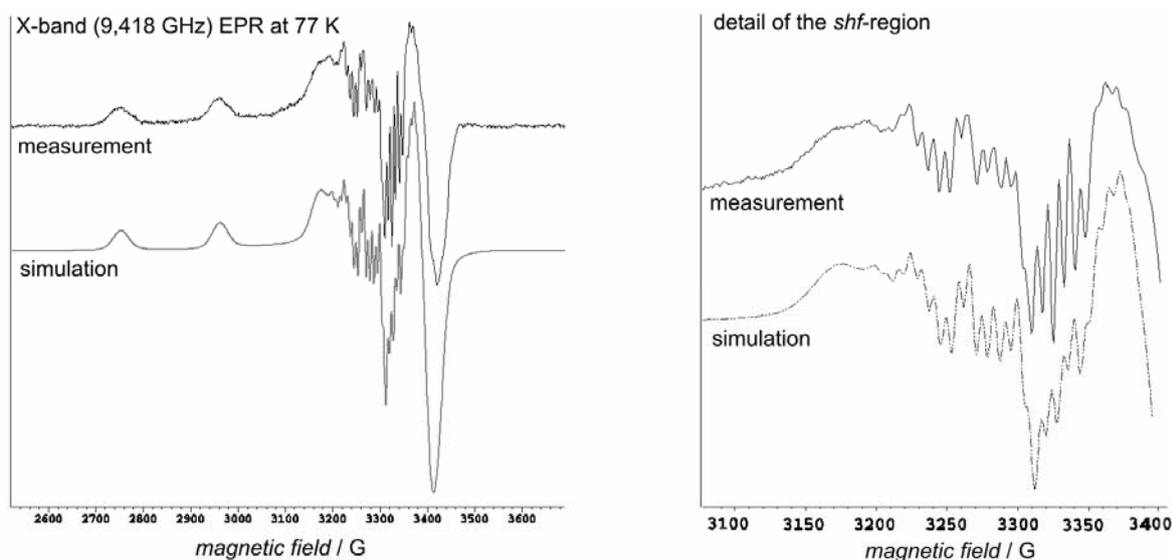
Figure 67: X-band EPR spectrum of strand [**D4-L-a/b**+en+Cu] containing one copper(II)salen base pair (left: whole spectrum, right detail of the shf region).

The measurement of duplex [**D9-L-a/b**+2en+2Cu], containing two neighbored copper(II)salen complexes, yielded an EPR spectrum depicted Figure 68.
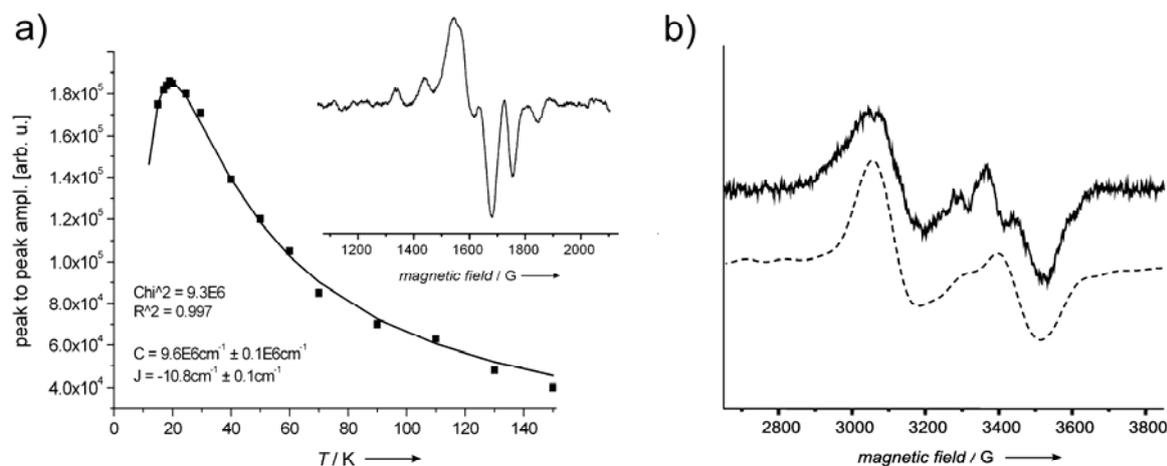
Figure 68: EPR spectroscopic determination of the Cu^{2+}-Cu^{2+}-distance and magnetic interaction in the duplex [**D9-L-a/b**+2en+2Cu]. a) The temperature dependence of the half-field signal (double integrated intensity) shows an anti-ferromagnetic coupling between the two metal centers with a coupling constant J = -10 cm^{-1} ± 2 cm^{-1} (inset = half-field signal at 45 K); b) depiction of the CW X-band EPR spectrum of [**D9-L-a/b**+2en+2Cu] (solid line: measurement, dotted line: simulation). The dipolar coupling constant D leads to a Cu^{2+}-Cu^{2+}-distance of 4.2 ± 0.5 Å.

The interpretation of the spectra by *Schiemann* showed that the two Cu^{2+}-ions couple in an antiferromagnetic manner with an exchange coupling constant J = -10 cm^{-1} ± 2 cm^{-1} as calculated from the temperature dependence of the half-field signal using a modified Bleaney-Bowers equation (Figure 68a).[232]

The Cu^{2+}-Cu^{2+}-distance r = 4.2 ± 0.5 Å was calculated from the measured dipolar coupling constant D = 370 ± 10 G = $1.39 \cdot 10^4 \cdot g \cdot r^{-3}$ (Figure 68b).[231]

4.5   Interplay of salen complex formation and DNA sequence

4.5.1 Complex formation in different sequence context

The comparison of melting points and mass spectrometric experiments for the different synthesized oligonucleotides with one or more salen ligand precursors revealed, that the arrangement of salicylic aldehydes in the oligonucleotides and the surrounding sequence context can have a significant influence on the salen complex formation. On the other hand, the driving force of complex formation inside the DNA double helix has major implications on duplex stability and in special cases even duplex secondary structure. This Chapter discusses examples of salicylic aldehyde-containing DNA strands, which show a more complex behavior than the "standard duplex" **D4-L-a/b** used throughout the rest of this thesis.

4.5.1.1 A palindromic hairpin with the ligand in its middle

The first oligonucleotide containing one salicylic aldehyde nucleobase synthesized for this work was the palindromic 13mer **D1-L** (5'-TGTACG**L**CGTACA-3'). It was planned that the single strand undergoes dimerization to the corresponding double strand (**D1-L**)$_2$ which is capable of forming a metal-salen complex inside the double helix. However, under the chosen conditions the melting curve of (**D1-L**)$_2$ showed a rather broad transition, which indicated hairpin formation instead of hybridization to a double strand (Chapter 4.4.2.2). Furthermore, the melting point was almost independent of the chosen DNA concentration, which is another very strong evidence for the exclusive presence of a hairpin with the ligand sitting in its loop (Figure 69).
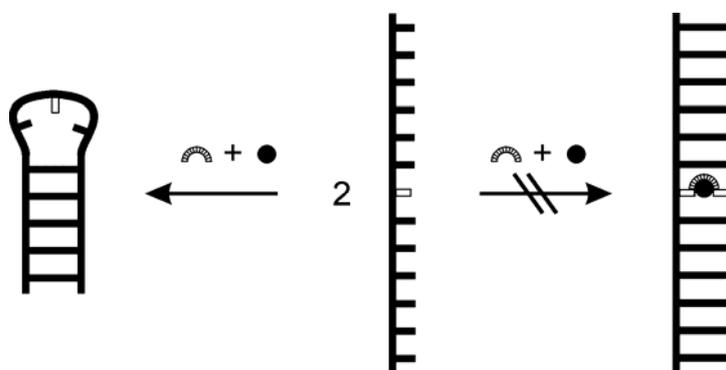
Figure 69: Hairpin vs. double strand formation of the palindromic self complementary strand **D1-L**.

Based on this behavior, it was not surprising that the addition of ethylenediamine and metal ions such as Cu^{2+} or Mn^{2+} did not result in any effect on the melting point of the oligonucleotide **D1-L**.

This observations lead to the synthesis of the non-palindromic duplex **D4-L-a/b** and the other related double strands described in this work. A proper hybridization of two single strands to give a double strand with a melting point of at least 30 °C was found to be important for handling of the duplexes at room temperature and a clean assembly of metal-salen complexes inside the double helix.

4.5.1.2　Duplexes with the ligands in shifted positions

In order to investigate in more detail how the preorganization of the salicylic aldehydes in the duplex affects the metal-salen complex formation, the position of two salicylic aldehydes in the oligonucleotide sequence was systematically varied as depicted in Figure 70a.
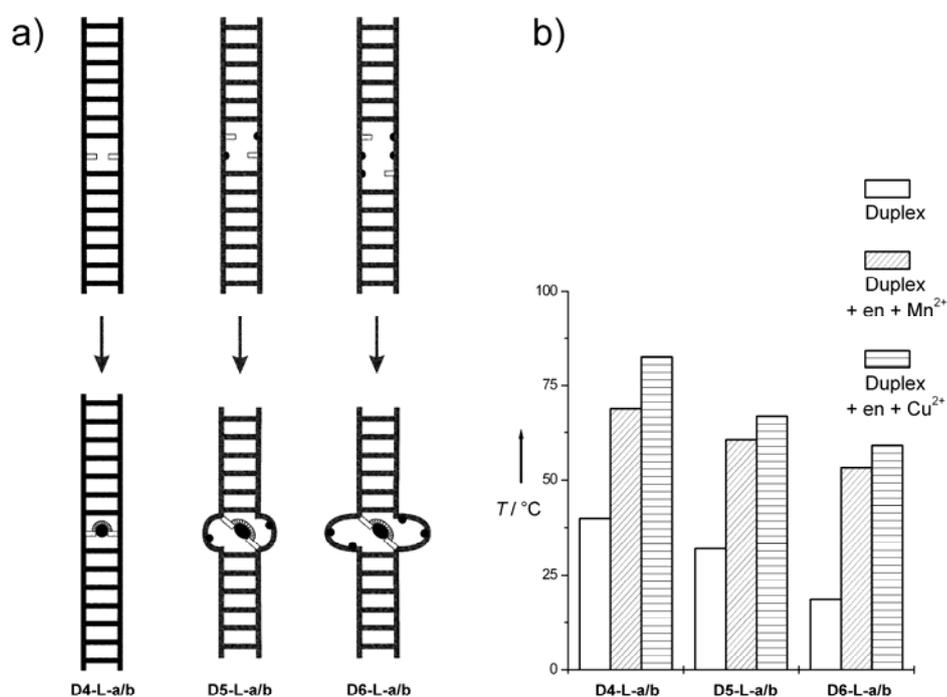
Figure 70: Comparison of the thermal stabilities of duplexes **D4-L-a/b**, **D5-L-a/b** and **D6-L-a/b** without any additives, with en and Mn^{2+} and with en and Cu^{2+}.

A graphical comparison of the determined thermal stabilities of the original strand **D4-L-a/b** with the sequences **D5-L-a/b** and **D6-L-a/b** is displayed in Figure 70b (for

details on sequence see Table 3 in Chapter 4.3.1). In these constructs the simple tetrahydrofuran derived spacers **D** (black bulges in Figure 70a, see Figure 42) were chosen as counterbase to the aldehydes to avoid unwanted interaction with the ligands. The melting points of the bare duplexes decreased by about 8 K with the loss of the first and by another 14 K with loss of a second **AT**-base pair. The values for the strands after assembly of the metal-salen base pair followed the same trend (Table 5).

However, duplexes **D5-L-a/b** and **D6-L-a/b** in which the aldehydes are shifted by one or two positions, respectively, are still able to form interstrand salen complexes with ethylenediamine and manganese or copper as the metal.

Complex formation even works, when the salicylic aldehydes are shifted (like in **D6-L-a/b)** but separated by an **AT**-base pair as in the duplex **D4-L-a/D8-L-b** (Figure 71).

<div align="center">
5'-CACATTALTGTTGTA-3'

3'-GTGTALTTACAACAT-5'
</div>

Figure 71: The sequence of duplex **D4-L-a/D8-L-b**.

The addition of ethylenediamine and Cu^{2+} to this duplex leads to a complex melting behavior, which differs significantly from the melting curve of the pure duplex (not shown). Furthermore, mass spectrometric analysis shows the quantitative formation of the duplex containing one copper salen complex (calculated for [**D4-L-a/D8-L-b**+en+Cu^{2+}-2H_2O-11H^+]$^{9-}$: 1020.7297; found 1020.7259).

Consequently, the formation of the salen complex in the duplex [**D4-L-a/D8-L-b**+en+Cu] must have broken the **AT**-base pair between the two salicylic aldehydes. The formation of the salen complex is obviously so strong that it forces the DNA duplexes to accept unfavorable double helix structures and even one broken base pair.

That the double helix, however, plays a role in complex formation became obvious when the single strand composition of the duplex was analyzed. No homoduplexes (a/a or b/b) were detected by mass spectrometric analysis. The metal was always complexed inside the "correct" heteroduplexes a/b. These results show that the two single strands have to form a stable duplex before metal ion complexation can occur. Once the duplex is formed, however, complex formation is taking place even if the double helix is distorted afterwards.

Formation of [**D4-L-a/D8-L-b**+en+Cu] demonstrates that the complex formation is able to override sequence information.

Double helix **D7-L-a/b**, in which the facing salicylic aldehydes are flanked by the spacers **D** (see Figure 42) on both sides showed a similar behavior in the melting point experiments (Table 5).

4.5.2 Brick-wise elongation of overlapping sequences

On the way towards DNA duplexes containing several metal ions, different approaches were tested. One attempt to generate longer DNA sequences containing several metal ions is based on the consecutive assembly of overlapping sequences (Figure 72).
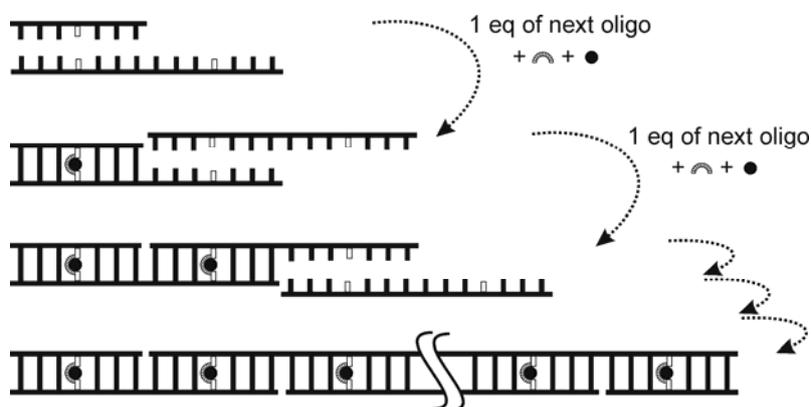
Figure 72: Brick-wise approach to long strands containing numerous metals inside the double helix. For this purpose, the four oligonucleotides depicted in Figure 73 were synthesized.

D17-L-a[e]   5'-CTCLTGG

D17-L-a   CGTLGTCCTCLTGG-3'

D17-L-b   3'-GAGLACCGCALCAG

D17-L-b[e]   GAGLACC-5'
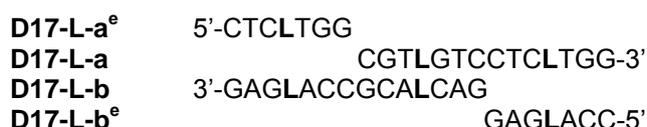
Figure 73: Sequences of the overlapping sequences **D17-L-a** and **D17-L-b** and the terminating strands **D17-L-a**[e] and **D17-L-b**[e].

The experiment was anticipated to proceed in the following way: First one equivalent of the end-piece **D17-L-a**[e] was supposed to hybridize with one equivalent of the complementary sequence **D17-L-b** by cooling the solution from a temperature above the melting point to a temperature below T_M. Addition of excess ethylenediamine and one equivalent of metal ions (e.g. Cu^{2+}) should then lead to a stable duplex containing one metal-salen base pair. The addition of 1 eq of fragment **D17-L-a** should then hybridize to the overhanging stretch of single strand and addition of Cu^{2+} again was supposed to fix the hybridized strands irreversibly and so on.

However, when the experiments were performed, it turned out that the strands would not hybridize in the planned way and no interstrand salen complexes were formed. When **D17-L-a^e** was mixed with **D17-L-b**, ethylenediamine and Cu^{2+}, the short single strand **D17-L-a^e** remained completely unreacted whereas the longer single strand **D17-L-b** formed an intrastrand copper-salen complex as proven by mass spectrometry (see more on unspecific hairpin formation in Chapter 4.5.3). Neither the use of Mn^{2+} instead of Cu^{2+} nor changing the concentrations, order of compound addition, reaction times and temperatures was successful.

Interestingly, when the two end-pieces **D17-L-a^e** and **D17-L-b^e** were hybridized and en and Cu^{2+} were added, the corresponding duplex [**D17-L-a^e/b^e**+en+Cu] was indeed formed quantitatively (see appendix, Figure 101, Chapter 7.1).

An explanation for the failure of this approach might be that the reaction is under control of the kinetically favored intrastrand complex formation. The overlapping sequences were with seven base pairs probably too short to ensure a proper hybridization of the strands. Furthermore, prior to addition of ethylenediamine and a metal salt, one of the seven base pairs (**LL**) must even be considered to be a mismatch. We believe that a lack of a proper double-stranded preorganization is the reason for the failure. The strands containing two salicylic aldehydes strongly tend to form unspecific hairpin structures (see next Chapter) and in this way the intended brick-wise elongation to give a longer sequence was impeded. A solution to this problem might be the use of longer overlapping sequences with a higher **GC** contend.

4.5.3 (Unspecific) hairpin formation and dynamics

Despite the successful experiments to coordinate several (two to ten) metal ions inside one DNA duplex (Chapter 4.6), a number of other tested sequences containing more than one salicylic aldehyde showed problems to form the desired interstrand complex. The formation of hairpins by intrastrand metal-salen complex assembly was observed in these cases even when the oligonucleotide sequence would not allow a proper hairpin formation in unmodified DNA.

Generally, it was found that this complication occurred when the hybridization of the strands could not be ensured, either because of the reaction conditions (concentration, temperature) or because of an intrinsic instability of the double strand.

The problem of duplex stability is a function of **GC**-content and number and position of salicylic aldehydes in the oligonucleotides. Prior to complex formation, the salicylic aldehyde base-pairs **LL** must be considered to be mismatches and positioning of several of these mismatches in a narrow region of the sequence surely leads to destabilization of the duplex. Especially in sequences in which two salicylic aldehydes are separated by one native nucleobase the formation of single strand hairpins was observed when the destabilizing effect of the **LL** mismatches was not compensated by the separating base pair (Figure 74).
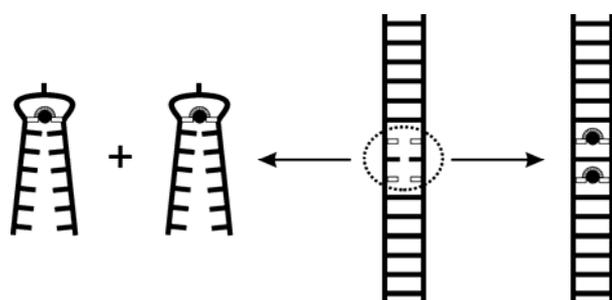
Figure 74: Unspecific hairpin formation vs. double strand formation of complementary strands **D12-L-a** and **D12-L-b**. Indicated by a dashed circle is the unstable middle region of the duplexes.

The results of the complexation experiments with the duplexes **D10-L-a/b** (one **AT** base-pair between two **LL** base-pairs), **D11-L-a/b** (one **GC** base-pair between two **LL** base-pairs) and **D12-L-a/b** (one **DD** base-pair between two **LL** base-pairs) are summarized in Table 7.

Duplex	Base pair between ligands	Observation in ESI MS
D10-L-a/b	**AT**	no duplex, noisy ESI spectrum
D11-L-a/b	**GC**	clean duplex formation
D12-L-a/b	**DD**	no duplex, mostly hairpin salen formation of **D12-L-a** and **D12-L-b**

Table 7: Results of the ESI mass spectrometric measurements of duplexes **D10-L-a/b**, **D11-L-a/b** and **D12-L-a/b** containing excess ethylenediamine (3.3 eq) and two equivalents of Cu^{2+} (DNA concentration 30 μM in 100 mM NH_4OAc, pH 8). **D** = tetrahydrofuran spacer.

Only in the case of a separating **GC** base pair, duplex formation won over the unspecific hairpin formation. It is noteworthy that the reaction products [**D12-L-a**+en+Cu] and [**D12-L-b**+en+Cu] containing the intrastrand copper-salen complex bridging over three consecutive nucleobases might be considered as the smallest possible hairpin structure imaginable. A structural model of the covalently

closed macrocycle formed by this reaction is depicted in Figure 75. The macrocycle has a ring size of 25 atoms (smallest perimeter).
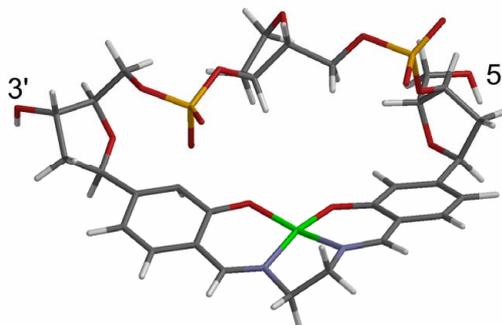
Figure 75: Molecular model of the covalent 25-membered macrocycle formed by the formation of an intrastrand salen complex in the strand **D12-L-a** (semi empiric equilibrium geometry optimization, PM3; light grey: H; dark grey: C; red: O; orange: P; blue: N; green: Cu^{2+}).[233]

Going from one native base-pair between to pairs of salicylic aldehydes to higher numbers of separating base-pairs another interesting observation was made: When a sample of the strand **D13-L-a/b** (containing three *Watson-Crick*-base pairs between the salicylic aldehydes) was treated with excess ethylenediamine and two equivalents of Cu^{2+}, mass spectrometry initially revealed the exclusive formation of the single strand hairpins [**D13-L-a**+en+Cu] and [**D13-L-b**+en+Cu]. However, when the same sample was stored at room temperature for several days, a slow conversion of the single strand hairpins to the corresponding double strand [**D13-L-a/b**+2en+2Cu] was observed (Figure 76).
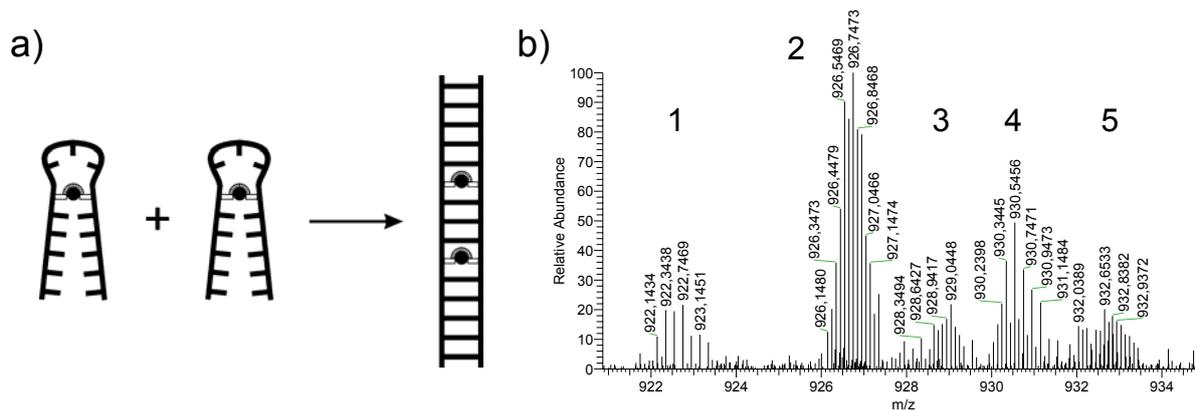
Figure 76: A slow conversion of the two unspecific hairpin structures [**D13-L-a**+en+Cu] and [**D13-L-b**+en+Cu] to the double helix [**D13-L-a/b**+2en+2Cu] containing two copper-salen complexes was observed by ESI mass spectrometry. a) Schematic depiction of the process; b) ESI-MS spectrum showing the sample 10 days after its preparation. The transformation into the species [**D13-L-a/b**+2en+2Cu] is not yet completely finished. The following species can be identified: (1) [**D13-L-a**+en+Cu], (2) [**D13-L-a/b**+2en+2Cu], (3) [**D13-L-a/b**+2en+2Cu+Na], (4) [**D13-L-b**+en+Cu] over [**D13-L-a/b**+2en+2Cu+K] and (5) [**D13-L-a**+en+Cu+Na+K].

The unspecific hairpin formation is a kinetically controlled process leading to metastable intermediates, which only slowly transform to the thermodynamic favored duplex. These experiments seemed to be very sensitive to the reaction conditions (temperature, incubation time) and the reproducibility was troublesome. Therefore, it was not possible to quantify the conversion process of [**D13-L-a**+en+Cu] and [**D13-L-b**+en+Cu] into [**D13-L-a/b**+2en+2Cu] in a kinetic study.

Another reason for an unavoidable unspecific hairpin formation was given when one of the complementary strands was in excess over its counter strand in the reaction mixture. This was sometimes a result of the unprecise determination of the oligonucleotide concentration. Figure 102 in the appendix (Chapter 7.1) shows the example of an experiment where the preparation of duplex **D14-L-a/b** contained a slight excess of the single strand **D14-L-a**. Addition of ethylenediamine and Cu^{2+} consequently gave a mixture of the duplex [**D14-L-a/b**+2en+2Cu] and the single strand hairpin [**D14-L-a**+en+Cu].

In the case of duplex **D9-L-a/b** where two salicylic aldehydes are directly neighbored, no unspecific hairpin formation by intrastrand salen complex formation was observed. Reaction of **D9-L-a/b** with ethylenediamine and Cu^{2+} yielded the product [**D9-L-a/b**+2en+2Cu] with two copper-salen complexes stacking on top of each other. The objection could be made that maybe both strands form intrastrand salen complexes instead of two stacking interstrand salen complexes (Figure 77).
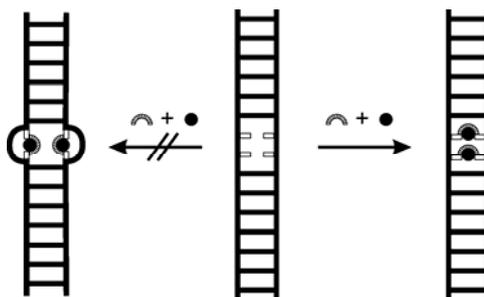
Figure 77: Two hypothetic ways the two metal-salen complexes can assemble inside the duplex **D9-L-a/b**.

This scenario could, however, be disproved by the fact that a single stranded sample **D9-L-a** or **D9-L-b** did not yield any intrastrand salen complex. Furthermore, the small distance between the directly neighbored salicylic aldehydes does not allow for a complex formation, which becomes evident from a corresponding structural computer model (not shown). More data on the successful stacking of two and more metals is discussed in Chapter 4.6.

In contrast, DNA sequences **D2-L** and **D3-L** were prepared with the intention to form hairpins [**D2-L**+en+metal] and [**D3-L**+en+metal] exclusively and so they did. Experiments on the complexation of various metals by hairpin **D2-L** are presented in Chapter 4.4.4. Hairpin **D3-L** carries the metal-base pair right next to a **TTTT**-loop, so that the metal complex closes the hairpin thereby presenting the metal to the core of a chiral cavity. In this case, too, formation of the metal-salen complexes either with Mn^{2+} or Cu^{2+} was observed in the thermal de- and renaturing curves.

4.5.4 Reaction of single strands

The reaction of oligonucleotide single strands containing two salicylic aldehydes to intrastrand hairpins as a side reaction to the formation of metal-containing duplexes was discussed in the preceding Chapter. But also single strands containing only one salicylic aldehyde were found to react with ethylenediamine and a metal ion to yield presumably a complex of a tridentate Schiff-base ligand and a further loosely bound ligand or solvent molecules (Figure 78). Metal-complexes of this type were described in the literature before.[234]
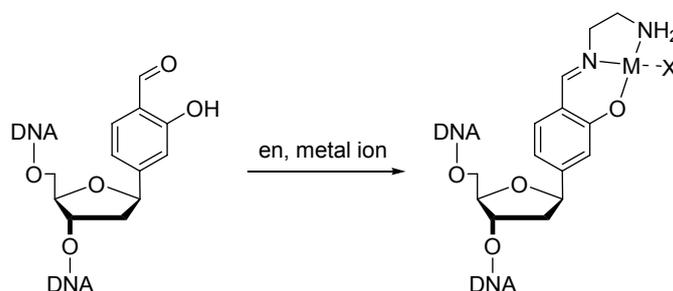
Figure 78: Expected structure of a single strand metal-aldimine complex (X = loosely bound ligand from solvent).

The evidence for this reaction was given by ESI mass spectrometry. The found masses could be assigned to the reaction product of the single strand plus one molecule of ethylenediamine plus one metal ion minus one molecule of water and minus a number of H^+-ions corresponding to the charge of the used metal ion. Even when a mixture of complementary single strands was treated with ethylenediamine and an excess of metal ions prior to hybridization of the sample, the formation of the single strand metal-complexes instead of the desired duplex was observed in some cases (observed e.g. for sequence **D16-L-a/b** containing an excess of Cu^{2+}).
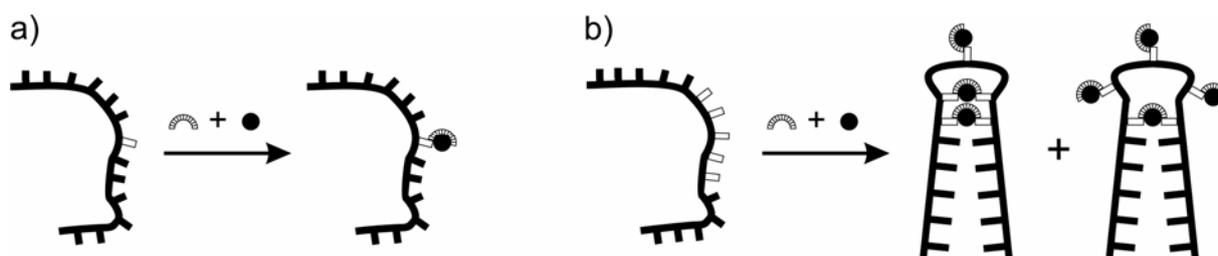
Figure 79: Schematic formation of the single strand copper complexes in strands containing the salicylic aldehyde nucleobases. a) one salicylic aldehyde per strand; b) single strands containing five salicylic aldehydes react to a mixture of a doubly bridged species carrying one extra copper complex and a singly bridged species carrying three extra copper complexes (one possible isomer shown).

An interesting situation was observed with the strands containing an odd number (three or more) of salicylic aldehydes in close proximity: The single strand **D18-L-b**, for example could be transformed into the compounds [**D18-L-b**+3en+3Cu] and [**D18-L-b**+4en+4Cu], respectively. From the stoichiometry of water molecules lost in the reaction it can be anticipated, that the constitution of the strands is according to Figure 79b. The corresponding ESI mass spectrum can be found in the appendix (Figure 103, Chapter 7.1).

4.6   Metal stacks and arrays

A special interest behind the incorporation of several metal-base pairs into one DNA duplex is the desire to construct metal arrays which provide new perspectives for the nanotechnological exploitation of the DNA structure as a molecular wire or electronic switch or for the generation of artificial multi-metal ribozymes. Furthermore, access to a variable set of multidentate ligands is of great interest to study metal interactions in homo- or hetero-multimetallic coordination compounds.

4.6.1 Two metal-salen complexes inside one duplex

To test the metal-salen base pair concept for its suitability to coordinate more than one metal ion inside a DNA double helix, the duplexes **D14-L-a/b** (containing two remote salen ligands separated by three *Watson-Crick* base pairs) and **D9-L-a/b** (containing two directly neighbored salen ligands) were prepared. In both of these duplexes two copper-salen complexes could be successfully assembled by addition of excess ethylenediamine (en) and two equivalents of Cu^{2+}. The analysis by ESI-

ICR mass spectrometry showed a quantitative reaction to the expected reaction products

[**D14-L-a/b**   +2en+2Cu^{2+}–4H$_2$O–4H$^+$]   and   [**D9-L-a/b**   +2en+2Cu^{2+}–4H$_2$O–4H$^+$] (Figure 80). Furthermore, a thermal de- and renaturation study with the duplex **D14-L-a/b** showed significant changes of the melting curves in absence and presence of ethylenediamine and/or Cu^{2+} (see Chapter 4.4.2.4).
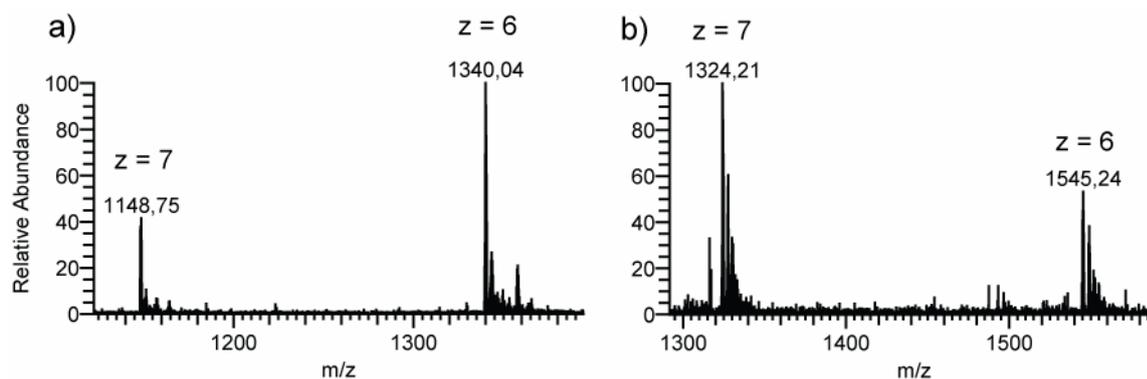
Figure 80: ESI-ICR spectra of a) [**D14-L-a/b**+2en+2Cu] showing the measured mass of the highest peaks. Lowest weight isotopomer mass found for [**D14-L-a/b**+2en+2Cu^{2+}–4H$_2$O–10H$^+$]$^{6-}$: 1339.3717; calculated for [C$_{264}$H$_{319}$N$_{89}$O$_{152}$P$_{24}$Cu$_2$]$^{6-}$: 1339.3705 and b) [**D9-L-a/b**+2en+2Cu] showing the measured mass of the highest peaks. Lowest weight isotopomer mass found for [**D9-L-a/b**+2en+2Cu^{2+}–4H$_2$O–10H$^+$]$^{7-}$: 1323.6397; calculated for [C$_{308}$H$_{372}$N$_{99}$O$_{176}$P$_{28}$Cu$_2$]$^{7-}$: 1323.6344.

EPR experiments on the two-copper system [**D9-L-a/b**+2en+2Cu] allowed the determination of a Cu^{2+}-Cu^{2+}-distance of ca 3.9 Å which indicates a longitudinal expanding of the DNA duplex when compared to the distance which is extracted from a computed structural model (Chapter 4.4.6).

The problem of unspecific hairpin formation in single strands containing more than one salicylic aldehyde arising from intramolecular salen complex formation was already discussed in Chapter 4.5.3. The duplexes **D9-L-a/b** and **D14-L-a/b**, however, did not suffer from this side reaction.

4.6.2 Homo-polynuclear metal stacks inside DNA

Several examples of metal stacking in crystalline bulk matter have been succeeded by just a few examples of defined multinuclear metal-complexes in solution, most of them which are complicated to synthesize and only stable in dry organic solvents (see Chapter 3.4.3). So far, only one example of stacking of up to five consecutive copper atoms by means of metal-base pairs in DNA was fully characterized.[123]

The extension of the metal-salen base pair concept to the synthesis of multinuclear DNA-based metal complexes with up to ten metal ions stacked linearly atop each other inside a DNA double helix is shown in Figure 81. The successful stacking of 10 metal ions inside the duplex means that a complete turn of the double helix ranging over a distance of 3.4 nm is substituted by an artificial construct.[235]
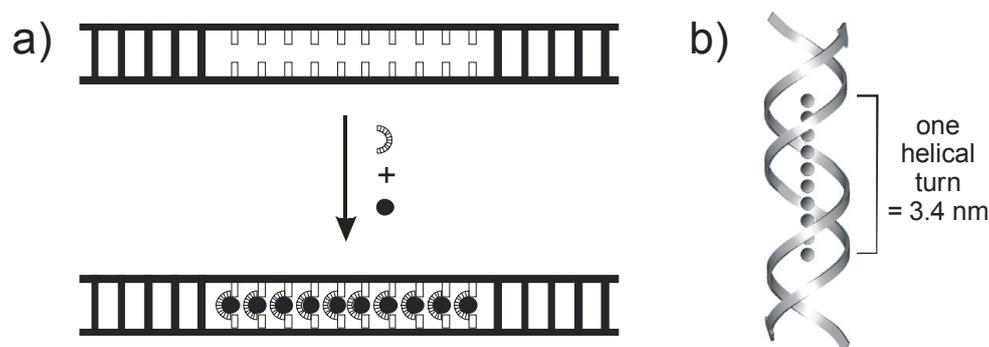
Figure 81: Depiction of the assembly of ten metal-salen base pairs inside a DNA duplex. a) assembly principle starting from the preorganized duplex; b) dimension of the metal stack assuming a B-DNA like secondary structure.

The synthesis of the oligonucleotides **D18-L-a/b** and **D19-L-a/b** was accomplished according to the same protocols, which were used before for the incorporation of a single modification. An excellent coupling fidelity of the ligand precursor in the automated DNA synthesis was found to be a prerequisite for the successful generation of the oligonucleotides containing up to 10 salicylic aldehydes in high purities and yields. A stretch of five *Watson-Crick* base pairs on either end of the duplexes **D18-L-a/b** and **D19-L-a/b** was chosen to provide an optimal preorganization of the system for the succeeding complex formation.

Figure 82a displays the characteristic UV spectral changes of the duplex [**D19-L-a/b** +10en] upon titration of Cu^{2+} ions into the solution. The overlaid curves show isosbestic points at λ = 342 nm and λ = 398 nm. Similar curves were obtained for [**D18-L-a/b** +5en+5Cu] (Figure 82b). A plot of the absorption maximum of the copper salen chromophore at λ = 360 nm against the copper concentration shows a linear rise up to a ratio of duplex to Cu^{2+} of about 1 : 10 for duplex **D19-L-a/b** and a ratio of 1 : 5 for duplex **D18-L-a/b** (Figure 83).
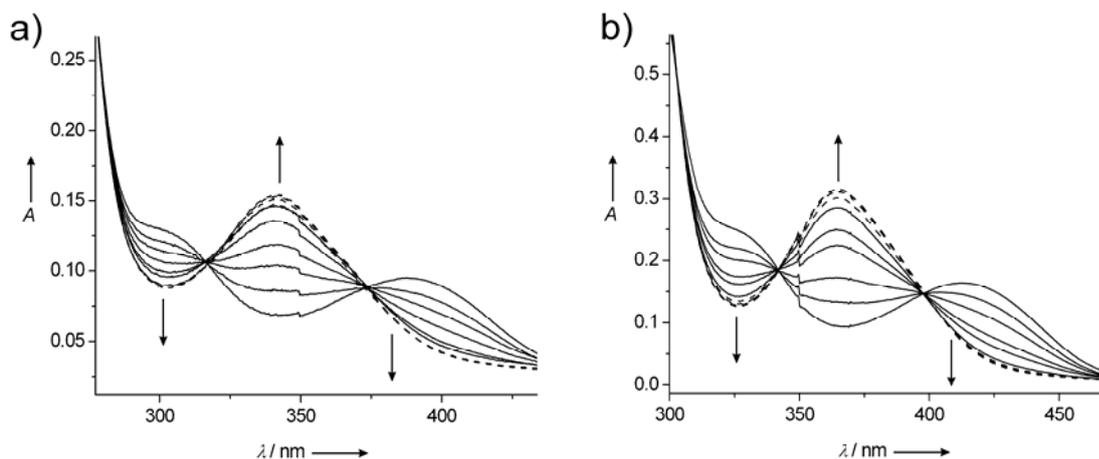
Figure 82: Titration of [**D18-L-a/b**+5en] and [**D19-L-a/b**+10en] with Cu^{2+}. a) Overlay of UV-Vis spectra of 30 μM [**D18-L-a/b**+5en+xCu] at various concentrations of Cu^{2+} (x = 0 eq to 9 eq in steps of 1 eq); b) Overlay of UV-Vis spectra of 6 μM [**D19-L-a/b**+10en+xCu] at various concentrations of Cu^{2+} (x = 0 eq to 18 eq in steps of 2 eq). The samples contained 10 mM CHES buffer and 150 mM NaCl.
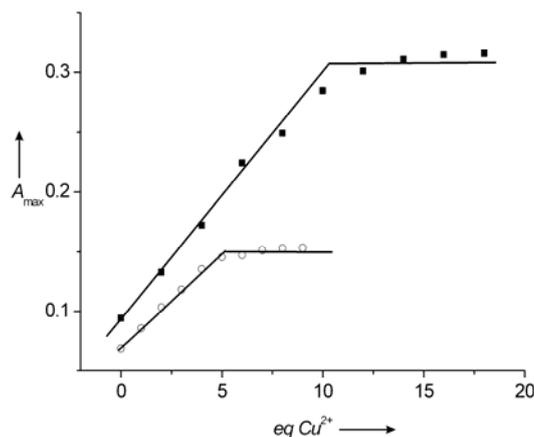
Figure 83: Plot of the absorption maximum A_{max} of the copper-salen system against the ratio $[Cu^{2+}]/[duplex]$ for [**D18-L-a/b**+5en+xCu] (open circles) and [**D19-L-a/b**+10en+xCu] (black boxes).

Temperature dependent circular dichroism spectra of duplex **D19-L-a/b** in absence or presence of ethylenediamine and Mn^{2+} can be found in Chapter 4.4.3.2 (Figure 62). In contrast to the bare duplex **D19-L-a/b**, the CD spectra of [**D19-L-a/b**+10en+10Mn] did not change when the temperature was raised. This is a clear sign for the high structural stability of the duplex caused by the multiple metal-salen crosslinks.

The correct assembly of 5 and 10 metal-salen complexes inside the double strands **D18-L-a/b** and **D19-L-a/b**, respectively, was further supported by ESI-ICR mass spectrometric measurements.

Clean mass spectra with the Cu^{2+} containing samples were, however, complicated to observe. Frequently, broad mass distributions in the spectra around the expected

molecular mass were obtained. Furthermore, under the conditions chosen for the ESI experiments, excess Cu^{2+} in solution lead to the formation of adducts containing more Cu^{2+} atoms than salen ligands. In the case of duplex [**D18-L-a/b**+5en], addition of 5 equivalents of Cu^{2+} yielded [**D18-L-a/b**+5en+5Cu] but addition of 10 equivalents gave rise to a mass spectrum which might be assigned to the species [**D18-L-a/b**+5en+9Cu] (see appendix, Figure 104 and Figure 105, Chapter 7.1).

When Mn^{2+} was used to assemble the stacked salen complexes inside the oligonucleotides, the mass spectra were of much higher quality. Addition of en and Mn^{2+} to the duplex **D19-L-a/b** yielded mass spectrometric data which were in full agreement with a structure containing 10 manganese-salen complexes. We believe that the reason for this is the reduced tendency of the manganese ions to form unspecific complexes.

Figure 84 shows an ESI-ICR spectrum of the reaction product [**D19-L-a/b**+10en+10Mn^{3+}-20H$_2$O-20H$^+$]$^{10+}$ of duplex **D19-L-a/b** with 10 molecules of ethylenediamine and 10 manganese ions under loss of 20 equivalents of water and 20-fold deprotonation. Again, the salen-bound manganese was oxidized to Mn^{3+} under aerobic conditions. This process was also shown to happen for the system [**D19-L-a/b**+10en+10Mn] by mass spectrometry.
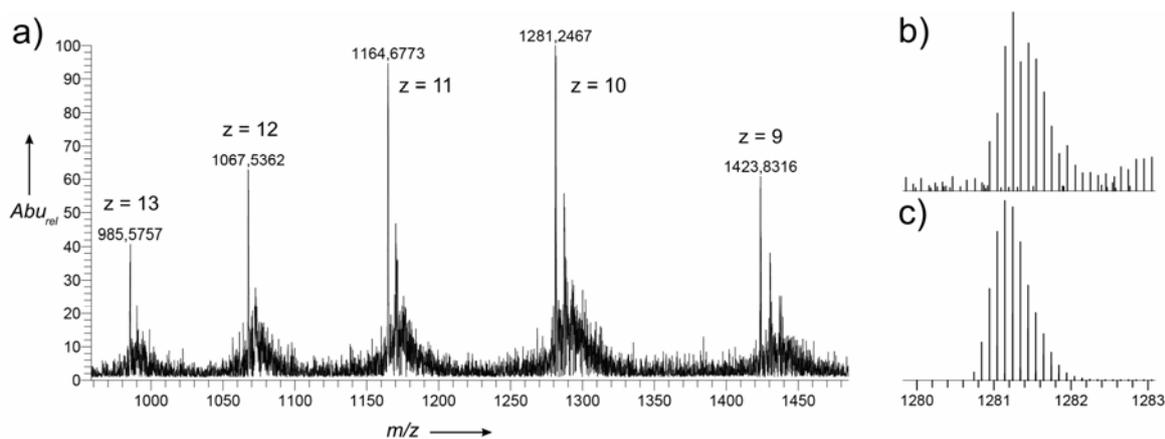
Figure 84. a) ESI-ICR mass spectrum of [**D19-L-a/b**+10en+10Mn]. The measured *m/z* values for *z* = 9..10 are in excellent agreement with the calculated masses. b) Measured isotope pattern for [**D19-L-a/b**+10en+10Mn^{3+}-20H$_2$O-40H$^+$]$^{10-}$. c) Simulated isotope pattern for the lowest isotopomer of [C$_{450}$H$_{502}$N$_{100}$O$_{236}$P$_{38}$Mn$_{10}$]$^{10-}$.

The mass spectra of [**D18-L-a/b**+5en+5Mn^{3+}-10H$_2$O-10H$^+$]$^{5+}$ and [**D19-L-a/b**+10en+10Cu^{2+}-20H$_2$O-20H$^+$] can be found in the appendix, Figure 106

and Figure 107, Chapter 7.1. A graphical representation of ten metal-salen complexes inside the double helix [**D19-L-a/b**+10en+10Mn] is depicted in Figure 85.
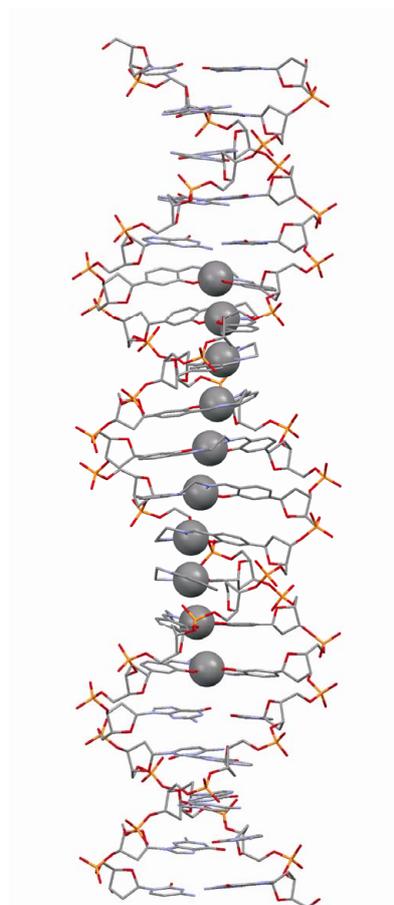
Figure 85: Computer model of [**D19-L-a/b**+10en+10Mn] representing a plausible structure of ten metal-salen complexes assembled inside the DNA double helix.[236]

When the metal complexation experiment was performed with the strand **D20-L**, which consists exclusively of 8 salicylic aldehyde nucleobases **25**, no distinct species [**D20-L**+8en+8M] was obtained but a dark precipitate was formed after several hours. This precipitate most likely is a (branched and crosslinked) polymer consisting of the oligonucleotides, which are randomly connected with each other by multiple metal-salen complexes.

4.6.3 Hetero-polynuclear stacks: controlled mixing of metals inside DNA

After we could show that metal stacking inside the DNA with the salen ligand is possible, a strategy was worked out to complex different metals inside the same duplex in a predetermined fashion. The coordination of two different metals required a second ligand with orthogonal selectivity. The **TT**-mismatch shown by *Marzilli* and

others to coordinate a Hg^{2+} ion selectively was chosen as a the second coordination site besides the salen complex (see Chapter 3.3.1).

According to the sequences of duplexes **D18-L-a/b** and **D19-L-a/b**, the 15mer duplexes **D22-L-a/b** and **D23-L-a/b** as well as the 20mer duplexes **D24-L-a/b** and **D25-L-a/b** were designed. They form a double helix prior to the addition of the metal ions to provide a preorganized geometry for the assembly of the stacked metal complexes. The modular synthesis of the oligonucleotides easily allowed a programming of the sequence of the two different ligands and thereby the defined arrangement of the coordinated metals (Figure 86).

5'-GCGCG**TLTLT**GGCCG-3'　　　　　　　5'-GCGCG**LTLTLTLTLT**GGCCG-3'
3'-CGCGC**TLTLT**CCGGC-5'　　　　　　　3'-CGCGC**LTLTLTLTLT**CCGGC-5'

D22-L-a/b　　　　　　　　　　　　　　**D24-L-a/b**

5'-GCGCG**LTTTL**GGCCG-3'　　　　　　　5'-GCGCG**LTTTTLLLLL**TGGCCG-3'
3'-CGCGC**LTTTL**CCGGC-5'　　　　　　　3'-CGCGC**LTTTTLLLLL**TCCGGC-5'
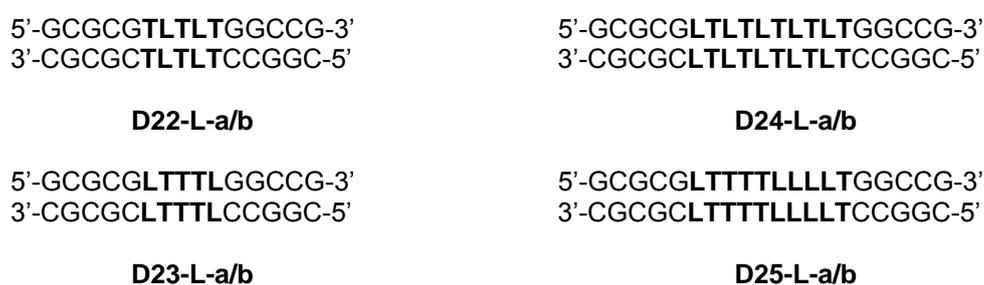
D23-L-a/b　　　　　　　　　　　　　　**D25-L-a/b**

Figure 86: The sequences **D22-L-a/b**, **D23-L-a/b**, **D24-L-a/b** and **D25-L-a/b** which were synthesized for the programmed assembly of mixed metal stacks.

After hybridization of the strands, first excess ethylenediamine was added, then Cu^{2+} and finally Hg^{2+}. The assembly process is schematically shown for duplex **D25-L-a/b** in Figure 87.
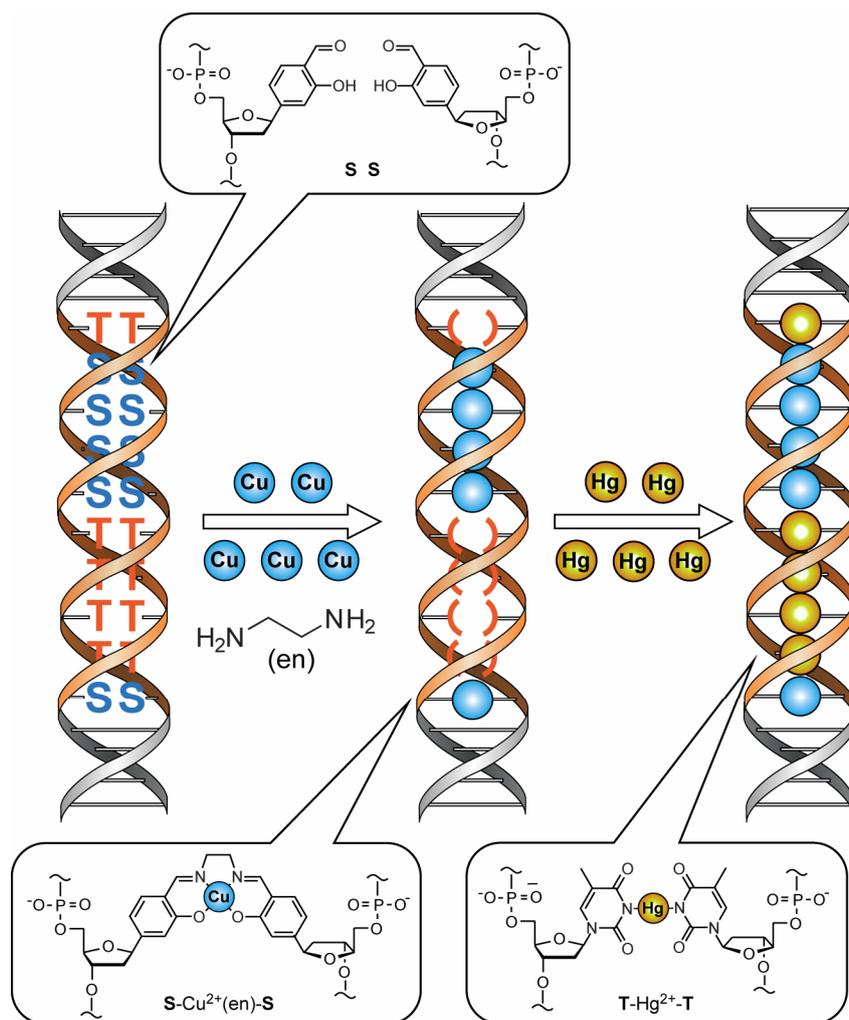
Figure 87: Schematic representation of the assembly of the programmed metal stack in **D25-L-a/b**. Only the metal-coordinating core sequence is depicted.

The metal coordination was followed by CD spectroscopic titration experiments. The formation of the desired products was further confirmed by ESI mass spectrometry. The obtained results are discussed below for the isomers **D22-L-a/b** and **D23-L-a/b** (Figure 88 and Figure 89) and the isomers **D24-L-a/b** and **D25-L-a/b** (Figure 90 and Figure 91).
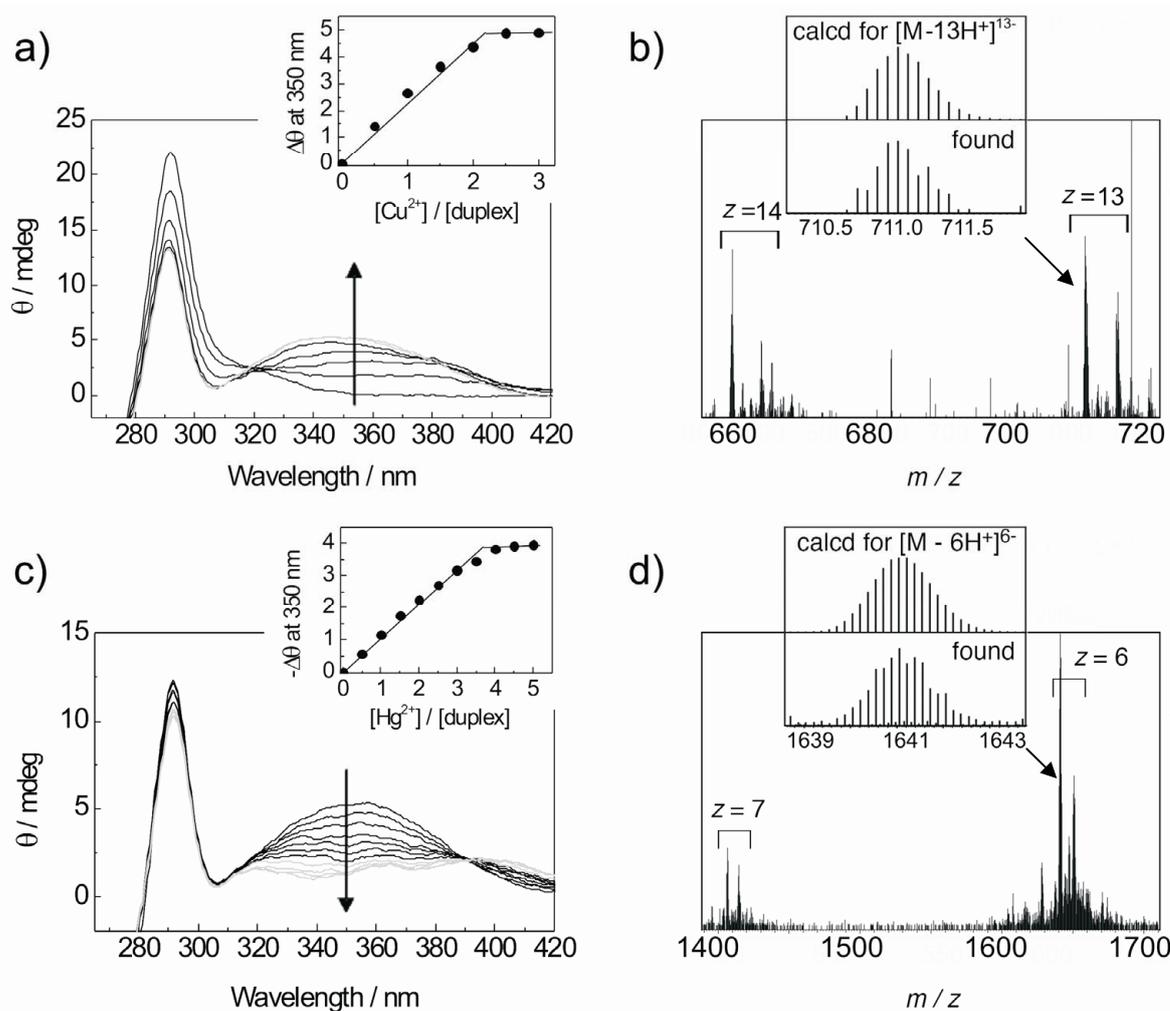
Figure 88: Assembly of a mixed five-metal stack in the order Hg^{2+}-Cu^{2+}-Hg^{2+}-Cu^{2+}-Hg^{2+} inside duplex **D22-L-a/b**. a) CD spectral changes at various concentrations of Cu^{2+} at 25 °C. [**D22-L-a/b**] = 15 µM in 1 mM ethylenediamine, 10 mM CHES (pH 9.0) and 20 mM $NaNO_3$ (inset: plot of circular dichroic changes at 350 nm against the ratio of $CuSO_4$ to **D22-L-a/b**); b) ESI-ICR mass spectrum of [**D22-L-a/b**+2en+2Cu] ($C_{302}H_{376}N_{96}O_{182}P_{28}Cu_2$); c) CD titration of [**D22-L-a/b**+2en+2Cu] with Hg^{2+}; d) ESI-ICR mass spectrum of [**D22-L-a/b**+2en+2Cu+3Hg] ($C_{302}H_{370}N_{96}O_{182}P_{28}Cu_2Hg_3$). For each charge z in the ESI spectra the first large peak corresponds to the bare molar ion of the metal-DNA assembly; the following peaks are adducts with Na^+, K^+ and/or NH_4^+.

The titration of the duplex **D22-L-a/b** with Cu^{2+} clearly showed the incorporation of two copper ions inside the DNA duplex (Figure 88a). The CD spectrum features an isosbestic point at 319 nm and shows a positive Cotton effect of the absorption band of the natural DNA bases, which decreases upon addition of Cu^{2+}. Simultaneously, the salen-ligand centered absorption band around 350 nm, which shows no ellipticity in the absence of Cu^{2+}, displays an increasing positive Cotton effect when Cu^{2+} is added until a ratio of [Cu^{2+}]/[duplex] = 2.0 is reached. The resulting product was confirmed by ESI mass spectrometry to be [**D22-L-a/b**+2en+2Cu] (found: 710.95 (z = 13), calculated for [M - 13H$^+$]$^{13-}$: 710.95) (Figure 88b).[237] Subsequent titration of Hg^{2+} ions into the same solution caused the positive CD-band around 350 nm to gradually

decrease linearly with the ratio of [Hg^{2+}]/[duplex] from 0.0 to about 3.0 (Figure 88c). The bimetallic ion stack inside the DNA double helix was confirmed by ESI-MS to be [**D22-L-a/b**+2en+2Cu+3Hg] (found: 1641.05 (z = 6), calculated for [M - $6H^+$]$^{6-}$: 1640.97) (Figure 88d). These experiments unambiguously show that the duplex **D22-L-a/b** quantitatively and site-selectively forms a pentanuclear complex with two Cu^{2+} ions and three Hg^{2+} ion in the order, Hg^{2+}-Cu^{2+}-Hg^{2+}-Cu^{2+}-Hg^{2+}.

The titration of Cu^{2+} and Hg^{2+} to the isomeric duplex **D23-L-a/b** likewise yielded a metal stack inside the DNA double helix in the order Cu^{2+}-Hg^{2+}-Hg^{2+}-Hg^{2+}-Cu^{2+} (Figure 89).
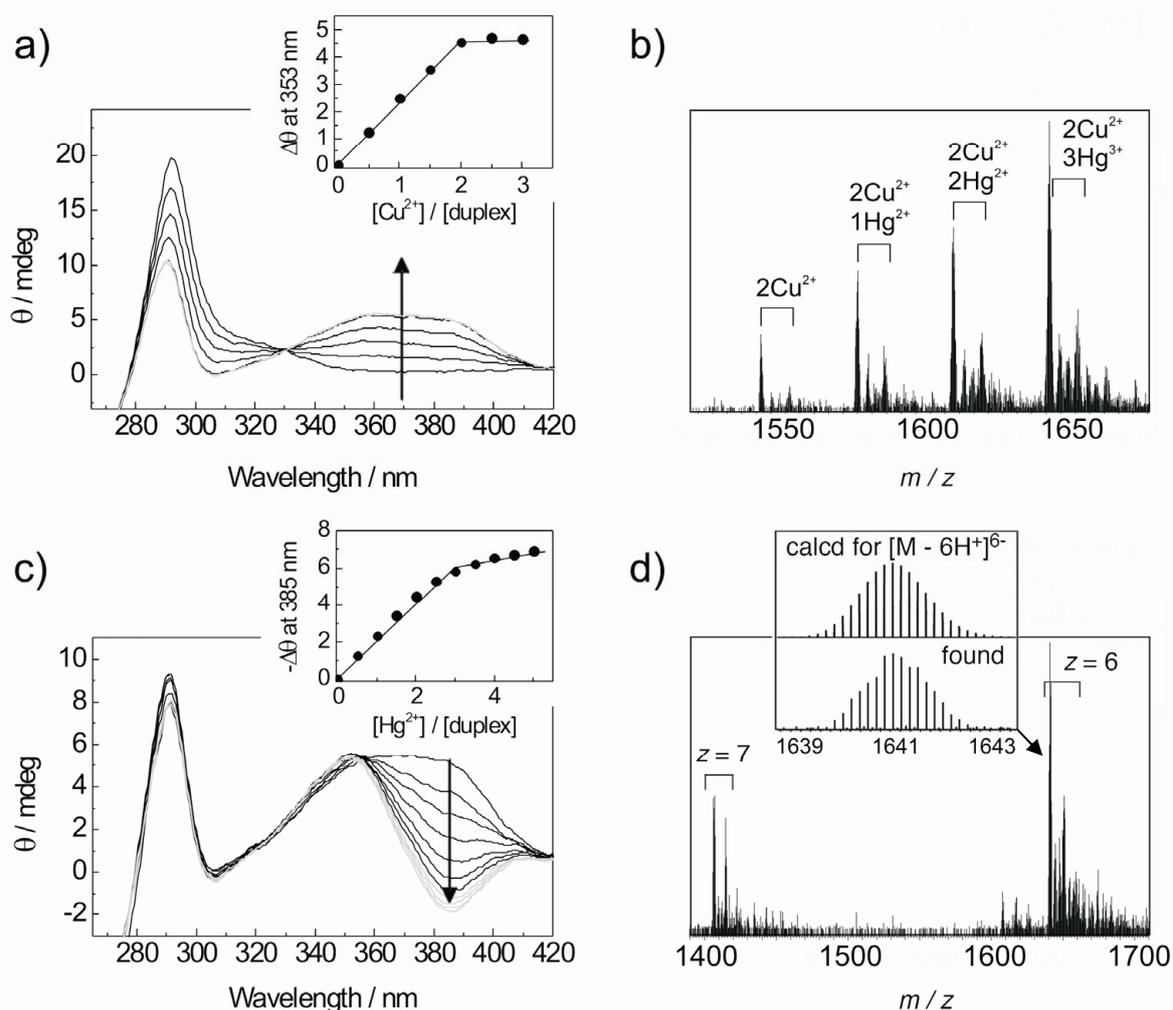
Figure 89: Assembly of a mixed five-metal stack in the order Cu^{2+}-Hg^{2+}-Hg^{2+}-Hg^{2+}-Cu^{2+} inside duplex **D23-L-a/b**. a) CD spectral changes at various concentrations of Cu^{2+} at 25 °C. [**D23-L-a/b**] = 15 μM in 1 mM ethylenediamine, 10 mM CHES (pH 9.0) and 20 mM $NaNO_3$ (inset: plot of circular dichroic changes at 353 nm against the ratio of $CuSO_4$ to **D23-L-a/b**); b) ESI-ICR mass spectrum of a sample of [**D23-L-a/b**+2en+2Cu] with only a slight excess of Hg^{2+}: the ability of the system to coordinate up to maximal three Hg^{2+} ions becomes evident; c) CD titration of [**D23-L-a/b**+2en+2Cu] with Hg^{2+}; d) ESI-ICR mass spectrum of [**D23-L-a/b**+2en+2Cu+3Hg] ($C_{302}H_{370}N_{96}O_{182}P_{28}Cu_2Hg_3$). For each charge z in the ESI spectra the first large peak corresponds to the bare molar ion of the metal-DNA assembly; the following peaks are adducts with Na^+, K^+ and/or NH_4^+.

A remarkable different behavior of the isomeric systems **D22-L-a/b** and **D23-L-a/b** was observed in the mass spectrometric measurements. When the oligonucleotide samples were treated with the same amount of ethylenediamine (30 eq), Cu^{2+} (3 eq) and Hg^{2+} (8 eq), only duplex **D22-L-a/b** with the central sequence **TLTLT** showed a quantitative uptake of all 5 metal ions in the mass spectrum. The sample of duplex **D23-L-a/b** with the central sequence **LTTTL**, however, gave signals belonging to the species   [**D23-L-a/b**+2en+2Cu],   [**D23-L-a/b**+2en+2Cu+1Hg], [**D23-L-a/b**+2en+2Cu+2Hg] and [**D23-L-a/b**+2en+2Cu+3Hg]. The coordination of all three Hg^{2+} ions inside the DNA was therefore under these conditions not complete. The reason for this behavior might be that the structural preorganization of the **TT**-mismatch as a mercury binding site has a pronounced influence on the binding constants of the concerned **TT**-sites. Whereas all **TT**-sites in **D22-L-a/b** are "stitched" together by the flanking **GC** stretches and the central copper-salen complexes, the three neighbored **TT**-sites in **D23-L-a/b**, in contrast, seem to form a mispaired "bubble" structure with higher structural flexibility. This seems to result in a diminished capability of Hg^{2+} binding, which is expressed by a smaller binding constant and in turn the need of higher Hg^{2+} concentrations to yield a complete saturation.

Generally it was found, that a ca. twofold excess of Hg^{2+} ions in the reaction mixture was necessary to ensure that all mass spectrometrically observed duplexes contain the expected number of mercury ions. This is in contrast to the quantitative coordination of Hg^{2+} to all the **TT** mismatches in the duplexes (1 : 1 ratio of Hg^{2+} to **TT**) measured by the CD titration experiments. The reason for this discrepancy might be either a decrease of the Hg^{2+} binding constant of the system or a loss of Hg^{2+} ions in the gas phase under the electro spray ionization conditions.

Also for duplexes **D24-L-a/b** and **D25-L-a/b**, the titrations of the metal ions were monitored by CD spectroscopy and the product formation was confirmed by mass spectrometry.[238]
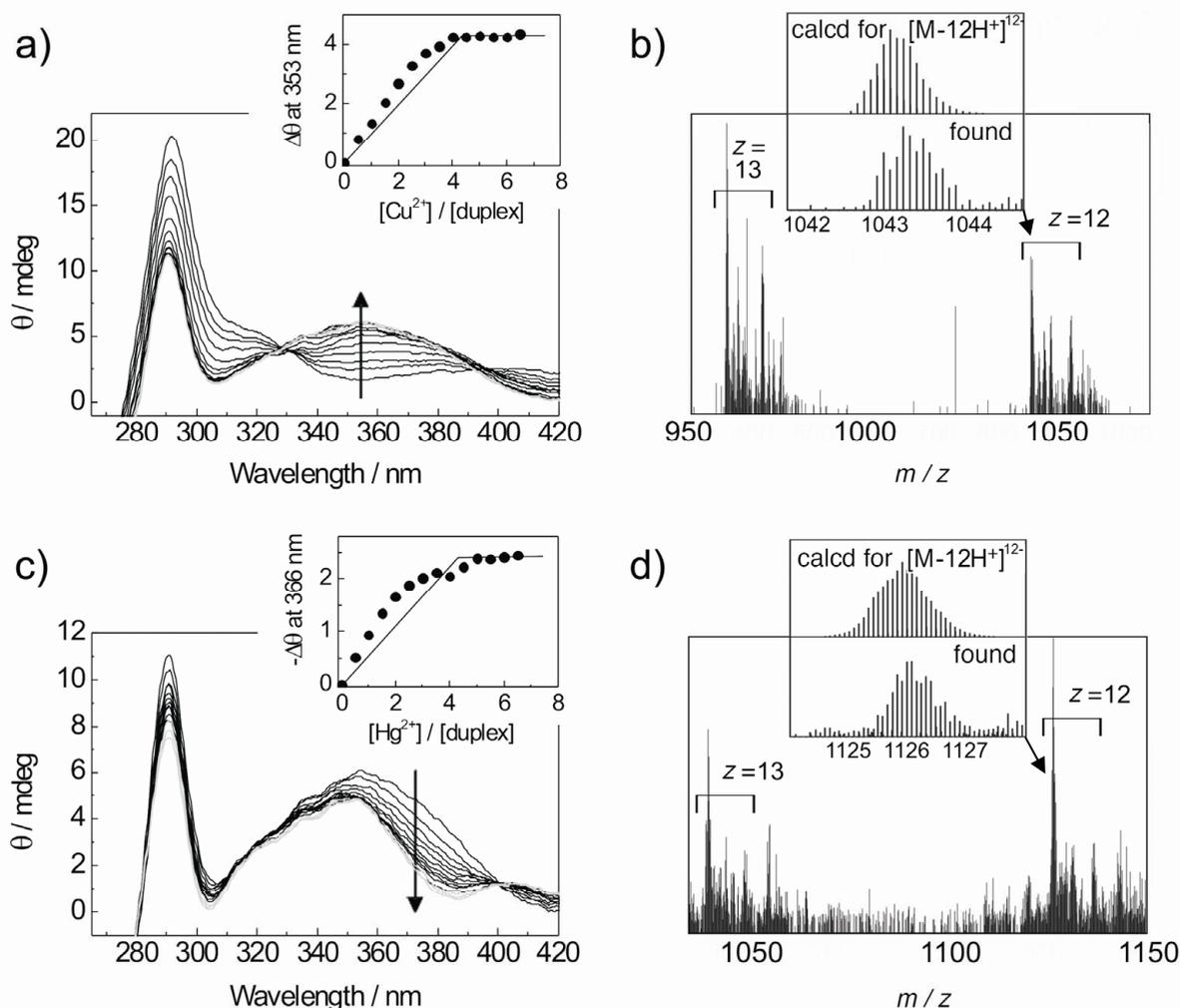
Figure 90: Assembly of the ten-metal stack Cu^{2+}-Hg^{2+}-Cu^{2+}-Hg^{2+}-Cu^{2+}-Hg^{2+}-Cu^{2+}-Hg^{2+}-Cu^{2+}-Hg^{2+} inside duplex **D24-L-a/b**. a) CD spectral changes at various concentrations of Cu^{2+} at 25 °C. [**D24-L-a/b**] = 15 μM in 1 mM ethylenediamine, 10 mM CHES (pH 9.0) and 20 mM $NaNO_3$ (inset: plot of circular dichroic changes at 353 nm against the ratio of $CuSO_4$ to **D24-L-a/b**); b) ESI-ICR mass spectrum of [**D24-L-a/b**+5en+5Cu] ($C_{420}H_{512}N_{110}O_{246}P_{38}Cu_5$); c) CD titration of [**D24-L-a/b**+2en+2Cu] with Hg^{2+}; d) ESI-ICR mass spectrum of [**D24-L-a/b**+5en+5Cu+5Hg] ($C_{420}H_{502}N_{110}O_{246}P_{38}Cu_5Hg_5$). For each charge z in the ESI spectra the first large peak corresponds to the bare molar ion of the metal-DNA assembly; the following peaks are adducts with Na^+, K^+ and/or NH_4^+.

127
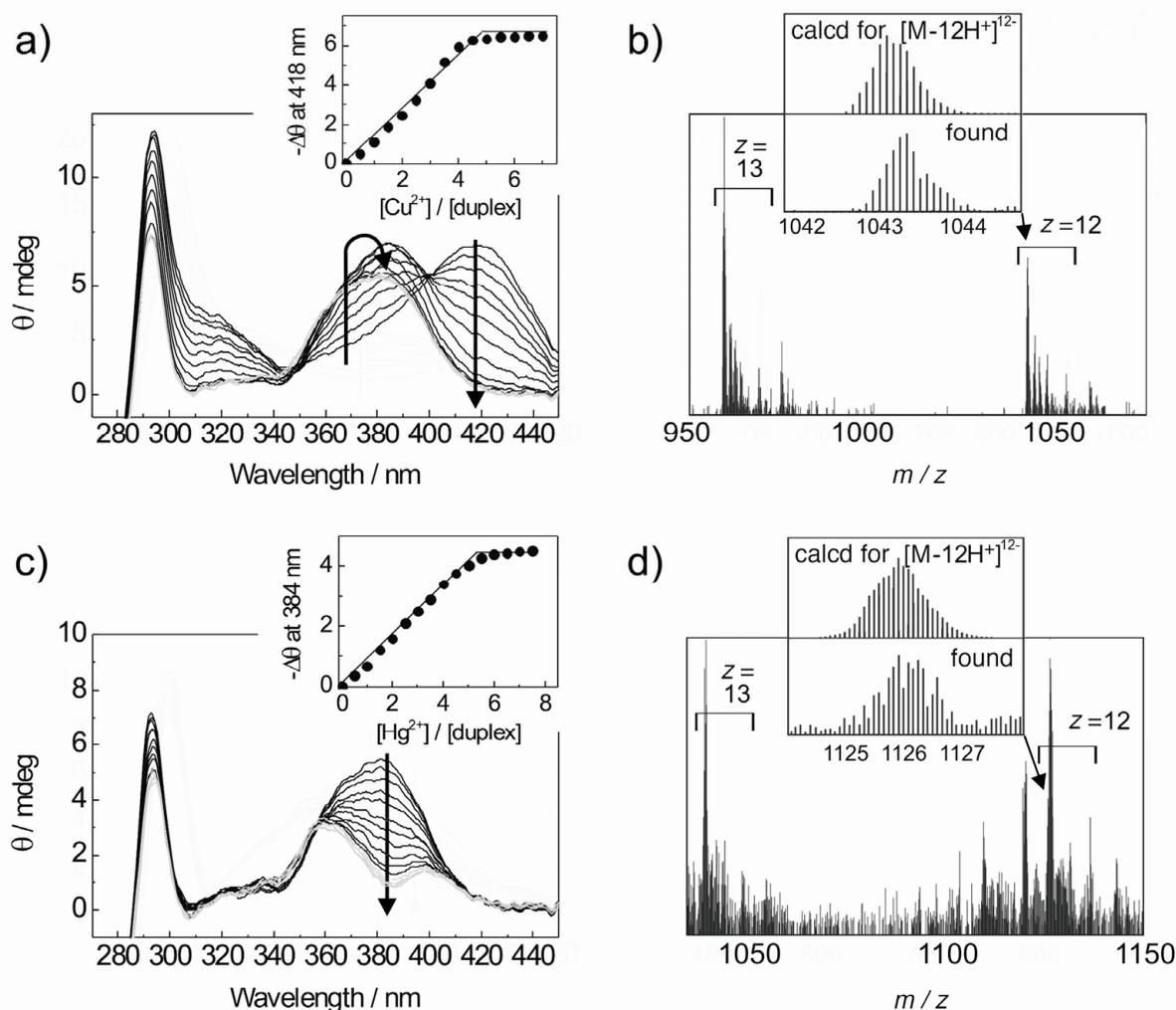
Figure 91: Assembly of the ten-metal stack Cu^{2+}-Hg^{2+}-Hg^{2+}-Hg^{2+}-Hg^{2+}-Cu^{2+}-Cu^{2+}-Cu^{2+}-Cu^{2+}-Hg^{2+} inside duplex **D25-L-a/b**. a) CD spectral changes at various concentrations of Cu^{2+} at 25 °C. [**D25-L-a/b**] = 15 μM in 1 mM ethylenediamine, 10 mM CHES (pH 9.0) and 20 mM $NaNO_3$ (inset: plot of circular dichroic changes at 418 nm against the ratio of $CuSO_4$ to **D25-L-a/b**); b) ESI-ICR mass spectrum of [**D25-L-a/b**+5en+5Cu] ($C_{420}H_{512}N_{110}O_{246}P_{38}Cu_5$); c) CD titration of [**D25-L-a/b**+2en+2Cu] with Hg^{2+}; d) ESI-ICR mass spectrum of [**D25-L-a/b**+5en+5Cu+5Hg] ($C_{420}H_{502}N_{110}O_{246}P_{38}Cu_5Hg_5$). For each charge z in the ESI spectra the first large peak corresponds to the bare molar ion of the metal-DNA assembly; the following peaks are adducts with Na^+, K^+ and/or NH_4^+.

When Cu^{2+} was added to duplex [**D25-L-a/b**+5en], the CD spectra featured an isosbestic point at 347 nm and showed a decreasing positive Cotton effect of the absorption band of the natural DNA bases (Figure 91a). Simultaneously, the absorption band around 420 nm decreased until a ratio of [Cu^{2+}]/[duplex] = 5 was reached, showing the complexation of 5 Cu^{2+} ions inside the duplex.

That the assembly of the multiple metal complexes inside the double helix was accompanied by significant structural changes could be assumed from the development of the CD-spectra during the titration of [**D25-L-a/b**+5en] with Cu^{2+}. Up to the addition of 3.5 equivalents of Cu^{2+}, the curves featured an additional isosbestic

point at 400 nm, when more Cu^{2+} was added the following curves deviated from this isosbestic point. Around 380 nm a positive CD-band increased in intensity from 0 to 3.5 equivalents of Cu^{2+} but subsequently decreased from 3.5 to 5 equivalents of Cu^{2+} (and stopped changing above 5 equivalents).

Formation of the expected product [**D25-L-a/b**+5en+5Cu] was confirmed by ESI-MS (found: 962.97 for $z = 13$, calculated for $[M - 13H^+]^{13-}$: 962.98) (Figure 91b). Subsequent titration of Hg^{2+} ions into the solution caused the positive CD band around 380 nm to gradually decrease until the ratio of $[Hg^{2+}]$/[duplex] reached now again 5.0 (Figure 91c). Formation of the bimetallic ion stack inside the DNA double helix [**D25-L-a/b**+5en+5Cu+5Hg] was again confirmed by ESI-MS (found: 1039.34 for $z = 13$, calculated for $[M - 13H^+]^{13-}$: 1039.35) (Figure 91d). These experiments unambiguously showed that the duplex **D25-L-a/b** quantitatively and site-selectively forms a heterodecanuclear complex with precisely five Cu^{2+} ions and five Hg^{2+} ions in the order Cu^{2+}-Hg^{2+}-Hg^{2+}-Hg^{2+}-Hg^{2+}-Cu^{2+}-Cu^{2+}-Cu^{2+}-Cu^{2+}-Hg^{2+}. Likewise duplex **D24-L-a/b** incorporated ten metal ions in the order Cu^{2+}-Hg^{2+}- Cu^{2+}-Hg^{2+}- Cu^{2+}-Hg^{2+}- Cu^{2+}-Hg^{2+}- Cu^{2+}-Hg^{2+} (Figure 90).

In parallel with the work on programmable metal arrays presented here, the group of *K. Tanaka* and *M. Shionoya* managed to assemble similar DNA duplexes containing two kinds of metal ions based on their pyridine-pyridine base pair **11** for the complexation of Hg^{2+} and the hydroxypyridone ligand system **12** for the complexation of Cu^{2+}. They were, however, not able to prepare mixed metal arrays with more than five stacked ions in total. The results of their work will soon be published together with the data presented in this thesis.[239]

4.7 Conclusion and outlook (part I)

Several approaches for the development of a new metal-base pair culminated in the successful preparation of the metal-salen base pair, which was assembled inside DNA duplexes from salicylic aldehyde precursors upon addition of ethylenediamine and a suitable metal cation.

The preparation of the ligand nucleoside afforded the preparation of a protected salicylic aldehyde **28** and the glycosyl donor **29**, which were reacted together in a copper-mediated *C*-glycosylation as the key step. The resulting salicylic aldehyde nucleobase **25** and the corresponding salen complex **42** were characterized by X-ray crystallography.

The *C-C*-coupling of the protected salicylic aldehyde **28** to the activated 3'*O*-methylxylose backbone sugar **64** was achieved and the corresponding nucleoside **61** could be isolated. However, the yields were so low that the project was dismissed and no pyranosyl-oligonucleotides were prepared.

The synthesis of metal-base pairs carrying a hydroxyphenyl-oxazoline ligand **43** failed at the glycosylation step. The related 3-(2-oxazolidinylidene-)indol-2-one nucleoside **52** could be incorporated as a modified nucleobase into oligonucleotides but metal binding was not observed.

From the protected salicylic aldehyde nucleobase **27**, a phosphoramidite **40** was prepared and incorporated into various oligonucleotides by automated DNA synthesis. Inside the DNA duplex, the assembly of the metal-salen base pair was studied by thermal de- and renaturing experiments (DNA melting curves), UV and CD spectroscopy, high resolution mass spectrometry and high pressure liquid chromatography. Oligonucleotides containing one and two copper(II)-salen complexes were further characterized by EPR spectroscopy.

The assembly of the metal-salen base pair was shown to be a cooperative process. The salen ligand was formed from the preorganized salicylic aldehydes and ethylenediamine first and subsequent coordination of the metal ion fixed the crosslink. This resulted in a tremendous stabilization of the duplex structure expressed in melting point increase of over 42 K.

A variety of diamines and metal ions such as Cu^{2+}, Mn^{3+}, Fe^{3+}, VO^{2+} and Ni^{2+} were used for the complex formation inside the duplex. This process was found to be so

strong, that sequence information of the double strand could be overridden by the metal-salen formation.

Incorporation of multiple ligand precursors into one DNA duplex allowed the controlled stacking of up to ten transition metal ions inside the double helix atop of each other. By combining the metal-salen base pair concept with the capability of **TT**-mismatches, which allow to bind Hg^{2+}-ions, the generation of mixed-metal-ion, multinuclear coordination compounds with a defined number of metal ions arranged in a determined one dimensional spatial relationship was achieved. Up to five Cu^{2+} ions plus five Hg^{2+} ions were thus arranged in a linear fashion.

The synthesis of further orthogonal ligand systems may open up the possibility to mix other metal ions and more than two metal ions inside the same DNA duplex.

Substituted diamine building blocks may be used to introduce functions such as steric bulk, chirality, additional metal coordinating sites or nodes for linking the oligonucleotide to other nanoscopic units in molecular architectures.

All discussed oligonucleotides have been prepared by means of automated solid phase synthesis. An enzymatic approach starting from a triphosphate of the salicylic aldehyde nucleobase might allow the synthesis of much longer metal-salen containing duplexes. These could be used in surface mounted electronic setups.

The EPR spectrum of two stacked Cu^{2+}-ions showed an antiferromagnetic coupling between the metal centers. EPR measurements and STM based experiments of duplexes containing more (and other) metal ions will open the possibility to study the electronic behavior of these systems in more detail.

X-ray analysis of the prepared metal-salen containing double strands is currently under way. It will hopefully yield more structural information about the homo- and heterometallic stacks.

A combination of the metal-base pair concept with the well established sequence-based techniques for the construction of complex DNA architectures with branches and junctions (Chapter 3.1.3) might eventually allow a convenient synthesis of programmable constructs with several metal binding sites spatially arranged in all three dimensions. This may open up interesting perspectives for molecular electronics and the mimicry of multimetal-enzymes.

The metal-salen complex inside the DNA might be used as a biocompatible, enantioselective catalyst amenable to optimization by evolutionary algorithms.

5   Part II: Coordinating metals on the exterior of the DNA double helix

5.1   Aims of project (part II)

As a subsidiary project of this thesis, some approaches were investigated to allow binding of metals to the exterior of DNA strands as an alternative way to generate nanoscale conducting materials from DNA templates.

In the first approach, metal ligands should be connected via a spacer moiety to the C5-position of uridine nucleobases. Corresponding DNA double strands were anticipated to form stable duplexes with the bound ligands protruding into the major groove. A continuous decoration of double strands with a multitude of these ligands could be used to aggregate metal ions along the whole DNA strand, thereby equipping it with new electronic or magnetic properties.

A second approach was based on the modular, postsynthetic labeling of oligonucleotides containing alkyne modified anchor nucleobases by "click chemistry" (Chapter 3.1.3.). A ligand capable of coordinating a nanoscopic gold cluster should be prepared to realize the specific aggregation of these clusters along DNA duplexes. The equidistantly arranged gold clusters were anticipated to display interesting electronic properties resulting from the coupling of their quantum behavior.[240]

5.2   Synthesis of ligand-modified uridine compounds

This Chapter briefly summarizes the synthesis of hydroxyphenyl-oxazoline nucleoside **67** and benzotriazole nucleoside **68** (Figure 92).
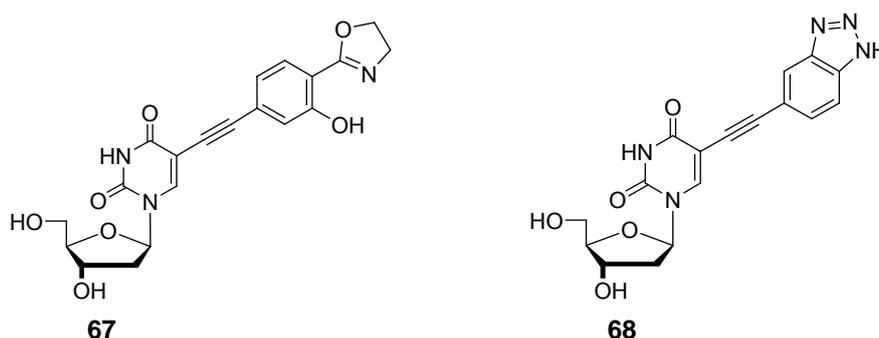
Figure 92: Hydroxyphenyl-oxazoline-uridine nucleoside **67** and benzotriazole-uridine nucleoside **68**.

The hydroxyphenyl-oxazoline ligand was already introduced in Chapter 4.2.3 where the attempts to couple it to 2'-deoxyribose were described to generate a new kind of metal-base pair. Unfortunately, the copper-mediated *C*-glycosylation could not be realized with this ligand.

However, another way of tethering the hydroxyphenyl-oxazoline ligand to a nucleobase was found to be possible by a sequence of two *Sonogashira* coupling reactions. The synthesis of the hydroxyphenyl-oxazoline nucleoside is depicted in Scheme 19.
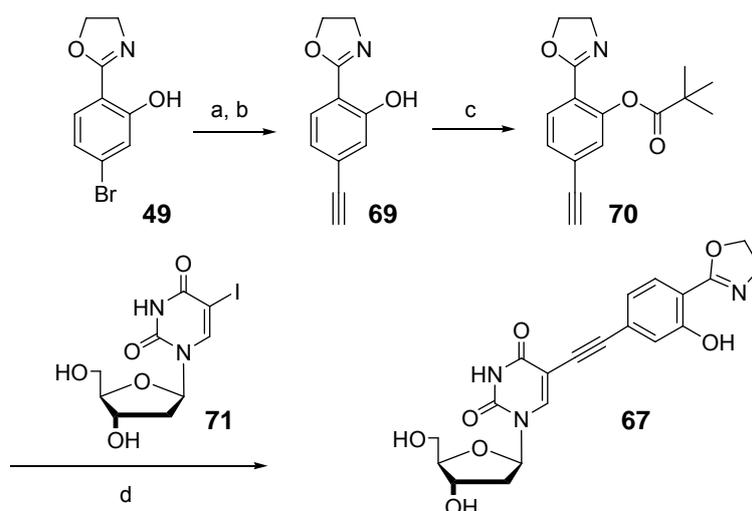
Scheme 19: Synthesis of hydroxyphenyl-oxazoline nucleoside **67**. a) TMS-acetylene, PdCl$_2$(PPh$_3$)$_2$, CuI, NEt(*iso*-Pr)$_2$, THF; b) K$_2$CO$_3$, MeOH, 75 % over 2 steps; c) pivaloyl chloride, NEt(*iso*-Pr)$_2$, cat. DMAP, CH$_2$Cl$_2$, 91 %; d) 5-iodouridin **71**, PdCl$_2$(PPh$_3$)$_2$, CuI, NEt(*iso*-Pr)$_2$, DMF, 23 %.

The synthesis started from compound **49** which was already introduced in Chapter 4.2.3. A *Sonogashira* coupling of **49** with trimethylsilyl-acetylene and subsequent cleavage of the silyl protecting group resulted in the formation of 2-[4-alkinyl-2-hydroxyphenyl-]oxazoline **69**. Protection of the free hydroxyl group with pivaloyl chloride yielded intermediate **70**, which was successfully coupled using a second *Sonogashira* coupling to commercially available 5-iodouridin **71**. The column chromatographic purification of the reaction product was found to be difficult due to extensive "smearing" of the material on the column material (silica, eluent: MeOH : CHCl$_3$). Slow recrystallization of the pre-purified material from methanol surprisingly yielded the deprotected compound **67** lacking the pivaloyl group (Figure 93).
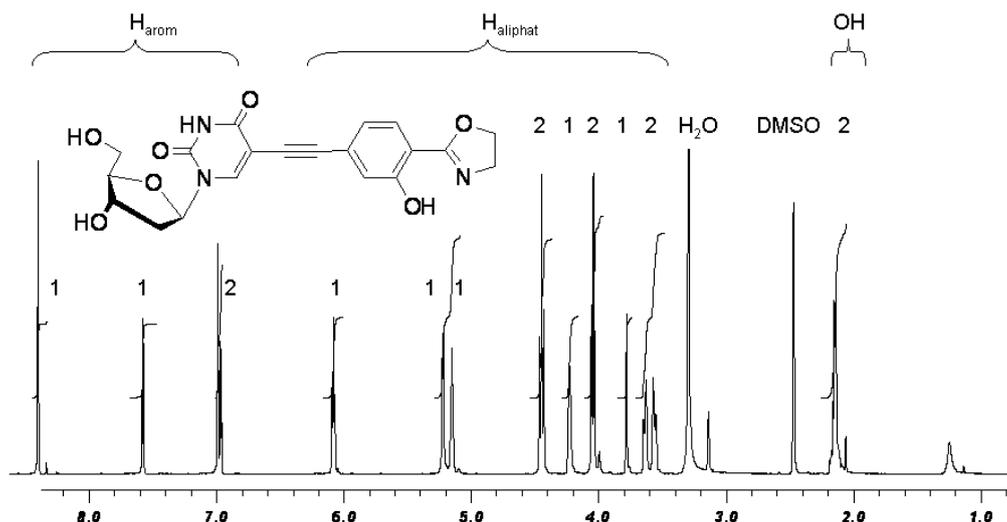
Figure 93: ^{1}H-NMR of nucleoside **67** showing that the pivalic ester is not present any more in the final product after recrystallization from methanol. This result is in agreement with mass spectrometric data. The relative integral values are indicated above the signals (600 MHz, D$_6$-DMSO).

The readily possible cleavage of the pivaloyl ester from the hydroxyl group of the hydroxyphenyl-oxazoline ligand is in good agreement with the difficulties to protect this position, as already described in Chapter 4.2.3. Here, the lability of the protecting group in combination with the presence of methanol as solvent presumably resulted in cleavage of the pivalic ester by means of a transesterification reaction.

When this ligand-modified nucleoside is intended to be used in solid-phase DNA synthesis, this hydroxyl group must be reliably equipped with a protecting group to prevent side reactions. Consequently, either extended treatment with nucleophilic solvents such as methanol has to be prevented or a change of the protecting strategy has to be considered. In the course of this work, however, this task was not further pursued.

On the other hand, compound **68** was successfully incorporated into oligonucleotides, although difficulties in finding suitable protecting groups were also encountered in this case.[241] **68** is another example of a 5-substituted uridine nucleosides, which exhibits base pairing properties like uridine (or thymidine) and displays the alkyne bound residue (here benzotriazole) into the major groove of a DNA double helix.

Benzotriazole is a commonly used metal complexing agent and it has been used as an anti-corrosive agent for copper and silver by forming surface monolayers to prevent oxidation.[242, 243]

More than 20 different monomeric benzotriazole-metal complexes were reported[244], among them for example the copper(II)complex [Cu(benzotriazole)$_4$(H$_2$O)$_2$](BF$_4$)$_2$[245] and the silver(I)complex [Ag(benzotriazole)$_2$]NO$_3$[246].

Benzotriazoles were extensively used for anchoring a variety of analytes to silver surfaces or colloids to make them amenable for their identification and quantification by Surface Enhanced Resonance Raman Spectroscopy (SERRS).[247, 248] Of special interest are benzotriazole-labeled DNA strands, which were detected by this method in concentrations down to 8 x 10^{-13} M.[249, 250]

So far, one limitation to these techniques was that tethering of a single benzotriazole anchor group to oligonucleotides was only possible at the 5'-terminus of a DNA strand by using the monomethoxytrityl protected benzotriazole-phosphoramidite depicted in Figure 94.[251]
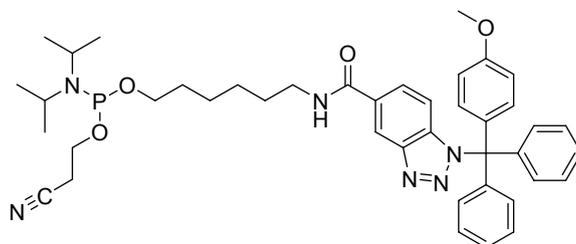
Figure 94: The monomethoxytrityl protected benzotriazole-phosphoramidite prepared by *Graham et al.*

In this thesis, a method is described for the incorporation of several benzotriazole-bound nucleosides by phosphoramidite chemistry without expecting to cause major disturbances of the DNA structure.

A further motivation to synthesize a nucleoside building block carrying a benzotriazole functionality came from the interest in DNA metallization, which is investigated in the *Carell* group.[55] It was anticipated, that attachment of benzotriazole to DNA strands would enhance the specific binding of metal ions or reduced clusters composed of a metal such as silver.

For these reasons, a synthesis of a protected benzotriazole phosphoramidite applying a new protecting strategy for benzotriazoles was developed and DNA strands containing these building blocks were produced.

Intuitively, a sequence of (1) ligand preparation (2) protection of the ligand and (3) *Sonogashira* coupling to 5-iodouridin would be the most appealing route to the protected phosphoramidite **72**, which was needed to incorporate **68** into oligonucleotides by solid phase DNA synthesis.

The strategy elaborated in this work, however, does not start from a benzotriazole precursor, although 4-substituted benzotriazoles are readily available. The reason is that the *N*-protection of unsymmetrical benzotriazoles leads to an almost inseparable mixture of the three isomers depicted in Figure 95.
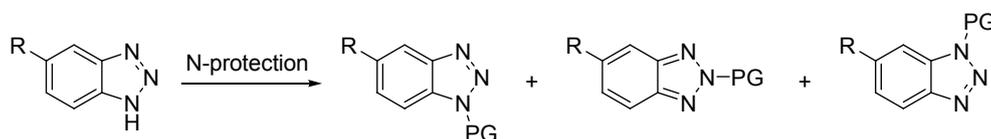
Figure 95: The N-protection of unsymmterically substituted benzotriazoles leads to a mixture of three isomers.

To circumvent this problem, a synthesis was developed which selectively introduces the needed protecting group on one of the nitrogen atoms before the heterocyclic structure of the benzotriazole ring is finally established (Scheme 20).
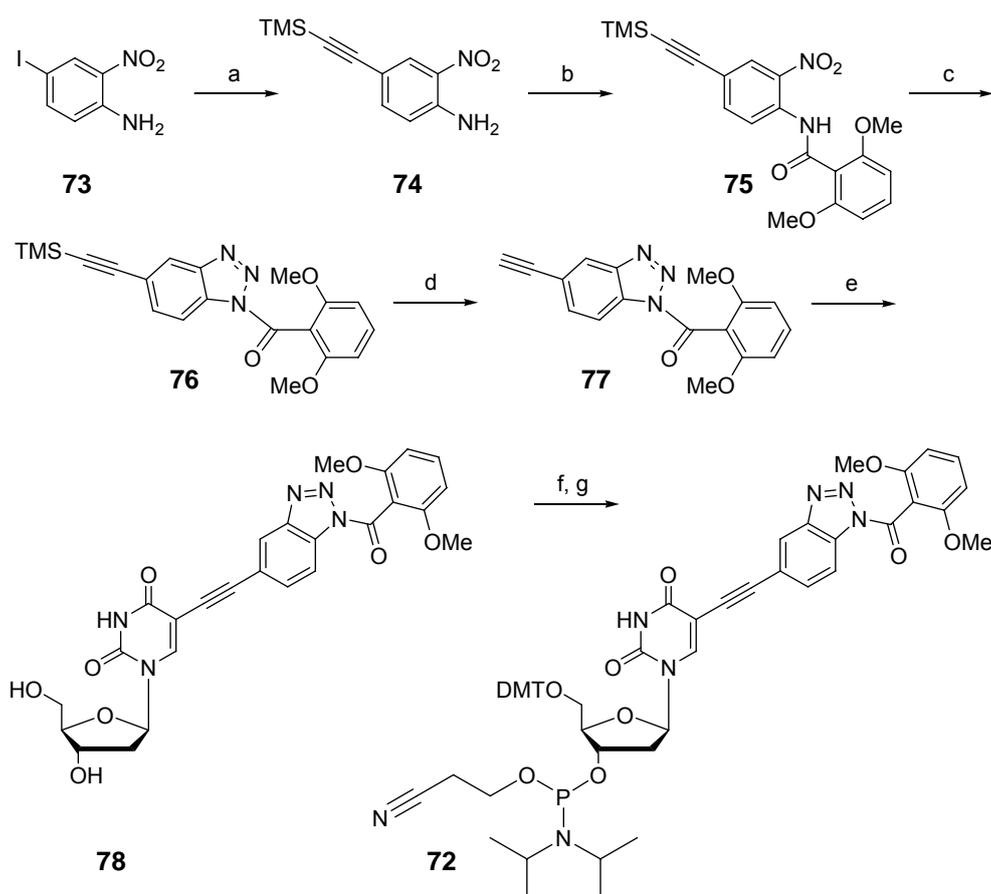
Scheme 20: Synthesis of the protected benzotriazole phosphoramidite **72**. a) TMS-acetylene, PdCl$_2$(PPh$_3$)$_2$, CuI, diethylamine, THF, 91 %; b) 2,6-dimethoxybenzoylchloride, di-*iso*-propylamine, CH$_2$Cl$_2$, 95 %; c) Fe, HOAc, then HCl, NaNO$_3$, H$_2$O, 50 % over 2 steps; d) TBAF, THF; - 78 °C, 85 %; e) 2'-deoxy-5-iodo-uridine, Pd(PPh$_3$)$_4$, CuI, DMF, sonification, 83 %; f) DMTCl, pyridine, 84 %; g) (*i*Pr$_2$N)(OCH$_2$CH$_2$CN)PCl, NEt(*iso*-Pr)$_2$, THF, 66 %.

First, 4-iodo-2-nitroaniline **73** was reacted in a *Sonogashira* coupling to intermediate **74** according to a literature procedure.[252, 253] Subsequently, the protecting group for the free nitrogen atom of the later benzotriazole was introduced.

Benzotriazole is not easy to protect.[254] In fact benzotriazole and *N*-oxygen substituted benzotriazoles are used as good leaving groups and behave similar to halogens in nucleophilic substitutions. This behavior is similar to *N*-substituted imidazoles. Consequently, the reaction with a protecting reagent like an acyl chloride yields a benzotriazole "amide", which is much more prone to nucleophilic cleavage than "real" amides. Indeed this was found to be a problem when acyl protecting reagents like pivaloyl chloride or simple benzoyl chloride were used. Therefore, the 2,6-dimethoxybenzoyl group was established as a new way of protecting benzotriazoles in a reliable way. It was chosen because the methoxy groups on the aromatic ring donate enough electron density into the amide functionality to prevent a cleavage of the *C-N* bond by weak nucleophiles.

For the same reason, also imidazoles can be protected with the 2,6-dimethoxybenzoyl group.[255] Trityl or benzyl protection of the benzotriazole which was reported by Graham *et al.* could not be used due to the high lability of these groups against the acidic conditions encountered during DNA synthesis.[251, 256]

Introduction of the protection group onto the only free amino group of **74** to yield **75** was followed by a direct sequence of nitro-group reduction and benzotriazole ring closure to give a single isomer of compound **76**. Subsequently, the TMS group was removed from the alkyne to yield compound **77**, which was coupled in a *Sonogashira* reaction to 5-iodouridin **71**. The resulting nucleoside **78** was finally converted into the 5'-DMT protected compound **79** and then into phosphoramidite **72** by standard procedures.

The following two DNA strands were prepared by solid phase oligonucleotide synthesis (Figure 96).

D26-B   5'-**B**ACAACATTAATG**B**C-3'
D27-B   5'-TACAACA**B**TAATGTG-3'

Figure 96: Benzotriazole (**B**) containing oligonucleotides **D26-B** and **D27-B** prepared in this work.

The 2,6-dimethoxybenzoyl protecting groups on the benzotriazoles could be completely removed by the treatment of the oligonucleotides with aq. ammonia : EtOH = 3 : 1, which is the common reagent for cleavage and

deprotection of synthesized DNA (Chapter 4.3.1). This showed that the application of the special protecting group strategy was successful in this case. The DNA concentration in solution was estimated according to the standard UV spectroscopic methods taking into account the molar extinction coefficient of the free benzotriazole-uridine nucleoside **68** (ε = 14000 l · mol^{-1} · cm^{-1}). Figure 97 shows the high resolution ESI mass spectra of the strands **D26-B** and **D27-B**, which confirm the proper incorporation and deprotection of the benzotriazole units.
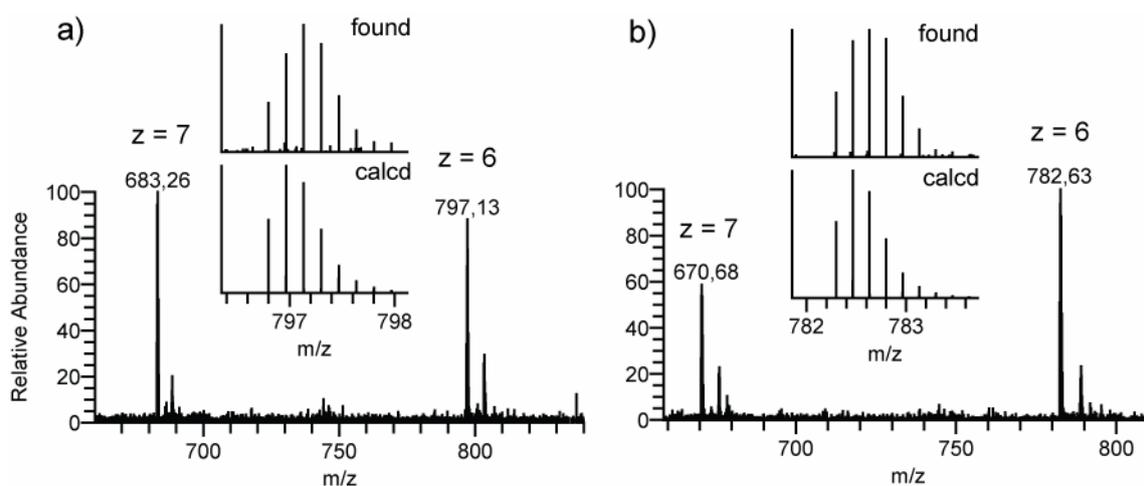
Figure 97: ESI mass spectra of **D26-B** and **D27-B**. a) Found for [**D26-B**-6H$^+$]$^{6-}$:796.7994; calculated for [$C_{161}H_{182}N_{60}O_{87}P_{14}$]$^{6-}$: 796.7993; b) Found for [**D27-B**-6H$^+$]$^{6-}$: 782.2977; calculated for [$C_{155}H_{181}N_{59}O_{87}P_{14}$]$^{6-}$: 782.2974.

Initial studies on the metal-binding abilities of these strands by the same mass spectrometric experiments described already for the salen-containing DNA strands did, however, not result in the observation of bound metal ions. The reason for this behavior might be that the metal-benzotriazole bond is not strong enough to survive mass spectrometry. More information about the metal-binding capabilities of the benzotriazole-DNA might be obtained from future UV, IR and especially Resonance Raman Spectroscopic Experiments.

More information on the synthesis of the benzotriazole-phosphoramidite and the incorporation into DNA strands can be found in the research report of *A. Keilbach*.

5.3   "Clicking" of gold clusters to DNA via glutathione-bisazide

The use of "click chemistry"[54] for the simple introduction of functionalities onto the alkyne carrying DNA strands was used here to bind ligand-stabilized gold nanoclusters which carry azide groups (Figure 98).
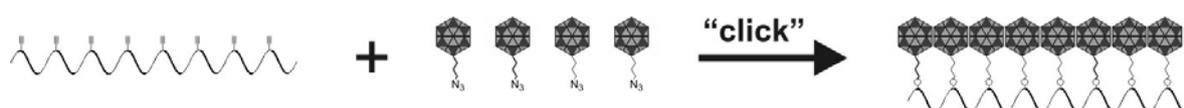
Figure 98: Principle of "clicking" azide-labeled clusters to alkyne-modified DNA strands.

The binding of single gold clusters to biomolecules such as DNA has been reported before[15, 257] and several gold-labeling techniques for imaging purposes are commercially available (e.g. Rubigold^{TM} and Nanogold^{TM}).[258, 259] The controlled binding of multiple gold clusters along the entire length of DNA strands is, however, still a challenging task.

Therefore, the simple peptidic compound glutathione which is known to effectively stabilize gold clusters in aqueous solutions[260, 261] was modified with azide functionalities by simple peptide chemistry to yield compound **80**. The synthesis is summarized in Scheme 21.[187]
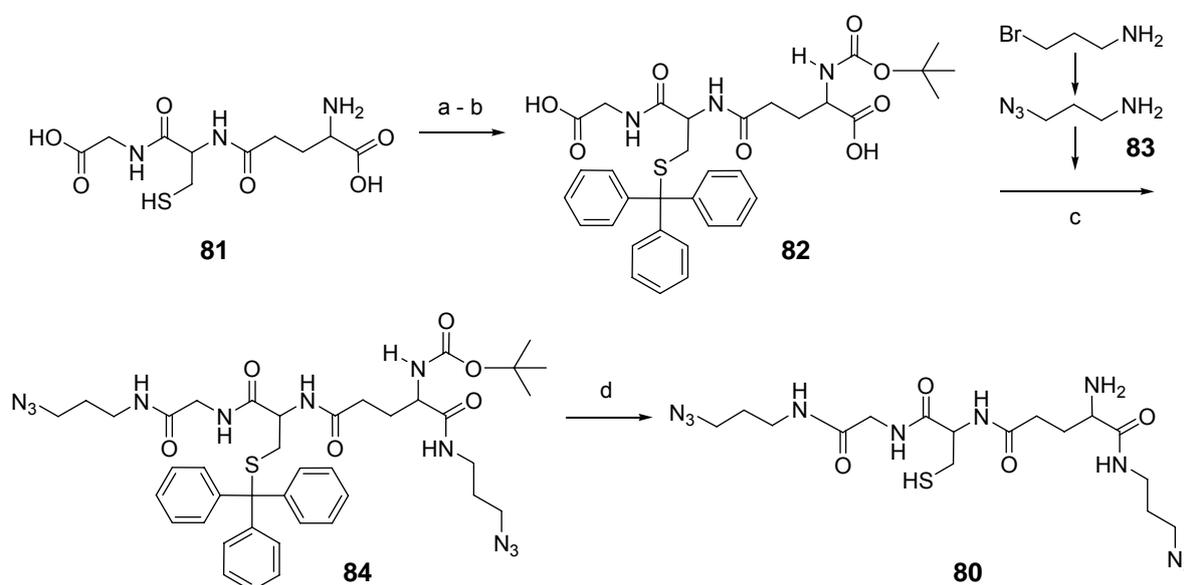
Scheme 21: Synthesis of glutathione-bisazide **80**. a) Ph₃CH, CH₃COOH, BF₃ · OEt₂, 59 %; b) BOC₂O, NaOH, H₂O, dioxane, 90 %; c) carbonyldiimidazole, THF, then 3-aminopropylazide, 68 %; d) TFA, H₂O, Et₃SiH, CH₂Cl₂, 80 %.

First, glutathione **81** was S-trityl and N-BOC protected to yield compound **82** according to standard procedures.[262] Subsequently, it was coupled with two equivalents of 3-aminopropylazid **83** (prepared from 3-aminopropylbromide)[263] to

give the protected bisazide **84**. The IR spectrum of this compound showed a strong absorption at 2094 cm^{-1}, which is typical for the azide group. Finally, the protecting groups were removed by treatment with trifluoroacetic acid and triethylsilane as a cation scavenger to result in the formation of the water-soluble product **80**. The product was finally purified by reversed phase HPLC chromatography. The comparison of the NMR spectra of **80** with those of free glutathione and the high resolution ESI mass spectrum confirmed the identity of the compound.

This compound was used by *M. Fischler* in the group of *Prof. U. Simon* (RWTH Aachen) for the synthesis of glutathione-bisazide-stabilized gold clusters.[264] Therefore, a mixture of HAuCl$_4$ and glutathione-bisazide was subjected to reduction by sodium borohydride and the formed gold clusters were purified by centrifugation and gel electrophoresis.[265] Subsequently, alkyne-modified DNA strands[58], which were bound to a mica surface, were treated with the azide-labeled gold clusters and a Cu(I) catalyst to perform the "click reaction".[264] Although these studies are currently still ongoing, first AFM pictures of rather short oligonucleotide strands (ca. 300 bp) show a selective binding of the gold clusters to the DNA (Figure 99).
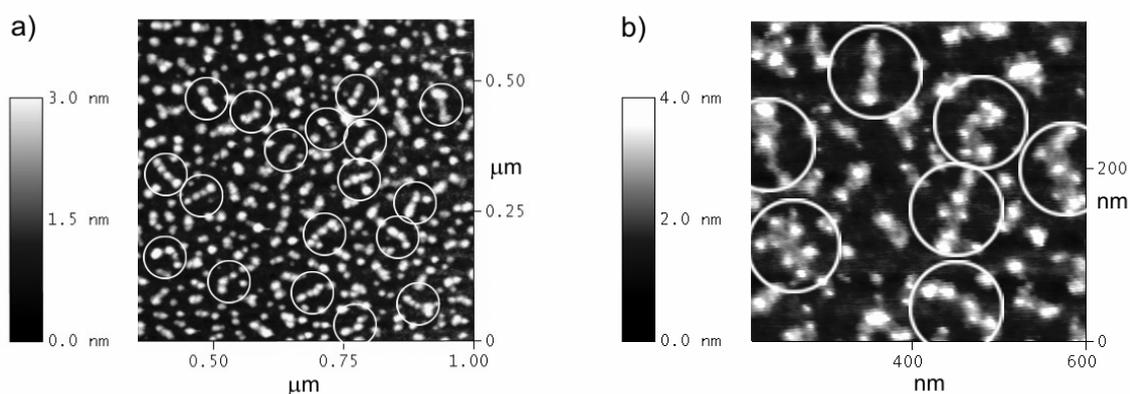
Figure 99: AFM image of glutathione-bisazide-stabilized gold clusters bound to an alkyne-tagged DNA template on a mica surface.

5.4   Conclusion and outlook (part II)

In the forgoing Chapters, two approaches for the coordination of metals to the exterior of DNA were described. Two modified nucleosides with ligands attached via alkyne linkers were synthesized and one of them (benzotriazole nucleoside **68**) was successfully incorporated into oligonucleotides. Metal coordination was, however, not yet observed with these DNA strands.

An extensive screening of experimental factors such as different metal ions, pH and salt additives will be necessary to find suitable conditions for the controlled binding of metal ions to these constructs. Surface analysis techniques such as AFM or STM might then enable a characterization of the DNA duplexes with metal ions attached to their outer periphery.

The "click chemistry" approach of binding azide-functionalized, ligand-stabilized gold clusters to alkyne-tagged oligonucleotides was successful as seen by AFM measurements. Up to now, the oligonucleotides used in these experiments were rather short sequences (ca. 300 bp). Longer alkyne-tagged oligonucleotides have been prepared in the Carell group, recently. Performing the "click reaction" with these strands should allow the preparation of cluster-decorated DNA stretches of sufficient length to be able to contact them with nanoscopic electrodes in a special STM setup. It would be very interesting to measure *I/U*-diagrams (current/voltage diagrams) in these systems and compare the data to the results obtained from measurements of the continuously metallized DNA strands discussed in Chapter 3.1.3.

6   Experimental part

6.1   Materials and methods

Chemicals were purchased from Sigma-Aldrich, ACROS or Lancaster and used without further purification. Solvents used were of reagent grade and purified by usual methods. Reactions were monitored on Merck Silica 60 F_{254} TLC plates. Detection was done by irradiation with UV light (254 nm) and staining with acidic 2,4-dinitrophenylhydrazine solution in ethanol. Flash chromatography was performed on Silica 60 (Merck, 230-400 mesh). NMR spectra were recorded on the following spectrometers: *Varian Oxford 200, Bruker AC 300, Varian XL 400* and *Bruker AMX 600*. The chemical shifts (δ) are given in ppm, the coupling constants (J) in Hz. Mass spectra were recorded on the following machines: Finnigan MAT 95 (EI), *Bruker Autoflex II* (MALDI-TOF) and Thermo Finnigan LTQ-FT (ESI-ICR). IR spectra were measured on a *Nicolet 510* FT-IR spectrometer in a KBr matrix or with a diamond-ATR (*Attenuated Total Reflection*) setup.

6.2   DNA synthesis, cleavage and purification

DNA oligonucleotides were synthesized on a PerSeptive Biosystems Expedite 8900 Synthesizer and an *Äkta Oligopilot 10 (Amersham Biosciences)* using Ultramild Bases and reagents (Glen Research) and following standard phosphoramidite protocols. The coupling times and phosphoramidite amounts for the salicylic aldehyde nucleosides were similar to those for the natural bases. Trityl values showed good incorporation of the modified nucleosides. After additional treatment with 2 % dichloroacetic acid + 1 % H_2O in dichloromethane to remove the acetal protecting groups (1 h for up to two salicylic aldehydes, 2 h for strands with more aldehydes), the controlled pore size glass (CPG) solid support was subjected to conc. $NH_{3\,(aq)}$: EtOH = 3 : 1 for 12 h at r.t. for cleavage of the strands. The solvents were removed in a SpeedVac concentrator and the pellet redissolved in bidest. water. Analytics and purification were performed on Merck LaChrome HPLC systems using 5μ Silica-C_{18} RP columns and 0.1 M NHEt$_3$OAc in (H_2O) : (MeCN : H_2O = 8 : 2) as eluent. The purified fractions were concentrated, desalted on Waters Sepac-C_{18} cartridges and concentrated again. The concentration was estimated by UV

spectroscopy following standard procedures taking into account the molar extinction coefficient for the ligandoside **6** (ε = 10290 l $\cdot$ mol^{-1} $\cdot$ cm^{-1}), which was measured on a Cary 100 UV-Vis spectrometer.

More information on DNA synthesis and the cleavage of the special protecting groups of the salicylic aldehydes is given in Chapter 4.3.

6.3   Melting point experiments

Melting profiles were measured on a Cary 100 UV-Vis spectrometer using quartz glass cuvettes with 1 cm path length. The samples contained 150 mM NaCl, 10 mM buffer (see Table 5 in Chapter 4.4.2) and 3 μM of each strand in a final volume of 1 mL. They were covered with 2 mm of silicon oil and tightly plugged. The measurements were repeated several times with independent sample preparations. First, the oligonucleotides were hybridized by slowly cooling the samples down from 85 °C to r.t. Addition of ethylenediamine (10 μL of a 10 mM freshly prepared stock solution) and metal-sulfate (concentration see Table 5 in Chapter 4.4.2) was followed by an incubation time of 5 h at 27 °C. The melting profiles started with a denaturing run (0 °C to 85 °C, for Cu^{2+}: 95 °C) with a slope of 0.5 °C/min. At least two denaturing and two renaturing ramps were performed and averaged for evaluation of the melting point (T_M = zero-crossing of sec. derivative of the 320 nm-background corrected change in hyperchromicity at 260 nm). The measurements of the samples containing Mn^{2+} and the DNA duplex reproducibly showed a strong hysteresis between the de- and renaturing profiles, which can be associated with a thermal instability of the Mn^{2+} salen complex when exposed to temperatures above T_M for elongated times. In these cases, the de- and renaturing curved were treated separately and two individual melting temperatures for the heating and cooling process were calculated.

6.4   UV and CD spectra and titrations

UV spectra and titrations were measured on a Cary 100 UV-Vis spectrometer using quartz glass cuvettes with 1 cm path length and 1 mL volume. The sample preparation was the same as for the melting point experiments (see also Table 4 in Chapter 4.4.1). For measurements above 280 nm, the chosen DNA concentration was 30 μM for double strands containing one pair of salicylic aldehydes and reduced

to 6 μM for the strands containing 10 pairs of salicylic aldehydes. Blank spectra (aqueous solution of particular buffer and salt) were carefully measured for every individual cuvette separately.

CD titrations were measured on a JASCO J 810 CD-spectropolarimeter using quartz glass cuvettes with 1 cm path length. The sample preparation was similar to the procedures used for the UV measurements. At least 10 spectra were accumulated in each case with a scanning speed of 200 nm/s.

Blank spectra (aqueous solution of particular buffer and salt) for the CD measurements were carefully measured for every individual cuvette separately, ensuring always the same cuvette orientation in the sample holder. In temperature-dependent measurements, one individual blank for each temperature was acquired. For the titrations, addition of a ca. 30-fold excess of ethylenediamine was followed by incubation at room temperature for 1 h. The metal was added as a solution of its sulfate in portions of 0.1 – 0.2 equivalents with respect to the DNA concentration in a volume of 1 – 2 μL with an Eppendorf precision pipette. At least 15 min (but max 1 h) was waited after each metal addition before the next curve was measured.

6.5   ESI mass spectrometry

A Thermo Finnigan LTQ-FT ESI-ICR mass spectrometer was used for the mass spectrometric characterization of the metal containing duplexes. The metal-DNA samples were prepared by hybridizing equimolar amounts of both single strands (30 μM) in 100 mM ammonium acetate buffer (pH 8) and subsequent incubation with the diamine and the corresponding metal salt overnight at room temperature.

ESI spectra of DNA strands were measured in flow injection analysis mode or coupled to chromatographic separation (eluent: 2 mM $NHEt_3OAc$ in H_2O : MeCN). In flow injection mode, 2 μL sample (30 μM DNA, 100 mM NH_4OAc) was injected in a steady flow of H_2O : MeCN = 8 : 2 (200 μL/min). The capillary temperature was 300 °C, spray voltage 4-5 kV (negative mode).

6.6   Synthesis of the salicylic aldehyde nucleobase

4-Bromo-salicylic aldehyde 31
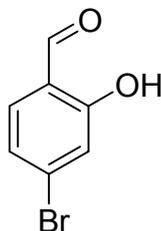
3-Bromophenol **30** (1.0 g, 5.8 mmol), $MgCl_2$ (830 mg, 8.7 mmol) and triethylamine (3.1 mL, 22 mmol) were dissolved in 30 mL dry acetonitrile and stirred at r.t. for 20 min. Paraformaldehyde (1.17 g, 39.0 mmol) was added and the mixture refluxed under stirring for 8 h. Then, water was added and the mixture was acidified with dil. hydrochloric acid (pH 2). The solution was extracted with diethylether twice and the combined organic extracts were washed with sat. $NaCl_{(aq)}$ three times and dried over Na_2SO_4. Removal of the solvents *in vacuo* and column chromatography (silica, hexane : EtOAc = 19 : 1) yielded a colorless oil, which slowly crystallized (571 mg, 2.84 mmol, 49 %).

R_f (hexane : EtOAc = 9 : 1) = 0.4; **¹H-NMR** (200 MHz, $CDCl_3$): δ 7.17 (1 H, dd, J = 8.3, 1.7 Hz), 7.20 (1 H, d, J = 1.7 Hz), 7.42 (1 H, d, J = 8.3 Hz), 9.86 (1 H, s), 11.12 (1 OH, s); **¹³C-NMR** (75 MHz, $CDCl_3$): δ 119.9, 121.5, 123.9, 132.4, 134.9, 162.4, 196.2; **EI-MS** (pos., 70 eV): m/z = 200 $[M]^+$, 172 $[M - CHO]^+$.

2-(4-Bromo-2-hydroxyphenyl)-1,3-dioxane 32
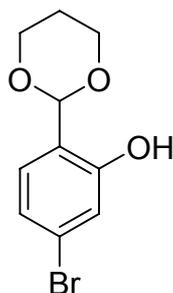
4-Bromosalicylic aldehyde (1.3 g, 6.4 mmol) **31** was combined with triethylorthoformiate (1.2 mL, 7.0 mmol) and 1,3-propanediol (1.9 mL, 26 mmol). A catalytic amount of tetra-*n*-butylammoniumtribromide (310 mg, 0.64 mmol) was added and the mixture was stirred for 3 d at r.t. The reaction was ended by adding sat. $NaHCO_3$ (aq) until pH 7 was reached. The mixture was extracted twice with ethyl acetate and the combined organic extracts were washed with dil. $NaHCO_3$ (aq) and dried over Na_2SO_4. The solvents were removed *in vacuo* and the raw material purified by column chromatography (silica, hexane : EtOAc = 10 : 1) to yield 1.4 g, 5.5 mmol, 86 %) of a colorless oil.

R$_f$ (hexane : EtOAc = 9 : 1) = 0.4; **^{1}H-NMR** (200 MHz, CDCl$_3$): δ 1.52 (1 H, d, *J* = 13.8), 2.15-2.35 (1 H, m), 4.00 (2 H, dt, *J* = 12.2, 2.4 Hz) 4.30 (2 H, dd, *J* = 10.7, 5.1 Hz), 5.61 (1 H, s), 6.98 (1 H, dd, *J* = 8.3, 1.7 Hz), 7.03 (1 H, d, *J* = 8.3 Hz), 7.07 (1 H, d, *J* = 1.7 Hz), 8.00 (1 OH, s); **^{13}C-NMR** (50 MHz, CDCl$_3$): δ 25.9, 67.7, 102.8, 120.7, 121.5, 123.0, 123.9, 129.1, 156.4; **IR** (KBr): ν = 2973, 2862, 1614, 1578, 1486, 1383, 1342, 1279, 1234, 1186, 1151, 1097, 988, 950, 921, 895, 860, 801, 645 cm^{-1}. **EI-HRMS** (pos., 70 eV): calc. for C$_{10}$H$_{11}$BrO$_3$ [M]$^+$: 257.9892, found: 257.9903.

2-(4-Bromo-2-(tri-iso-propylsilyloxy)-phenyl)-1,3-dioxane 28
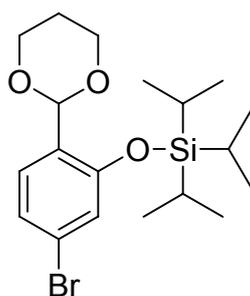
2-(4-Bromo-2-hydroxyphenyl)-1,3-dioxane **32** (1.3 g, 4.8 mmol) was dissolved in dry CH_2Cl_2 (30 mL) and 1.9 mL (12.1 mmol) NEt(*iso*-Pr)$_2$ was added. At 0 °C, tri-*iso*-propylsilyltriflat (2.5 g, 8.2 mmol) was added drop wise. After stirring for 12 h at r.t., water was added and the mixture was extracted two times with CH_2Cl_2. The combined organic extracts were washed with H_2O and sat. NaCl$_{(aq)}$ and dried over Na_2SO_4 . After removal of the solvents *in vacuo* the resulting oil was subjected to column chromatography (first pure hexane to elute excess silyl reagent, then

hexane : EtOAc = 30:1). The resulting colorless oil (1.7 g, 4.2 mmol, 87 %) was intensively dried in high vacuum before it was used for the next step.

R_f (hexane : EtOAc = 9 : 1) = 0.5; **^{1}H-NMR** (300 MHz, CDCl$_3$): δ 1.13 (18 H, d, J = 7.1 Hz), 1.24 - 1.36 (3 H, m), 1.41 (1 H, d, J = 13.7 Hz), 2.13-2.30 (1 H, m), 3.93 (2 H, dt, J = 2.5, 12.4 Hz) 4.22 (2 H, dd, J = 5.0, 10.6 Hz), 5.80 (1 H, s), 6.93 (1 H, d, J = 1.9 Hz), 7.09 (1 H, dd, J = 8.3, 1.9 Hz), 7.45 (1 H, d, J = 8.3 Hz); **^{13}C-NMR** (75 MHz, CDCl$_3$): δ 13.5, 18.4, 26.2, 67.9, 94.4, 121.8, 123.0, 124.5, 128.6, 129.1, 154.3; **IR** (diamond-ATR): ν = 2945, 2892, 2866, 1593, 1572, 1486, 1465, 1404, 1268, 1236, 1150, 1121, 1098, 988, 926, 882, 842, 805, 755, 683, 659, 643 cm^{-1}; **FAB-MS** (pos.): 415.5 [M+H]$^+$; **EA** calc. for C$_{19}$H$_{31}$BrO$_3$Si: C 54.93; H 7.52; found: C 54.60; H 7.72.

Protected nucleoside 38
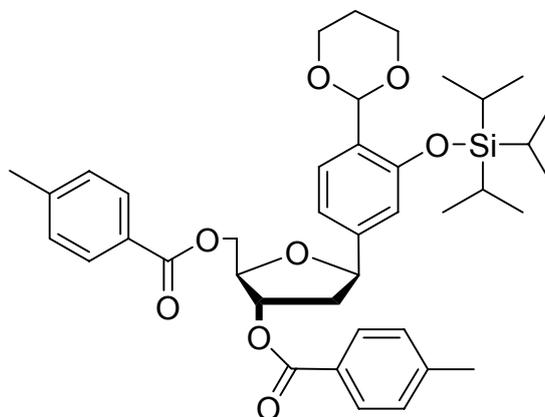
A solution of compound **28** (7.1 g, 17.1 mmol) in 40 mL freshly distilled diethylether was cooled to – 78 °C and 22.9 mL (35.9 mmol) *t*-BuLi in pentane (1.57 M) was added dropwise over one hour. The reaction was kept at – 78 °C with stirring for 3 hours and subsequently transfer-cannuled to a precooled (– 78 °C) suspension of copper(I)bromide-disulfide complex (1.8 g, 8.6 mmol) in 10 mL ether. The reaction mixture was carefully warmed to – 30 °C for 20 min whereby the solids dissolved. A yellow solution resulted which was immediately cooled down to – 78 °C and transfer-cannuled to a precooled solution of 2.2 g (5.7 mmol) α-3',5'-bistoluoyl-1'-ribosyl chloride (**29**) in 20 mL dry CH$_2$Cl$_2$. The reaction mixture was allowed to warm up to r.t. overnight. Then, 20 mL sat. NH$_4$Cl$_{(aq)}$, 1 mL 2 M ammonia and

100 mL ether were added and the organic phases were separated. The aqueous phases were extracted twice with 100 mL ether and the organic phases combined. After washing twice with water, once with sat. $NaCl_{(aq)}$ and drying over Na_2SO_4, the solvents were removed *in vacuo* and the resulting oil was purified by flash column chromatography (silica, hexane : EtOAc = 9 : 1). 1.3 g (1.9 mmol, 33 %) of the desired β-anomer elutes short before 1.8 g (2.6 mmol, 45 %) of the α-anomer.

Analytical data for the β-anomer: R_f (hexane : EtOAc = 4 : 1) = 0.3; **^{1}H-NMR** (400 MHz, CDCl$_3$): δ 1.05 (18 H, d, *J* = 6.5 Hz), 1.25 (3 H, sept), 1.40 (1 H, d, *J* = 12.8 Hz), 2.08-2.15 (1 H, m), 2.15-2.24 (1 H, m), 2.38 (3 H, s), 2.42 (3 H, s), 2.50 (1 H, dd, *J* = 13.7, 4.9 Hz), 3.93 (2 H, td, *J* = 11.9, 1.8 Hz), 4.21 (2 H, dd, *J* = 11.0, 4.9 Hz), 4.54 (3 H, m), 5.19 (1 H, dd, *J* = 11.0, 5.0 Hz), 5.55 (1 H, d, *J* = 5.8 Hz), 5.85 (1 H, s), 6.90 (1 H, s), 6.93 (1 H, d, *J* = 8.0 Hz), 7.19 (2 H, d, *J* = 8.0 Hz), 7.26 (2 H, d, *J* = 8.0 Hz), 7.56 (1 H, d, *J* = 7.9 Hz), 7.89 (2 H, d, *J* = 8.2 Hz), 7.96 (2 H, d, *J* = 8.2 Hz); **^{13}C-NMR** (75 MHz, CDCl$_3$): δ 13.35, 18.36, 22.02, 22.08, 26.30, 42.13, 65.41, 67.94, 77.50, 80.64, 83.20, 97.74, 115.62, 118.58, 127.45, 127.74, 128.57, 129.49, 129.56, 129.58, 130.09, 130.14, 143.07, 144.12, 144.49, 153.65, 166.50, 166.76; **IR** (KBr) v = 2947, 2867, 1719, 1612, 1508, 1466, 1420, 1271, 1178, 1150, 1100, 999, 929, 753, 689 cm^{-1}; **EI-HRMS** (pos.): calc. for $C_{40}H_{52}O_8Si$ $[M]^+$: 688.3421, found: 688.3426.

## Sugar-deprotected nucleoside 27
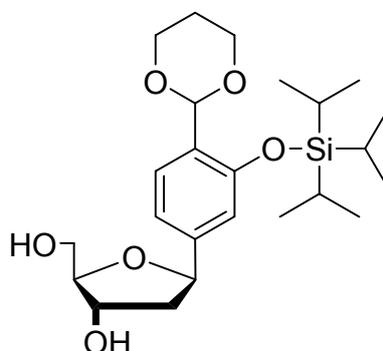
Compound **38** (750 mg, 1.09 mmol) was dissolved in 14 mL dry methanol and 331 mg (2.40 mmol) K_2CO_3 were added. The suspension was stirred for 2 h at r.t. until all solids had dissolved. The yellow solution was diluted with 50 mL chloroform

and 50 mL water. The aqueous phase was separated and extracted three times with CHCl$_3$. The combined organic extracts were washed with sat. NaCl$_{(aq)}$ and dried over Na$_2$SO$_4$. After removal of the solvents *in vacuo* the raw material was purified by flash column chromatography (silica, CHCl$_3$: MeOH = 50 : 1) to yield 353 mg (0.78 mmol, 72 %) of a colorless oil.

R$_f$ (CHCl$_3$: MeOH = 9 : 1) = 0.4; **^{1}H-NMR** (200 MHz, CDCl$_3$): δ 1.12 (18 H, d, J = 6.5 Hz), 1.21 - 1.34 (3 H, m), 1.41 (1 H, d, J = 13.4 Hz), 1.80 - 1.99 (1 H, m), 2.14 - 2.27 (2 H, m), 3.80 (1 H, dd, J = 11.6, 4.2 Hz), 3.69 (1 H, dd, J = 11.5, 5.1 Hz), 3.85 - 4.05 (3 H, m), 4.23 (2 H, dd, J = 11.7, 5.0 Hz), 4.38 (1 H, d, J = 5.9 Hz), 5.12 (1 H, dd, J = 10.2, 5.6 Hz), 5.86 (1 H, s), 6.80 (1 H, d, J = 1.4 Hz), 6.90 (1 H, dd, J = 7.9, 1.4 Hz), 7.55 (1 H, d, J = 7.9 Hz); **^{13}C-NMR** (150 MHz, CDCl$_3$): δ 11.99, 17.02, 24.85, 43.03, 62.52, 66.55, 72.64, 78.61, 86.20, 96.32, 114.60, 117.24, 126.39, 127.06, 142.40, 152.17; **IR** (KBr) v = 2926, 2868, 1611, 1578, 1503, 1465, 1420, 1285, 1237, 1151, 1099, 1000, 927, 884, 687 cm^{-1}; **EI-HRMS** (pos): calc. for C$_{24}$H$_{39}$O$_6$Si [M-H]$^+$: 451.2516, found: 451.2529.

DMT protected nucleoside 39
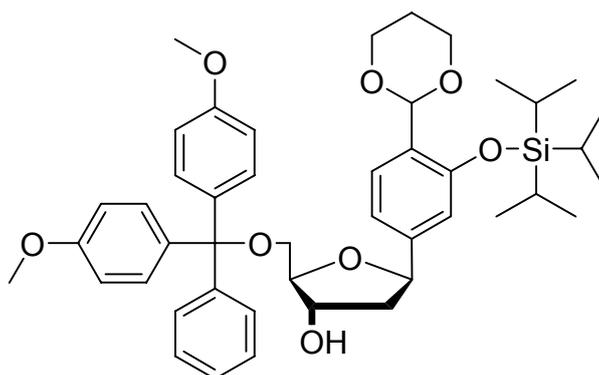
317 mg (0.70 mmol) of **27** was coevaporated twice with 6 mL dry pyridine. Then, it was dissolved in 3.2 mL pyridine and stirred over molsieves 4 Å for 2 h. 260 mg (0.77 mmol) 4,4'-dimethoxytritylchloride were added and the reaction was stirred for 2 h at r.t. Subsequently, 2 mL of dry MeOH were added, the mixture stirred for 1 h, filtrated and the solvents removed *in vacuo*. Flash chromatography (silica, hexane : EtOAc = 9 : 1, + 0.1 % pyridine) yielded 339 mg (0.45 mmol, 67 %) of a colorless oil.

R_f (hexane : EtOAc = 1 : 1) = 0.4; **^{1}H-NMR** (600 MHz, CDCl$_3$): δ 1.07 (18 H, dd, J = 7.5, 2.8 Hz), 1.21 - 1.28 (3 H, m), 1.40 (1 H, d, J = 13.5 Hz), 1.80 (OH, d, J = 2.0 Hz), 1.86 (1 H, ddd, J = 13.3, 10.0, 6.1 Hz), 2.14 – 2.26 (2 H, m), 3.16 (1 H, dd, J = 9.5, 6.9 Hz), 3.39 (1 H, dd, J = 9.6, 4.6 Hz), 3.79 (6 H, s), 3.93 (2 H, td, J = 12.4, 2.1 Hz), 4.01 (1 H, psept, J = 7.0, 4.6, 2.8 Hz), 4.21 (2 H, d, J = 11.3 Hz), 4.36 (1 H, d, J = 3.0 Hz), 5.07 (1 H, dd, J = 9.9, 5.7 Hz), 5.84 (1 H, s), 6.71 (1 H, d, J = 1.0 Hz), 6.82 (4 H, d, J = 8.8 Hz), 6.94 (1 H, d, J = 7.9, 1.0 Hz), 7.21 (1 H, t, J = 7.3 Hz), 7.27 (2 H, t, J = 7.5 Hz), 7.33 (4 H, d, J = 8.8 Hz), 7.44 (2 H, d, J = 7.4 Hz), 7.52 (1 H, d, J = 8.0 Hz); **^{13}C-NMR** (150 MHz, CDCl$_3$): δ 13.15, 18.19, 26.07, 43.68, 55.36, 64.57, 67.69, 74.92, 79.62, 86.24, 86.43, 97.53, 113.31, 115.77, 118.26, 126.95, 127.42, 128.00, 128.32, 130.18, 136.16, 143.91, 144.92, 153.07, 158.64; **IR** (KBr) ν = 2946, 2866, 1610, 1579, 1509, 1465, 1426, 1396, 1285, 1251, 1177, 1151, 1099, 1035, 997, 828, 687, 584 cm^{-1}; **EI-HRMS** (pos.): calc. for C$_{45}$H$_{57}$O$_8$Si [M-H]$^+$: 753.3822, found: 753.3793.

Ligand nucleoside phosphoramidite 40
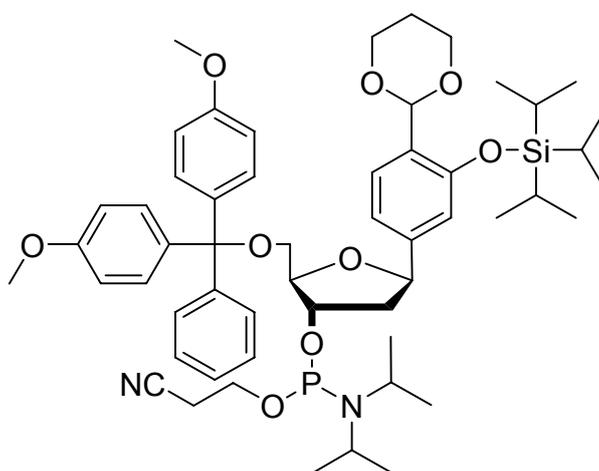
74 mg (0.10 mmol) of **39** was coevaporated twice with 2 mL dry THF and finally dissolved in 2 mL degassed THF. Then, 74 μL (0.40 mmol) NEt(*iso*-Pr)$_2$ and 36 μL (0.17 mmol) (*i*Pr$_2$N)(OCH$_2$CH$_2$CN)PCl were added and the reaction mixture was stirred for 2 h. The solvents were removed *in vacuo* and the residue was taken up into 1 mL of degassed EtOAc and purified by column chromatography under an atmosphere of protecting gas (desactivated silica, hexane : EtOAc = 5 : 1, + 0.1 % pyridine, all solvents degassed). The solvent was distilled off in high vacuum yielding

a mixture of diastereomers as a colorless oil (75 mg, 0.078 mmol, 78 %), which was stored no longer than several days at − 20 °C prior to its use in DNA synthesis.

R$_f$ (hexane : EtOAc = 9 : 1) = 0.1 (double spot); **^{1}H-NMR** (600 MHz, CDCl$_3$): δ 1.07 (18 H, d, *J* = 7.4 Hz), 1.09 - 1.30 (17 H, m), 1.39 (1 H, d, *J* = 13.3 Hz), 1.80 (1 H, ddd, *J* = 5.9, 11.0, 12.8 Hz), 2.14 - 2.33 (2 H, m), 2.48 (1 H, dd, *J* = 6.5, 2.3 Hz), 2.60 (1 H, t, *J* = 6.4 Hz), 3.13 - 3.31 (2 H, m), 3.52 - 3.65 (2 H, m), 3.68 - 3.75 (1 H, m), 3.77 (3 H, s), 3.78 (3 H, s), 3.93 (2 H, td, *J* = 12.0, 2.2 Hz), 4.21 (2 H, dd, *J* = 11.6, 5.7 Hz), 4.46 (1 H, dd, *J* = 10.8, 6.0 Hz), 5.02 - 5.09 (1 H, m), 5.84 (1 H, s), 6.72 (1 H, dd, *J* = 4.2, 1.5 Hz), 6.77 - 6.83 (4 H, m), 6.95 - 7.01 (1 H, m), 7.17 - 7.22 (1H, m), 7.22 - 7.35 (6 H, m), 7.40 - 7.47 (2 H, m), 7.50 - 7.55 (1 H, m); **^{13}C-NMR** (150 MHz, CDCl$_3$): δ 12.97, 18.01, 20.20 + 20.31 (2 diast.), 24.42 + 24.60 (2 diast.), 25.89, 29.68 + 30.31 (2 diast.), 41.78 + 43.26 (2 diast.), 46.19, 55.18, 63.96, 67.52, 79.77, 85.52, 85.82, 86.10, 97.38, 113.06, 113.20, 115.63, 117.45, 118.26, 126.70, 127.23, 127.75, 127.85, 128.25, 130.07, 143.62, 144.81, 149.71, 158.41; **^{31}P-NMR** (80 MHz, CDCl$_3$): δ 149.0, 149.5; **IR** (KBr) ν = 2924, 2852, 2250, 1610, 1582, 1509, 1465, 1424, 1396, 1252, 1179, 1152, 1100, 1035, 999, 829 cm^{-1}; **ESI-HRMS** (pos.): calc. for C$_{54}$H$_{76}$N$_2$O$_9$PSi [M]$^+$: 955.5058, found: 955.5083.

6.7   Synthesis of a monomeric copper salen complex

**Deprotected ligand-nucleoside 25**
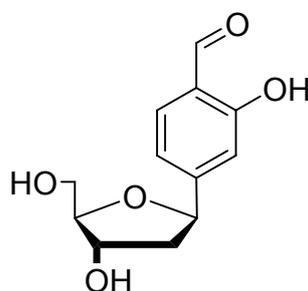
Sugar-deprotected nucleoside **27** (85 mg, 0.17 mmol) was dissolved in 2 mL dry THF, 1.7 eq Bu$_4$NF (1.1 M sol. in THF) was added and stirred for 3 h at r.t. Then, 200 μL concentrated HCl and one drop of water were added and stirred for another 2 h. 10 mL water was added and the mixture was extracted thrice with 20 mL Et$_2$O. The

combined organic extracts were dried over Na_2SO_4, the solvents removed *in vacuo* and the raw product was purified by flash column chromatography (silica, $CHCl_3$: MeOH = 9 : 1). The resulting brown solid was purified by recrystallization from EtOAc to yield 15 mg (0.06 mmol, 32 %) of colourless needles.

R_f ($CHCl_3$: MeOH = 9 : 1) = 0.3; **^{1}H-NMR** (400 MHz, CD_3OD): δ 1.90 (1 H, ddd, J = 13.1, 10.4, 5.9 Hz), 2.26 (1 H, ddd, J = 13.1, 10.4, 5.9 Hz), 3.68 (2 H, psept, J = 5.1, 11.6 Hz), 3.98 (1 H, dt, J = 5.1, 2.4 Hz), 4.32 (1 H, dt, J = 5.9, 1.9 Hz), 5.13 (1 H, dd, J = 10.4, 5.6 Hz), 7.03 (1 H, s), 7.06 (1 H, dd, J = 8.0, 1.4 Hz), 7.66 (1H, d, J = 8.0 Hz), 9.98 (1 H, s); **^{13}C-NMR** (100 MHz, CD_3OD): δ 44.81, 64.01, 74.28, 80.85, 89.50, 115.13, 118.50, 121.87, 134.11, 153.82, 162.79, 196.86; **IR** (diamond-ATR): ν = 3262 (m), 2897 (m), 1650 (s), 1628 (s), 1434 (m), 1348 (m), 1309 (s), 1177 (m), 1153 (s), 1087 (s), 1051 (s), 988 (s), 956 (m), 874 (m), 810 (s), 680 (m) cm^{-1}; **ESI-HRMS** (neg.): calc. for $C_{12}H_{13}O_5$ [M-H]$^-$: 237.0757, found: 237.0771; **X-ray** structure: see Chapter 4.2.2 and reference [183].

Salen ligand 41
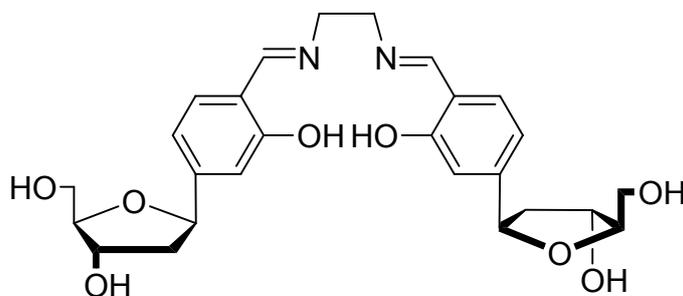
The fully deprotected ligand **25** (45 mg, 0.19 mmol) was dissolved in 10 mL dry MeOH and 0.5 eq. ethylenediamine (6.32 μL, 0.095 mmol) was added. The color of the solution changes to yellow and a microcrystalline yellow material precipitates within several days. The reaction was also carried out in CD_3OD in the NMR tube and quantitative conversion was observed by NMR spectroscopy.

^{1}H-NMR (400 MHz, CD_3OD): δ 1.90 (1 H, ddd, J = 13.2, 10.4, 5.9 Hz), 2.21 (1 H, dtd, J = 12.5, 5.2, 1.7 Hz), 3.53-3.76 (3 H, m), 3.95 (2 H, s), 4.30 (1 H, m), 5.07 (1 H, dd, J = 10.4, 5.6 Hz), 6.83-6.93 (2, m), 7.30 (1H, dd, J =19.2, 8.0 Hz), 8.43 (1 H, s);

^{13}C-NMR (100 MHz, CD$_3$OD): δ 44.85, 59.59, 63.83, 73.95, 80.63, 88.71, 114.38, 115.96, 117.88, 131.75, 147.55, 162.14, 166.12; **IR** (diamond-ATR): ν = 3253 (w), 2890 (w), 2853 (w), 2428 (s), 1984 (w), 1627 (s), 1429 (m), 1372 (m), 1265 (m), 1186 (w), 1138 (m), 1089 (m), 1055 (s), 1021 (s), 976 (s), 938 (m), 898 (m), 866 (m), 816 (s), 808 (s), 755 (m) cm^{-1}; **ESI-HRMS** (pos.): calc. for C$_{26}$H$_{33}$O$_8$N$_2$ [M+H]$^+$: 501.2231, found: 501.2229.

Cu-salen complex 42
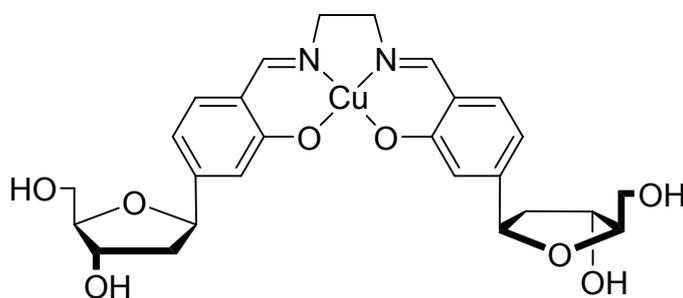
A solution of salen ligand **41** (50 mg, 0.10 mmol) in 5 mL dry MeOH was combined with a methanolic solution of Cu(acac)$_2$ (26 mg, 0.10 mmol) and heated under reflux for 10 min. The color changed from yellow over green to purple. Slowly cooling down a sat. methanolic solution yielded small dichrotic green-purple crystals which were used for crystallographic examination.

IR (diamond-ATR): ν = 3305 (m), 2919 (w), 2888 (w), 1634 (s), 1614 (s), 1526 (s), 1482 (m), 1427 (s), 1387 (m), 1322 (s), 1302 (m), 1312 (m), 1187 (m), 1064 (s), 1038 (s), 998 (s), 966 (s), 959 (s), 873 (s), 795 (s) cm^{-1}; **ESI-HRMS** (pos.): calc. for C$_{26}$H$_{31}$O$_8$N$_2$Cu [M+H]$^+$: 562.1371, found: 562.1369. **X-ray** structure: see Chapter 4.2.2 and reference [184].

6.8   Synthesis of a 3-(2-oxazolidinylidene-)indol-2-one nucleoside

Protected 3-dichlormethylen-indol-2-one nucleoside 57
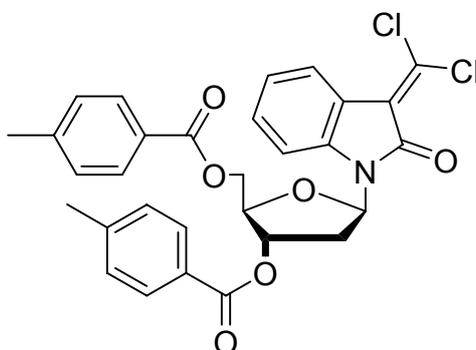
To a stirred suspension of 3-dichlormethylene-indol-2-one **56** (2.0 g, 9.4 mmol) in dry acetonitrile (70 mL) was added 1,8-diazabicyclo[5.4.0]undec-7-ene (1.4 mL, 9.4 mmol). The resulting clear red solution stirred 5 min. Then 2'-deoxyribosyl chloride **29** (4.0 g, 10 mmol) was added. The mixture then turned greenish black and stirred an additional 17 h. The solvent was removed and the reaction mixture was separated by column chromatography on two successive columns. The first column (CH$_2$Cl$_2$: MeOH = 19 : 1) gave an impure isomeric mixture which was then separated on a second column (CHCl$_3$: EtOAc = 39 : 1) to give β-**57** (0.97 g, 18%) which elutes short before its isomer α-**57** (1.0 g, 19%) as yellow solids.

β-**57**: **R$_f$** (hexane : EtOAc = 9 : 1) = 0.3; **^{1}H-NMR** (300 MHz, CDCl$_3$): δ 7.97 (5 H, m), 7.25 (5 H, m), 7.03 (1 H, dt, *J* = 7.7, 1.0 Hz), 6.92 (1 H, td, *J* = 7.8, 1.3 Hz), 6.42 (1 H, dd, *J* = 8.9, 6.1 Hz), 5.76 (1 H, ddd, *J* = 7.1, 3.6, 2.7 Hz), 4.80 (1 H, dd, *J* = 12.2, 3.3 Hz), 4.69 (1 H, dd, *J* = 12.1, 3.8 Hz), 4.46 (1 H, ddd, *J* = 3.5, 3.5, 3.5 Hz), 3.10 (1 H, ddd, *J* = 14.1, 9.4, 7.1 Hz), 2.43 (6 H, s), 2.38 (1 H, ddd, *J* = 14.1, 6.1, 2.4 Hz); **^{13}C-NMR** (75 MHz, CDCl$_3$): δ 194.2, 166.6, 166.5, 163.9, 144.8, 144.4, 139.4, 133.5, 130.7, 130.2, 130.2, 129.7, 127.3, 126.9, 125.0, 124.9, 123.1, 121.5, 111.4, 82.3, 81.8, 74.6, 64.3, 34.3, 22.1; **IR** (diamond-ATR): ν = 3413, 2945, 2929, 1710, 1610, 1596,1468, 1448, 1377, 1364, 1311, 1268, 1195, 1178, 1125, 1099, 1083, 1016, 932, 834, 744, 710 cm^{-1}; **EI-MS** (pos., 70 eV): calc. for C$_{30}$H$_{25}$Cl$_2$NO$_6$ [M]$^+$ 565.1; found 565.1; **APCI-HRMS** (pos.): calc. for C$_{30}$H$_{26}$Cl$_2$NO$_6$ [M+H]$^+$ 566.1132; found 566.1120.

α-**57**: **R$_f$** (hexane : EtOAc = 9 : 1) = 0.2; **^{1}H-NMR** (600 MHz, CDCl$_3$): δ 8.04 (1 H, d, J = 7.8 Hz), 7.95 (4 H, d, J = 8.1 Hz), 7.39 (1 H, d, J = 7.9 Hz), 7.29 (1 H, dt, J = 7.8, 1.1 Hz), 7.26 (4 H, m), 7.11 (1 H, dt, J = 7.8, 0.8 Hz), 6.49 (1 H, t, J = 6.9 Hz), 5.63 (1 H, ddd, J = 7.8, 4.4, 3.3 Hz), 4.83 (1 H, ddd, J = 3.7, 3.7, 3.7 Hz), 4.63 (1 H, dd, J = 12.0, 4.4 Hz), 4.55 (1 H, dd, J = 12.0, 3.7 Hz), 2.95 (1 H, ddd, J = 15.2, 7.6, 7.6 Hz), 2.85 (1 H, ddd, 14.5, 6.4, 4.8 Hz), 2.44 (3 H, s), 2.41 (3 H, s); **^{13}C-NMR** (75 MHz, CDCl$_3$): δ 208.8, 168.2, 168.0, 165.6, 146.3, 146.0, 141.0, 134.9, 132.3, 131.7, 131.6, 131.5, 128.7, 128.5, 126.6, 126.5, 124.6, 123.1, 112.8, 84.8, 83.6, 77.1, 66.7, 36.6, 32.8, 23.6, 23.6.

Protected 3-(2-oxazolidinylidene-)indol-2-one nucleoside 58
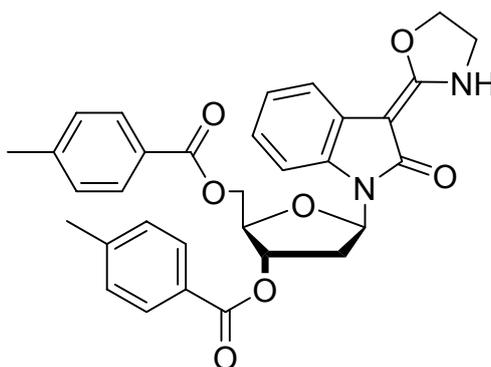
To a stirred solution of **57** (0.89 g, 1.6 mmol) in dry THF (12 mL) was added ethanolamine (0.30 mL, 5.0 mmol). The reaction was stirred for 17 h, over which time the yellow solution became colorless with a white precipitate. The solvent was removed *in vacuo*, the remaining residue was dissolved in CH$_2$Cl$_2$ and the solution was washed with water and dried over Na$_2$SO$_4$. After removal of the solvents, the raw material was purified by column chromatography (CH$_2$Cl$_2$: MeOH = 19 : 1) to give the β-nucleoside β-**58** (0.30 g, 35%) as a white-bluish foam. The α-nucleoside α-**57** could be reacted with ethanolamine in the same way to yield α-**58**.

β-**58**: **R$_f$** (CHCl$_3$: MeOH = 9 : 1) = 0.8; **^{1}H-NMR** (600 MHz, CDCl$_3$): δ 8.55 (1 H, NH, s), 7.99 (4 H, dd, J = 22.2, 8.2 Hz), 7.41 (1 H, d, J = 7.5), 7.26 (5 H, m), 6.96 (1 H, t, J = 7.6 Hz), 6.68 (1 H, td, J = 7.7, 1.1 Hz), 6.57 (1 H, dd, J = 9.1, 6.1 Hz), 5.80 (1 H, m), 4.78 (1 H, dd, J = 12.0, 3.5 Hz), 4.71 (1 H, dd, J = 12.1, 4.0), 4.69 (2 H, td, J =

8.0, 2.9 Hz), 4.46 (1 H, dd, *J* = 7.3, 3.7 Hz), 3.85 (2 H, td, *J* = 8.0, 1.7 Hz), 3.21 (1 H, ddd, *J* = 14.3, 9.1, 7.7 Hz), 2.43 (3 H, s), 2.42 (3 H, s), 2.35 (1 H, ddd, *J* = 8.3, 6.1, 2.2 Hz); ^{13}**C-NMR** (150 MHz, CDCl$_3$): δ 168.89, 166.52, 166.291, 165.00, 144.28, 143.95, 133.58, 129.94, 129.93, 129.31, 129.31, 127.24, 126.93, 124.05, 121.91, 121.50, 118.31, 110.19, 81.85, 81.05, 79.31, 74.82, 69.14, 64.46, 42.70, 34.26, 21.84, 21.84; **IR** (diamond-ATR): ν = 3238, 3051, 2982, 2923, 2884, 1716, 1666, 1608, 1593, 1567, 1468, 1446, 1369, 1312, 1269, 1198, 1178, 1148, 1080, 1047, 1018, 982, 934, 842, 774, 752, 733, 687, 656 cm^{-1}; **EI-HRMS** (pos.): calc. for C$_{32}$H$_{30}$N$_2$O$_7$ [M]$^+$ 554.2048; found 554.2075.

α-**58: R$_f$** (CHCl$_3$: MeOH = 9 : 1) = 0.7; ^{1}**H-NMR** (600 MHz, CDCl$_3$): δ 8.52 (1 H, NH, s), 7.91 (4 H, dd, *J* = 17.1, 8.1 Hz), 7.37 (2 H, t, *J* = 8.0), 7.18 (4 H, dd, *J* = 24.2, 8.1 Hz), 6.96 (1 H, t, *J* = 7.4 Hz), 6.92 (1 H, t, *J* = 7.6 Hz), 6.58 (1 H, t, *J* = 7.5 Hz), 5.58 (1 H, ddd, *J* = 8.1, 4.1, 4.1 Hz), 4.77 (1 H, dt, *J* = 3.9, 3.9 Hz), 4.60 (2 H, dt, *J* = 8.3, 2.1 Hz), 4.55 (1 H, dd, *J* = 11.8, 4.8 Hz), 4.48 (1 H, dd, *J* = 11.8, 3.9 Hz), 3.75 (2 H, ddd, *J* = 7.6, 7.6, 5.7 Hz), 2.85 (2 H, m), 2.36 (3 H, s), 2.32 (3 H, s); ^{13}**C-NMR** (150 MHz, CDCl$_3$): δ 169.2, 166.8, 166.6, 165.2, 144.6, 144.3, 133.6, 130.2, 130.2, 129.6, 127.4, 127.2, 124.6, 122.2, 121.8, 118.6, 110.4, 82.6, 82.5, 81.4, 75.9, 75.8, 70.6, 69.4, 65.4, 43.0, 35.1, 22.1; **EI-MS** (pos.): calc. for C$_{32}$H$_{30}$N$_2$O$_7$ [M]$^+$ 554.2; found 554.2.

## 3-(2-oxazolidinylidene-)indol-2-one nucleoside β-52
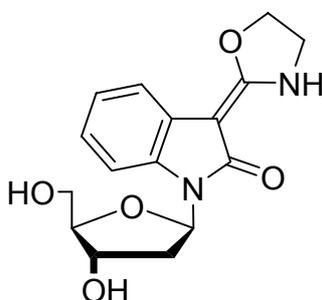
To a stirred suspension of β-**58** (141 mg, 0.254 mmol) in dry methanol was added K$_2$CO$_3$ (84 mg, 0.610 mmol). The reaction was monitored by TLC (CH$_2$Cl$_2$: MeOH = 19 : 1). After stirring 3 days, the reaction was quenched with water and extracted with CHCl$_3$. Purification by column chromatography

(CH_2Cl_2 : MeOH = 9 : 1) gave β-**52** (44 mg, 54%) as a white powder wich was immediately used in the next step.

^{1}H-NMR (200 MHz, $CDCl_3$): δ 2.10 (1 H, dd), 2.50 (2 H, OH, br), 3.20 (1 H, m), 3.70-4.00 (4 H, m), 4.10 (1 H, s), 4.70 (3 H, m), 6.30 (1 H, dd), 7.05 (3 H, s), 7.45 (1 H, t), 8.65 (1 H, NH, br); **EI-MS** (pos.): calc. for $C_{24}H_{15}NO_6$ [M]$^+$ 413.1; found 412.8.

DMT-protected 3-(2-oxazolidinylidene-)indol-2-one nucleoside β-59
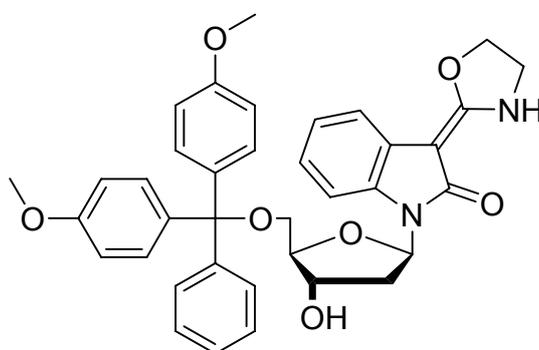
β-**52** (44 mg, 0.138 mmol) was stirred in dry pyridine with molecular sieve 4 Å for 1 h, then DMT-Cl (67 mg, 0.172 mmol) was added. The reaction was monitored by TLC (CH_2Cl_2 : MeOH = 19 : 1). After 16 h, the reaction was quenched with MeOH, washed with H_2O, extracted with CH_2Cl_2 and dried over Na_2SO_4. Purification by column chromatography (CH_2Cl_2 : MeOH = 19 : 1) gave β-**59** (10 mg, 65%) as a yellow-green oil.

R_f ($CHCl_3$: MeOH = 9 : 1) = 0.5; **^{1}H-NMR** (400 MHz, $CDCl_3$): δ 2.13 (1 H, ddd, J = 10.2, 6.7, 3.4 Hz), 2.91 (1 H, dt, J = 13.6, 8.0 Hz), 3.44 (2 H, ddd, J = 14.7, 10.1, 4.6 Hz), 3.69 (2 H, t, J = 8.3 Hz), 3.74 (6 H, s), 4.02 (1 H, dd, J = 8.7, 4.3 Hz), 4.54 (2 H, ddd, J = 16.8, 13.7, 8.4 Hz), 4.67 (1 H, q, J = 3.9 Hz), 6.50 (1 H, t, J = 7.4 Hz), 6.72 (1 H, dt, J = 7.8, 1.1 Hz), 6.77 (4 H, d, J = 8.9 Hz), 6.96 (1 H, dt, J = 7.5, 0.6 Hz), 7.16-7.26 (3 H, m), 7.28 (1 H, d, J = 8.2 Hz), 7.36 (4 H, d, J = 8.7 Hz), 7.41 (1 H, dd, J = 7.6, 0.7 Hz), 7.48 (2 H, d, J = 7.8 Hz); **^{13}C-NMR** (100 MHz, $CDCl_3$): δ 37.39, 42.99, 55.64, 64.26, 69.36, 72.77, 79.59, 81.53, 84.68, 86.82, 110.94, 113.56, 118.42, 121.62, 122.15, 124.24, 127.18, 128.24, 128.72, 130.60, 133.97, 136.37,

145.33, 158.87, 165.20, 168.96; **IR** (diamond-ATR): ν = 3320, 3057, 2929, 2836, 1731, 1661, 1605, 1574, 1507, 1467, 1443, 1361, 1299, 1246, 1175, 1148, 1086, 1030, 984, 933, 827, 775, 749, 701, 684 cm^{-1}; **FAB-MS** (pos.): calc. for $C_{37}H_{36}N_2O_7$ [M]$^+$ 620.3; found 620.2; **APCI-HRMS** (pos.): calc. for $C_{37}H_{36}N_2O_7$ [M]$^+$ 620.2517; found 620.2514.

DMT-protected 3-(2-oxazolidinylidene-)indol-2-one phosphoramidite β-60
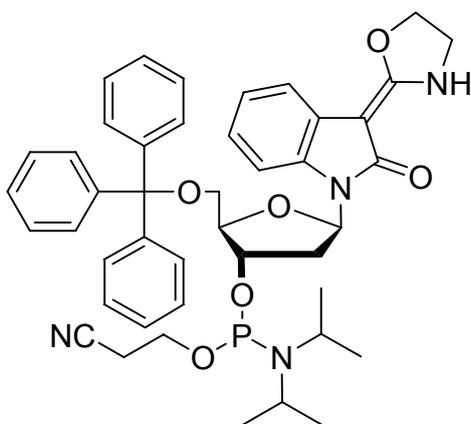
55 mg (0.089 mmol) of the DMT protected nucleoside β-**59** was coevaporated twice with 2.0 mL dry THF and finally dissolved in 1.5 mL degassed THF. Then, 55 μL (0.36 mmol) NEt(*iso*-Pr)$_2$ and 25 μL (0.11 mmol) (*i*Pr$_2$N)(OCH$_2$CH$_2$CN)PCl were added and the reaction mixture was stirred for 3 h until TLC control showed a complete transformation of the starting material. The solvents were removed *in vacuo* and the residue was taken up into 1 mL of degassed EtOAc and purified by column chromatography under an atmosphere of protecting gas (desactivated silica, hexane : EtOAc = 5 : 1, + 0.1 % pyridine, all solvents degassed). Silica gel chromatography, however, lead to partial decomposition and change of the color to dark green-blue. The solvent was distilled off in high vacuum yielding a mixture of product diastereomers and unidentified decomposition products which was nevertheless used in the automated DNA synthesis. The ^{1}H- and ^{13}C-NMR spectra confirm the coexistence of several species and were not interpretable due to their complexity (see discussion in Chapter 4.2.4).

^{31}P-NMR (80 MHz, CDCl$_3$): δ 15.35 (s, oxidized phosphorylating reagent), 132.26 and 132.89 (small, belonging to two diastereomers of a phosphorylated compound), 149.37 and 150.02 (large, belonging to two diastereomers of another phosphorylated compound) (Figure 100). **ESI-HRMS** (pos.): calc. for C$_{46}$H$_{53}$N$_4$O$_8$P$_1$Na$_1$ [M+Na]$^+$: 843.3499; found 843.3482.
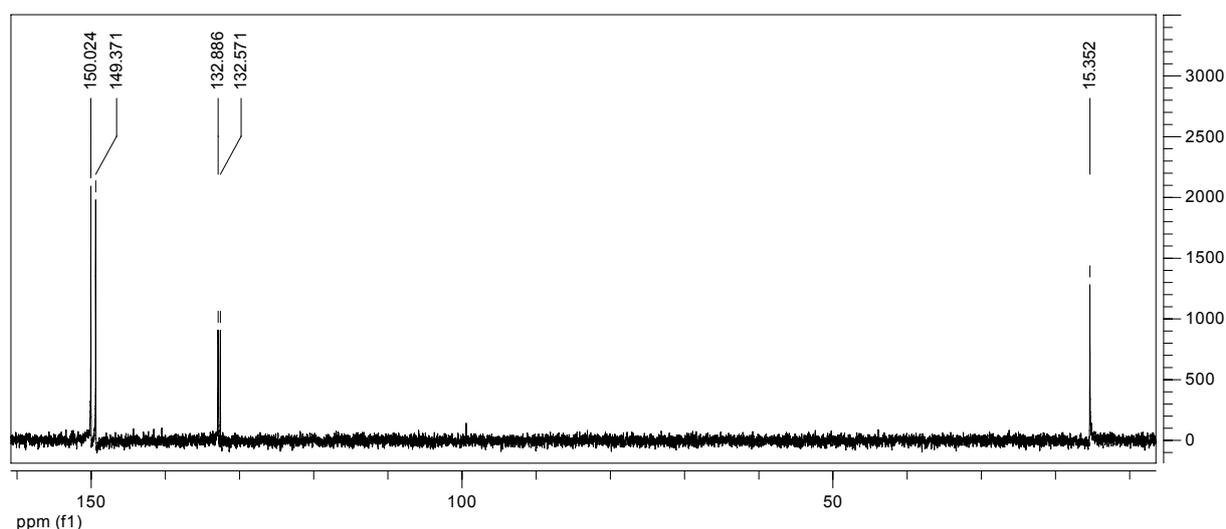
Figure 100: ^{31}P-NMR spectrum of the product mixture of the phosphorylation of nucleoside β-**59**.

6.9   Synthesis of 3'-O-methyl-xylopyranosyl nucleosides

1',2',4'-Tri-*O*-toluoyl-3'-*O*-methyl-α,β-D-xylopyranose 62
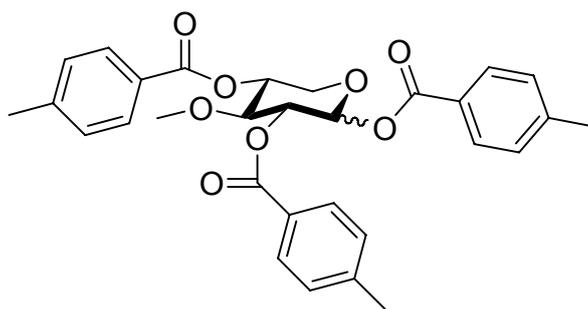
3'-*O*-methyl-α,β-D-xylofuranose (3.04 g, 18.5 mmol) was dissolved in 30 mL dry pyridine under a protecting gas atmosphere. Then, 8.68 mL (65.7 mmol, 3.6 eq) toluoyl chloride was added slowly. After addition of 50 mg DMAP, the mixture was stirred for 60 h at r.t. Subsequently, the solvent was removed from the yellow solution *in vacuo* and the remaining residue was extracted twice with CHCl$_3$. The organic extracts were combined and washed once with sat. NaHCO$_{3\ (aq)}$ and twice with H$_2$O.

After drying with Na_2SO_4 the raw material was subjected to column chromatography (silica gel, pentane : EtOAc = 10 : 1 → 6 : 1) to yield 5.78 g (11.2 mmol, 61 %) of compound **62** as a colorless resin. The product is a mixture of anomers with a ratio of $\alpha : \beta$ = 2 : 1. Separation of the anomers was not necessary for the following transformations.

R_f (hexane : EtOAc = 4 : 1) = 0.4 (double spot); **^{1}H-NMR** (200 MHz, CDCl$_3$): α-Isomer: δ 2.35-2.49 (9 H, m), 3.58 (3 H, s), 3.81-3.97 (1 H, m), 4.10-4.24 (2 H, m) 5.29 (1 H, dt, J = 8.7, 4.6 Hz), 5.40 (1 H, dd, J = 4.6, 4.0 Hz), 6.58 (1 H, d, J = 3.4 Hz), 7.07-7.34 (6 H, m), 7.85-8.03 (6 H, m); β-Isomer: δ 2.35-2.49 (9 H, m), 3.62 (3 H, s), 3.81-3.97 (1 H, m) 4.44 (1 H, dd, J = 12.7, 3.2 Hz), 5.20 (1 H, q, J = 4.1 Hz), 5.40 (1 H, t, J = 4.6 Hz), 6.28 (1 H, d, J = 3.7 Hz), 7.07-7.34 (6 H, m), 7.85-8.03 (6 H, m); **^{13}C-NMR** (50 MHz, CDCl$_3$): α-Isomer: δ 21.9 (3C), 60.6, 62.1, 70.6, 71.3, 78.7, 90.7; β-Isomer: δ 21.9 (3C), 59.3, 61.5, 68.4, 68.9, 76.7, 92.1; α-Isomer + β-Isomer: 129.3, 129.3, 129.4, 129.5, 129.6, 130.0, 130.4, 144.3, 144.3, 144.7, 165.5, 166.0 (2C); **IR** (diamond-ATR): ν = 3036, 2951, 1717, 1611, 1448, 1409, 1309, 1257, 1177, 1089, 1015, 958, 838, 748, 689 cm^{-1}; **EI-MS** (pos.): 399 [M-Tol-CO]$^+$; **ESI-MS** (pos.): 541 [M + Na]$^+$, 557 [M + K]$^+$; **APCI-HRMS** (pos.): calc. for $C_{30}H_{31}O_8$ [M+H]$^+$: 519.2013; found 519.2032.

## 2',4'-Di-*O*-toluoyl-3'-*O*-methyl-α-D-xylopyranosylchloride 63
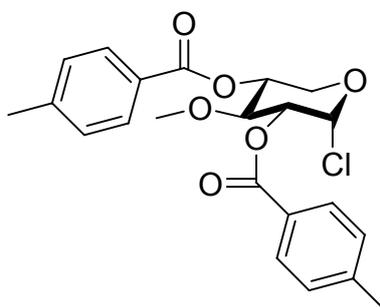
20 mg $ZnCl_2$ were molten in a Schlenk flask in high vacuum by heating with a hot air blower and allowed to cool down under an atmosphere of N_2 protecting gas. Subsequently, 1.7 mL dry CHCl$_3$, 500 mg 1',2',4'-tri-*O*-toluoyl-3'-*O*-methyl-α,β-D-xylopyranose **62** (0.97 mmol) and 0.68 mL (7.60 mmol, 8.0 eq) dichloromethyl-

methylether were added. The mixture was heated to 50 °C for 2 h and stirred at room temperature for 16 h. Subsequently, the solvent was removed *in vacuo* and the raw material was subjected to a quick column chromatography (silica gel, pentane : EtOAc = 10 : 1) to yield 248 mg (0.59 mmol, 62 %) of the glycosyl chloride **63** as a colorless oil or foam which had to be stored at − 20 °C under protecting gas to prevent decomposition.

R_f (hexane : EtOAc = 9 : 1) = 0.4; **^{1}H-NMR** (200 MHz, CDCl$_3$): δ 2.36 (6 H, s), 3.51 (3 H, s), 3.92 (1 H, t, J = 11 Hz), 4.04 (1 H, t, J = 9.4 Hz), 4.12 (1 H, dd, J = 11.0, 6.1 Hz), 5.08-5.23 (1 H, m), 5.13 (1 H, dd, J = 9.8, 3.9 Hz), 6.33 (1 H, d, J = 3.9 Hz), 7.16-7.25 (4 H, m), 7.85-8.01 (4 H, m); **^{13}C-NMR** (50 MHz, CDCl$_3$): δ 21.9 (2C), 61.3, 61.7, 70.7, 73.7, 78.2, 92.3, 126.6 (2C), 126.8 (2C), 130.0 (2C), 130.2 (2C),144.6, 144.7, 165.7 (2C); **IR** (diamond-ATR): ν = 3037, 2940, 1719, 1612, 1449, 1409, 1378, 1313, 1258, 1176, 1091, 1020, 942, 838, 748, 689, 636 cm^{-1}; **EI-MS** (pos.): 418 [M]$^+$, 383 [M − Cl]$^+$; **ESI-MS** (pos.): 437 [M − Cl + OMe + Na]$^+$, 453 [M − Cl + OMe + K]$^+$; **EA**: calc. for C$_{22}$H$_{23}$ClO$_6$: C: 63.08; H: 5.53; Cl: 8.46; found: C: 62.92; H: 5.37.

2',4'-Di-*O*-toluoyl-3'-*O*-methyl-α-D-xylopyranosyl bromide 64
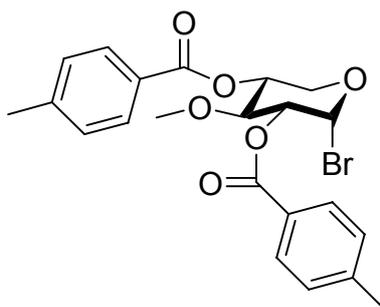
The fully protected sugar 1',2',4'-tri-*O*-toluoyl-3'-*O*-methyl-α,β-D-xylopyranose **62** (0.55 g, 1.06 mmol) was dissolved in 7 mL dry CH$_2$Cl$_2$ and 0.26 mL acetic anhydride was added to ensure complete absence of H$_2$O. Subsequently, the mixture was cooled to 0 °C and 1.5 mL HBr in HOAc (33 %) was added slowly. After stirring for 1 h at 0 °C and 2 h at 10 °C the mixture was stored in a refridgerator (4 °C) overnight. Subsequently, the solution was diluted with 50 mL cold CH$_2$Cl$_2$ and quickly washed with cold H$_2$O, cold diluted NaHCO$_{3\,(aq)}$ and cold sat. NaCl$_{(ap)}$ and dried over MgSO$_4$.

The solvent was removed *in vacuo* at room temperature upon which 290 mg (0.63 mmol, 59%) of a slightly yellow oil resulted. Attempts to purify the product by column chromatography resulted in complete hydrolysis of the compound on the silica gel, so the raw material was used immediately for the further experiments. NMR spectroscopy revealed ca. 90 % purity. The impurities probably were hydrolysis or elimination products.

^{1}H-NMR (200 MHz, CDCl$_3$) δ 2.35 (6 H, s), 3.50 (3 H, s), 3.71-4.21 (3 H, m), 4.95 (1 H, dd, J = 9.5, 3.9 Hz), 5.18 (1 H, ddd, J = 10.8, 9.4, 5.9 Hz), 6.66 (1 H, d, J = 3.9 Hz), 7.20 (4 H, d, J = 8.0), 7.89 (2 H, d, J = 8.1 Hz), 7.93 (2 H, d, J = 8.1 Hz); **^{13}C-NMR** (50 MHz, CDCl$_3$): δ 21.25, 21.27, 60.65, 62.61, 69.80, 72.38, 78.26, 89.15, 125.87, 126.02, 128.80, 128.83, 129.33, 129.49, 143.89, 144.02, 164.85, 164.97; **IR** (diamond-ATR): ν = 3481, 3038, 2944, 2656, 2550, 1710, 1673, 1612, 1419, 1314, 1262, 1177, 1094, 1049, 1020, 946, 838, 749, 688 cm^{-1}; **APCI-HRMS** (pos.): calc. for C$_{22}$H$_{24}$O$_6$Br [M+H]$^+$: 463.0751; found: 463.0751.

2',4'-Di-*O*-toluoyl-1'-phenyl-3'-*O*-methyl-β-D-xylopyranose 65
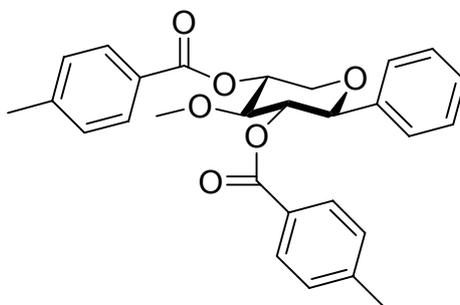
18 mg (0.75 mmol) magnesium turnings were activated by stirring under protecting gas for several h. A solution of 118 mg (0.75 mmol) bromobenzene in 100 μL dry THF was treated with molsieves 4 Å and an aliquot was added to the magnesium. The Grignard reaction initiated after short heating with a hot air blower and the remaining bromobenzene solution was added slowly. When all solids were dissolved, the slightly brown solution was cooled to − 78 °C and transferred to a precooled suspension of 77 mg (0.38 mmol) copper(I)bromide-disulfide complex in 1 mL dry THF. The orange suspension was carefully warmed to 0 °C and transferred after 5 min to a 0 °C cold solution of 100 mg (0.25 mmol) of the xylosyl chloride **63** in 1 mL

dry THF. The yellow mixture was allowed to warm up to r.t. slowly which resulted in a color change to brown. After 2 h, 2 mL sat. $NH_4Cl_{(aq)}$ and 20 mL ether were added and the organic phases were separated. The aqueous phases were extracted twice with 10 mL ether and the organic phases were combined. After washing twice with water, once with sat. $NaCl_{(aq)}$ and drying over Na_2SO_4, the solvents were removed *in vacuo* and the resulting oil was purified by flash column chromatography (silica gel, hexane : EtOAc = 10 : 1). 90 mg (0.20 mmol, 80 %) of *C*-glycoside **65** were obtained which crystallized in long needles from the solvent right after leaving the chromatography column. X-ray crystallography showed a β-configuration of the *C*-glycosidic bond.

R$_f$ (hexane : EtOAc = 9 : 1) = 0.3; **^{1}H-NMR** (200 MHz, CDCl$_3$): δ 2.39 (3 H, s), 2.43 (3 H, s), 3.47 (3 H, s), 3.54 (1 H, t, *J* = 10.8 Hz), 3.90 (1 H, t, *J* = 9.3 Hz), 4.36-4.48 (2 H, m), 5.30-5.45 (2 H, m), 7.15-7.42 (9 H, m), 7.81 (2 H, d, *J* = 8.3 Hz), 7.97 (2 H, d, *J* = 8.2 Hz); **^{13}C-NMR** (75 MHz, CDCl$_3$): δ 22.02, 22.08, 60.48, 67.99, 72.06, 74.71, 81.96, 83.61, 127.35, 127.43, 127.56, 128.77, 128.99, 129.44, 129.61, 129.98, 130.15, 137.33, 144.09, 144.49, 164.93, 165.93; **IR** (diamond-ATR): ν = 3034, 2995, 2950, 2928, 2850, 1727, 1711, 1609, 1454, 1310, 1256, 175, 1104, 1084, 1042, 1018, 994, 973, 910, 837, 748, 697, 689 cm^{-1}; **APCI-HRMS** (pos.): calc. for C$_{28}$H$_{29}$O$_6$ [M+H]$^+$: 461.1959; found: 461.1936; **X-ray** structure: see Figure 39, Chapter 4.2.5. The crystallographic data is listed in the appendix, Chapter 7.2.

Ligand-substituted 3'-*O*-methyl-β-D-xylopyranoses 61 and 66
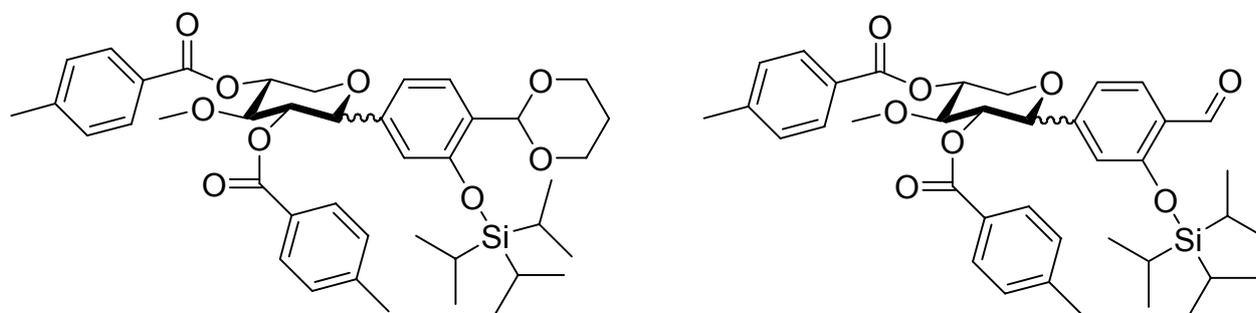
A solution of compound **28** (620 mg, 1.50 mmol) in 5 mL freshly distilled diethylether was cooled to – 78 °C and 1.9 mL (3.00 mmol) *t*-BuLi in pentane (1.57 M) was added

dropwise over 20 min. The reaction was kept at – 78 °C with stirring for 3 h and subsequently transfer-cannuled to a precooled (– 78 °C) suspension of copper(I)bromide-disulfide complex (150 mg, 0.75 mmol) in 2 mL ether. The reaction mixture was carefully warmed to – 30 °C for 20 min whereby the solids dissolved and a yellow solution resulted which was immediately cooled down to – 78 °C and transfer-cannuled to a precooled solution of 140 mg (0.3 mmol) methylxylosyl bromide **64** in 3 mL dry CH_2Cl_2. The orange reaction mixture was allowed to warm up to r.t. overnight. Then, 5 mL sat. $NH_4Cl_{(aq)}$, 0.2 mL 2 M ammonia and 20 mL ether were added and the organic phases were separated. The aqueous phases were extracted twice with 20 mL ether and the organic phases were combined. After washing twice with H_2O, once with sat. $NaCl_{(aq)}$ and drying over Na_2SO_4, the solvents were removed *in vacuo* and the resulting oil was purified by flash column chromatography (silica, hexane : EtOAc = 20 : 1 → 10 : 1). Besides the usual side products of the cuprate addition (ligand dimer, various sugar derivatives) both anomers of the *C*-glycoside without the acetal protecting group could be separately isolated (yield not determined). Furthermore, 62 mg (0.086 mmol, 29%) of the desired *C*-glycoside could be isolated as an inseparable anomeric mixture.
The procedure for separating the anomers is discussed in Chapter 4.2.5.

α-**66** (free aldehyde): **R$_f$** (hexane : EtOAc = 4 : 1) = 0.5; **^{1}H-NMR** (200 MHz, $CDCl_3$) δ 0.98 (9 H, dd, *J* = 3.0 Hz), 1.02 (9 H, d, *J* = 3.0 Hz), 1.11-1.32 (3 H, m), 2.28 (6 H, s), 3.62 (3 H, s), 3.81 (1 H, s), 4.11 (1 H, dd, *J* = 12.9, 1.8 Hz), 4.27 (1 H, d, *J* = 13.4 Hz), 4.89 (1 H, s), 5.01 (1 H, s), 5.21 (1 H, s), 6.84-6.99 (5 H, m), 7.07 (1 H, d, *J* = 7.3 Hz), 7.58-7.76 (5 H, m), 10.37 (1 H, s).

β-**66** (free aldehyde): **R$_f$** (hexane : EtOAc = 4 : 1) = 0.6; **^{1}H-NMR** (200 MHz, $CDCl_3$) δ 0.97 (9 H, d, *J* = 4.1 Hz), 1.01 (9 H, d, *J* = 4.1 Hz), 1.09-1.30 (3 H, m), 2.33 (3 H, s), 2.36 (3 H, s), 3.39 (3 H, s), 3.45 (1 H, t, *J* = 10.5 Hz), 3.82 (1 H, t, *J* = 9.2 Hz), 4.29-4.41 (2 H, m), 5.13-5.37 (2 H, m), 6.87 (1 H, s), 6.90 (1 H, d, *J* = 8.7 Hz), 7.14 (2 H, d, *J* = 8.2 Hz), 7.21 (2 H, d), 7.58 (1 H, d, *J* = 7.9 Hz), 7.75 (2 H, d, *J* = 8.2 Hz), 7.89 (2 H, d, *J* = 8.2 Hz), 10.37 (1 H, s); **FAB-MS** (pos.): 617.8 [M-*i*Pr]$^+$, 661.8 [M+H]$^+$, 683.8 [M+Na]$^+$. The ^{1}H-NMR of β-**66** is printed in Chapter 4.2.5.

α-**61** (acetal protected): **R$_f$** (hexane : EtOAc = 4 : 1) = 0.4; **^{1}H-NMR** (200 MHz, $CDCl_3$) δ 0.98 (9 H, d, *J* = 3.1 Hz), 1.02 (9 H, d, *J* = 3.1 Hz), 1.08-1.25 (3 H, m), 1.31 (1 H, d,

J = 13.4 Hz), 2.00-2.22 (1 H, m), 2.26 (3 H, s), 2.28 (3 H, s), 3.60 (3 H, s), 3.74-3.92 (3 H, m), 4.02-4.28 (4 H, m), 4.84 (1 H, s), 4.98 (1 H, s), 5.16 (1 H, s), 5.73 (1 H, s), 6.81 (1 H, s), 6.83 (2 H, d, J = 7.8 Hz), 6.95 (2 H, d, J = 7.9 Hz), 7.01 (1 H, d, J = 8.2 Hz), 7.45 (1 H, d, J = 7.9 Hz), 7.65 (2 H, d, J = 8.3 Hz), 7.66 (2 H, d, J = 8.2 Hz).

β-**61** (acetal protected): **R$_f$** (hexane : EtOAc = 4 : 1) = 0.4; The ^{1}H-NMR was of very low intensity and resolution. However it showed clearly the success of reprotecting the aldehyde. A ^{13}C-NMR spectrum was only measured for a mixture of α-**61** + β-**61** and at least one of the corresponding free aldehydes. It could not be fully interpreted due to its complexity. **FAB-MS** (pos.): 675.2 [M-iPr]$^+$, 719.3 [M+H]$^+$.

## 6.10 Synthesis of a hydroxyphenyl-oxazoline-uridine nucleoside

2-(4-Bromo-2-hydroxyphenyl-)oxazoline 49
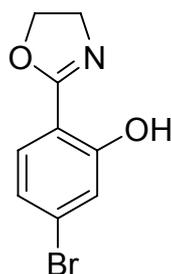
7.0 mg (0.05 mmol) dry ZnCl$_2$ was molten in a Schlenk flask in high vacuum by heating with a hot air blower and allowed to cool down under an atmosphere of N$_2$ protecting gas. 5 mL dry chlorobenzene, 198 mg (1.00 mmol) 4-bromo-2-hydroxy-benzonitrile **48** and 90 μL (1.50 mmol) dry ethanolamine were added and the mixture was refluxed under protecting gas for 4 h. Afterwards, the mixture was taken up in 20 mL MeOH : CH$_2$Cl$_2$ = 1:1, transferred to a round bottom flask and 10 g silica gel were added. All solvents were removed at the rotary evaporator and the solids were transferred on a silica gel column. The product was eluted with hexane : EtOAc = 10 : 1 to yield 149 mg (0.61 mmol, 62 %) of a slightly pink powder. The use of Cd(OAc)$_2$ as catalyst resulted in yields up to 89 % but the ZnCl$_2$ method was preferred due to the high toxicity of cadmium.

R_f (hexane : EtOAc = 4 : 1) strongly dependent on concentration of the compound on the silica plate; **^{1}H-NMR** (200 MHz, CDCl$_3$) δ 4.09 (2 H, t, J = 9.2 Hz), 4.44 (2 H, t, J = 9.2 Hz), 7.00 (1 H, dd, J = 8.4, 1.5 Hz), 7.20 (1 H, d, J = 1.4 Hz), 7.49 (1 H, d, J = 8.4 Hz), 12.34 (1 H, s); **^{13}C-NMR** (75 MHz, CDCl$_3$): 53.50, 67.04, 109.90, 120.15, 122.11, 127.25, 129.10, 160.54, 165.92; **IR** (KBr): ν = 3446, 2960, 2860, 1642, 1570, 1484, 1399, 1365, 1301, 1273, 1227, 1139, 1067, 935, 911, 872, 819, 795, 743, 669, 571, 543 cm^{-1}; **APCI-HRMS** (pos.): calc. for C$_9$H$_9$NO$_2$Br [M+H]$^+$: 241.9811; found: 241.9801.

2-(4-Ethinyl-2-hydroxyphenyl-)oxazoline 69
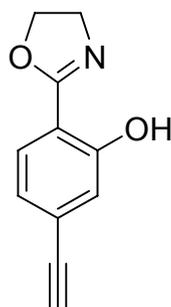
A mixture of 20 mL dry THF and 10 mL *N,N*-di-*iso*-propylethylamine was degassed three times by evacuation and application of nitrogen gas. Then, 1.50 g (6.20 mmol) 2-(4-bromo-2-hydroxyphenyl)-oxazoline 49, 60 mg (0.32 mmol, 5 mol%) CuI and 131 mg (0.19 mmol, 3 mol%) Pd(PPh$_3$)$_2$Cl$_2$ were added. The color of the mixture changed from pink over yellow to orange. Subsequently, 1.3 mL (0.92 g, 9.40 mmol) trimethylsilylacetylene were added slowly and the mixture was heated to 80 °C for 14 h. Then, all solvents were removed *in vacuo* and the residue was taken up in 50 mL MeOH and 1.00 g (7.20 mmol) K$_2$CO$_3$ were added to remove the trimethylsilyl protecting group. After stirring for 1.5 h at r.t., the suspension was filtered and the filtrate was neutralized with an acidic ion exchange resin (Dowex 50 W). The mixture was filtered again and all solvents were removed from the filtrate *in vacuo*. The remaining yellow oil was purified by flash column chromatography (silica gel, pentane : EtOAc = 10 : 1 → 1 : 1) to yield 0.87 g (47.0 mmol, 75 %) of 2-(4-ethynyl-2-hydroxyphenyl)-oxazoline **69** as a yellow resin.

R_f (hexane : EtOAc = 9 : 1) = 0.4; **^{1}H-NMR** (600 MHz, CDCl$_3$) δ 3.14 (1 H, s), 4.11 (2 H, t, J = 9.5 Hz), 4.43 (2 H, t, J = 9.5 Hz), 6.99 (1 H, dd, J = 8.0, 1.5 Hz), 7.13 (1 H, d, J = 1.5 Hz), 7.59 (1 H, d, J = 8.0 Hz).; **^{13}C-NMR** (150 MHz, CDCl$_3$): δ 53.68, 67.11, 79.09, 83.28, 111.42, 120.47, 122.56, 126.93, 128.14, 159.62, 165.99; **IR** (Nujol): ν = 3310, 2963, 2932, 2854, 2359, 1640, 1560, 1465, 1392, 876, 821 cm^{-1}; **APCI-HRMS** (pos.): calc. for C$_{11}$H$_{10}$NO$_2$ [M+H]$^+$: 188.0706; found 188.0702.


2-(4-Ethinyl-2-pivalyloxyphenyl-)oxazoline 70
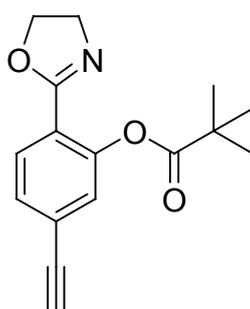
0.77 g (4.1 mmol) 2-(4-ethynyl-2-hydroxyphenyl)-oxazoline **69** were dissolved under a protecting gas atmosphere in 20 mL dry CH$_2$Cl$_2$ and 20 mg DMAP and 1.76 mL (1.33 g, 10.3 mmol) N,N-di-iso-propylethylamine were added. After slow addition of 0.86 mL (0.84 g, 7.0 mmol) pivalic acid chloride at 5 °C, the reaction mixture was stirred for 14 h at r.t. Then, H$_2$O was added and the organic layer was washed with 5 % Na$_2$CO$_3$ $_{(aq)}$, H$_2$O and sat. NaCl$_{(aq)}$ and dried over NaSO$_4$. The solvent was removed *in vacuo* and the raw material was purified by column chromatography (silica gel, pentane : EtOAc = 7 : 1) to yield 1.0 g (3.8 mmol, 91 %) of compound **70** as a yellow oil.

R_F (CHCl$_3$: MeOH = 9 : 1) = 0.8; **^{1}H-NMR** (300 MHz, CDCl$_3$): δ 1.28 (9 H, s), 3.08 (1 H, s), 3.99 (2 H, t, J = 9.3 Hz), 4.33 (2 H, t, J = 9.3 Hz), 6.77 (1 H, d, J = 8.0, 1.5 Hz), 7.09 (1 H, d, J = 1.5 Hz), 7.80 (1 H, d, J = 8.0 Hz); **^{13}C-NMR** (75 MHz, CDCl$_3$): δ 27.20, 54.90, 67.14, 79.91, 126.99, 129.31, 130.78 (C$_{quart.}$ not determined).

Hydroxyphenyl-uridine nucleoside 67
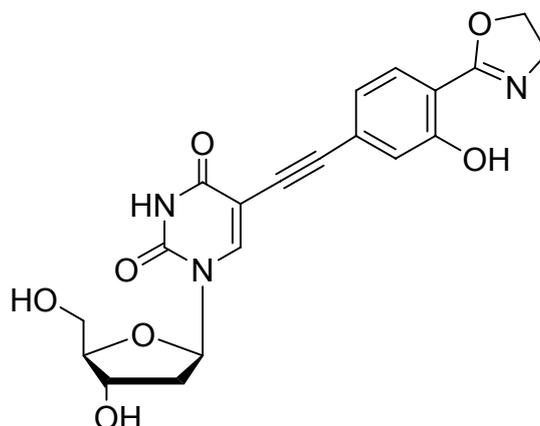
A mixture of 0.5 mL dry DMF and 1 mL *N,N*-di-*iso*-propylethylamine was degassed three times by evacuation and application of nitrogen gas. Then, 71 mg (0.20 mmol) 2'-deoxy-5-iodouridine **71**, 68 mg (0.25 mmol) 2-(4-ethynyl-2-pivaloyloxyphenyl)-oxazoline **70**, 3 mg (0.016 mmol) CuI and 3 mg (0.004 mmol) Pd(dppf)Cl$_2$ were added. The reaction mixture was heated to 80 °C for 14 h. Subsequently, the solvents were removed *in vacuo* and the residue was taken up in 1 mL of methanol. 3 g silica gel were added, the solvents removed again and the remaining material was subjected to column chromatography (CHCl$_3$: MeOH = 9 : 1). During the chromatography and the time in methanolic solution, the pivaloyl protecting group underwent transesterification onto methanol and the non-protected nucleoside **67** precipitatet slowly from the solution in form of a brown, microcrystalline material (19 mg, 0.046 mmol, 23 %). Attempts to generate crystals for X-ray measurements were unsuccessful.

R$_f$ (CHCl$_3$: MeOH = 9 : 1) = 0.3; **^{1}H-NMR** (600 MHz, D$_6$-DMSO): δ 2.09-2.20 (2 H, m), 3.57 (1 H, td, *J* = 12.3, 3.9 Hz), 3.65 (1 H, td , *J* = 12.1, 3.9 Hz), 3.79 (1 H, dd, *J* = 6.7, 3.3 Hz), 4.06 (2 H, t, *J* = 9.4 Hz), 4.24 (1 H, q, *J* = 4.1 Hz), 4.46 (2 H, t, *J* = 9.4 Hz), 5.21 (1 H, t, *J* = 4.7 Hz), 5.26 (1 H, d, *J* = 4.3 Hz), 6.09 (1 H, t, *J* = 6.5 Hz), 6.99 (1 H, dd, *J* = 8.0, 1.6 Hz), 7.02 (1 H, dd, *J* = 1.5, 0.4 Hz), 7.61 (1 H, d, *J* = 8.0 Hz), 8.44 (1 H, s), 11.72 (1 H, s), 12.38 (1 H, s); **^{13}C-NMR** (150 MHz, D$_6$-DMSO): δ 40.44, 53.13, 60.91, 67.37, 69.98, 85.05, 85.13, 87.77, 91.29, 97.82, 110.47, 118.56, 121.92, 127.37, 128.27, 144.77, 149.55, 158.99, 161.45, 165.13; **IR** (diamond-ATR): ν = 3490, 3431, 3171, 3070, 2935, 2843, 1698, 1674, 1628, 1609, 1562, 1464, 1430,

1394, 1356, 1290, 1274, 1231, 1186, 1146, 1102, 1053, 1003, 928, 875, 808, 786, 756, 676 cm^{-1}; **ESI-HRMS** (neg.): calc. for $C_{20}H_{18}N_3O_7$ [M–H]$^-$: 412.1151; found: 412.1139.

6.11 Synthesis of a benzotriazole-uridine nucleoside

2,6-Dimethoxy-*N*-(2-nitro-4-trimethylsilylethynyl-phenyl)-benzamide 75
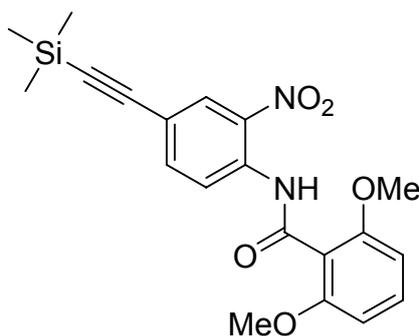

A solution of 2-nitro-4-trimethylsilylethinyl-aniline **74** (0.50 g, 2.1 mmol) in 10 mL dry CH_2Cl_2 was prepared and first 0.48 mL (5.0 mmol) di-*iso*-propylamine and subsequently a solution of 2,6-dimethoxybenzoylchloride (1.02 g, 5.0 mmol) in 12 mL CH_2Cl_2 was slowly added. The clear mixture was stirred for 12 h after which TLC control confirmed the complete transformation of the starting material. The reaction mixture was mixed with 20 mL H_2O and the aqueous phase was extracted thrice with chloroform. The combined organic extracts were washed once with sat. $NaCl_{(aq)}$ and dried over $NaSO_4$. After removal of the solvents *in vacuo* the raw material was purified by column chromatography (silica gel, hexane : EtOAc = 4 : 1) to yield 0.8 g (2.0 mmol, 95%) of the product as yellow crystalline material.

R$_f$ (hexane : EtOAc = 4 : 1) = 0.5; **^{1}H-NMR** (400 MHz, CDCl3): δ 0.27 (9 H, s), 3.86 (6 H, s), 6.63 (2 H, d, *J* = 8.5 Hz), 7.36 (1 H, t, *J* = 8.4 Hz), 7.72 (1 H, dd, *J* = 8.8, 2.0 Hz), 8.31 (1 H, d, *J* = 1.8 Hz), 9.0 (1 H, d, *J* = 8.8 Hz), 10.68 (1 H, s, NH); **^{13}C NMR** (150 MHz, CDCl3): δ 0.03 (3C), 56.25 (2C), 96.44, 102.41, 104.40 (2C), 115.04, 118.49, 122.50, 129.22, 132.13, 135.20, 136.07, 138.92, 158.07 (2C), 164.63; **IR** (diamond-ATR): ν = 3310, 3134, 3000, 2966, 2838, 2165, 1687, 1615, 1592, 1564, 1536, 1500, 1472, 1460, 1432, 1343, 1297, 1262, 1250, 1238, 1216, 1144, 1117, 1106, 1055, 937, 859, 845, 792, 760, 747, 702, 670, 635 cm^{-1};

EI-MS (pos.): 398 [M]$^+$, 165 [DMBz]$^+$; **EI-HRMS** (pos.): calc. for $C_{20}H_{22}N_2O_5Si$ [M]$^+$: 398.1297; found: 398.1280.

### *N*-1-(2,6-Dimethoxybenzoyl)-5-trimethylsilylethynyl-benzotriazole 76
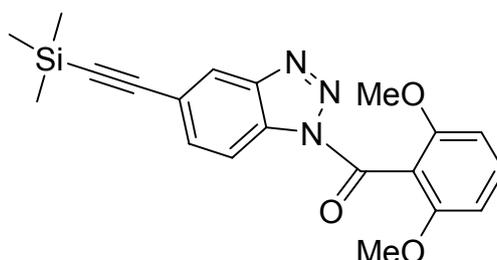
Under a N_2 protecting gas atmosphere, 0.80 g (2.00 mmol) of compound **75** was dissolved in 60 mL glacial acetic acid. To the heavily stirred yellow solution, an excess of iron powder (0.56 g, 10.0 mmol) was added. The mixture was warmed to 70 °C for 5 h after which another 0.28 g (5.00 mmol) of iron powder was added and the stirring was continued for 12 h at 70 °C. When thin layer chromatography (hexane : EtOAc = 4 : 1) showed complete conversion, excess iron was removed with a magnet from the reaction mixture and the reduction product was used for the next reaction without purification or removal of solvent. For achieving the ring closure to the benzotriazole, the flask was cooled to 5 °C in an ice bath and 15 mL H_2O and 9 mL 1M HCl were added. Then a solution of 0.18 g (2.6 mmol) $NaNO_3$ in 2 mL H_2O was slowly dripped into the well stirred mixture without allowing the temperature to rise above 5 °C. Five minutes after the addition, the ice bath was removed and the mixture was stirred for another 20 min at r.t. After removal of all solvents *in vacuo* the remaining brown oil was extracted thrice with $CHCl_3$ and the combined organic extracts were freed from acid by treatment with sat. $NaHCO_3$ (aq). Removal of the solvent was followed by column chromatography (silica gel, $CHCl_3$) to yield **76** as a colorless solid (363 mg, 0.96 mmol, 50 % over two steps).

R$_f$ (hexane : EtOAc = 4 : 1) = 0.4; **^{1}H-NMR** (400 MHz, CDCl₃): δ 0.29 (9 H, s), 3.76 (6 H, s), 6.67 (2 H, d, *J* = 8.5 Hz), 7.46 (1 H, t, *J* = 8.5 Hz), 7.76 (1 H, dd, *J* = 8.5, 1.4 Hz), 8.20 (1 H, dd, *J* = 1.5, 0.8 Hz), 8.3 (1 H, d, *J* =8.0 Hz). **^{13}C-NMR** (150 MHz, CDCl₃): δ 0.03 (3C), 56.16 (2C), 95.53, 103.86, 104.15 (2C), 112.45, 112.71, 114.60,

133.95, 121.51, 123.67, 131.00, 132.98, 158.23, 165.33; **FAB-MS** (pos.): 402 [M+Na]$^+$, 379 [M]$^+$, 306 [M-TMS]$^+$, 165 [DMBz]$^+$, 73 [TMS]$^+$.

### *N*-1-(2,6-Dimethoxybenzoyl)-5-ethynyl-benzotriazole 77
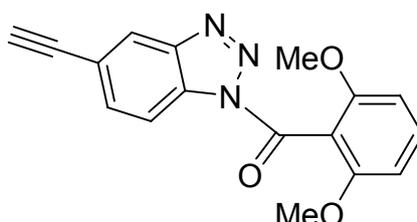
The TMS-protected alkyne **76** (0.26 g, 0.68 mmol) was dissolved in 15 mL THF, cooled to − 78 °C and 0.82 mL of a 1M Bu$_4$NF solution in THF was added. After stirring for 30 min, H$_2$O was added and the reaction mixture was extracted thrice with CHCl$_3$. The combined organic extracts were washed once with sat. NaCl$_{(aq)}$ and dried over Na$_2$SO$_4$. Purification by column chromatography (silica gel, CHCl$_3$) yielded **77** as colorless solid (188 mg, 0.58 mmol, 85 %).

R$_f$ (CHCl$_3$) = 0.6; **^{1}H-NMR** (600 MHz, CDCl$_3$): δ 3.17 (1 H, s), 3.76 (6 H, s), 6.67 (2 H, d, *J* = 8.5 Hz), 7.46 (1 H, t, *J* = 8.5 Hz), 7.79 (1 H, dd, *J* =8.5, 1.4 Hz), 8.26 (1 H, m), 8.40 (1 H, d, *J* = 8.5 Hz); **^{13}C-NMR** (150 MHz, CDCl$_3$): δ 56.01 (2C), 78.10, 82.48, 104.00 (2C), 112.26, 114.65, 117.09, 122.43 (2C), 129.24, 131.99, 135.36, 138.84, 157.84, 164.43; **IR** (diamond-ATR): ν = 3281, 3108, 3076, 3016, 2986, 2942, 2839, 1718, 1590, 1475, 1430, 1369, 1320, 1256, 1225, 1104, 1050, 948, 906, 883, 836, 783, 750, 719, 677, 640, 627, 606 cm^{-1}; **EI-MS** (pos.): 326 [M]$^+$, 165 (DMBz); **EI-HRMS** (pos.) calc. for C$_{17}$H$_{14}$N$_2$O$_5$: 326.0902; found: 326.0889.

Benzotriazole-uridine nucleoside 78
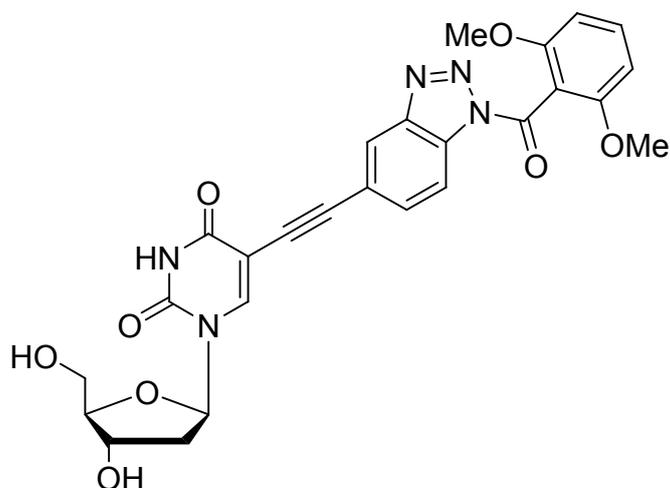
2'-Deoxy-5-iodo-uridine **71** (290 mg, 0.82 mmol), Pd(PPh3)4 (139 mg, 0.12 mmol) und CuI (46 mg, 0.24 mmol) were dissolved in 4 mL DMF and degassed three times by evacuation and application of nitrogen gas. Then, a degassed solution of 0.32 g (0.98 mmol) **77** in 4 mL DMF was added over 45 min. Subsequently, the mixture was ultrasonicated for 45 min and stirred at r.t. for 12 h. After removal of the solvent *in vacuo* and chromatographic purification (silica gel, EtOAc), **78** was obtained as a yellowish solid (0.36 g, 0.68 mmol, 83 %)

Rf (EtOAc) = 0.6; **^{1}H-NMR** (600 MHz, D$_6$-DMSO): δ 2.20 (2 H, m), 3.63 (1 H, m), 3.68 (1 H, m), 3.70 (6 H, s), 3.84 (1 H, m), 4.28 (1 H, m), 5.21 (1 H, t, *J* = 4.8 Hz), 5.27 (1 H, d, *J* = 4.3 Hz), 6.15 (1 H, t, *J* = 6.5 Hz), 6.87 (2 H, d, *J* = 8.5 Hz), 7.57 (1 H, t, *J* = 8.5 Hz), 7.89 (1 H, dd, *J* = 8.5, 1.2 Hz), 8.32 (1 H, d, *J* = 7.7 Hz), 8.38 (1 H, s), 8.50 (1 H, s); **^{13}C-NMR** (150 MHz, D$_6$-DMSO): δ 40.17, 56.06 (2C), 60.68, 69.76, 83.64, 84.86, 87.51, 90.49, 97.57, 104.34 (2C), 111.42, 114.14, 120.96, 122.58, 129.78, 133.13, 133.92, 144.50, 145.54, 149.31, 157.31 (2C), 161.26, 164.57; **IR** (diamond-ATR): ν = 3394, 3056, 2937, 2840, 1694, 1596, 1477, 1459, 1434, 1368, 1324, 1292, 1258, 1224, 1109, 1054, 917, 874, 823, 782, 749, 722, 693, 639 cm^{-1}; **FAB-MS** (pos.): 686 [M+NBA]$^-$, 532 [M-H]$^-$; **APCI-HRMS** (pos.): calc. for C$_{26}$H$_{24}$O$_8$N$_5$ [M+H]$^+$: 534.1619; found: 534.1602.

DMT-protected benzotriazole-uridine nucleoside 79
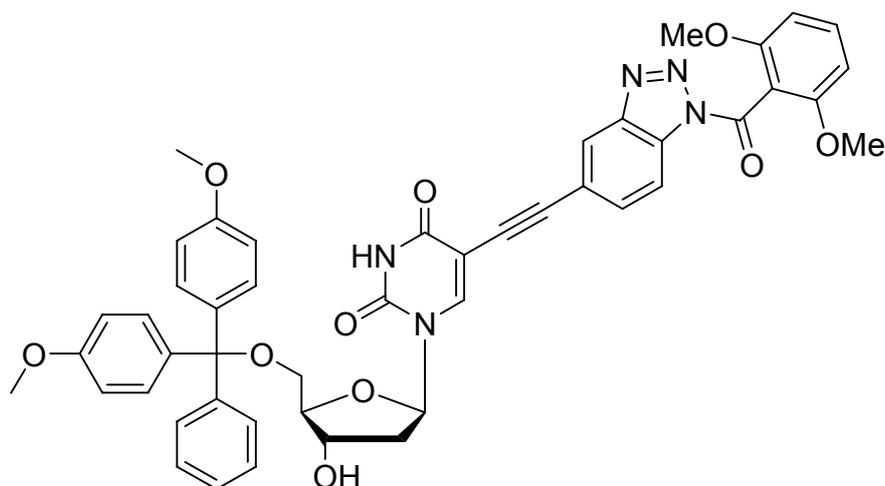
Compound **78** (0.33 g, 0.62 mmol) wass stirred for 12 h in 7 mL pyridine over molsieves (4 Å). Then, DMT-Cl (0.23 g, 0.68 mmol) was added and stirring was continued for 48 h. Removal of the solvent *in vacuo* and chromatographic purification (CHCl$_3$: MeOH = 9 : 1 + 0.1 % pyridine) yielded nucleoside **79** as a yellowish resin (0.43 g, 0.52 mmol, 84 %).

R$_f$ (CHCl$_3$: MeOH = 10 : 1 + 0.1 % py) = 0.4; **^{1}H-NMR** (400 MHz, CDCl$_3$): δ 2.38 (1 H, m), 2.62 (1 H, m), 3.31 (1 H, q, *J* = 10.8, 3.2 Hz), 3.50 (1 H, m), 3.65 (3 H, s), 3.66 (3 H, s), 3.74 (6 H, s), 4.20 (1 H, s), 4.62 (1 H, m), 6.43 (1 H, t, *J* = 6.8 Hz), 6.65 (2 H, d, *J* = 8.5 Hz), 6.77 (2 H, d, *J* = 2.1 Hz), 6.79 (2 H, d, *J* = 2.1 Hz), 7.12 (1 H, t, *J* = 7.5 Hz), 7.19 (1 H, m), 7.25 (2 H, t, *J* = 7.7 Hz), 7.36 (2 H, d, *J* = 1.7 Hz), 7.39 (2 H, d, *J* = 1.7 Hz), 7.46 (3 H, m), 7.70 (1 H, m), 8.13 (1 H, d, *J* = 8.5 Hz), 8.37 (1 H, s), 9.68 (1 H, s, NH); **^{13}C-NMR** (150 MHz, CDCl$_3$): δ 41.78, 55.1 (2C), 55.97 (2C), 63.47, 72.31, 80.86, 85.99, 86.88, 87.08, 92.57, 100.14, 103.96 (2C), 112.31, 113.33 (2C), 114.03, 120.64, 123.04, 127.02, 128.04, 129.87, 130.59, 132.77, 133.53, 135.47, 142.78, 144.42, 145.80, 149.30, 158.00, 158.56, 161.40, 165.125; **IR** (diamond-ATR): ν = 3453, 3190, 3066, 2936, 2837, 1697, 1596, 1508, 1477, 1456, 1371, 1292, 1248, 1175, 1110, 1031, 916, 824, 789, 754, 702, 639 cm^{-1}; **FAB-MS** (pos.): 859 [M+Na]$^+$, 837 [M+H]$^+$, 303 [DMT]$^+$, 161 [DMBz]$^+$; **FAB-HRMS** (pos.): calc. for C$_{46}$H$_{43}$N$_5$O$_{10}$ [M+H]$^+$: 836.2951; found: 836.2932.

DMT-protected benzotriazole-uridine phosphoramidite 72
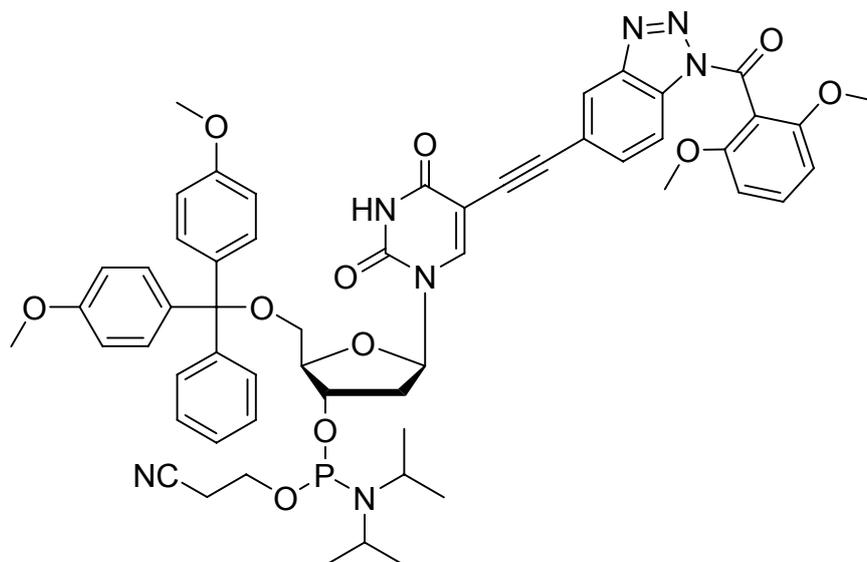
DMT protected nucleoside **79** (242 mg, 0.29 mmol) was coevaporated twice with 5 mL dry THF and finally dissolved in 5 mL dry, degassed THF. Then, 198 μL (1.16 mmol) NEt(*iso*-Pr)$_2$ and 109 μL (116 mg, 0.49 mmol) (*i*Pr$_2$N)(OCH$_2$CH$_2$CN)PCl were added and the reaction mixture was stirred for 3 h until TLC control showed a complete transformation of the starting material. The solvents were removed *in vacuo* and the residue was purified by column chromatography under an atmosphere of protecting gas (desactivated silica, CHCl$_3$: MeOH = 9 : 1, + 0.1 % pyridine, all solvents degassed) to yield the phosphoramidite **72** as a colorless resin (197 mg, 0.19 mmol, 66 %) which was used immediately in the automated DNA synthesis.

R$_f$ (CHCl$_3$: MeOH = 10 : 1 + 0.1 % py) = 0.8; **^{31}P-NMR** (200 MHz, CDCl$_3$): δ 149.66, 150.10; **IR** (diamond-ATR): ν = 3405, 2941, 2839, 2735, 2513, 2350, 2253, 1707, 1597, 1508, 1477, 1460, 1452, 1444, 1366, 1293, 1249, 1218, 1176, 1111, 1054, 1031, 991, 916, 827, 789, 755, 703, 639 cm^{-1}; **APCI-HRMS** (pos.): calc. for C$_{56}$H$_{59}$O$_{11}$N$_7$P [M+H]$^+$: 1036.4005; found 1036.4023.

6.12 Synthesis of a glutathione-bisazide

Trt-Boc-Protected Glutathion-bis-azide 84
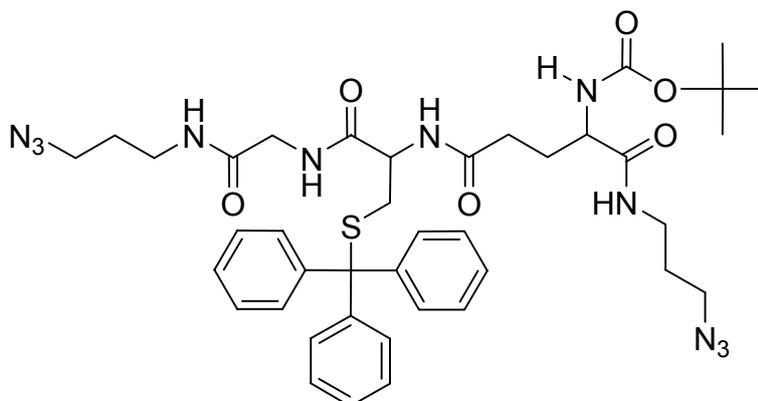
200 mg (0.31 mmol) of the protected glutathione **82**[262] were dissolved in 5 mL dry THF and 100 mg (0.62 mmol) carbonyldiimidazole were added. After 30 min stirring at room temperature, 62 mg (0.62 mmol) 3-aminopropylazide **83**[263] was added and the mixture was stirred for 14 h. Then, the solvent was removed *in vacuo* and the yellow raw material was subjected to column chromatography (silica gel, CHCl$_3$: MeOH = 10 : 1) which yielded 168 mg (0.21 mmol, 68 %) of the diazide **84** as a yellowish powder.

R$_f$ (CHCl$_3$: MeOH = 9 : 1) = 0.7; **^{1}H-NMR** (400 MHz, D$_6$-DMSO): δ 1.37 (9 H, s), 1.56–1.74 (5 H, m), 1.74–1.86 (1 H, m), 2.08–2.22 (2 H, m), 2.35-2.42 (2 H, m), 3.04–3.15 (4 H, m), 3.27-3.34 (4 H, m), 3.53 (1 H, dd, *J* = 16.6, 5.4 Hz), 3.67 (1 H, dd, *J* = 16.6, 6.2 Hz), 3.82 (1 H, dd, *J* = 14.4, 8.5 Hz), 4.19 (1 H, dd, *J* = 13.9, 6.7 Hz), 6.88 (1 H, d, *J* = 7.9 Hz), 7.22–7.37 (15 H, m), 7.64 (2 H, t, *J* = 5.9 Hz), 7.87 (1 H, t, *J* = 5.6 Hz), 8.17–8.25 (2 H, m); **^{13}C-NMR** (150 MHz, CDCL$_3$): δ 28.45, 28.72, 28.76, 32.02, 32.05, 32,81, 36.94, 37.11, 43.63, 49.14, 49.21, 53.24, 53.74, 67.59, 127.21, 128.32, 129.64, 144.36, 156.14, 169.14, 170.77, 171.93, 173.04; **IR** (diamond-ATR): ν = 3291, 3060, 2934, 2094, 1646, 1520, 1444, 1366, 1247, 1163, 1083, 1031, 855, 743, 699, 675, 616 cm^{-1}; **EI-HRMS** (pos.): calc. for C$_{40}$H$_{51}$N$_{11}$O$_6$SNa [M+Na]$^+$: 836.3642; found: 836.3647.

Glutathion-bis-azide 80
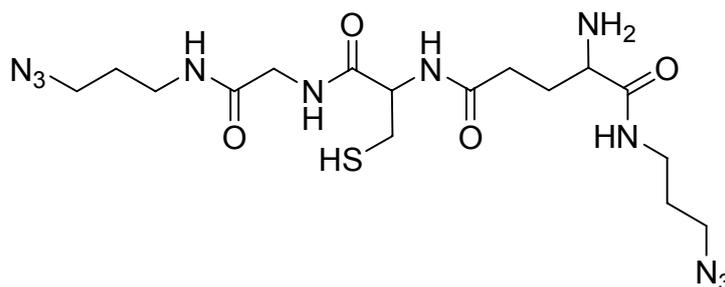
100 mg (0.12 mmol) of the protected glutathione-bis-azide **84** were dissolved in 10 mL CH_2Cl_2 and 300 μL H_2O, 300 μL triethylsilane and 10 mL trifluoroacetic acid were added. After stirring for 1 h at r.t., all solvents were removed *in vacuo* and the residue was taken up into 5 mL H_2O. The suspension was filtered and the water was removed from the filtrate by lyophilisation to yield 42 mg (0.09 mmol, 80 %) of the free glutathione-bis-azide **80** as a yellowish powder, which could be further purified by reverse phase HPLC (0.1 % TFA in H_2O : MeCN).

¹H-NMR (600 MHz, D_2O): δ 1.79-1.90 (4 H, m), 2.19-2.25 (2 H, m), 2.54 (2 H, t, J = 7.0 Hz), 3.06 (2 H, dd, J = 14.2, 9.0 Hz), 3.30 (1 H, dd, J = 14.1, 4.8 Hz), 3.32-3.46 (8 H, m), 3.91-3.99 (2 H, m), 4.03 (1 H, t, J = 6.6 Hz), 4.75 (1 H, m, SH ?), 8.13 (2 H, t, J = 6.7 Hz, NH ?), 8.67 (1 H, t, J = 7.6 Hz, NH ?), 8.83 (2 H, d, J = 5.9 Hz, NH ?). Of the 7 heteroatom-bound hydrogens, only 6 were observed; **¹³C-NMR** (100 MHz, CD_3OD): δ 26.53, 28.10, 29.62, 29.68, 31.74, 37.78, 38.10, 43.57, 50.01, 50.04, 53.95 ($C_{methine}$), 57.59 ($C_{methine}$), 169.84 (C_{quart}), 171.41 (C_{quart}), 173.03 (C_{quart}), 174.40 (C_{quart}); **MALDI-MS** (pos.): 472.3 $[M+H]^+$, 494.3 $[M+Na]^+$; **ESI-HRMS** (pos.): calc. for $C_{16}H_{30}N_{11}O_4S$ $[M+H]^+$: 472.2197; found: 472.2195.

7 Appendix

7.1 Further selected ESI spectra
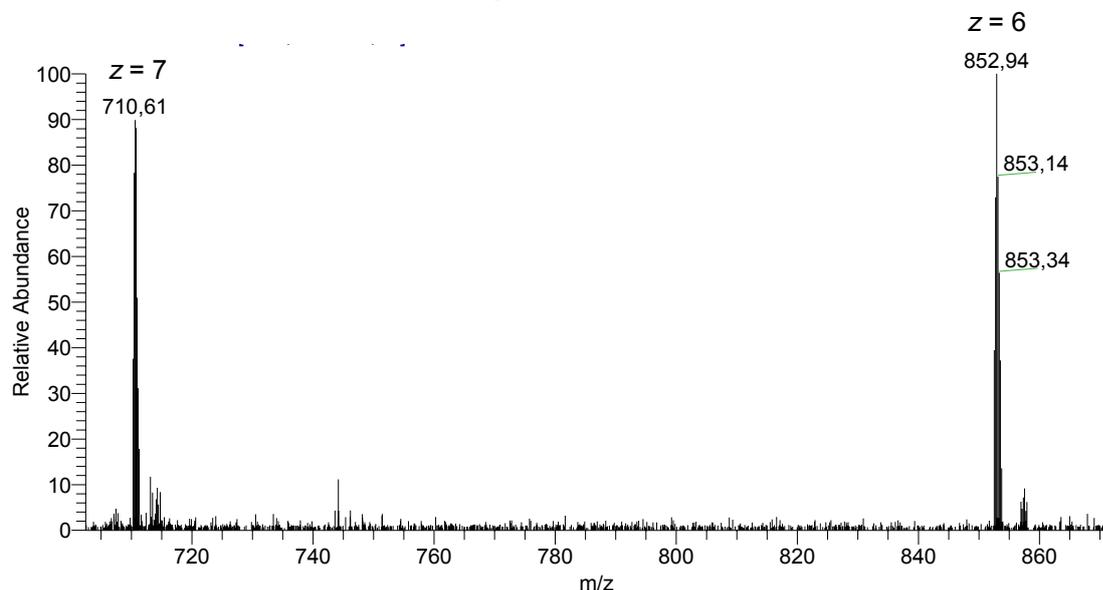
Figure 101: ESI-ICR spectrum of [**D17-L-a^e/b^e**+en+Cu]. Lowest weight isotopomer mass found for [**D17-L-a^e/b^e**+en+Cu^{2+}–H$_2$O–8H$^+$]$^{6-}$: 710.2810; calculated for [C$_{142}$H$_{170}$N$_{48}$O$_{80}$P$_{12}$Cu$_1$]$^{6-}$: 710.2804.
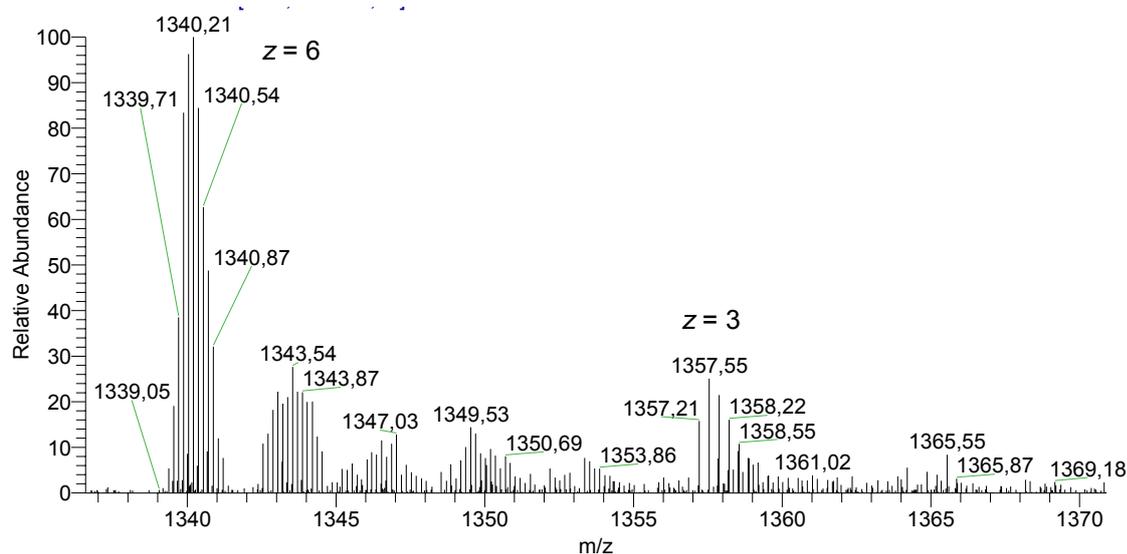

Figure 102: Example for the copper complexation of a sample preparation of duplex **D14-L-a/b** containing an excess of oligonucleotide **D14-L-a**. Besides the expected species [**D14-L-a/b**+2en+2Cu] (*m/z* = 1339.38) and its salt adducts (1343-1355) also the signal of the unspecific hairpin [**D14-L-a**+en+Cu] (*m/z* = 1357.21) containing one intramolecular copper-salen complex was observed.
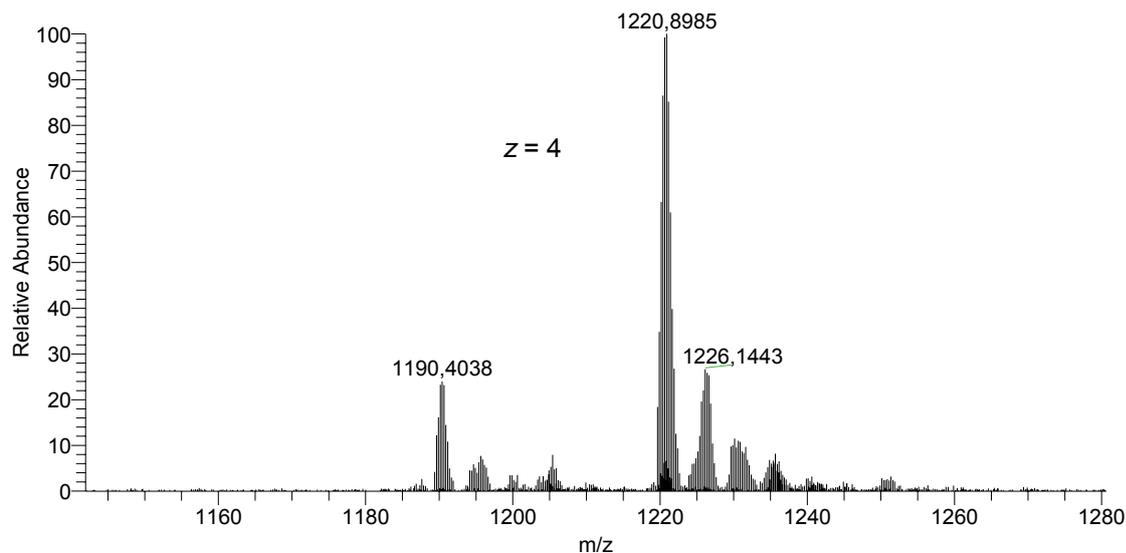
Figure 103: ESI-ICR spectrum of single strand **D18-L-b** containing an excess of en and Cu^{2+}. Two different species according to Figure 79 were identified. Found for [**D18-L-b**+3en+3Cu-5H_2O-10H^+]$^{4-}$: 1189.4018, calculated for [$C_{160}H_{190}N_{44}O_{88}P_{14}Cu_3$]$^{4-}$: 1189.3984. Found for [**D18-L-b**+4en+4Cu-5H_2O-12H^+]$^{4-}$: 1219.6481, calculated for [$C_{162}H_{196}N_{46}O_{88}P_{14}Cu_4$]$^{4-}$: 1219.6441.
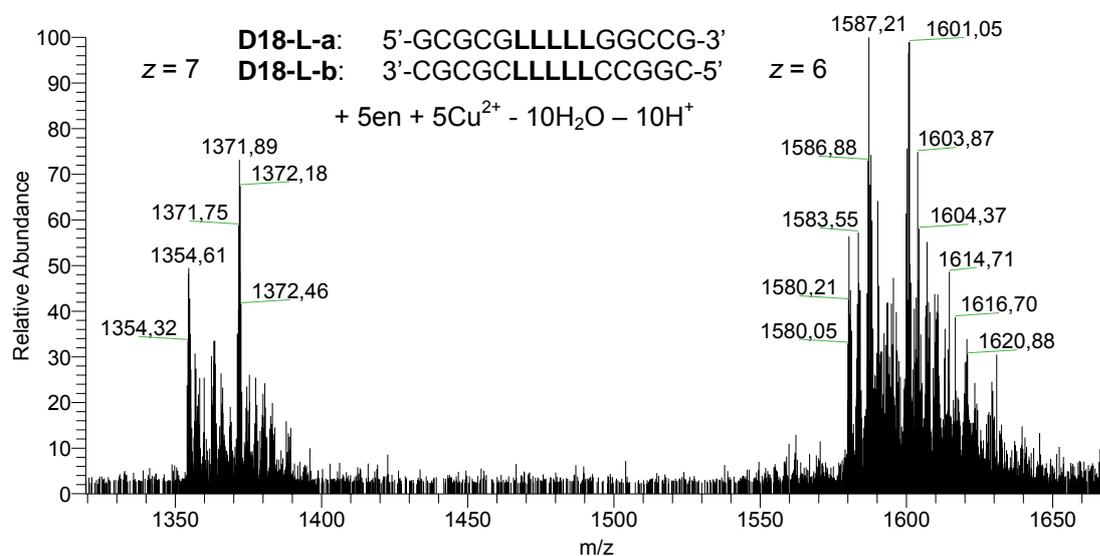
Figure 104: ESI-ICR spectrum of [**D18-L-a/b**+5en+5Cu] showing the measured mass of the highest peaks. Lowest weight isotopomer mass found for [**D18-L-a/b**+5en+5Cu^{2+}–10H_2O–17H^+]$^{7-}$: 1353.6085; calculated for [$C_{320}H_{375}N_{90}O_{176}P_{28}Cu_5$]$^{7-}$: 1353.6036.
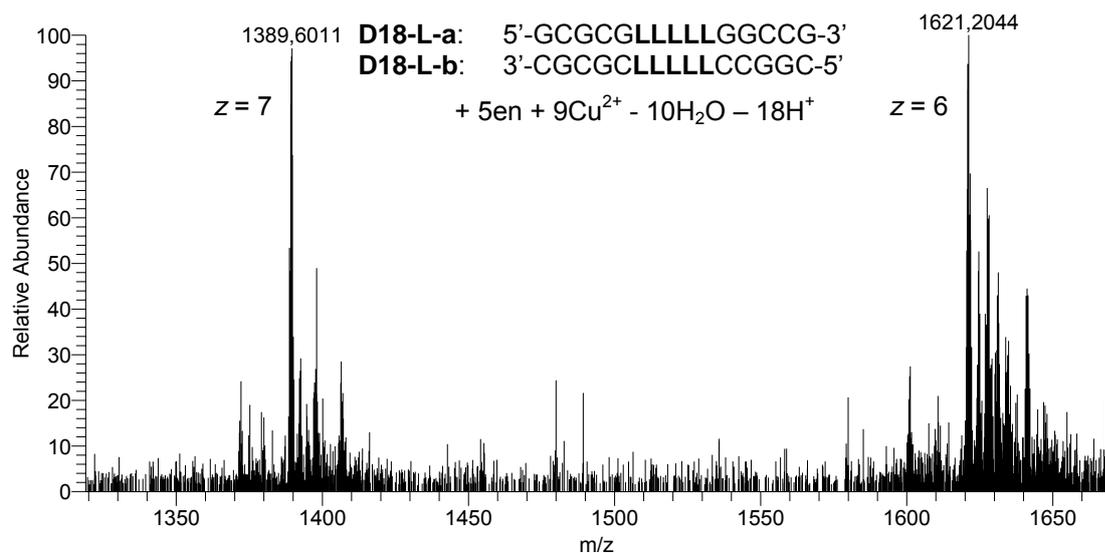
Figure 105: ESI-ICR spectrum of the duplex [**D18-L-a/b**+5en] containing excess Cu^{2+}. The peaks presumably represent [**D18-L-a/b**+5en+9Cu] although the deviation between found and calculated exact masses is higher than for the other examples. Lowest weight isotopomer mass found for [**D18-L-a/b**+5en+9Cu^{2+}–10H$_2$O–25H$^+$]$^{7-}$: 1388.1781; calculated for [C$_{320}$H$_{367}$N$_{90}$O$_{176}$P$_{28}$Cu$_9$]$^{7-}$: 1388.4116.
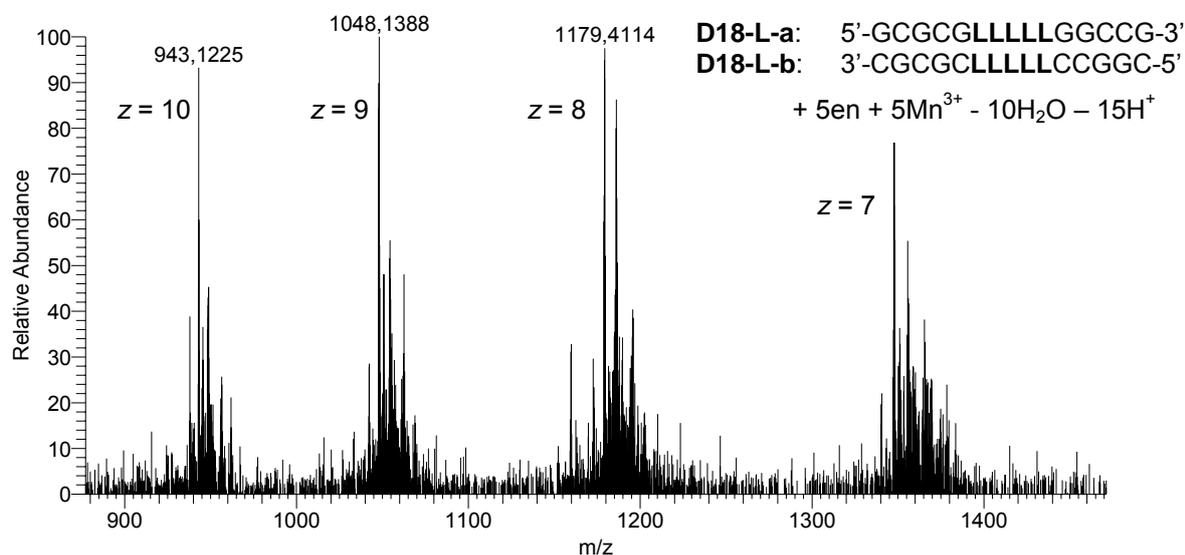

Figure 106: ESI-ICR spectrum of [**D18-L-a/b**+5en+5Mn] showing the measured mass of the highest peaks. Lowest weight isotopomer mass found for [**D18-L-a/b**+5en+5Mn^{3+}–10H$_2$O–24H$^+$]$^{9-}$: 1047.5814; calculated for [C$_{320}$H$_{368}$N$_{90}$O$_{176}$P$_{28}$Mn$_5$]$^{9-}$: 1047.5791.
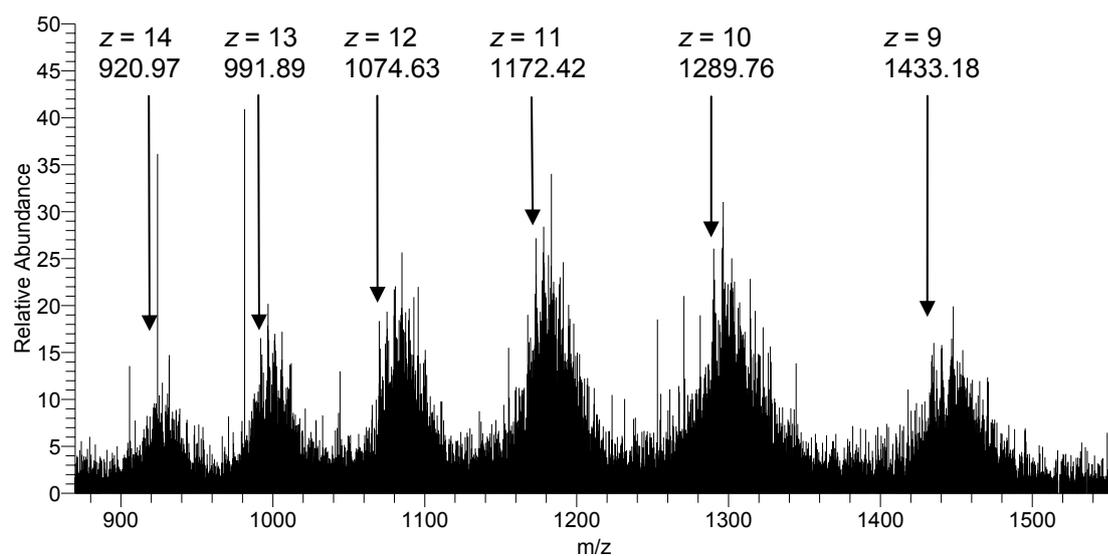
Figure 107: ESI-ICR spectrum of the duplex **D19-L-a/b**+10en+10Cu]. The arrows indicate the calculated values for the lowest weight isotopomer masses of [**D19-L-a/b**+10en+10Cu^{2+}-20H$_2$O-20H$^+$] at different charges z.

7.2   *Crystallographic data*

The Crystallographic data of compounds **25**[183] and **42**[184] can be obtained free of charge from The Cambridge Crystallographic Data Centre.

Crystal data and structure refinement for **65**:[266]

|	
Habitus, colour	needle, colourless
Crystal size	$0.28 \times 0.18 \times 0.10$ mm^3
Crystal system	Orthorhombic
Space group	P2(1)2(1)2 Z = 4
Unit cell dimensions	a = 10.4385(5) Å $\alpha = 90°$.
	b = 39.626(2) Å $\beta = 90°$.
	c = 5.9554(4) Å $\gamma = 90°$.
Volume	2463.4(2) Å^3
Cell determination	12281 peaks with Theta 2.0 to 23.1°.
Empirical formula	C28 H28 O6
Formula weight	460.50
Density (calculated)	1.242 Mg/m^3
Absorption coefficient	0.087 mm^{-1}
F(000)	976

Data collection:

Diffractometer type	IPDS2
Wavelength	0.71073 Å
Temperature	193(2) K
Theta range for data collection	2.02 to 25.00°.
Index ranges	-12<=h<=12, -47<=k<=46, -7<=l<=7
Data collection software	STOE WinXpose (X-Area)
Cell refinement software	STOE WinCell (X-Area)
Data reduction software	STOE WinIntegrate (X-Area)

Solution and refinement:

Reflections collected	24477
Independent reflections	4271 [R(int) = 0.1205]
Completeness to theta = 25.00°	97.6 %
Observed reflections	2621[I>2sigma(I)]
Reflections used for refinement	4271
Flack parameter (absolute struct.)	1.0(16)
Largest diff. peak and hole	0.136 and -0.156 e.Å^{-3}
Solution	Direct methods / difference fourier
Refinement	Full-matrix least-squares on F^2
Treatment of hydrogen atoms	Calculated positions, equivalent isotropic U's
Programs used	SHELXS-97 (Sheldrick, 1990)
	SHELXL-97 (Sheldrick, 1997)
	SHELXTL, STOE IPDS2 software
Data / restraints / parameters	4271 / 0 / 310
Goodness-of-fit on F^2	0.938
R index (all data)	wR2 = 0.1109
R index conventional [I>2sigma(I)]	R1 = 0.0526

Atomic coordinates and equivalent isotropic displacement parameters (Å^2) for **65**. U(eq) is defined as one third of the trace of the orthogonalized U^{ij} tensor.

	x	y	z	U(eq)	Occupancy
O2	0.5918(2)	0.14852(7)	0.9619(3)	0.0458(6)	1
O3	0.5578(3)	0.19540(7)	1.1685(4)	0.0565(7)	1
O5	0.6495(2)	0.04965(7)	1.4018(4)	0.0516(7)	1
O1	0.3556(2)	0.09209(7)	1.2213(4)	0.0556(7)	1
O4	0.7387(2)	0.11593(7)	1.2956(4)	0.0591(7)	1
O6	0.5852(3)	0.04567(8)	1.7610(4)	0.0691(9)	1
C14	0.7369(4)	0.23103(10)	0.9014(6)	0.0488(9)	1
C13	0.6949(3)	0.19851(10)	0.8479(5)	0.0409(8)	1
C3	0.6279(3)	0.10090(10)	1.1991(6)	0.0453(9)	1
C12	0.6082(3)	0.18171(10)	1.0091(6)	0.0444(9)	1

C21	0.6500(4)	0.03498(10)	1.6095(6)	0.0513(10)	1
C18	0.7367(3)	0.18341(10)	0.6500(6)	0.0474(9)	1
C22	0.7330(3)	0.00532(11)	1.6178(5)	0.0462(9)	1
C6	0.3082(4)	0.13818(10)	0.9778(6)	0.0493(9)	1
C15	0.8197(3)	0.24782(10)	0.7591(6)	0.0504(9)	1
C23	0.8110(3)	-0.00488(11)	1.4400(6)	0.0536(10)	1
C1	0.4069(3)	0.11231(10)	1.0431(5)	0.0484(9)	1
C4	0.5653(4)	0.07791(10)	1.3668(6)	0.0507(10)	1
C19	0.9539(4)	0.25134(12)	0.4074(6)	0.0666(12)	1
C11	0.2153(3)	0.14844(11)	1.1290(7)	0.0568(11)	1
C7	0.3113(4)	0.15323(12)	0.7690(7)	0.0672(12)	1
C17	0.8179(3)	0.20116(11)	0.5082(6)	0.0499(10)	1
C25	0.8815(4)	-0.05377(11)	1.6497(6)	0.0603(11)	1
C16	0.8607(3)	0.23311(11)	0.5613(6)	0.0483(10)	1
C5	0.4394(4)	0.06500(10)	1.2794(6)	0.0569(10)	1
C2	0.5325(3)	0.12808(10)	1.1329(6)	0.0465(9)	1
C24	0.8841(4)	-0.03403(12)	1.4584(7)	0.0605(11)	1
C9	0.1277(5)	0.18733(12)	0.8632(8)	0.0733(13)	1
C10	0.1262(4)	0.17255(12)	1.0707(8)	0.0685(12)	1
C26	0.8032(4)	-0.04346(13)	1.8244(7)	0.0680(12)	1
C8	0.2232(5)	0.17737(13)	0.7113(7)	0.0790(15)	1
C27	0.7303(4)	-0.01454(11)	1.8102(6)	0.0596(11)	1
C28	0.9583(5)	-0.08581(13)	1.6637(8)	0.0829(15)	1
C20	0.8496(4)	0.11395(14)	1.1590(8)	0.0808(15)	1

Bond lengths [Å] and angles [°] for **65**.

O2-C12	1.356(4)
O2-C2	1.441(4)
O3-C12	1.213(4)
O5-C21	1.367(4)
O5-C4	1.439(4)
O1-C5	1.427(5)
O1-C1	1.433(4)
O4-C20	1.418(5)
O4-C3	1.422(4)
O6-C21	1.205(4)
C14-C15	1.382(5)
C14-C13	1.397(5)
C13-C18	1.392(5)
C13-C12	1.478(5)
C3-C4	1.502(5)
C3-C2	1.519(5)
C21-C22	1.461(5)
C18-C17	1.388(5)
C22-C27	1.390(5)
C22-C23	1.396(5)
C6-C7	1.380(5)
C6-C11	1.384(5)
C6-C1	1.505(5)
C15-C16	1.382(5)
C23-C24	1.389(6)
C1-C2	1.547(5)
C4-C5	1.503(5)
C19-C16	1.519(5)
C11-C10	1.378(6)
C7-C8	1.371(6)
C17-C16	1.379(5)
C25-C24	1.382(5)
C25-C26	1.385(5)
C25-C28	1.504(6)
C9-C10	1.367(6)
C9-C8	1.403(7)
C26-C27	1.379(6)
C12-O2-C2	116.9(3)

C21-O5-C4	117.7(3)
C5-O1-C1	111.8(3)
C20-O4-C3	114.1(3)
C15-C14-C13	120.0(4)
C18-C13-C14	119.4(3)
C18-C13-C12	123.3(4)
C14-C13-C12	117.3(3)
O4-C3-C4	109.8(3)
O4-C3-C2	110.0(3)
C4-C3-C2	108.5(3)
O3-C12-O2	122.8(3)
O3-C12-C13	124.9(4)
O2-C12-C13	112.3(3)
O6-C21-O5	121.7(4)
O6-C21-C22	126.2(3)
O5-C21-C22	112.0(3)
C17-C18-C13	119.3(4)
C27-C22-C23	118.3(4)
C27-C22-C21	118.1(3)
C23-C22-C21	123.6(3)
C7-C6-C11	118.4(4)
C7-C6-C1	120.8(3)
C11-C6-C1	120.8(3)
C16-C15-C14	120.9(4)
C24-C23-C22	120.1(4)
O1-C1-C6	108.5(3)
O1-C1-C2	106.6(3)
C6-C1-C2	113.2(3)
O5-C4-C3	107.6(3)
O5-C4-C5	108.6(3)
C3-C4-C5	110.9(3)
C10-C11-C6	120.9(4)
C8-C7-C6	120.8(4)
C16-C17-C18	121.6(4)
C24-C25-C26	117.6(4)
C24-C25-C28	120.9(4)
C26-C25-C28	121.5(4)
C17-C16-C15	118.8(4)
C17-C16-C19	120.4(3)
C15-C16-C19	120.8(4)
O1-C5-C4	111.3(3)
O2-C2-C3	107.5(3)
O2-C2-C1	110.3(3)
C3-C2-C1	111.0(3)
C25-C24-C23	121.7(4)
C10-C9-C8	118.1(4)
C9-C10-C11	121.1(4)
C27-C26-C25	121.7(4)
C7-C8-C9	120.7(4)
C26-C27-C22	120.7(4)

Anisotropic displacement parameters (Å^2) for **65**.
The anisotropic displacement factor exponent takes the form: $-2\pi^2[\,h^2\,a^{*2}U^{11} + ... + 2\,h\,k\,a^*\,b^*\,U^{12}\,]$

	U^{11}	U^{22}	U^{33}	U^{23}	U^{13}	U^{12}
O2	0.0560(15)	0.0368(17)	0.0446(12)	-0.0003(11)	0.0128(11)	-0.0045(12)
O3	0.0659(16)	0.0453(18)	0.0582(15)	-0.0042(13)	0.0127(13)	0.0011(14)
O5	0.0633(17)	0.0483(18)	0.0431(13)	0.0040(12)	0.0064(11)	0.0103(14)
O1	0.0515(15)	0.0523(18)	0.0629(16)	0.0120(13)	0.0112(12)	-0.0023(13)
O4	0.0522(15)	0.057(2)	0.0679(16)	-0.0074(14)	-0.0005(13)	-0.0091(14)
O6	0.094(2)	0.068(2)	0.0454(14)	0.0018(14)	0.0136(15)	0.0146(18)
C14	0.049(2)	0.045(3)	0.052(2)	0.0026(18)	-0.0030(17)	0.0029(19)
C13	0.0404(18)	0.039(2)	0.0430(18)	0.0030(16)	-0.0036(15)	0.0021(17)
C3	0.045(2)	0.043(2)	0.0478(19)	-0.0024(16)	0.0031(16)	-0.0069(18)
C12	0.044(2)	0.040(3)	0.049(2)	-0.0004(18)	-0.0006(18)	0.0064(17)
C21	0.061(2)	0.050(3)	0.042(2)	0.0021(19)	-0.0010(18)	-0.010(2)

C18	0.049(2)	0.039(3)	0.054(2)	-0.0040(18)	-0.0020(18)	0.0018(18)
C22	0.048(2)	0.047(3)	0.0434(18)	0.0009(17)	-0.0047(16)	-0.0112(19)
C6	0.051(2)	0.045(3)	0.052(2)	-0.0033(18)	-0.0029(18)	-0.0040(19)
C15	0.052(2)	0.041(3)	0.058(2)	0.0018(19)	-0.0079(18)	-0.0056(19)
C23	0.054(2)	0.055(3)	0.051(2)	0.0127(19)	0.0042(18)	0.000(2)
C1	0.055(2)	0.047(3)	0.0431(19)	0.0007(17)	0.0081(17)	-0.0025(19)
C4	0.055(2)	0.046(3)	0.051(2)	-0.0006(18)	0.0093(18)	0.006(2)
C19	0.061(3)	0.068(3)	0.071(3)	0.012(2)	0.003(2)	-0.017(2)
C11	0.050(2)	0.060(3)	0.060(2)	0.000(2)	0.0017(18)	0.003(2)
C7	0.080(3)	0.064(3)	0.057(2)	0.007(2)	-0.002(2)	0.011(3)
C17	0.047(2)	0.055(3)	0.048(2)	0.0003(18)	0.0022(17)	-0.004(2)
C25	0.056(2)	0.063(3)	0.062(2)	0.006(2)	-0.006(2)	0.002(2)
C16	0.042(2)	0.056(3)	0.047(2)	0.0052(18)	-0.0049(16)	-0.0048(19)
C5	0.065(3)	0.045(3)	0.061(2)	0.0141(19)	0.009(2)	-0.003(2)
C2	0.051(2)	0.047(3)	0.0406(18)	0.0025(16)	0.0106(16)	-0.0022(18)
C24	0.054(2)	0.063(3)	0.064(2)	0.006(2)	0.0095(19)	0.004(2)
C9	0.072(3)	0.055(3)	0.093(3)	-0.007(3)	-0.027(3)	0.005(2)
C10	0.055(3)	0.064(3)	0.087(3)	-0.006(2)	0.005(2)	0.005(2)
C26	0.081(3)	0.067(3)	0.056(2)	0.014(2)	-0.004(2)	0.003(3)
C8	0.110(4)	0.067(4)	0.060(3)	0.001(2)	-0.026(3)	0.001(3)
C27	0.075(3)	0.059(3)	0.045(2)	0.0056(19)	0.0050(19)	0.000(2)
C28	0.082(3)	0.070(4)	0.098(3)	0.013(3)	-0.007(3)	0.019(3)
C20	0.053(2)	0.082(4)	0.108(4)	0.016(3)	0.011(2)	0.003(2)

Hydrogen coordinates and isotropic displacement parameters (Å^2) for **65**.

	x	y	z	U(eq)	Occupancy
H14	0.7084	0.2416	1.0356	0.059	1
H3	0.6531	0.0877	1.0631	0.054	1
H18	0.7099	0.1612	0.6123	0.057	1
H15	0.8489	0.2698	0.7978	0.060	1
H23	0.8141	0.0081	1.3061	0.064	1
H1	0.4265	0.0976	0.9110	0.058	1
H4	0.5517	0.0902	1.5116	0.061	1
H193	1.0351	0.2389	0.4025	0.100	1
H192	0.9692	0.2742	0.4646	0.100	1
H191	0.9176	0.2527	0.2559	0.100	1
H11	0.2130	0.1387	1.2748	0.068	1
H7	0.3753	0.1468	0.6639	0.081	1
H17	0.8447	0.1911	0.3713	0.060	1
H52	0.4547	0.0508	1.1454	0.068	1
H51	0.3982	0.0508	1.3955	0.068	1
H2	0.5128	0.1424	1.2666	0.056	1
H24	0.9372	-0.0406	1.3364	0.073	1
H9	0.0659	0.2039	0.8231	0.088	1
H10	0.0626	0.1790	1.1764	0.082	1
H26	0.7997	-0.0566	1.9575	0.082	1
H8	0.2269	0.1875	0.5668	0.095	1
H27	0.6776	-0.0081	1.9330	0.072	1
H283	0.9334	-0.1009	1.5410	0.124	1
H282	0.9417	-0.0969	1.8080	0.124	1
H281	1.0497	-0.0805	1.6514	0.124	1
H203	0.8680	0.0903	1.1244	0.121	1
H202	0.9226	0.1238	1.2390	0.121	1
H201	0.8350	0.1264	1.0190	0.121	1

Torsion angles [°] for **65**.

C15-C14-C13-C18	-0.4(5)
C15-C14-C13-C12	179.0(3)
C20-O4-C3-C4	131.2(3)
C20-O4-C3-C2	-109.5(4)
C2-O2-C12-O3	-12.1(5)
C2-O2-C12-C13	166.9(3)

C18-C13-C12-O3	-170.7(3)
C14-C13-C12-O3	9.9(5)
C18-C13-C12-O2	10.3(4)
C14-C13-C12-O2	-169.0(3)
C4-O5-C21-O6	-2.0(5)
C4-O5-C21-C22	176.2(3)
C14-C13-C18-C17	-0.8(5)
C12-C13-C18-C17	179.8(3)
O6-C21-C22-C27	6.0(6)
O5-C21-C22-C27	-172.1(3)
O6-C21-C22-C23	-176.6(4)
O5-C21-C22-C23	5.3(5)
C13-C14-C15-C16	1.0(5)
C27-C22-C23-C24	-0.5(5)
C21-C22-C23-C24	-177.9(4)
C5-O1-C1-C6	174.9(3)
C5-O1-C1-C2	-62.9(4)
C7-C6-C1-O1	-158.0(4)
C11-C6-C1-O1	24.6(5)
C7-C6-C1-C2	83.9(4)
C11-C6-C1-C2	-93.5(4)
C21-O5-C4-C3	148.3(3)
C21-O5-C4-C5	-91.6(4)
O4-C3-C4-O5	-68.3(4)
C2-C3-C4-O5	171.5(3)
O4-C3-C4-C5	173.1(3)
C2-C3-C4-C5	52.9(4)
C7-C6-C11-C10	1.5(6)
C1-C6-C11-C10	178.9(4)
C11-C6-C7-C8	-1.0(7)
C1-C6-C7-C8	-178.5(4)
C13-C18-C17-C16	1.6(5)
C18-C17-C16-C15	-1.0(5)
C18-C17-C16-C19	177.5(3)
C14-C15-C16-C17	-0.3(5)
C14-C15-C16-C19	-178.8(3)
C1-O1-C5-C4	62.8(4)
O5-C4-C5-O1	-174.5(3)
C3-C4-C5-O1	-56.5(4)
C12-O2-C2-C3	-119.2(3)
C12-O2-C2-C1	119.6(3)
O4-C3-C2-O2	63.4(3)
C4-C3-C2-O2	-176.5(3)
O4-C3-C2-C1	-175.9(3)
C4-C3-C2-C1	-55.8(4)
O1-C1-C2-O2	179.1(3)
C6-C1-C2-O2	-61.7(4)
O1-C1-C2-C3	60.1(4)
C6-C1-C2-C3	179.3(3)
C26-C25-C24-C23	-0.1(6)
C28-C25-C24-C23	178.1(4)
C22-C23-C24-C25	0.5(6)
C8-C9-C10-C11	-0.3(7)
C6-C11-C10-C9	-0.8(7)
C24-C25-C26-C27	-0.2(6)
C28-C25-C26-C27	-178.4(4)
C6-C7-C8-C9	-0.1(7)
C10-C9-C8-C7	0.7(7)
C25-C26-C27-C22	0.1(7)
C23-C22-C27-C26	0.2(6)
C21-C22-C27-C26	177.8(4)

185

References

7.3 Abbreviations

A	adenine (adenosine)		IR	Infrared (spectroscopy)
A	absorption		J	coupling constant
acac	acetylacetonate		λ	wavelength
AFM	Atomic Force Microscopy		LC-MS	Liquid Chromatography-Mass Spectrometry
A_{max}	absorption maximum		M	molecule or molar
A_{norm}	normed absorption		m/z	mass/charge
APCI	Atmospheric Pressure Chemical Ionisation		MALDI	Matrix Assisted Laser Desorption Ionisation
ATR	Attenuated Total Reflection		mdeg	milli degree (ellipticity)
bp	base pair(s)		Me	methyl
Bu	butyl		min	minute(s)
C	cytosine (cytidine)		MS	Mass Spectrometry
cat.	catalytic		NBA	3-nitrobenzylic alcohol
CD	Circular Dichroism		NMR	Nuclear Magnetic Resonance
CHES	N-cyclohexyl-2-aminoethanesulfonic acid		NOESY	Nuclear Overhauser Effect SpectroscopY
d	day(s)		OAc	acetyl
DMAP	4-N,N-dimethylaminopyridine		Ph	phenyl
DMBz	dimethoxybenzoyl		phen	1,2-phenylenediamine
DMF	N,N-dimethylformamide		R	organic residue
DMSO	dimethylsulfoxide		r.t.	room temperature
DMT	4,4'-dimethoxytrityl		rel. int.	relative intensity
DNA	deoxyribonucleic acid		RF	retention factor
dppf	1,1'-Bis(diphenylphosphanyl)ferrocen)		RNA	ribonucleic acid
ε	extinction coefficient		RP	Reverse Phase
EA	Elementary Analysis		salen	N,N-bis-salicylidene-ethylenediamine
Ed.	editor(s)		sat.	saturated
edh	O,O'-ethylenedihydroxylamine		SEM	trimethylsilylethoxymethyl
EDTA	ethylenediamine-tetra-acetate		STM	Scanning Tunneling Microscopy
EI	Electron Impact		T	thymine (thymidine)
en	ethylenediamine		TBAF	tetra-n-butylammonium fluoride
EPR	Electron Paramagnetic Resonance		TES	triethylsilyl
eq	equivalent(s)		THF	tetrahydrofuran
ESI	Electro Spray Ionisation		TIPS	tri-iso-propylsilyl
Et	ethyl		TLC	thin layer chromatography
FAB	Fast Atom Bombardement		T_M	melting temperature
FT	Fourier Transformation		TOF	time of flight
G	guanine (guanosine)		Tol	toluoyl
h	hour(s)		TRIS	tris(hydroxymethyl)aminomethane
HEPES	N-(2-hydroxyethyl)piperazine-N'-2-ethanesulfonic acid		UV	Ultraviolet (spectroscopy)
HPLC	High Performance Liquid Chromatography		z	charge
HRMS	High Resolution Mass Spectrometry		$\tilde{\nu}$	wave number
I	intensity			
iPr	iso-propyl			

8 References

[1]   H. Lodish, A. Berk, SL Zipursky. P. Matzudaira, D. Baltimore and J. Darnell, "*Molecular Cell Biology*", **1999**, *4th edition*, WH Freeman and Co, New York.

[2]   J. D. Watson, F. H. C. Crick, *Nature* **1953**, *171*, 737.

[3]   W. Saenger, "*Principles of Nucleic Acid Structure*", **1984**, Springer, New York.

[4]   K. M. Guckian, B. A. Schweitzer, R. X.-F. Ren, C. J. Sheils, D. C. Tahmassebi, E. T. Kool, *J. Am. Chem. Soc.* **2000**, *122*, 2213-2222.

[5]   R. P. Feynman, *Engeneering and Science* **1960**, *23*, 22-36.

[6]   V. Balzani, M. Venturi, A. Credi (Eds.), *"Molecular Devices and Machines"* **2003**, *Wiley-VCH*, Weinheim.

[7]   J.-M. Lehn, *"Supramolecular Chemistry",* **1995***, Wiley-VCH*, Weinheim.

[8]   Examples include all kinds of quantum dot applications, UV-light blocking nano particles, thin-film lithium-ion batteries and nano-structured surfaces.

[9]   See for example on http://www.nano.gov/ and http://www.foresight.org/.

[10]   N. C. Seeman, *Angew. Chem. Int. Ed.* **1998**, *37*, 3220-3238.

[11]   M. Scheffler, A. Dorenbeck, S. Jordan, M. Wüstefeld, G. von Kiedrowski, *Angew. Chem.* **1999**, *111* (22), 3513 – 3518.

[12]   A. Chworos, I. Severcan, A. Y. Koyfman, P. Weinkam, E. Oroudjev, H. G. Hansma, L. Jaeger, *Science* **2004**, *306*, 2068-2072.

[13]   E. Ennifar, P. Walter, B. Ehresmann, C. Ehresmann, P. Dumas, *Nature Struct. Biol.* **2001**, *8*, 1064.

[14]   P. W. K. Rothemund, *Nature* **2006**, *440*, 297-302.

[15]   C. Niemeyer, *Angew. Chem. Int. Ed.* **2001**, *40*, 4128-4158.

[16]   S. E. Baker, W. Cai, T. L. Lasseter, K. P. Weidkamp, R. J. Hamers, *Nano Lett.* **2002**, *2*, 1413–1417.

[17]   K. A. Williams, P. T. M. Veenhuizen, B. G. de la Torre, R. Eritja, C. Dekker, *Nature* **2002**, *420*, 761.

[18]   N. C. Seeman, *Trends Biochem. Sci.* **2005**, *30*, 119-125.

[19]   C. Mao, W. Sun, Z. Shen, N. C. Seeman, *Nature* **1999**, *397*, 144-146.

[20]   H. Yan, X. Zhang, Z. Shen, N. C. Seeman, *Nature* **2002**, *415*, 62-65.

[21]   W. B. Sherman, N. C. Seeman, *Nano Lett.* **2004**, *4*, 1203–1207.

[22]   J-S. Shin, N A. Pierce, *J. Am. Chem. Soc.* **2004**, *126*, 10834–10835.

[23]   J. A. Doudna, T. R. Cech, *Nature* **2002**, *418*, 222-228.

[24]   A. C. Forster, S. Altman, *Science* **1990**, *249*, 783−786.

[25]   J. W. Szostak, C. Wilson, *Nature* **1995**, *374*, 777.

[26]   R.R. Breaker, *Curr. Opin. Chem. Biol.* **1997**, *1*, 26-31.

[27]   Y. Li, R.R. Breaker, *Curr. Opin. Struct. Biol.* **1999**, *9*, 315-323.

[28]   G.M. Emilsson, R.R. Breaker, *Cell. Mol. Life Sci.* **2002**, *59*, 596-607.

[29]   C.-H. B. Chen, D. S. Sigman, *J. Am. Chem. Soc.* **1988**, *110*, 6570.

[30]   J. K. Bashkin, E. I. Frolova, U. Sampath, *J. Am. Chem. Soc.* **1994**, *116*, 5981-5982.

[31]   G. R. Dreyer, P. B. Dervan, *Proc. Natl. Acad. Sci. U.S.A.* **1985**, *82*, 968.

References

[32]   D. Magda, S. Crofts, A. Lin, D. Miles, M. Wright, J. L. Sessler, *J. Am. Chem. Soc.* **1997**, *119*, 2293-2294.

[33]   J. Brunner, A. Mokhir, R. Krämer, *J. Am. Chem. Soc.* **2003**, *125*, 12410-12411.

[34]   I. Boll, R. Krämer, J. Brunner, A. Mokhir, *J. Am. Chem. Soc.* **2005**, *127*, 7849-7856.

[35]   I. Boll, E. Jentzsch, R. Krämer, A. Mokhir, *Chem. Comm.* **2006**, 3447-3449.

[36]   G. Roelfes, B.L. Feringa, *Angew. Chem. Int. Ed.* **2005**, *44*, 3230-3232.

[37]   G. Roelfes, A.J. Boersma, B.L. Feringa, *Chem. Commun.* **2006**, 635-637*.

[38]   X. Li and D. R. Liu, *Angew Chem. Int. Ed.* **2004**, *43*, 4848–4870.

[39]   Z. J. Gartner, B. N. Tse, R. Grubina, J. B. Doyon, T. M. Snyder and D. R. Liu, *Science* **2004**, *305*, 1601–1605.

[40]   M. W. Kanan, M. M. Rozenman, K. Sakurai, T. M. Snyder and D. R. Liu, *Nature* **2004**, *431*, 545–549.

[41]   65 D. M. Rosenbaum and D. R. Liu, *J. Am. Chem. Soc.*, **2003**, *125*, 13924–13925.

[42]   T. Carell, C. Behrens, J. Gierlich, *Org. Biomol. Chem.* **2003**, *1*, 2221-2228.

[43]   B. Giese, *Curr. Opin. Chem. Biol.*, 2002, **6**, 612–618.

[44]   G. B. Schuster, *Acc. Chem. Res.*, 2000, **33**, 253–260.

[45]   J. P. Pouget, T. Douki, M. J. Richard and J. Cadet, *Chem. Res. Toxicol.*, 2000, **13**, 541–549.

[46]   A. Schwögler, L. T. Burgdorf, T . Carell, *Angew. Chem. Int. Ed.* **2000**, *39*, 3918 –3920.

[47]   T. J. Meade, J. F. Kayyem, *Angew. Chem. Int. Ed. Engl.* **1995**, *34*, 352-354.

[48]   C. J. Murphy, M. R. Arkin, Y. Jenkins, N. D. Ghatlia, S. H. Bossmann, N. J. Turro, J. K. Barton, *Science* **1993**, *262*, 1025-1029.

[49]   S. Breeger, U. Hennecke, T. Carell, *J. Am. Chem. Soc.* **2004**, *126*, 1302 – 1303.

[50]   S. Breeger, M. von Meltzer, U. Hennecke, T. Carell, *Chem. Eur. J.* **2006**, *12*,6469 – 6477.

[51]   D. Porath, A. Bezryadin, S. deVries, C. Dekker, Nature **2000**, *403*, 635-638.

[52]   E. Braun, Y. Eichen, U. Sivan, G. Ben-Yoseph, *Nature* **1998**, *391*, 775-778.

[53]   K. Keren, R. S. Berman, E. Buchstab, U. Sivan, E. Braun, *Science* **2003**, *302*, 1380-1382.

[54]   H. C. Kolb, M. G. Finn, K. B. Sharpless, *Angew. Chem. Int. Ed.* **2001**, *40*, 2004-2021.

[55]   G. A. Burley, J. Gierlich, M. R. Mofid, H. Nir, S. Tal, Y. Eichen, T. Carell, *J. Am. Chem. Soc.* **2006**, *128*, 1398-1399.

[56]   L. Zhu, P. S. Lukerman, J. W. Canary and N. C. Seeman, *J. Am. Chem. Soc.*, **2003**, *125*, 10178–10179.

[57]   M. D. Sørensen, M. Petersen and J. Wengel, *Chem. Commun.*, **2003**, 2130–2131.

[58]   J. Gierlich, G. A. Burley, P. M. E. Gramlich, D. M. Hammond, T. Carell, *Org. Lett.* **2006**, *8*, 3639-3642.

[59]   K. V. Gothelf, T. H. LaBean, *Org. Biomol. Chem.* **2005**, *3*, 4023-4037.

[60]   J. S. Choi, C. W. Kang, K. Jung, J. W. Yang, Y. G. Kim and H. Y. Han, *J. Am. Chem. Soc.* **2004**, *126*, 8606–8607.

[61]   K. M. Steward and L. W. McLaughlin, *J. Am. Chem. Soc.* **2004**, *126*, 2050–2057.

[62]   K. M. Steward, J. Rojo and L. W. Mclaughlin, *Angew. Chem. Int. Ed.* **2004**, *43*, 5808–5811.

[63]   J. L. Czlapinski, T. L. Sheppard, *J. Am. Chem. Soc.* **2001**, *123*, 8618–8619.

[64]   J. L. Czlapinski, T. L. Sheppard, *ChemBioChem* **2004**, *5*, 127-129.

[65]   J. L. Czlapinski, T. L. Sheppard, *Chem. Commun.* **2004**, 2468-2469.

References

[66]   K. V. Gothelf and R. S. Brown,*Chem. Eur. J.*, **2005**, *11*, 1062–1069.

[67]   M. Nielsen, A. H. Thomsen, E. Cló, F. Kirpekar and K. V. Gothelf, *J. Org. Chem.* **2004**, *69*, 2240–2250.

[68]   K. V. Gothelf, A. H. Thomsen, M. Nielsen, E. Cló and R. S. Brown, *J. Am. Chem. Soc.* **2004**, *126*, 1044–1046.

[69]   R. S. Brown, M. Nielsen and K. V. Gothelf, *Chem. Commun.* **2004**, 1464–1465.

[70]   M. Nielsen, V. Dauksaite, J. Kjems and K. V. Gothelf, *Bioconjugate Chem.* **2005**, *16*, 681–685.

[71]   L. Kværnø, J. Wengel, *Chem. Commun.* **2001**, 1419–1424.

[72]   J. Kurreck, *Eur. J. Biochem.* **2003**, *270*, 1628–1644.

[73]   Kisakürek, M. Volkan, Rosemeyer, Helmut (Eds.) „*Perspectives in Nucleoside and Nucleic Acid Chemistry* “ **2000**, *Wiley-VCH*, Weinheim.

[74]   M. Manoharan, *Antisense Nucleic Acid Drug Dev.* **2002**, *12*, 103–128.

[75]   M. J. Gait, *Cell. Mol. Life Sci.* **2003**, *60*, 844–853.

[76]   U. Galderisi, A. Cascino, A. Giordano, *J. Cell. Physiol.* **1999**, *181*, 251-257.

[77]   A. Okamoto, K. Tainaka, Y. Ochi, K. Kanatania, I. Saito, *Mol. BioSyst.* **2006**, *2*, 122–127.

[78]   R. P. Iyer, L.R. Phillips, W.Egan, J.B. Regan, S. L. Beaucage, *J. Org. Chem.* **1990**, *55*, 4693-4699.

[79]   S. Obika, D. Nanbu, Y. Hari, J. Andoh, K. Morio, T. Doi, T. Imanishi, *Tet. Lett.* **1998**, *39*, 5401-5404.

[80]   S. K. Singh, P. Nielsen, A. A. Koshkin, J. Wengel *Chem. Commun.* **1998**, 455-456.

[81]   L. Zhang, A. Peritz, E. Meggers, *J. Am. Chem. Soc.* **2005***, 127*, 4174-4175.

[82]   P. E. Nielsen, M. Egholm, *"An introduction to PNA" in Peptide Nucleic Acids* **2004**, *2nd Edition,* Horizon Bioscience, Wymondham (UK), 1-36.

[83]   F. Seela, A. Jawalekar, *Helv. Chim. Acta* **2002**, *85*, 1857-1868.

[84]   F. Seela, H. Debelak, *Nucleic Acids Res.* **2000**, *28*, 3224.

[85]   A. Kornberg, T. A. Baker, *DNA Replication*, 2nd ed.; W. H. Freeman: New York, **1992**.

[86]   M. Ober, H. Mueller, C. Pieck, J. Gierlich, T. Carell, *J. Am. Chem. Soc.* **2005**, *127*, 18143-18149.

[87]   D. R. Lesser, M. R. Kurpiewski, L. Jen-Jacobson, *Science* **1990**, *250*, 776-778.

[88]   S. A. Smith, S. B. Rajur, L. W. McLaughlin, *Nature Struct. Biol.* **1994**, *1*, 18-22.

[89]   B. A Schweitzer,. E. T. Kool, *J. Am. Chem. Soc.* **1995**, *117*, 1863-1872.

[90]   K. M. Guckian, B. A. Schweitzer, R. X.-F. Ren, C. J. Sheils, P. L. Paris, D. C. Tahmassebi, E. T. Kool, *J. Am. Chem. Soc.***1996**, *118*, 8182-8183.

[91]   H. Liu, J. Gao, S. R. Lynch, Y. D. Saito, L. Maynard, E. T. Kool, *Science* **2003**, *302*, 868 – 871.

[92]   E. Hammersten, *Biochem. Z.* **1924**, *144*, 383.

[93]   S.D. Wettig, D.O. Wood and J.S. Lee, *J. Inorg. Biochem.* **2003**, *94*, 94–99.

[94]   M. Egli, *Chem. & Biol.* **2002**, *9*, 277-286.

[95]   J. Schliepe, U. Berghoff, B. Lippert, D. Cech, *Angew. Chem. Int. Ed. Engl.* **1996**, *35*, 646-648.

[96]   S. Katz, *J. Am. Chem. Soc.* **1952**, *74*, 2238-2245.

[97]   C. A. Thomas, *J. Am. Chem. Soc.* **1954**, *76*, 6032-6034..

[98]   S. Katz, *Biochim. Biophys. Acta* **1963**, *68*, 240-253..

[99]   L. D. Kosturko, C. Folzer, R. F. Stewart, *Biochemistry* **1974**, *13*, 3949-3952.

[100] N. Davidson, J. Widholm, U. S. Nandi, R. Jensen, B. M. Olivera, J. C. Wang, *Biochemistry* **1965**, *53*, 111.

References

[101]   D. W. Gruenwedel, M. K. Cruikshank, *J. Inorg. Biochem.* **1991**, *43*, 29-36.

[102]   E. Buncel, C. Boone, H. Joly, R. Kumar, A. R. J. Norris, *Inorg. Biochem.* **1985**, *25*, 61-73.

[103]   Z. Kuklenyik, L. G. Marzilli, *Inorg. Chem.* **1996***, 35*, 5654-5662.

[104]   A. Ono, H. Togashi, *Angew. Chem. Int. Ed.* **2004**, *43*, 4300–4302.

[105]   Y. Miyake, H. Togashi, M. Tashiro, H. Yamaguchi, S. Oda, M. Kudo, Y. Tanaka, Y. Kondo, R. Sawa, T. Fujimoto, T. Machinami, A. Ono, *J. Am. Chem. Soc.* **2006**, *128*, 2172-2173.

[106]   J. S. Lee, L. J. P. Latimer, R. S. Reid, Biochem. Cell Biol. **1993**, *71*, 162-168.

[107]   P. Aich, S. L. Labiuk, L. W. Tari, L. J. T. Delbaere, W. J. Roesler, K. J. Falk, R. P. Steer, J. S. Lee, *J. Mol. Biol.* **1999**, *294*, 477-485.

[108]   P. Aich, R. J. S. Skinner, S. D. Wettig, R. P. Steer, J. S. Lee, *J. Biomol. Str. & Dyn.* **2002**, *20*, 93-98.

[109]   A. Rakitin, P. Aich, C. Papadopoulos, Yu. Kobzar, A. S. Vedeneev, J. S. Lee, J. M. Xu, *Phys. Rev. Lett.* **2001**, *86*, 3670-3673.

[110]   W.I. Sundquist and S. Lippard. *Coordination Chem. Rev.* **1990**, *100*, 293-322.

[111]   W. Bannwarth, W. Pfleiderer, F. Müller, *Helv. Chim. Acta* **1991**, *74*, 1991-1999.

[112]   D. J. Hurley, Y. Tor, *J. Am. Chem. Soc.* **1998**, *120*, 2194-2195.

[113]   K. Tanaka, M. Shionoya, *J. Org. Chem.* **1999**, *64*, 5002-5003.

[114]   M. Tasaka, K. Tanaka, M. Shiro, M. Shionoya, *Supramol. Chem.* **2001**, *13*, 671-675.

[115]   K. Tanaka, M. Tasaka, H. Cao, M. Shionoya, *Eur. J. Pharm. Sci.* **2001***, 13*, 77-83.

[116]   H. Cao, K. Tanaka, and M. Shionoya, *Chem. Pharm. Bull.,* **2000**, *48*, 1745-1748.

[117]   E. Meggers, P. L. Holland, W. B. Tolman, F. E. Romesberg, P. G. Schultz, *J. Am. Chem. Soc.* **2000,** *122,* 10714-10715.

[118]   N. Zimmermann, E. Meggers, P. G. Schultz, *Bioorg. Chem.* **2004**, *32*, 13-25.

[119]   N. Zimmerman, E. Meggers, P. G. Schultz, *J. Am. Chem. Soc.* **2002**, *124*, 13684-13685.

[120]   R. Wing, H. Drew, T. Takano, C. Broka, S. Tanaka, K. Itakura, R. E. Dickerson, *Nature* **1980**, *287*, 755-758.

[121]   S. Atwell, E. Meggers, G. Spraggon, P. G. Schultz, *J. Am. Chem. Soc.* **2001**, *123*, 12364-12367.

[122]   K. Tanaka, Y. Yamada, M. Shionoya, *J. Am. Chem. Soc.* **2002**, *124*, 8802-8803.

[123]   T. Tanaka, A. Tengeiji, T. Kato, N. Toyama, M. Shiro, M. Shionoya, *J. Am. Chem. Soc.* **2002**, *124*, 12494-12498.

[124]   Y. Takezawa, K. Tanaka, M. Shionoya, poster presentation at „*COE Symposium for Young Scientists on Frontiers of Molecular Science*", August 25-26, **2006**, Koshiba Hall, University of Tokyo.

[125]   K. Tanaka, A. Tengeiji, T. Kato, N. Toyama, M. Shionoya, *Science* **2003**, *299*, 1212-1213.

[126]   H. Zhang, A. Calzolari, R. Di Felice, *J. Phys. Chem. B* **2005**, *109*, 15345-15348.

[127]   L. Zhang, E. Meggers, *J. Am. Chem. Soc.* **2005**, *127*, 4174 -4175.

[128]   H. Weizman, Y. Tor, *J. Am. Chem. Soc.* **2001**, *123*, 3375-3376.

[129]   C. Brotschi, A. Häberli, C. J. Leumann, *Angew. Chem. Int. Ed.* **2001** , *40* ,3012-3014.

[130]   C. Brotschi, C. J. Leumann, *Nucleosides, Nucleotides & Nucleic Acids* **2003**, *22*, 1195-1197.

[131]   C. Switzer, S. Sinha, P. H. Kim, B. D. Heuberger, *Angew. Chem.* **2005**, *117*, 1553-1556; *Angew. Chem. Int. Ed. Engl.* **2005**, *44*, 1529-1532.

References

[132]   C. Switzer, D. Shin, *Chem. Commun.* **2005**, 1342-1344.

[133]   D-L. Popescu, T. J. Parolin, C. Achim, *J. Am. Chem. Soc.* **2003**, *125*, 6354-6355.

[134]   H. Thielert, P. Pfeiffer, *Chem. Ber.* **1938,** *71***,** 1399-1403.

[135]   R. H. Bailes, M. Calvin, *J. Am. Chem. Soc.* **1947**, *69,* 1886-1893.

[136]   Statistics generated by SciFinder Scholar 2006 upon searching for substructures of the basic
        salen ligand containing any metal.

[137]   T. P. Yoon, E. N. Jacobsen, *Science* **2003**, *299*, 1691.

[138]   Zhang, W.; Loebach, J. L.; Wilson, S. R.; Jacobsen, E. N., *J. Am. Chem. Soc.* **1990**, *112*, 2801.

[139]   Irie, R.; Noda, K.; Ito, Y.; Matsumoto, N.; Katsuki, T., *Tetrahedron Lett.* **1990**, *31*, 7345.

[140]   E. M. McGarrigle, D. G. Gilheany, *Chem. Rev.* **2005**, 10*5*, 1563-1602.

[141]   T. Katsuki, *Adv. Synth. & Cat.* **2002**, *344*, 131.

[142]   T. Katsuki, *Coord. Chem. Rev.* **1995**, *140*, 189.

[143]   M. Tokunaga, J. F. Larrow, F. Kakiuchi, E. N. Jacobsen, *Science* **1997**, *277*, 936.

[144]   A. Bencini, I. Ciofini, M. G. Uytterhoeven, *Inorg. Chim. Acta* **1998**, *274*, 90-101.

[145]   H. Miyasaka, R. Clerac, W. Wernsdorfer, L. Lecren, C. Bonhomme, K.-I. Sugiura, M. Yamashita,
        Angew. Chem. **2004**, *116*, 2861 – 2865.

[146]   T. Glaser, M. Heidemeier, T. Weyhermüller, R.-D. Hoffmann, H. Rupp, P. Müller, *Angew. Chem.*
        2006, *118*, 6179-6183.

[147]   K. Sato, M. Chikira, Y. Fujii, A. Komatsu, *Chem. Commun.* **1994**, 625-626.

[148]   S. S. Mandal, U. Varshney, S. Bhattacharya, *Bioconjugate Chem.* **1997**, *8*, 798-812.

[149]   S.E. Rokita, C. J. Burrows in „*DNA and RNA Binders*", Wiley VCH **2003**, *Vol. 1*, 126-145.

[150]   D. J. Gravert, J. H. Griffin, *J. Org. Chem.* **1993**, *58*, 820-822.

[151]   A. S. Kumbhar, S. G. Damle, S. T. Dasgupta, S. Y. Rane, A. S. Kumbhar, *J. Chem. Research (S)*
        1999, 98-99.

[152]   S. Routier, J.-L. Bernier, M. J. Waring, P. Colson, C. Houssier, C. Bailly, *J. Org. Chem.* **1996**, *61*,
        2326-2331.

[153]   J. G. Muller, L. A. Kayser, S. J. Paikoff, V. Duarte, N. Tang, R. J. Perez, S. E. Rokita, C. J.
        Burrows, *Coord. Chem. Rev.* **1999**, *185-186*, 761-774.

[154]   J. S. Miller (Ed.), „*Extended linear chain compounds*", Plenum Press, New York **1982**, *Vol. 1-3*.

[155]   W. A. Little, *Phs. Rev. A* **1964**, *134*, 1416.

[156]   H. Reihlen, E. Flohr, *Ber. Dtsch. Chem. Ges.* **1934***, 67*, 2010.

[157]   B. M. Craven, D. Hall, *Acta Cryst.* **1961**, *14*, 475-480.

[158]   K. A. Hofmann, G. Bugge, *Ber. Dtsch. Chem. Ges.* **1908**, *41*, 312.

[159]   K. Krogmann, *Angew. Chem. 1969*, *81*, 10-17.

[160]   L. Malatesta, F. Canziani, *J. Inorg. Nucl. Chem.* **1961**, *19,* 81.

[161]   M. Albrecht, *Angew. Chem. Int. Ed.* **2005**, *44*, 6448-6451.

[162]   J.-M. Lehn, A. Rigault, J. Siegel, J. Harrowfield, B. Chevrier, D. Moras, *Proc. Natl. Acad. Sci. USA*
        1987, *84*, 2565-2569.

[163]   Y.-H. Chen, C.-C. Lee, C.-C. Wang, G.-G. Lee, S.-Y. Lai, F.-Y. Li, C.-Y. Mou, S.-M. Peng, *Chem.
        Commun.* **1999**, 1667-1668.

References

[164]   I. P. Chen, M.-D. Fu, W.-H. Tseng, J.-Y. Yu, S.-H. Wu, C.-J. Ku, C. Chen, S.-M. Peng, *Angew. Chem.* **2006**, *118*, 5946-5950.

[165]   M. Albrecht, S. Mirtschin, M. de Groot, I. Janser, J. Runsink, G. Raabe, M. Kogej, C. A. Schalley, R. Fröhlich, *J. Am. Chem. Soc.* **2005**, *127*, 10371-10387.

[166]   Diploma thesis, Yvonne Söltl, LMU München, Dept. f. Chemie u. Biochemie, **2005**.

[167]   G. H. Clever, Y. Söltl, H. Burks, W. Spahl, T. Carell, *Chem. Eu. J.* **2006**, *12*, 8708 - 8718.

[168]   S. Akine, T. Taniguchi, T. Nabeshima, *Chem. Lett.* **2001**, *7*, 682.

[169]   A. Okamoto, K. Tainaka, I. Saito, *Tetrahedron Letters* **2002**, *43*, 4581-4583.

[170]   T. Mitsui, A. Kitamura, M. Kimoto, T. To, A. Sato, I. Hirao, Ichiro; S. Yokoyama, *J: Am. Chem. Soc.* **2003**, *125*, 5298-5307.

[171]   M. Shionoya, K. Tanaka, *Bull. Chem. Soc. Jpn.* **2000**, *73*, 1945-1954.

[172]   N. U. Hofsløkken, L. Skattebøl, *Acta Chem. Scand.* **1999**, *53*, 258.

[173]   R. Gopinath, S. J. Haque, B. K. Patel, *J. Org. Chem.* **2002**, *67*, 5842.

[174]   Sall, D.J. et al, *J. Med. Chem.* **1997**, *40*, 2843-2857.

[175]   G. Casiraghi, G. Casnati, G. Puglia, G. Sartori, G. Terenghi, *J. Chem. Soc. Perkin I* **1980**, *9*, 1862-1865.

[176]   M. Takeshita, C. N. Chang, F. Johnson, S. Will, and A. P. Grollman, *J. Biol. Chem.* **1987**, *262*, 10171-10179.

[177]   U. Wichai, S. A. Woski, *Org. Lett.***1999**, *1*, 1173-1175.

[178]   C. B. Reese, Q. Wu, *Org. Biomol. Chem.* **2003**, *1*, 3160-3172.

[179]   R. Bihovsky, C. Selick, I. Guisti, *J. Org. Chem.* **1988**, *53*, 4026-4031.

[180]   N. Griesang, C. Richert, *Tet. Lett.* **2002**, *43*, 8755-8758.

[181]   H.-C. Zhang, G. D. Daves Jr., *J. Org. Chem.* **1992**, *57*, 4690-4696.

[182]   G. Zemplén, E. Pascu, *Ber. Dtsch. Chem. Ges.* **1929**, *62*, 1613.

[183]   CCDC 271234 contains the crystallographic data for this compound. These data can be obtained free of charge via www.ccdc.cam.ac.uk/conts/retrieving.html (or from the Cambridge Crystallographic Data Centre, 12, Union Road, Cambridge CB2 1EZ, UK; fax: (+44) 1223-336-033; or deposit@ccdc.cam.ac.uk).

[184]   CCDC 602317 contains the crystallographic data for this compound. These data can be obtained free of charge from The Cambridge Crystallographic Data Centre via www.ccdc.cam.ac.uk/data_request/cif.

[185]   a) D. Hall, T.N. Waters, *J. Chem. Soc.* **1960**, 2644; b) L. C. Nathan, J. E. Koehne, J. M. Gilmore, K. A. Hannibal, W. E. Dewhirst, T. D. Mai, *Polyhedron* **2003**, *22*, 887; c) L. Dyers Jr., S. Y. Que, D, VanDerveer, X. R. Bu, *Inorganica Chimica Acta* **2006**, *359*, 197.

[186]   W. Saenger, *Principles of Nucleic Acid Structure*, Springer, New York, **1984**, p. 9-27.

[187]   Bachelor thesis, Tanja Köpping, LMU München, Dept. f. Chemie u. Biochemie, **2005**.

[188]   E.A. Ison, R.A. Corbin, M.M. Abu-Omar, *J. Am. Chem.Soc.* **2005**, *127*, 11938-11939.

[189]   A.J. Davenport, D.L. Davies, J. Fawcett, D.R. Russell, *J. Organomet. Chem.* **2006**, *691*, 2221-2227.

[190]   J.H. Hwang, M.M. Abu-Omar, *Tet. Lett.* **1999**, *40*, 8313-8316.

References

[191]   Y. Kijima, N. Asai, S. Tamura, N. Kishij, *Optronics* **1997**, *184*, 148-152.

[192]   G. Helmchen, A. Pfaltz, *Acc. Chem. Res.* **2000**, *33*, 336-345.

[193]   Patent: A. M. Lago, „Preparation of substituted 2-hydroxy-3-phenoxypropylamines as calcilytic compounds", PCT Int. Appl. **2000**, 42 pp, CODEN: PIXXD2, WO 2000045816, A1 20000810, CAN 133:163944, AN 2000:553416.

[194]   M. Schinnerl, M. Seitz, A. Kaiser, O. Reiser, *Org. Lett.* **2001**, *3*, 4259-4262.

[195]   T. W. Greene, P. G. M. Wuts, *„Protective groups in Organic Synthesis"* **1999**, *3rd edition*, John Wiley & Sons, New York.

[196]   Research Project (advanced Organic Chemistry), Heather Burks, LMU München, Dept. f. Chemie u. Biochemie, **2003 - 2004**.

[197]   D. Borrmann, R. Wegler, *Chem. Ber.* **1969**, *102*, 64-70.

[198]   A. Corsico Coda, G. Desimoni, P. Quadrelli, P.P. Righetti, G. Tacconi, *Gaz. Chim. Ital.* **1987**, *117*, 301-305.

[199]   Because the expected phosphoramidite contained a second phosphorylated compound as impurity which might have been an isomer phosphorylated at the oxazoline-nitrogen, the possibility exists, that the isolated oligonucleotide is the product of an unwanted chain elongation at the ligand's nitrogen atom. The outcome of the melting experiments carried out with the double strands containing the nucleoside **52**, however, suggest that this is not the case and the strands have the correct configuration.

[200]   Goodnow Jr., R.A.; Richou, A.-R.; Tam, S., *Tetrahedron Lett.* **1997**, *38*, 3195-3198.

[201]   Nielsen, P.E., *Acc. Chem. Res.* **1999**, *32*, 624-630.

[202]   Eschenmoser, A.; Kisakürek, M.V., *Helv. Chim. Acta* **1996**, *79*, 1249-1259.

[203]   Orgel, L. *Science* **2000**, *290*, 1306-1307.

[204]   Eschenmoser, A.; Krishnamurthy, R.; Guntha, S.; Scholz, P.; Schöning, K.-U., *Science* **2000**, *290*, 1347-1351.

[205]   Eschenmoser, A.; Micura, R.; Bolli, M., *Chemistry & Biology* **1997**, *4*, 309-320.

[206]   Eschenmoser, A.; Krishnamurthy, R.; Wagner, T.; Reck, F.; Beier, M., *Science* **1999**, *283*, 699-703.

[207]   Eschenmoser, A., *Science* **1999**, *284*, 2118-2124.

[208]   Eschenmoser, A.; Krishnamurthy, R.; Huynh, H.K.; Stanek, M.; Wippo, H.; Jungmann, O., *Org. Lett.* **1999**, *1*, 1527-1530.

[209]   Schlönvogt, I.; Pitsch, S.; Lesueur, C.; Eschenmoser, A.; Jaun, B., *Helv. Chim. Acta.* **1996**, *79,* 2316-2345.

[210]   M. Egli, P. S. Pallan, R. Pattanayek, C. J. Wilds, P. Lubini, G. Minasov, M. Dobler, C. J. Leumann, A. Eschenmoser, *J. Am. Chem. Soc.* **2006**; *128*, 10847-10856.

[211]   Dissertation, Christoph Behrens, Philipps Universität Marburg, Fachbereich Chemie, **2003**.

[212]   Diploma thesis, Johannes Gierlich, Philipps Universität Marburg, Fachbereich Chemie, **2003**.

[213]   A. Schwögler, T. Carell, *Helv. Chim. Acta* **2000**, 83, 2452-2463.

[214]   H. Gross, I. Farkas, *Chem. Ber.* **1960**, *93*, 95-99.

[215]   M. Mach, U. Schlueter, F. Mathew, B. Fraser-Reid, K. C. Hazen, *Tetrahedron* **2002**, *58*, 7345-7354.

References

[216]   M. J. Gait (Ed.), „*Oligonucleotide Synthesis - A Practical Approach*" **1984**, IRL Press, Oxford.

[217]   R. Nomura, Y. Hasegawa, M. Ishimoto, T. Toyosaki, H. Matsuda, *J. Org. Chem.* **1992**, *57*, 7739-7724.

[218]   S. Akine, T. Taniguchi, T. Nabeshima, *Chem. Lett.* **2001**, *7*, 682.

[219]   G. H. Clever, K. Polborn, T. Carell, *Angew. Chem. Int. Ed.* **2005**, *44*, 7204 - 7208.

[220]   All melting point experiments with **D4-L-a/b** described in this study were carried out with 3 μM DNA and 150 mM NaCl but Tanaka et al. used lower concentrations (2 μM DNA and 50 mM NaCl) in a different buffer. The behavior of **D4-L-a/b** was also checked under these conditions for better comparability and it was found that lowering of the DNA and salt concentration led to a decrease of all measured absolute melting temperatures, but the difference between the TM prior and after assembly of the metal base pair became even larger.

[221]   J. F. Larrow, E. N. Jacobsen, *J. Org. Chem.* **1994**, *59*, 1939.

[222]   S. Zolezzi, A. Decinti, E. Spodine, *Polyhedron* **1999**, *18*, 897.

[223]   R. Klement, F. Stock, H. Elias, H. Paulus, P. Pelikán, M. Valko, M. Mazúr, *Polyhedron* **1999**, *18*, 3617.

[224]   R. S. Downing, F. L. Urbach, *J. Am. Chem. Soc.* **1969**, *91*, 5977.

[225]   G. M. Segers-Nolten, N. M. Sijtsema, C. Otto, *Biochemistry* **1997**, *36*, 13241.

[226]   N. Berova, K. Nakanishi, R. W. Woody (Ed.), *Circular Dichroism (Second Edition)*, New York, **2000**, *Wiley-VCH*, p. 713-718.

[227]   J. H. Banoub, R. P. Newton, E. Esmans, D. F. Ewing, G. Mackenzie, *Chem. Rev.* **2005**, *105*, 1869.

[228]   S. A. Hofstadler, R. H. Griffey, *Chem. Rev.* **2001**, *101*, 377.

[229]   J. L. Beck, M. L. Colgrave, S. F. Ralph, M. M. Sheil, *Mass. Spec. Rev.* **2001**, *20*, 61.

[230]   S.-W. Lee, S. Chang, D. Kossakovski, H. Cox, J. L. Beauchamp, *J. Am. Chem. Soc.* **1999**, *121*, 10152-10156.

[231]   The measurements were performed by Stephan Reitmeier and Prof. Olav Schiemann, TU München and Johann Wolfgang Goethe-Universität Frankfurt, **2005** – **2006**.

[232]   B. Bleaney, K. D. Bowers, *Proc. Roy. Soc. London Ser. A* **1952**, *214*, 451.

[233]   Spartan '02, **1991-2002**, *Wavefunction Inc.*, Irvine, USA.

[234]   M. I. F. Garcia, M. Fondo, G. A. M. Deibe, M. B. F. Fernandez, A. M. Gonzalez, *Z. Anorg. Allg. Chem.* **2000**, 626, 1985-1991.

[235]   G. H. Clever, T. Carell, *Angew. Chem.* **2006**, in press (DOI: anie.200603099).

[236]   Manual fitting of the X-ray-derived copper-salen complex geometry into an idealized model of a double stranded B-DNA with rise/base = 3.375 Å, twist/base = 36 ° (Spartan '02, **1991-2002**, *Wavefunction Inc.*, Irvine, USA).

[237]   The mass of the most abundant isotopomers of the simulation and measurement were compared because the peak of the lowest weight isotopomer was in most cases to small for an unambiguos assignment. Only 2 decimals are given fort these mass values.

[238]   Master thesis, Corinna Kaul, LMU München, Dept. f. Chemie u. Biochemie, **2006**.

[239]   K. Tanaka, G. H. Clever, Y. Takezawa, Y. Yamada, C. Kaul, M. Shionoya, T.Carell, *Nature Nanotech.* **2006**, in press (DOI: 10.1038/nnano.2006.141).

References

[240]   R. G. Osifchin, R. P. Andres, J. I. Henderson, C. P. Kubiak, R. N. Dominey, *Nanotechnology* **1996**, *7*, 412-416.

[241]   Research Project (advanced Organic Chemistry), Andreas Keilbach, LMU München, Dept. f. Chemie u. Biochemie, **2004**.

[242]   S. L. F. A. da Costa and S. M. L. Agostinho, *Corrosion* **1989**,*45*,472.

[243]   J. C. Rubim, I. G. R. Gutz, O. Sala, *J. Mol. Struct.* **1983**, *101*, 1-6.

[244]   J. C. Plakatouras, S. P. Perlepes, D. Mentzafos, A. Terzis, T. Bakas, V. Papaefthymiou, *Polyhedron* **1992**, *11*, 2657-2672.

[245]   A. N. Chebotarev, M. V. Shestakova, E. B. Rusanov, *Russ. J. Coord. Chem.,* **2002**, *28*, 601–602.

[246]   I. Soetofte, K. Nielsen, *Acta Chem. Scand. A.* **1983**, *37*, 891-895.

[247]   Z. Q. Tian, *J. Raman Spectrosc.* **2005**, *36,* 466–470.

[248]   A. M. Ingram, K. Stirling, K. Faulds, B. D. Moore, D.Graham, *Org. Biomol. Chem.* **2006**, *4*, 2869–2873.

[249]   D. Graham, W. E. Smith, A. M. T. Linacre, C. H. Munro, N. D. Watson and P. C. White, *Anal. Chem.* **1997**, *69*, 4703-4707.

[250]   D. Graham, B. J. Mallinder and W. E. Smith, *Angew. Chem. Int. Ed.* **2000**, *39*, 1061-1063.

[251]   R. Brown, W. E. Smith, D. Graham, *Tet. Lett.* **2001**, *42*, 2197-2200.

[252]   D. W. Price, J. M. Tour, *Tetrahedron* **2003**, *59*, 3131-3156.

[253]   D. W. Price, S. M. Dirk, F. Maya, J. M. Tour, *Tetrahedron* **2003**, *59,* 2497-2518.

[254]   A. R. Katritzky, X. Lan, J. Z. Yang, and O. V. Denisko, *Chem. Rev.* **1998**, *98*, 409-548.

[255]   S. Zaramella, R. Strömberg, E. Yeheskiely, *Eur. J. Org. Chem.* **2002**, 2633-2639.

[256]   D. McKeown, C. J. McHugh, A. McCabe, W. E. Smith, D. Graham, *Heterocycles* **2002**, *57*, 1227–1230.

[257]   M. Bendayan. *Science* **2001***, 291*, 1363-1365.

[258]   Nanoprobes Inc., Yaphank, NY, USA; www.nanoprobes.com.

[259]   Rubiona GbR, Herne, Germany; www.rubiona.de.

[260]   Y. Negishi, Y. Takasugi, S. Sato, H. Yao, K. Kimura, T. Tsukuda, *J. Am. Chem. Soc.* **2004,** *126*, 6518–6519.

[261]   C. J. Ackerson, M. T. Sykes, R. D. Kornberg, *Proc. Natl. Acad. Sci. USA* **2005**, *102*, 13383-13385

[262]   M. Gelinsky, R. Vogler, H. Vahrenkamp, *Inorg. Chim. Acta* **2003**, *344*, 230-238.

[263]   B. Carboni, A.Benalil, M. Vaultier, *J. Org. Chem.* **1993**, *58*, 3736-3741.

[264]   Cluster synthesis and results will appear in the dissertation of Monika Fischler, RWTH Aachen, Institut f. Anorganische Chemie.

[265]   Y. Negishi, K. Nobusada, T. Tsukuda, *J. Am. Chem. Soc.* **2005**, *127*, 5261 -5270,

[266]   Measured and solved by M. Marsch, Philipps Universität Marburg, Fachbereich Chemie, **2003**.

Curriculum Vitae

Personal Data

Family Name: Clever   Martial Status: Unmarried, no children
Given Names: Guido Heinrich   Nationality: German
Gender: Male   Date of Birth: 15.10.1976

School/Alt. Service/University

1987 – 1996   High school (Gymnasium) Sinzig, Germany. Graduation on June 21st '96 (grade: 1.6).
1996 – 1997   Alternative service in rescue service of German Red Cross (Training as paramedic).
1997 – 2003   Studies of chemistry at the Ruprecht-Karls **University, Heidelberg**.
Jul – Aug '99 Internship at **Bayer AG**, research centre Wuppertal-Elberfeld (*Dr. T. Kraemer*).
Aug 20th '99   **Pre-diploma exams** with distinction (grade: 1.0).
2000 – 2001   Semester abroad at the **University of Strathclyde, Glasgow, UK**. "Surface
               Enhanced Resonance Raman-Spectroscopy" (*Dr. D. Graham*, Dept. Inorg. Chemistry).
Sep – Oct '01 Internship at the **Institute for Molecular and Cell Biology, Singapore**
               working on "Oncoproteins of the Human Papilloma Virus" (*Prof. H.U. Bernard*).
2002 – 2003   **Diploma thesis** on "Redox-functionalized tetra(hetero)arylmethanes"
               (*Prof. T.J.J. Müller*, Dept. Org. Chemistry, Heidelberg).
Mar 17th '03   **Diploma** (grade: 1.1), subsidiary subject: molecular biology.
May 1st '03   **PhD thesis** in the group of *Prof. T. Carell* on "Metal-Base Pairs in DNA".
               First: **University of Marburg**, since Dec '03: **University of Munich**.

Stipends, Events

- Prize of the "Otto Hofmann Foundation" for pre-diploma.
- Prize of the "Dr. Sophie Bernthsen Fonds" for diploma.
- Prize of the "Dr. Klaus Römer Foundation" for PhD thesis.
- Oct 2003 – Sept 2005 Kekulé fellow of the "Fonds des Verbandes der Chem. Industrie".
- Apr 2001 – Mar 2003 fellow of the "Studienstiftung des Deutschen Volkes".
- Jul 2000 – Mar 2003 member of e-fellows.
- 26. – 28.10.05 Participation at the "Roche Symposium for Leading Chemists of the Next
  Decade", Basel, Switzerland.
- 27.04 – 05.05.01 Participation at two conferences of the "Northeast Section of the American
  Younger Chemists Committee" in Boston organized and promoted by the "Gesellschaft
  Deutscher Chemiker" (German Chemists Society) and the ACS.
- 13 – 17.09.00 Participation at the seminar "Silentium 2000" of McKinsey & Comp. in Rome, Italy.
- 26. – 30.06.00 Participation at the 50. Nobel-Laureate-Meeting in Lindau, sponsored by the
  "Klaus-Tschira Foundation" Heidelberg.

Further Activities

- 1990 – 2002   Volunteer in the German Red Cross.
- 2000 – 2002   Tutorial jobs at the department of chemistry, Heidelberg.
- Since 1999   Student member of the "Gesellschaft Deutscher Chemiker".
- 2001 – 2003   Planning and foundation of a "Younger Chemist's Committee"
                   branch in Heidelberg and election as head of the group, organization of
                   several lectures, social events and the international Conference
                   "Promoting Younger Chemist's 2002"
- 2004 – 2005   Leader of the "Younger Chemist's Committee" branch Munich.
                   Organization of the industry contact fair "Alpenforum 2005".

Languages

English (fluent), French (basics), Japanese (beginner).